PROGRAMA DE DOCTORADO
Investigación en Medicina

APLICACIONES CLÍNICAS DE MODELOS DE DINÁMICA DE FLUIDOS EN PATOLOGÍA RESPIRATORIA

CLINICAL APPLICATIONS OF FLUID DYNAMICS MODELS IN RESPIRATORY DISEASE

Ana Fernández Tena

PROGRAMA DE DOCTORADO
Investigación en Medicina

APLICACIONES CLÍNICAS DE MODELOS DE DINÁMICA DE FLUIDOS EN PATOLOGÍA RESPIRATORIA

CLINICAL APPLICATIONS OF FLUID DYNAMICS MODELS IN RESPIRATORY DISEASE

Ana Fernández Tena

RESUMEN (en Inglés)

Inhaled medication is the first line of treatment in diseases such as asthma or COPD. The effect of aerosol therapies depends on the dose deposited beyond the oropharyngeal region as well as its distribution in the lungs (central or peripheral airways, uniform or not uniform). If an aerosol is deposited at a suboptimal dose or in a region of the lung that is not affected by the pathology being treated, the efficacy of the treatment will be compromised.

Factors such as the size of the aerosol particles, breathing conditions, the geometry of the airways or mucociliary clearance mechanisms play a fundamental role in the lung deposition of aerosolized drugs. These peculiarities of each individual make it necessary to have available in clinical practice a method to personalize aerosolized therapies. A possibility is creating airway models that are exclusive for each patient using computational fluid dynamics (CFD) techniques in combination with high resolution computerized tomography (HRCT) images of the thorax. But the applications of CFD techniques in respiratory medicine are not only limited to the study of drug deposition in the lungs. CFD also allows knowing in depth the fluid-dynamic characteristics of the obstructive lung diseases, providing information that is not available through basic lung function tests.

To these ends, a model of the conducting airways was developed, based on thoracic CT images to obtain the geometry of the upper airways, trachea and main bronchi, and supplemented with algorithmic techniques for the development of the rest of the conducting airways. Because the fully developed model consists of 65,536 branches it was chosen to develop a simplified version of the model, in which only eight branches of the airways are fully developed. The boundary conditions in the developed branches are applied to their equivalent truncated ones through a user-defined function (UDF), allowing obtaining results of the function in the complete model operating just through eight branches. Also another UDF that allows the use of non-stationary boundary conditions in the model was developed, to simulate breathing conditions.

Obstructive lung diseases, particularly chronic bronchitis and emphysema, were simulated, obtaining FVC, FEV_1 and FEV_1/FVC results in agreement with the expected when performing a forced spirometry. Multiple simulations were also performed to check the deposition of inhaled particles. In normal breathing conditions, with a flow of 30 *L/min*, approximately 30% of the inhaled particles with a mass median aerodynamic diameter (MMAD) of 5 *μm* are going to be trapped in the oropharyngeal region, and an additional 20% in the first 4 generations of the airways. When increasing the MMAD to 20 *μm*, these values increase to 70 % and 30% respectively. With a higher flow rate, 75 *L/min*, 100% of the particles with MMAD of 20 *μm* are trapped in the oropharyngeal region. The use of inhalers with particles larger than 10 *μm* and flow rates over 30 *L/min* must be avoided, because the percentage of particles deposited before reaching the lungs is greater than 50%. These results are in agreement with the ones obtained by other authors.

Therefore, CFD is a very powerful technique, increasingly becoming more accessible to users, which provides valuable information to the study of the physiology of respiration, the fluid dynamic characteristics of various respiratory diseases, or to the knowledge of the mechanisms governing the pulmonary deposition of inhaled particles.

SR. DIRECTOR DE DEPARTAMENTO DE MEDICINA
SR. PRESIDENTE DE LA COMISIÓN ACADÉMICA DEL PROGRAMA DE DOCTORADO EN INVESTIGACIÓN EN MEDICINA

Acknowledgments

I wish these lines serve to express my most sincere gratitude to all those who contributed to the elaboration of this Doctoral Thesis with their personal and professional contributions.

To my supervisors Pere Casan and Eduardo Blanco, who trusted me from the beginning and have encouraged me to introduce myself in the world of computational fluid dynamics and particle deposition. Undoubtedly, without their help, this work would never have been possible.

To Amador Prieto, who has shown interest in this work from the beginning and has helped me understand the possibilities of computed tomography, obtaining images that I can only describe as fascinating.

To Keith Walters and Ira Katz, who kindly reviewed this work providing valuable suggestions to improve it.

To Manel Jordana, who made my stay in Hamilton easier, and Renée Labiris and all her investigation group, who made me feel like another member of the team.

To Mary and Dave, who welcomed me into their home, and who deserve my deepest affection.

To all my colleagues in the respiratory medicine department, for their interest in my work and their constant motivation.

To my father Joaquín, because without his encouragement and help I would not even had started this adventure.

And at last but not least, to my mother Ana, my husband Ángel and our beloved baby, for always being there.

Thank you very much.

Table of contents

INDEX

CHAPTER 1
Introduction

1.1. Interest in lung computational models

It is noteworthy that actually there is a great interest worldwide in the research of Computational Fluid Dynamics (CFD) techniques. In May of 2012, the Food and Drug Administration (FAD) in the United States announced a research project entitled "Predictive models of lung deposition for the safety and efficacy of inhaled drugs". The main objective was “to develop a computational fluid dynamics model of inhaled medication that may account for product characteristics and the physiological parameters of inhaled drugs on the total and regional deposition in the lungs". In particular, one of the main goals of this project was to improve the existing models by developing a geometry that can be used to investigate the drug deposition in the lower respiratory tract including the alveolar region. Another example of the interest raised by CFD techniques is that in the last worldwide CFD conferences, its application to medicine has an increasing presence. The Computational Fluid Dynamics Conference (raised in 1997), in 2003 created the field called “Food and Medical Engineering”, posteriorly renamed “Bio-engineering”. Initially, in 2003, just one abstract about blood circulation was presented, but each year this number increased (in 2007 they were presented seven abstracts about blood circulation and five about the movement of air in the respiratory system, and in 2012 three and one respectively). Another important CFD conference is the Computational and Mathematical Biomedical Engineering Conference, where, in 2013, a total number of 125 abstracts were sent, being 50 about the circulatory system and just 2 about the respiratory system. There are many other CFD conferences, and the medicine field is always present, especially dedicated to the circulatory system, but increasingly dedicated to the respiratory system.

1.2. The use of Computational Fluid Dynamics nowadays

CFD can be defined as the technique that attempts to use computers to simulate the movement of fluids. It is a branch of fluid mechanics that uses numerical methods and

algorithms to solve and analyse problems that involve fluid flows. CFD embraces a variety of technologies including mathematics, computer science, engineering and physics, and these disciplines have to be brought together to provide the means of modelling fluid flows. Such modelling is used in many fields of science and engineering but, if it is to be useful, the results that it yields must be a realistic simulation of a fluid in motion.

The increasing power of computers and its lower price have allowed the advance of CFD, in which the Navier-Stokes equations are solved in the domain under study. CFD packages available in the market are easy to use and sufficiently powerful to be used in the industry. With the proliferation of commercial programs, a growing number of experts have come in contact with these methods. However, some of the CFD features are often not well known, and therefore, the results obtained may not be correct. Therefore, it has become very important for the management of CFD having a good training in fluid dynamics and understanding the philosophy, capabilities and limitations of the system.

Some of the most popular applications of CFD in industry are car development, aerospace industry and wind turbine industries. In fact, in any application where there is any sort of fluid flow, CFD can bring benefit: climate modelling, distribution of aerosolized drugs by an inhaler, transport of gas or liquids in pipeline, etc.

As an example of the use of CFD for problems of scientific or engineering interest, consider the racing car industry, where CFD is an emerging science in the aerodynamic design area. During the last decade aerodynamicists found a growing interest in using computers and CFD methods to simulate wind tunnel tests or track conditions. CFD codes can simulate the flow over a car through mathematical modelling and solving of a discrete model. In fact, the wind tunnel technology has become insignificant alongside the rapid growth of CFD. With a wind tunnel, experiments are made by blowing wind over a real object in a controlled environment and measuring the aerodynamic forces that arise. In CFD the same experiment may be conducted in the form of a computer simulation. Nowadays CFD is a basic tool for the design and development of racing cars, helping wind tunnel research. In fact it's possible to test the car prior to any wind tunnel session, to pre-evaluate various configurations and submit to test only the most promising solutions. CFD substantially helps with understanding the phenomena involved in fluid flows, permitting accurate display and analysis of the information, with a level of detail that is hard to provide experimentally.

We all pass through life surrounded, and even sustained, by the flow of fluids. Blood moves through the vessels in our bodies, and air flows into our lungs. Our vehicles move through the Earth’s blanket of air or across its lakes and seas, powered by still

other fluids, such as fuel and oxidizer that mix in the combustion chambers of engines. Indeed, many of the environmental or energy-related issues we face today cannot possibly be confronted without detailed knowledge of the mechanics of fluids (Moin 1997).

1.3. Modelling of the lung using CFD

Applied to respiratory medicine, CFD would find the air velocity and pressure at all points of the airway, and how they change over time breathing. CFD has a promising future in the knowledge of the behaviour of air in the lungs, both in healthy people and in chronic respiratory diseases; in the study of particle deposition in the lungs, to enhance the deposition of inhaled drugs for the treatment of certain pathologies, and, in the other hand, to help preventing the deposition of air pollutants in the lungs (for example in mining workers).

CFD can also enhance the utility of common health tests used in clinical practice as the spirometry, CT (Computed Tomography), or SPECT (Single Photon Emission Computed Tomography).

CFD software searches for the detailed calculation of the movement of fluids through the use of computers, to solve the mathematical equations that govern the motion of a fluid. Thus it is possible to simulate the behaviour of a fluid. These equations, which define at any point of the space the velocity and pressure of a fluid, were discovered more than 150 years ago by the French engineer Claude Navier and the Irish mathematician George Stokes. These equations, which are partial differential equations, arise from applying Newton's second law to fluid motion, together with the assumption that the stress in a fluid is the sum of a diffusing viscous term and a pressure term. These equations are the same for any flow. The particularization to specific cases is defined by the boundary conditions and the initial values that were indicated.

Navier-Stokes equations are very complex, so its analytical solution is only possible in very elementary cases. The use of computers to obtain the numerical solution is the fact that has given rise to CFD. Even today, due to the computational complexity and the limitations of the most powerful computers, it is less efficient trying to use CFD techniques in cases where other techniques have achieved appropriate simplifications.

To solve the equations, the program will transform the differential equations into algebraic equations, and will solve them in a finite number of points in the space. So the first thing to do is to divide in small pieces (cells) the three-dimensional model of the airways, using a calculation mesh; the higher the number of points of this mesh, the greater the accuracy and realism of the simulation, but also it would be more difficult to be generated and resolved. In cases with a complex geometry, this phase can take days or even weeks. These issues will be discussed in more detail in Chapter 03.

Until the late '60s, the computers did not reach computational speeds sufficient to solve simple cases, such as laminar flow around a certain obstacle. Before that, the experimental studies were the basic means for calculation. Currently, experimental tests are still required for the testing of not very complex designs, but the advances in computers have allowed a significant reduction in the number of tests needed.

The advantages provided by the CFD analysis can be summarized in:

- Substantial reduction of time and costs in new designs.
- Ability to analyse systems or conditions very difficult to simulate experimentally.
- Level of detail practically unlimited.

However, CFD techniques also have some limitations. First, they are needed machines with large computational power (CFD researchers are regular users of the most powerful computers in the world), and software price is not yet accessible to the general public. Second, it requires a skilled workforce that is capable of running the programs and properly analyse the results. But the major drawback of CFD is that it is not always possible to obtain enough accurate results, and the ease of miscalculations. This is due to the need for simplifying the studied phenomenon so the hardware and software can be able to work with it. The results will be more accurate if the assumptions and simplifications applied were appropriate. We are going to consider, for example, the airflow in the airways. In theory, with the Navier-Stokes equations, the speed and air pressure at any point of the airways can be calculated. It is necessary to establish, with the equations, the initial and boundary conditions referred to the variables of study and to the solid surfaces. In this case, the conditions referred to the variables are defined by the velocity and pressure of the flow. The conditions of the solid surfaces are defined by their shape, mathematically expressed in appropriate coordinates.

As recondite as it is, the study of turbulence is a major component of the larger field of fluid dynamics, which deals with the motion of all liquids and gases. Similarly, the application of powerful computers to simulate and study fluid flows that happen to be

turbulent is a large part of the burgeoning field of CFD. In recent years, experts in fluid dynamics have used supercomputers to simulate flows in such diverse cases as the America's Cup racing yachts and blood movement through an artificial heart.

Its difficulty was expressed in 1932 by the British physicist Horace Lamb, who, in an address to the British Association for the Advancement of Science, reportedly said, "I am an old man now, and when I die and go to heaven there are two matters on which I hope for enlightenment. One is quantum electrodynamics, and the other is the turbulent motion of fluids. And about the first one I am rather optimistic". Of course, Lamb could not have foreseen the development of the modern supercomputers. These technological marvels are at last making it possible for engineers and scientists to gain fleeting but valuable insights into turbulence (Moin 1997).

1.4. Hypothesis and objectives of this work

The hypothesis of this work is that it is possible to simulate the behaviour of the air in the lungs in healthy people or in certain obstructive pathologies (such as chronic bronchitis and emphysema), employing a single path airway model that allows the simulation of the entire conducting airways but reducing computational costs, using CFD techniques. It is also possible to simulate the deposition of inhaled particles in the lungs in all of these situations.

The overall objective of this work is:

> ***To develop a model of computational fluid dynamics of the human airways that could be used to simulate the airflow in the conducting airways***.

Furthermore, this model should allow the investigation of specific diseases, such as chronic bronchitis and emphysema, and also the investigation of the deposition of pollutants or drugs in the airways.

To achieve the overall objective the following specific objectives were established:

1. Development of a complete path for the airflow along the conducting airways. This path must extend from the trachea until the beginning of the alveolar region, and should allow the simulation of airflow in the airways without including a large

number of branches or computing nodes. Therefore, the total calculation time must be maintained below a fair value.
2. Development and simulation of a realistic model for the upper airways and attachment to the model of the lower airways.
3. Investigation of a set of boundary conditions for the simulation, and selection of the most appropriate ones for predicting a realistic airflow field of the airways, both in the inspiration and expiration cycles.
4. Study of a group of airways diseases, such as chronic bronchitis and pulmonary emphysema, using specific morphologies for these pathologies, and different forms of breathing.
5. Research on the behaviour of pollutants and inhaled drugs in the whole model.
6. Establish new acting proposals based on the obtained results.
7. Investigation of a method for acquiring relevant information from medical examinations in order to develop specific models for specific people.

1.5. Structure of this document

This work is comprised by seven main chapters, references and three appendices.

Chapter 1, Introduction, remarks the importance of CFD techniques and their applications in industry and medicine, focusing in the respiratory field, are reviewed. Also the hypothesis and objectives of this work are indicated.

Chapter 2, Theoretical principles, provides an overview on the function, anatomy and physiology of the respiratory system; on the types of air pollutants with their composition, particle size and possible effects on health; on inhaled drugs, the devices available for their administration, and the factors that modify particle deposition in the lungs; on the most used lung function tests and their clinical applications; on obstructive lung diseases, focusing in COPD (chronic obstructive pulmonary disease) and asthma; and on the main lung models developed until now.

Chapter 3, Model development, focuses on the development of a realistic model of the complete human conducting airways, and the simplifications needed to achieve affordable computational costs without losing accuracy.

Chapter 4, Fluid-dynamic characteristics of COPD, deepens in the study of two of the main obstructive lung diseases, chronic bronchitis and emphysema, using the previously developed CFD model of the airways. Also, the correct functioning of the model is checked under different circumstances.

Chapter 5, Particle deposition, is centred on the simulation of particle deposition in the CFD model, studying both nasal and oral inhalation. The main factors that modify the deposition patterns are described, and several tips to enhance the entrance of inhaled drugs into the lungs are provided.

Chapter 6, Model customization, focuses on the adaptation of the CFD model to specific cases, employing HRCT images of the patients to obtain an approximation to their airway anatomy. Also the possibility of validating the model by means of SPECT or PET images is discussed.

Chapter 7, Conclusions and future works, collects the conclusions of the whole work and provides new fields of application for the CFD airway model developed.

References comprise the bibliographic references employed in this work by alphabetical order.

The appendices collect the published articles related to this thesis and the two different user defined functions that where developed for the correct functioning of the CFD airway model.

CHAPTER 2
Theoretical principles

2.1. The respiratory system

The respiratory system consists of a combination of organs that carry the air (oxygen) that is breathed into the bloodstream, and thence to the cells, to enable the growth and metabolic activity of the organism; and conversely, remove CO_2 from the blood (produced by the cellular metabolism) outside the body.

Breathing is an involuntary automatic process, in which oxygen from the inhaled air is extracted and waste gases are expelled with the breath, but it can also be voluntarily controlled during short periods of time. The number of inhalations and exhalations done by a person in one minute (respiratory rate) depends on the exercise, age, etc... Normal respiratory rate for an adult at rest ranges from 12 to 17 breaths per minute.

A human adult at rest makes approximately 26,000 respirations a day, while a new born takes 51,000 breaths a day under the same conditions. The air flowing in and out of the lungs, in each normal quiet breathing, is called tidal volume and is about 500 *mL*, while the total lung capacity of an adult person is about 5 *L*.

A brief description of the function, anatomy and physiology of the human respiratory system will be provided in the next sections.

2.1.1. Function

The main function of the respiratory system is the gas exchange between ambient air and the bloodstream, providing oxygen (O_2) from the air to the arterial blood, and eliminating carbon dioxide (CO_2) from the venous blood, produced by cell metabolism. This is essential for the homeostasis of the human body. In normal conditions, the values of these gases are expressed in table 2.1.

	Arterial blood	Mixed venous blood
pO_2 (*mmHg*)	80-100	35-40
pCO_2 (*mmHg*)	35-45	45-50
pH	7.35-7.45	7.30-7.35

Table 2.1: Normal values of respiratory gases in arterial and mixed venous blood (obtained from the pulmonary artery).

The respiratory tract is specially designed, both anatomically and functionally, so that air can reach the most distal areas of the lungs in the cleanest possible condition. Nasal hairs, nasal turbinates, vocal chords, the cilia of the bronchial epithelium, the sneeze and cough reflexes, etc., all contribute to this filtering process. And, on most occasions it is properly done. And if the particles present in breathed air finally achieve to deposit in the airways, these have a range of defence mechanisms in order to eliminate as many particles as possible, which will be furthered developed in chapter 2.3.3.5.

2.1.2. Anatomy

Human respiratory system can be divided into two parts:

- Driving system: consisting in the nostrils, mouth, pharynx, larynx, trachea and bronchi.

  It can be subdivided into upper airway and lower airway, being the lower edge of the cricoid cartilage, located in the larynx, the separation point between the two parts.

- Exchange system: consisting in alveolar ducts and sacs.

2.1.2.1. Upper Airways

The upper airways are composed by the nose, inner nasal cavity, paranasal sinuses, pharynx and larynx. The mouth is a structure that can participate in the respiration during an effort or in certain pathological situations.

- **Nostrils**: the nose is the superficial and front part of the nostrils. It is mainly composed by cartilaginous structures covered by skin, and it is located on the face. It has two holes called nares at its bottom, representing the external communication for the air inlet or outlet. Behind each naris there is a small space called nasal vestibule, whose internal walls have some thick hairs called vibrissae.

  Nostrils consist of two bone cavities separated by a septum, excavated inside the skull, and with their internal walls upholstered by a mucous membrane. They have a medial wall called nasal septum, and a lateral wall which contains the nasal conchae, which are bony prominences that communicate with the nasal sinuses. In the rear edge of the nostrils there are two holes called choanae, which open into nasopharynx, as seen in figure 2.1. Thereby they are the communication with the rest of the respiratory system (Rouvière 2002).

- **Mouth**: it is a cavity located in the face, under the nose, delimited by five walls:

  - Anterior wall: it is formed by the lips.
  - Side walls: they consist of the cheeks.
  - Lower wall: where the tongue is located.
  - Upper wall: is the palate, formed by a bony portion (hard palate, the palatal vault) and a membranous portion (soft palate).
  - Back wall: it is an irregular hole called fauces, which connects the mouth to the pharynx.

- **Pharynx**: it is a muscular and membranous organ with the shape of a tube that participates in breathing and swallowing. It is located in the neck, connecting the nose and mouth to the larynx and esophagus, so it allows the passage of air and food to the respiratory system and the digestive tract, respectively. In humans it is about five inches long, extending in front of the spine from the outer base of the skull until the 6^{th} or 7^{th} cervical vertebra.

  It can be divided into three parts (figure 2.1):

- Nasopharynx: also called upper pharynx because it starts in the back of the nasal cavity. The pharyngeal tonsils or adenoids are located there. Nasopharynx is limited superiorly by the cavum, anteriorly by the choanae, and inferiorly by the soft palate.
- Oropharynx: also called middle pharynx, because its front is connected to the oral cavity through the fauces. Above is limited by the soft palate and down by the epiglottis. The palatine tonsils are located there, between the anterior and posterior palatine pillars.
- Laryngopharynx: also called lower pharynx. It is composed by structures surrounding the larynx below the epiglottis. Between the pyriform sinuses is the entrance of the larynx bounded by the aryepiglottic folds (Rouvière 2002).

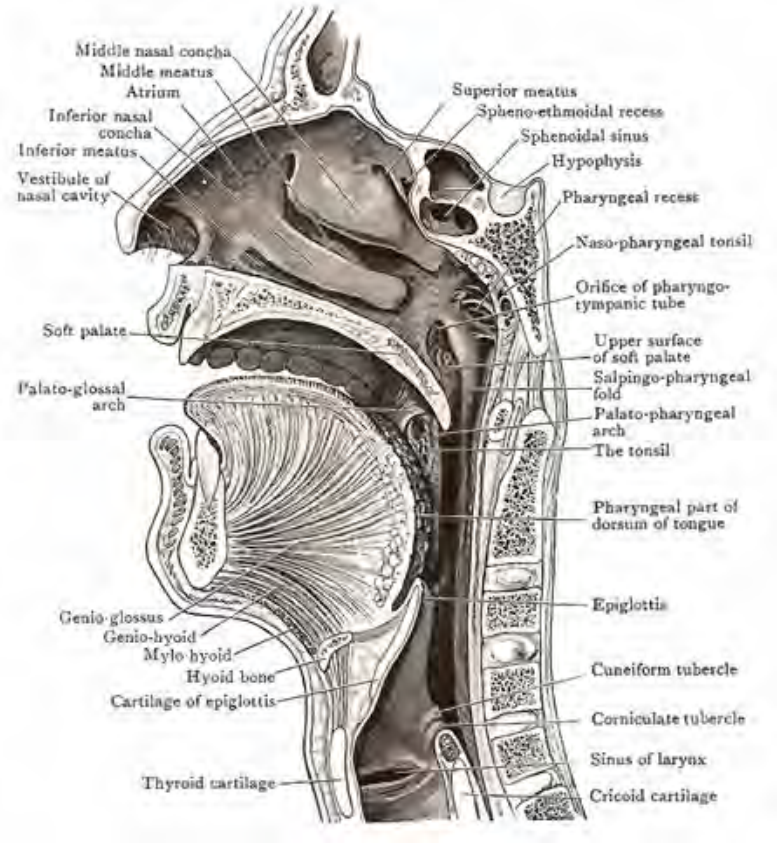

Figure 2.1: Anatomy of the nostrils and pharynx.

- **The Larynx**: tubular organ predominantly consisting of several cartilages with semilunar shape. It communicates the pharynx (located behind it) with the trachea.

  It is located in the anterior part of the neck, at the level of cervical vertebrae C3, C4, C5 and C6. It composed by the hyoid bone and several cartilages, which can be observed in figure 2.2: thyroid, cricoid, arytenoid, corniculate, cuneiform, epiglottis, sesamoids (anterior and posterior) and interaytenoid (Rouvière 2002).

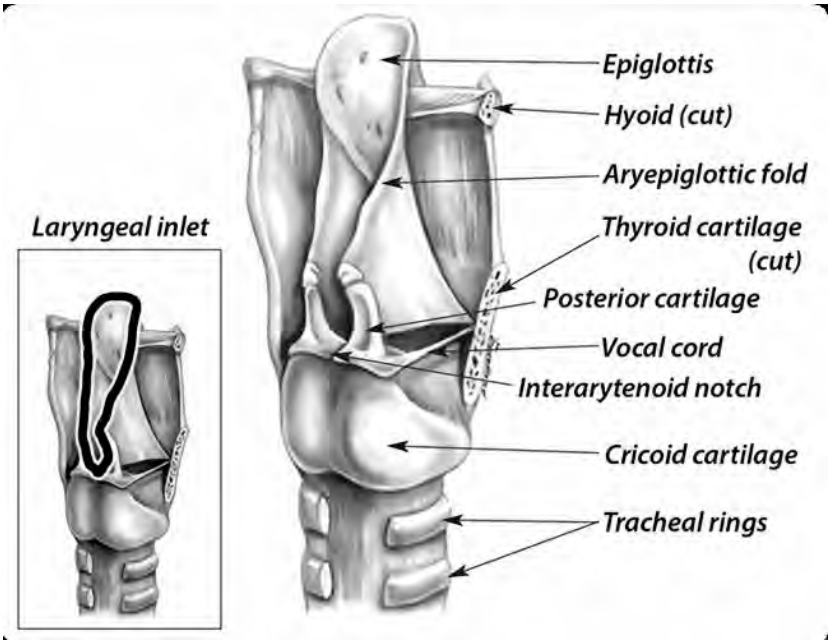

Figure 2.2: Anatomy of the larynx. The laryngeal inlet (marked with a black ring) includes the epiglottis, the paired aryepiglottic folds, the paired posterior cartilages, and the interarytenoid notch.

2.1.2.2. Lower Airways

Lower airways start at the trachea, which goes from the lower edge of the cricoid cartilage to the bronchial bifurcation, named main carina, situated at the same level as the fourth thoracic vertebra. In an adult, the trachea has a length between 10 and 15 *cm*, and a diameter around 2.5 *cm*. It is comprised by 18 to 24 cartilages, with horseshoe shape, united in the anterior region by fibro elastic tissue and in the posterior region by smooth muscle. The posterior region is called membranous zone.

The right main bronchus is shorter, wider and more vertical than the left one. It goes out of the trachea with an angle between 25 to 30 degrees. Its lumen measures about 16 *mm*, and its average length is about 2 *cm*. The right main bronchus subdivides in three lobar bronchia: upper, middle and lower. Its first ramification is the upper right bronchus, which subsequently divides in the apical, anterior and posterior segmental

bronchia. The ramifications for the middle and right lower lobes have a common origin in the intermediate bronchus. The middle lobe bronchus subdivides into lateral and medial segments. The lower lobe bronchus is the continuation of intermediate bronchus, and it divides into five different ramifications: apical, medial basal, anterior basal, lateral basal and posterior basal.

Left main bronchus goes out of the trachea with an angle about 45 degrees. It is substantially longer than the right one, with an average length of 5 *cm* and a diameter between 7 and 12 *mm*. It divides into left upper and left lower lobar bronchia. The left upper bronchus gives rise to three segmental bronchia: apicoposterior, anterior and lingular. Left lower bronchus divides into four segmental bronchia: inferior apical, anterior basal, lateral basal and posterior basal (Figure 2.3) (Rouvière 2002).

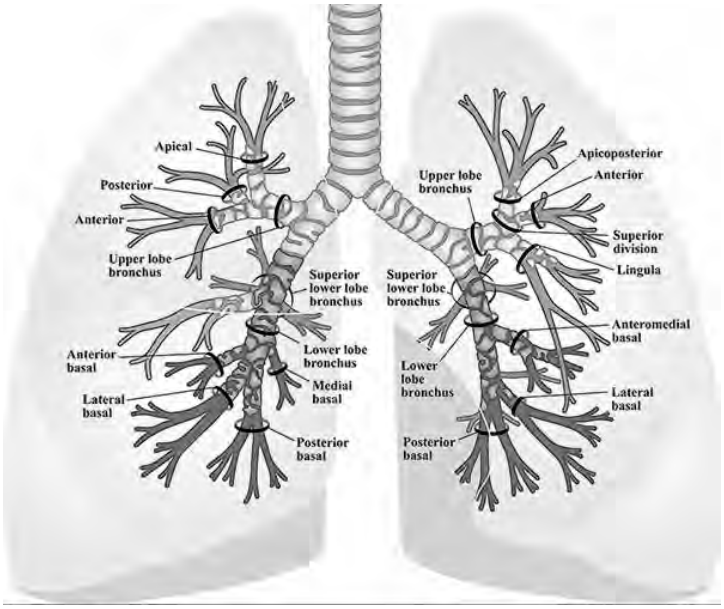

Figure 2.3: Anatomy of the bronchial tree. The trachea divides into the two main bronchia. Main left bronchus gives rise to the left upper and left lower lobar bronchia. Right main bronchus gives rise to the right upper, middle and right lower lobar bronchia.

From here, bronchia generally continue dividing in a dichotomous way until they reach a minimum of 23 generations, but also trifurcations and even some quadfurcations are described (Montesantos 2013). Generations 1, 2 and 3 have walls with cartilage, and are called bronchia. Generations from 4 to 16 are called bronchioles. This last one (16^{th}) is named terminal bronchiole, and it is the smallest portion of the airways lacking alveoli. Their diameter is about 1 mm. These first 16 generations comprise the conducting airway.

The acinus is the lung portion that depends from a terminal bronchiole. Each terminal bronchiole gives rise to three generations of respiratory bronchioles (generations 17, 18 and 19), which are the first structures that have some alveolar sacs in their walls. Respiratory bronchioles are followed by alveolar ducts (generations 20, 21 and 22) and alveolar sacs (generation 23). In this region gas exchange occurs, and it is named respiratory zone. Usually the respiratory zone is comprised by 2 to 5 generations of respiratory bronchioles, each of which opens in the alveolar ducts, with a short course, rapidly dividing into 10 to 16 alveoli (Rouvière 2002).

2.1.3. Physiology

Gas exchange is possible in the lungs if there is a contribution of air (ventilation) and blood (perfusion) to them. It is, therefore, necessary the integrity of the lung tissues, and a proper functioning of certain extrapulmonary factors, such as the brain ventilatory centres, the cardiac pump and the respiratory muscle pump.

Respiratory mechanics includes the study of the forces governing the movements of the lungs (pulmonary mechanics) and the thorax (thoracic mechanics), and also the resistance these forces have to overcome. Respiratory mechanics depend on some static properties, which govern the relations between pressure and volume, and some dynamic properties, which govern the relations between pressure and flow (Gea 2007).

2.1.3.1. Inspiration and expiration

The respiratory muscles are key elements of the breathing process. The contraction of the inspiratory muscles, primarily the diaphragm, external intercostals and parasternals muscles, produces a pressure difference between atmosphere and alveoli, causing the air to pass into the alveoli (inspiration). To understand this phenomenon it is necessary to know that the lungs are covered with two layers called

parietal pleura and visceral pleura, between which there is a virtual space called intrapleural space. In this space there is always (except under certain pathological conditions) a negative pressure in a greater or lesser degree, called pleural pressure (P_{pl}). This negative pressure keeps the lung inflated, attached to the chest wall. Furthermore it must be also taken into account that pressure in the alveoli is equivalent to pressure in the mouth (and hence to the atmospheric pressure) if there is no airflow and the glottis is opened, due to the physical principle of a tendency to equalize pressures between communicated compartments if there is no flow between them. Therefore, the pressure gradient between atmosphere and alveoli occurs because the contraction of the inspiratory muscles makes the P_{pl} to be even more negative. This negative pressure is not completely transmitted to the alveoli (alveolar pressure -P_{alv}-), since the resistance of the lung tissues opposes (transpulmonar pressure or elastically retraction pressure -P_{st}-), but sufficiently so there is some negativity in the alveoli compared to the atmosphere and thus the air enters into the lungs (Figures 2.4 and 2.5). Therefore, P_{alv} is the sum of P_{pl} and P_{st}:

$$P_{alv} = P_{pl} + P_{st} \tag{2.1}$$

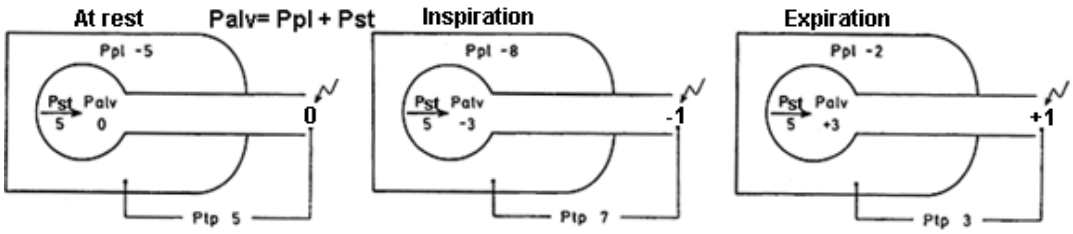

Figure 2.4: The pressure in the alveoli (P_{alv}) is equal to the sum of the pleural pressure (P_{pl}) and the transpulmonar pressure (P_{st}). P_{st} is always constant, and the P_{pl} varies along the respiratory cicle, so the P_{alv} is negative at inspiration (and the air enters into the lungs) and positive at expiration (the air exits the lungs).

Inspiration is an active process, since it requires the contraction of the inspiratory muscles.

Expiration, however, and under normal circumstances, is a passive process, it just happens by relaxation of the inspiratory muscles and the elastic recoil of the lungs. Upon relaxation of the inspiratory muscles, the P_{pl} becomes less negative again, while the P_{st} remains unchanged. P_{alv} therefore becomes slightly more positive than atmospheric pressure and therefore the air leaves the alveoli (Gea 2007).

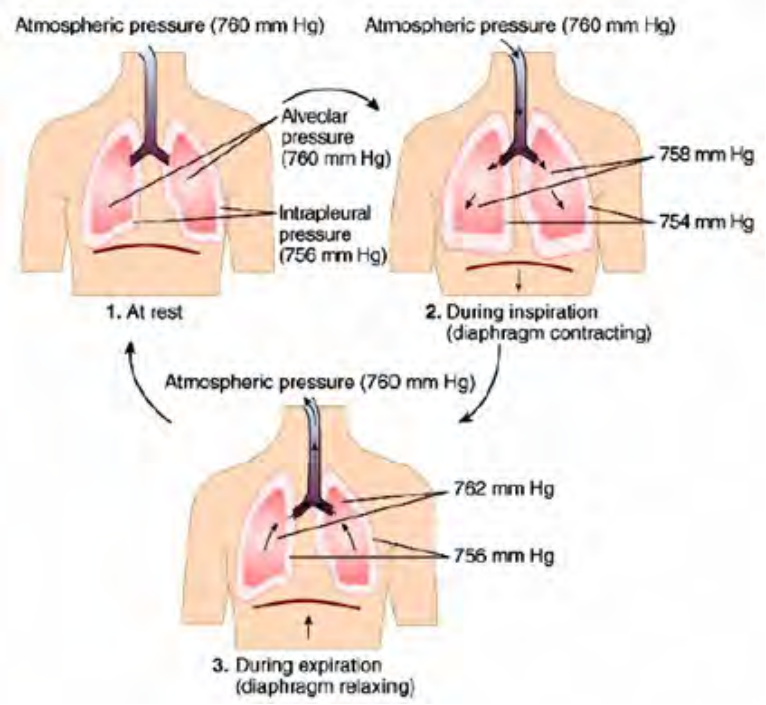

Figure 2.5: The measured values for P_{alv} and P_{pl} at rest, at inspiration and at expiration are shown.

Figure 2.6 summarizes the relationships between P_{alv} and P_{pl}, and the volume of air throughout the respiratory cycle.

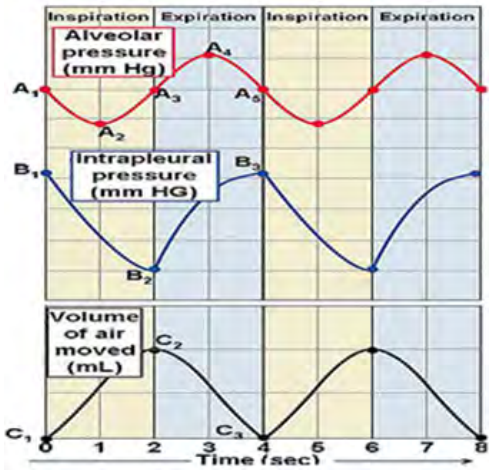

Figure 2.6: Relationship between P_{alv} and P_{pl} during the respiratory cycle. It can be seen how P_{alv} decreases in the inspiration so the air tends to enter into the lungs, and decreases in the expiration so the air exits the lungs. This is due to the changes in the P_{pl} throughout the respiratory cycle.

2.1.3.2. Static properties

The volume of air entering the lungs not only depends on the pressure gradient between the atmosphere and the alveoli, but also on the elastic properties of the lung-rib cage system. Distensibility (or lung compliance) is defined by the volume of air that can mobilize a given transpulmonar pressure gradient, which corresponds to the difference between P_{alv} and P_{pl}. Recall that the P_{alv} is equivalent to the pressure in the mouth. P_{pl} is usually considered equivalent to the esophageal pressure, when there is no inspiratory or expiratory air flow, which can be easily measured swallowing a pressure transducer. If the pressure in the esophagus and mouth are recorded along a forced expiration, it is generated a curve whose slope is the static lung compliance.

In contrast, lung elasticity is the tendency of the lung to recover its initial volume when the force that was deforming it disappears. Therefore it can be considered the opposite concept of distensibility (Gea 2007).

2.1.3.3 Dynamic properties

The dynamic properties of the respiratory system take into account the variable "time", so instead of referring to the relationship between pressure and volume, they refer to the relationship between pressure and flow. The most important dynamic mechanical property is airflow resistance, which is conditioned by the total pulmonary resistance. Total lung resistance is the sum of the resistance of the airway itself (R_{aw}) and the resistance of the lung parenchyma.

R_{aw} is equivalent to the 80 % of the total pulmonary resistance, and is directly proportional to the pressure gradient between mouth and alveoli in presence of airflow, and inversely proportional to the airflow itself. It mainly depends on the internal calibre of the airway. The flow is known to be transitional or turbulent in the trachea and large bronchi, while in the rest of the airway it is laminar.

An interesting phenomenon that depends on the correlation between the different

pressures acting on the respiratory system is the dynamic compression exerted on the airways. As mentioned above, during exhalation, air goes out of the alveoli. The closer to the mouth, the lower is the pressure inside the airway, due to the decreasing gradient. Therefore, there is a point at which the airway pressure is equal to the pressure found in the surrounding lung parenchyma. This point is called the equal pressure point or EPP. Beyond this point the airway tends to collapse because of the pressure in lung parenchyma. In normal circumstances, and at the start of expiration, the EPP is in large airways, which contain cartilage, preventing its collapse. As exhalation proceeds, the reduction in the volume implies a greater dynamic compression of the airways, and therefore moves the EPP to smaller airways with no cartilage. Thus, in healthy people, the collapse of the airway occurs only at very low lung volumes. However, in people with certain lung diseases the EPP moves to small airways at relatively high lung volumes, causing collapse of the airways and therefore air trapping (air enters into the lungs but then is not able to get out) , which is one of the causes of dyspnoea in these patients (Gea 2007).

2.2. Air pollution

Air pollution is an aspect of the environmental problems which is derived from our current model of development. Pollution refers to the presence in the atmosphere of any agent or combination of agents (physical, chemical or biological) in forms and concentrations that can be harmful to health, the welfare of population or harmful for plant or animal life. Depending on the affected environment, pollution can have different names: hydric pollution (water), atmospheric pollution (air) and soil contamination.

Among the most common air pollutants are aerosols, sulphur oxides, carbon monoxide, nitrogen oxides, hydrocarbons, ozone and carbon dioxide, mainly from burning fossil fuels (coal, oil and gas). The combustion of these raw materials is mainly produced in the process or the operation of the industry and road transport.

Past February 2011, Madrid and Barcelona, among many other European cities, were concerned at the warning from health authorities that breathing the city air could be harmful to health. Some air quality control stations in Madrid recorded nitrogen dioxide peaks above 40 $\mu g/m^3$, which is the acceptable limit under current legislation.

In the rush hour in the city, cars, many with diesel engines, start up, move a few feet, curb and start again. Every minute there are produced more contaminants, such as copper, antimony, tin, manganese, zinc, barium, metal from worn brakes, wheels and firm (called "rolling dust").

According to Querol (2008), Spanish urban air contains approximately 15% of rolling dust, 35% of ultrafine particles from the engines, 30% of nitrogen and sulphur oxides and 20% of mineral dust, mainly caused by city works. The vast majority of urban pollution comes from traffic (Figure 2.7), and some pollutants are not declining despite the efforts of automotive industry to make cars with fewer emissions. Diesel engines, which are increasingly widespread, emit more ultrafine particles and gases, compounding the problem.

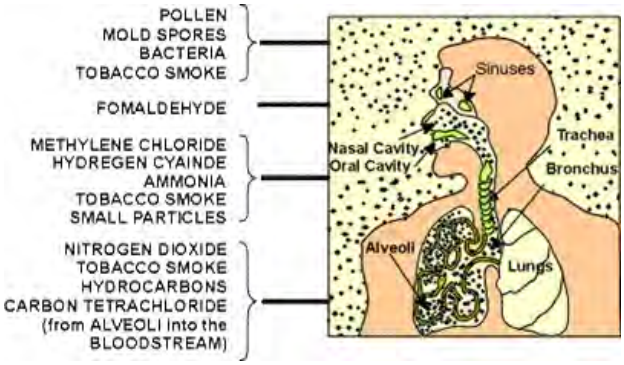

Figure 2.7: Most common inhaled particles from the air in the cities, and their capability to enter into the respiratory airways.

There is increasing evidence that ultrafine particles are dangerous. European Current laws on urban air quality only consider particles larger than 2.5 μm, although they should also legislate about these ultrafine particles.

In Spain, a total of 10.4 million people (i.e. 22% of the population) are breathing contaminated air with pollutant levels above the legally established ones in the Community legislation. However, if the recommendations of the World Health Organization (WHO) are considered, then 44.3 million people (i.e. 94% of the population) are breathing unhealthy air. The reason is that the WHO considers that the permissible limit for air pollution by particulate matter should be lowered to 20 $\mu g /m^3$ (currently it is established in 40 $\mu g/m^3$ annually).

2.2.1. Types of air pollutants

- **CFCs**: since 1960 it has been demonstrated that chlorofluorocarbons (CFCs, also known as "freons") have potentially negative effects: they contribute very significantly to the destruction of the ozone layer in the stratosphere, as well as increasing the greenhouse effect. Montreal protocol, approved on January 1st 1989, ended the production of most of these products. Used in refrigeration and air conditioning, they are released to the atmosphere at the time of the destruction of old equipment. Used as a propellant in aerosols, a part is released in each use. Nowadays, aerosols use other substitute gases (Baird 2001).
- **Carbon monoxide (CO)**: is one of the products of incomplete combustion. It is hazardous to humans and animals, since it fixes to the haemoglobin in blood, preventing the transport of oxygen in the organism. It is easily diluted in ambient air, but in a closed environment, its concentration makes it very toxic, and even fatal. The internal combustion engines of cars emits carbon monoxide into the atmosphere, so highly urbanized areas tend to have an excessive concentration of this gas up to concentrations of 50-100 *ppm*, rates that are hazardous to people's health (Aránguez 1999).
- **Carbon dioxide (CO_2)**: its concentration in the atmosphere is steadily increasing due to the use of fossil fuels as an energy source, causing the greenhouse effect.
- **Nitrogen monoxide (NO)**: it is a colourless gas and is slightly soluble in water. It is produced by burning fossil fuels in transport and industry. It oxidizes very rapidly into nitrogen dioxide (NO_2) and then in nitric acid (HNO_3), responsible of acid rain (World Health Organization 1987).
- **Sulphur dioxide (SO_2)**: the main source of SO_2 emissions into the atmosphere is the combustion of sulphur-containing coal. SO_2 from the combustion of sulphur is oxidized into sulphuric acid (H_2SO_4), which is also a component of acid rain. Acid rain is formed when the air's moisture combines with nitrogen monoxide or SO_2 emitted to the atmosphere. This chemical combination of gases and water vapour gives rise to sulphuric acid and nitric acids, substances that fall on the ground in form of precipitations or acid rain. Contaminants from acid rain can travel long distances, and the winds can move them thousands of miles before precipitating with dew, drizzle, rain, hail, snow or fog, that become acid when combined with those waste gases (World Health Organization 1979).

- **Methane (CH_4)**: methane is a gas formed when organic matter decomposes under conditions where oxygen is scarce, such as in swamps, marshes or rice fields. It is also produced in the process of digestion and defecation of herbivorous animals. Methane is a greenhouse gas that contributes to the global warming of the Earth, as it increases the heat retention capacity by the atmosphere (Baird 2001).
- **Ozone (O_3)**: ozone is a natural constituent of the atmosphere, but when its concentration is above some established levels it is considered a pollutant. Its concentration at sea level can range about 0.01 *mg/kg*. When pollution from exhaust gases from cars is high and solar radiation is intense, ozone levels increase and can reach up to 0.1 *mg/kg*. Plants may be affected in their development by small concentrations of ozone. People are also affected by ozone at concentrations between 0.05 and 0.1 *mg/kg*, as it causes irritation of the nose and throat, and dryness of mucous membranes of the upper respiratory tract (McKee 1993).

2.2.2. Particle composition and size

When referring to particulate matter pollution in the environment, it is important to consider that there is not a single homogeneous pollutant, but a set of pollutants varied enormously both in size and in composition. Therefore, air pollutants must be considered as a polydisperse aerosols. In aerosols with a polydisperse particle size distribution, the size is defined by the mass median aerodynamic diameter (MMAD), or diameter of a particle of mass equal to the average particle diameter of a population, meaning the diameter of a particle in which 50% of the aerosol mass is greater and the other 50% is smaller (Pritchard 1987). The aerodynamic diameter is the one corresponding to a sphere of density 1,000 kg/m^3 that has the same gravitational settling velocity as the particle in question:

$$d_{aerodynamic} = d_{particle}\left(\frac{\rho_p}{1{,}000}\right)^{1/2} \quad (2.2)$$

Figure 2.8 shows a diagram comparing the size of a human hair with other particle sizes.

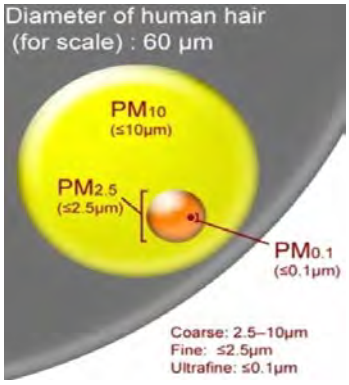

Figure 2.8: Comparative diameters in microns of different types of particles, using as reference the diameter of a human hair.

Figure 2.9 shows a comparative diagram with various sizes of particles contained in the air (in microns).

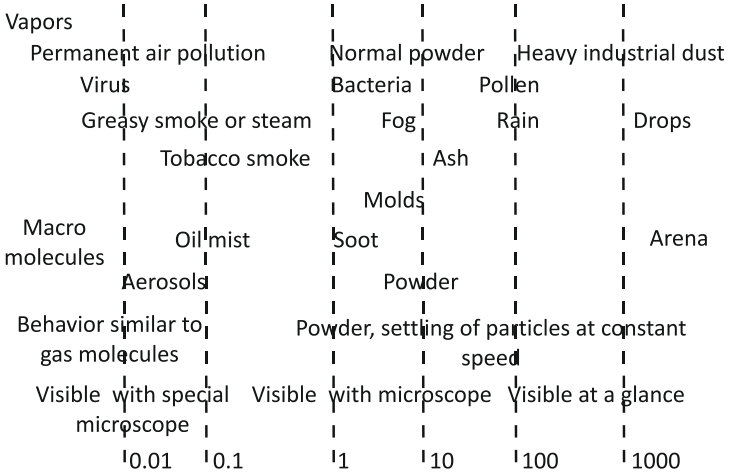

Figure 2.9: Sizes of various particles contained in the air (in microns).

In terms of its composition, particles are classified into:

- **Solid particles.** They may have a mineral or organic origin. The mineral particles are typically silica. In urban settings, carbon particles from incomplete combustion processes are very important. In indoor settings they are also important glass fibers or textiles. Organic particles have an animal or vegetable origin, such as bacteria, fungus, or pollen.
- **Liquid particles.** Such as small water droplets, aerosols, mists, etc.

Depending on its size, particles can be classified into:

- **Particles with aerodynamic diameter between 15 and 100 microns:** The overall content of ambient particles is known as total particulate matter. This includes all the particles that are suspended in the air, but generally, the particles larger than 15 microns are deposited by their weight and are rarely inhaled.
- **Particles with aerodynamic diameter between 5 and 10 microns:** The nose and trachea filter particles from 10 to 15 microns, preventing their entry into the lungs.

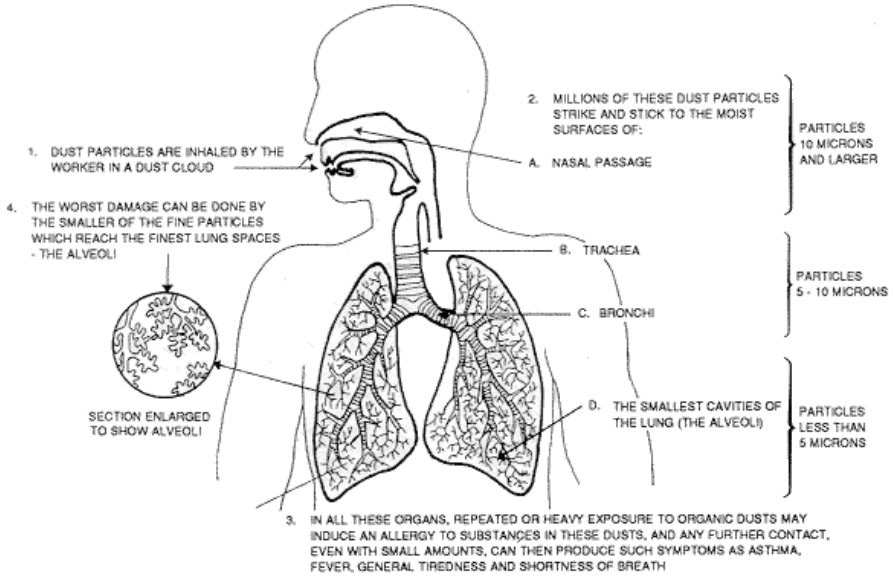

Figure: 2.10: Respiratory system and air pollution hazard areas in function of the inhaled particle size (Ontario Ministry of Agriculture, Food and Rural Affairs).

- **Particles with aerodynamic diameter between 2.5 and 5 microns:** The cilia of the respiratory epithelium of the trachea capture and expel particles of 3-5 microns that have broken through the nasopharynx, letting go into the lungs only particles with smaller diameters. These particles are considered the “respirable fraction” of an aerosol, as they can be delivered to the lungs for drug therapies.
- **Particles with aerodynamic diameter less than 2.5 microns:** These finer particles, known as the breathable suspended particulate, are the most important ones from the point of view of health.

Figure 2.10 shows a resume of these points.

2.2.3. Effects on health

The effect of particles on health is directly dependent on its size, since the human body is designed to remove larger particles and prevent its accumulation in the lungs, which ultimately are the filters that prevent the passage of fine particles to the bloodstream.

Numerous studies have linked air pollution with a wide range of health effects, but since the contaminant mixture contains many different substances, it is very difficult to link specific health problems with a particular pollutant. Detected effects could result from one or more air pollutants (Böhm 1982, Cordasco 1977, Neher 1994, Keller 1986).

The first evidence that air pollution is associated with adverse health effects was observed in London in December 1952 (Davis 2002). Several thousands of people died as a result of a special weather situation. A layer of cold air was trapped under a layer of warm air, so it could not rise. This phenomenon, known as thermal inversion, creates a natural roof, trapping polluted air near the ground. The inversion lasted four days. Since the weather was cold, the people of London burned a large amount of coal, which formed a fog throughout the city. The data explain that about 4,000 people died because of the fog and many more suffered severe respiratory problems.

Air pollution affects people in different ways. Factors such as health condition, age, lung capacity and the time of exposure to air pollution can influence how pollutants affect health.

Large particles of air pollutants can particularly affect the upper respiratory tract, while smaller particles can reach the distal airways and even the alveoli located in the deepest part of the lungs. Also, fine particles remain airborne for longer periods of time and can be transported over long distances. They are also more likely to pass directly from the lungs to the blood and other body parts. This could have a negative impact on health. People exposed to air pollutants may experience short or long term adverse effects. It has been observed a link between pollution in cities and increased emergency visits and hospital admissions due to lung and heart diseases, and strokes.

There are many studies analysing the impact of air pollution specifically in the lungs, as they are the gateway pollution in the body.

According to a report prepared by the European Topic Centre on quality Air and Climate Change (ETC/ACC), air pollution is associated with 455,000 premature deaths

each year in the 27 member states that make up the European Union (European Lung Foundation web).

Figure 2.11 shows the possible effects of air pollution on population's health

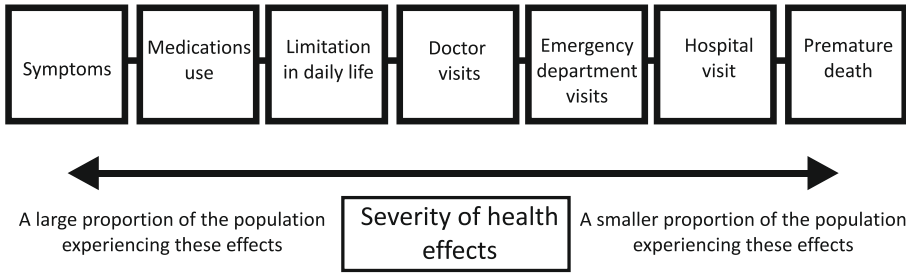

Figure 2.11: Possible effects of air pollution on population's health (reproduced from the original in Spanish, in the webpage of the European Lung Foundation).

2.3. Inhaled drugs

The particles that make up the air in the cities, and of which the respiratory system tries to be protected through several mechanisms (which will be furthered described in chapter 2.3.3.5), are called aerosols. But also are aerosols those devices used to transport liquid droplets or solid particles in a gaseous medium, and that today are widely used in medicine for the treatment of various pathologies. This is a paradox: an efficient system, designed to avoid certain particles from penetrating into the lungs, is at the same time used to intentionally deposit drugs in the airways and even for these to reach the alveoli in the best possible conditions.

The administration of inhaled drugs presents a series of advantages over systemic administration, making it preferable for the treatment of local diseases. Its effect on the airway is performed directly, without any metabolizing reaction, molecular conversion or absorption by another organ, which reduces the side effects and allows the achievement of greater treatment effectiveness. This makes the inhaled route essential for the treatment of respiratory diseases, particularly those related to bronchial obstruction.

2.3.1. Background

The treatment of respiratory diseases with inhaled steam has been traditionally done for centuries. The first bronchodilator drugs used were obtained from atropa belladonna and stramonium. The fruits of these plants contain atropine and hyoscyamine, with relaxing properties on bronchial muscle. These drugs were introduced in Europe at the beginning of nineteenth century in form of "asthma cigarettes", made with stramonium leaves, henbane and belladonna, which were very popular until few years ago.

In 1828, Schneider and Waltz developed an atomizer for mineral water sprays, called hidroconion, but it was also used as an inhaler. The first portable inhaler was created in 1856 by Sales-Giron, who worked as physician at a spa. It consisted of a manual liquid atomizer that enabled patients to administer inhaled balsamic infusions at home.

The discovery of adrenalin in 1901 by Takamine and Aldrich, and its inhaled administration for the first time in 1929 by Percy Camps (Camps 1929), initiated the search for the administration of new inhaled drugs, leading to improvements in the devices for their administration (Rau 2005).

2.3.2. Devices for the administration

The devices currently used for the administration of inhaled drugs can be divided into three types: nebulizers, metered-dose inhalers, and dry powder inhalers.

- **Nebulizers**: There are basically three types of nebulizers, jet ,ultrasonic, and with vibrating mesh technology (VMT). Jet nebulizers are based on the Bernoulli effect, according to which a compressed gas that passes through a narrow orifice creates a low pressure area upon exiting. If at this low-pressure point we connect a tube that has a thin layer of liquid, the low pressure will cause this liquid to be aspirated in small droplets. Ultrasonic nebulizers use piezoelectric crystals that vibrate at a high frequency within the nebulizing chamber, transmitting the vibratory energy to the

liquid that is in contact with it, converting said liquid into an aerosol (Martínez-Martínez 2003). Jet nebulizers can generally aerosolize most drug solutions, and ultrasonic nebulizers may not be effective if viscous suspensions or solutions are used (Newman 1995). VMT nebulizers have a mesh or membrane with 1000 to 7000 laser drilled holes that vibrates at the top of the liquid reservoir, and thereby pressures out a mist of very fine droplets through the holes. This technology is more efficient than the ultrasonic and jet nebulizers, allowing achieving shorter treatment times.

Nebulizers can administer high doses of medication in patients who are not able to coordinate or cooperate, and they are able to administer several substances mixed together in one same solution. The minimal inspiratory flow needed for the aerosol produced by a nebulizer to reach the lungs is 6–8 *L/min* (Newhouse 1976). However, there are high amounts of drug lost, as much of the medication is retained in the nebulizer dead-space, or it is lost in the room air during expiration. It has been estimated that only 10% of the dose that is initially placed in the nebulizer will be effectively deposited in the lungs (O'Callagan 1997), but with VMT nebulizers the lung deposition achieved can be greater (Daniels 2013, Conway 2012). The large droplets are deposited in the oropharynx, while the droplets are too small to penetrate in the lungs and are once again expelled during expiration.

Pulmonary deposition may be increased by modifying the patient's way of inhaling. Most patients inhale by using circulating volume. If the patient takes a deep breath and holds it in, the quantity of medication retained in the lungs may increase 14%–17% (Newman 1985). Probably the most practical way to modify the deposition pattern is to reduce the size of the droplets that are generated. This can be done with ultrasonic nebulizers by making the piezoelectric crystal vibrate at a greater frequency; with jet nebulizers this can be done by increasing the compressed gas flow (Mercer 1981).

- **Metered-dose Inhalers**: Metered dose inhalers (MDI) are devices used to administer aerosolized drugs that emit a fixed dose of medication with each pulse. They have a metallic chamber containing a suspension or solution of the drug with a liquid propellant that, at room temperature and atmospheric pressure, turns to its gaseous phase. A key piece in this system is the dosage valve, which releases at each pulse a controlled and reproducible dose of medication. The drug is released at a high speed (at more than 30 *m/s* through the mouthpiece) and in the form of particles with an MMAD of between 2 and 4 μm. MDI have a series of advantages, such as their small size (making them easy to handle), the exactness of the dosage, the possibility to fit them to holding chambers, the fact that they do not require

high flows to be inhaled and their low cost in general. Their main drawbacks are the difficulty inherent in synchronizing activation–inhalation and the low dose that reaches the lungs, which has been estimated at approximately 10%–20% of the dose emitted (Newman 1981, 1983). The high release speed and the large size of the particles generated mean that more than half of these impact in the oropharyngeal region (Newman 1981). Another drawback of MDI is the possible variation in the dose released at each pulse if the device is not correctly shaken (Altshuler 1957).

In the past, the propellant used was chlorofluorocarbons (CFC), but due to their harmful effects on the ozone layer, they have been banned by the United Nations. The substitute currently used in MDI is hydrofluoroalkanes (HFA) (Labiris 2003-II). HFA transform into their gaseous state at a higher temperature than CFC (Gabrio 1999), reducing the cold Freon effect, which is the interruption of breathing when the particles impact against the back wall of the oropharynx. There are currently on the market MDI-HFA with salbutamol, fluticasone, beclomethasone, anticholinergics, and the combination of salmeterol–fluticasone. The development of MDI with HFA has also been able to reduce the size of the aerosol droplets and, therefore, improve the lung deposition of the drug. In the case of beclomethasone–HFA, with an MMAD of 1.1 *m*, it has been demonstrated that up to 56% of the initial dose is deposited (Leach 1998 I & II, Leach 2006).

The optimal conditions for the inhalation of an aerosol using an MDI are to start breathing from functional residual capacity, activating at that moment the inhaler, inhale using an inspiratory flow less than 60 *L/min* and follow the inspiration with 10 *s* of apnea (Dolovich 1981). This method increases deposition by sedimentation in the peripheral areas of the airways. The minimal inspiratory flow necessary for its use is approximately 20 *L/min* (Newhouse 1976).

One way to avoid the lack of coordination between the patient and the device is to use inhalation chambers that fit on the mouthpiece of the MDI. The aerosol goes into the chamber and the particles that are too big impact against its wall and are retained there, while the smaller particles remain in suspension within the chamber until they are inhaled by the patient. In addition, the space that the chamber provides between the MDI and the mouth of the patient allows the aerosol to lose speed, reducing impaction against the oropharynx. In this manner, local adverse effects are reduced and lung deposition of the drug is increased (Ashworth 1991). It has been demonstrated that MDI used with inhalation chambers are as effective as nebulizers in the treatment of acute asthma attacks (Cates 2001).

Furthermore, with the aim of avoiding a lack of coordinated activation and inhalation, new MDI have been developed that automatically release the medication when the patient inhales, such as Autohaler™ and Easybreath™; these devices have been shown to improve the lung deposition of drugs in patients for whom coordination is difficult (Newman 1991). In addition, they require less inspiratory flow than conventional MDI, at around 18–30 *L/min*, which makes them more adequate for patients with physical limitations, children and the elderly (Giner 2000)

- **Dry Powder Inhalers**: Dry powder inhalers (DPI) were designed with the aim to eliminate the inherent coordination difficulties of MDI. They administer individual doses of drugs in a powder form contained in capsules that should be broken or opened before their administration (unidose systems), or in blisters that move around in a device or have powder reservoirs (multidose systems).

  Other advantages of DPI are that they do not require propellants for their administration, which makes them more respectful of the environment, and many of them have an indicator of the remaining doses. The main drawbacks are that patients perceive to a lesser degree the drug entering the airways, which may complicate treatment compliance, and its price, which is generally higher than in MDI. DPI should be stored in a dry setting, as humidity favours the agglomeration of the powder that can obstruct the inhalation system (Labiris 2003 II).

  The dose that reaches the lungs is similar to MDI, and less than 20% of the initial dose actually reaches the lungs. It has been demonstrated that if the inhalation technique is correct, there is no difference between the administration of a drug by means of DPI or MDI (Taburet 1994). The use of low inspiratory flow, humidity, and changes in temperature are all factors that have been shown to worsen the lung deposition of medications with DPI (Newhouse 2000).

  In the case of DPI, the “aerosol” is produced by the inspiratory effort of the patient (Taburet 1994). An inspiratory flow of at least 30 *L/min* is necessary for the powder medication to become dispersed and reach the lungs, which may be difficult to be done in the elderly, children or patients with severe respiratory disorder (Virchow 1994). The air is directed toward the container with loose powder, which generally consists of particles that are too large to penetrate the airway due to the formation of powder agglomerations or to the presence of large-sized particles that transport the drug, such as lactose. The dispersion of the powder into particles that enter into the inhaled fraction is produced by the formation of turbulent airflows inside the powder container, which break the powder agglomerations up into smaller sized particles and separate the transport particles from the drug (Concessio 1999). The

particles that are generated have a final MMAD that ranges from 1 to 2 μm (Terzano 1999, Hickey 2007). Every DPI has a different airflow resistance that determines the inspiratory effort necessary to disperse the powder. The greater the resistance of the device, the more difficult it is to generate the inspiratory effort, but at the same time the deposition of the drug in the lungs is greater (Chan 2003, Prime 1997).

2.3.3. Factors that modify the particle deposition

The main factors that influence the particle deposition in the lungs are listed in the next subsections.

2.3.3.1. Size and shape

The size and shape of particles are primary factors that condition their deposition in the lungs. Figure 2.12 shows a sketch of particle deposition in the airways. Depending on their size and shape, the particles can be deposited by means of four mechanisms:

- **Impaction**. This is the physical phenomenon by which the particles of an aerosol tend to continue on a trajectory when they travel through the airways, instead of conforming to the curves of the respiratory tract (Newhouse 1976). Particles with enough momentum (product of the mass and velocity) are affected by centrifugal forces at the points where the airflow suddenly changes direction, colliding with the airway wall. This mainly happens in the first 10 bronchial generations, where the air speed is high and the flow is turbulent (Lourenco 1982). This phenomenon mainly affects particles larger than 10 μm, which are mostly retained in the oropharyngeal region, especially if the drug is administered by dry powder inhalers (DPI) or metered-dose inhalers (MDI) (Heyder 1982). But it also affects the deposition of particles included in the respirable fraction (from 2 to 5 µm).

- **Interception**. This is mainly the case of fibers, which, due to their elongated shape, are deposited as soon as they contact the airway wall.

- **Sedimentation**. This is the physical phenomenon by which particles with sufficient mass are deposited due to the force of gravity when they remain in the airway for a sufficient length of time. This predominates in the last 5 bronchial generations, where the air speed is slow and the residence time is therefore longer (Lourenco 1982).

- **Suspension.** This is the phenomenon by which the particles of an aerosol move erratically from one place to another in the airways. This happens as a consequence of the Brownian diffusion of particles with an MMAD smaller than 0.5 *μm* when they reach the alveolar spaces, where the air speed is practically zero. These particles are generally not deposited and they are expelled once again upon exhalation.

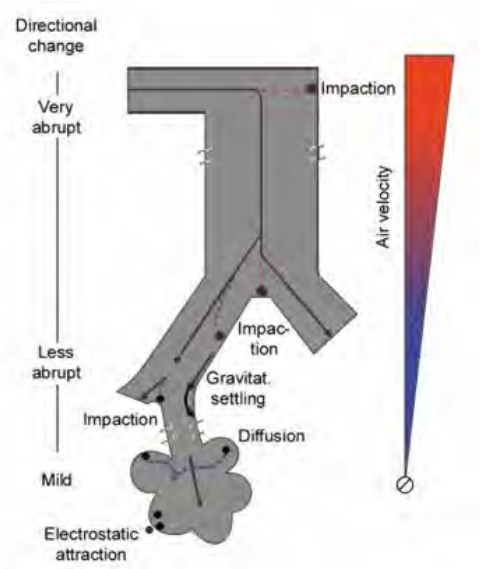

Figure 2.12: Main ways of particle deposition in the airways. When air velocity is high and the airflow suddenly changes direction, particles are deposited by impaction. As the air velocity decreases and the airflow has a more lineal direction, the particles tend to be deposited by sedimentation (mainly) or diffusion (in a lesser degree).

The particles of aerosolized drugs usually have a uniform shape and are symmetrical on several planes. They rarely are smaller than 1 *μm*, and therefore the predominating mechanisms are impaction and sedimentation (Aerosols 2006).

It can generally be considered that particles with an MMAD higher than 10 *μm* are deposited in the oropharynx, those measuring between 5 and 10 *μm* in the central

airways and those from 0.5 to 5 μm in the small airways and alveoli. Therefore, for topical respiratory treatment it is best to use particles with an MMAD between 0.5 and 5 μm. This is known as the respirable fraction of an aerosol (Jackson 1995).

2.3.3.2. Airway geometry

The probabilities of particle deposition by impaction increase when the particles themselves are larger, the inspiratory airflow is greater, the angle separating two branches is wider and the airway is narrower (Newman 1985).

In pathologies such as chronic bronchitis or asthma, which may alter the lung architecture with the appearance of bronchoconstriction, inflammation or secretion accumulation, the deposition of aerosolized drugs is modified. The smaller calibre of the airway increases air speed, producing turbulence in places where the flow is usually laminar. The airway obstruction also means that the air tends to be displaced toward unobstructed areas, and therefore the drug will also tend to be deposited mostly in healthy areas of the lung (Lippmann 1980).

2.3.3.3. Airflow velocity

Because particles are transported through the airways by an air current, their trajectories are affected by its characteristics. The air flow in the lungs is determined by the tidal volume and respiratory rate. Sbirlea-Apiou et al. (2007) demonstrated that in the first four generations of the airways, the deposition increases for any particle size as the inspiratory flow increases. However, the opposite happens in the last generations of the airways, where the deposition of particles is inversely proportional to this flow. This is due to the fact that the increased inspiratory flow reduces the residence time of the particles in the airway, therefore the effects of the severity and of the Brownian movement will be quite lower. Obviously, a minimal inspiratory flow is necessary to drag the particles toward the interior of the bronchial tree.

2.3.3.4. Humidity degree

The particles of aerosolized drugs can be hygroscopic to a greater or lesser extent. Hygroscopicity is the property of some substances to absorb and exhale humidity depending on the setting in which they are found. This means that they can get larger or smaller in size upon entering into the airways, with the consequent modification in the deposition pattern compared to what was initially expected. The diameter that a particle reaches after hygroscopic growth depends on its initial diameter, the intrinsic properties of the particle, and the environmental conditions in the airways. The mole fraction of water vapour contained in the airway has been demonstrated to be an important factor related with the increase in the MMAD of the aerosol particles (Lange 2000). In general, it is considered that hygroscopic growth does not have much of an effect in particles with MMAD less than 0.1 μm; meanwhile it is very intense in particles with MMAD larger than 0.5 μm (García Río 1997).

The hygroscopicity of molecules can be used to try to favour the deposition of inhaled drugs. Several studies have been developed, in which an aerosol was administered with a submicrometric or nanometric MMAD in order to reduce extrathoracic loss, taking advantage of later growth due to hygroscopicity, which enabled the particles to be retained within the lungs (Longest 2010, 2011).

2.3.3.5. Mucociliary system

Once deposited in the airways, the particles can be carried by the mucociliary system, degraded or absorbed into the systemic circulation or the lymph ducts (Lippmann 1980). The first of these mechanisms is found in the conducting airways (from the trachea to the terminal bronchioles), which have ciliated epithelium that are covered by two layers of mucus: a low-viscosity periciliary layer, or sol, and a thicker layer that covers the former, or gel. This biphasic layer of mucus protects the epithelium from dehydration, helping to humidify the air and providing a protective barrier by trapping inhaled particles (Basbaum 1989). The insoluble particles are trapped by the gel and

they are moved toward the pharyngolaryngeal region by the movements of the ciliated epithelium, where they are either coughed up or swallowed (Gail 1983, Satir 1990). The clearance speed depends on the number of ciliated cells and the cilia beat frequency, and it may be affected by factors that influence the function of the cilia or the quantity or quality of the mucus. In cystic fibrosis (CF), for example, very thick mucus is produced that does not correctly move along with the cilia. This is due to a mutation in the gene that codes the CFTR receptor, which regulates the passage of the chloride ion through the surface of the epithelial cells (Sevilla-Sánchez 2010).

The soluble particles are eliminated by absorptive mechanisms. The liposoluble molecules cross the respiratory epithelium by passive transport; the hydrosoluble molecules can cross the epithelial barrier either through the intercellular spaces or by active transport (by mechanisms of endocytosis and exocytosis) (Summers 1991). Once in the submucosal region, the particles can enter the systemic circulation, bronchial circulation or lymphatic system (Lippmann 1980). The particles that are deposited in the alveoli can be devoured and eliminated by the alveolar macrophages if they are insoluble particles (non-absorptive mechanism) (Brain 1970); if they are soluble, they can be absorbed into the systemic circulation (Folkesson 1996).

2.4. Lung function tests

A brief description of the main lung function test is provided in the next subsections.

2.4.1. Description

Lung function tests are a set of diagnostic techniques which aims to study several aspects of the functioning of the respiratory system. They prove an objective, accurate and reliable information. The spirometry is the main basic test and in many cases allows decisions for the patients.

The spirometry can be defined as the analysis of the lung volumes and the airflows under controlled circumstances. It is easily reproducible if suitable equipment and a technician with sufficient experience are available.

There are two kinds of spirometry, the simple spirometry and the forced spirometry. In the simple spirometry the patient, after a forced inspiration, expels all the air volume without a time limit. In the forced spirometry the patient has to expel all the air in the shortest time as possible. Nowadays the forced spirometry is the most important one from the clinical point of view.

Classically they have been used for spirometry two types of devices, the spirometer and the pneumotachograph. The spirometer is an instrument capable of measuring the lung volumes. The pneumotachograph measures the airflows. Nowadays the spirometers integrate both systems (García de Vinuesa 2010).

2.4.2. Determination

The forced spirometry is obtained asking the patient to make an intense, fast and prolonged expiration, after a forced inspiration. The spirometer allows obtaining volume/time and flow/volume graphics, which show the spirometric parameters. In these graphics, except in their first portion, the morphology is independent of the patient's effort. This happens in the moment when the pressures inside and outside the airway are equal, that is when airway collapses leading to dynamic airflow limitation.

The most important parameters obtained in the spirometry (Figure 2.13) are the forced vital capacity (FVC), which is the volume delivered during one expiration made as forcefully and completely as possible, starting from full inspiration, and the forced expiratory volume (FEV_1) in one second, which is the volume delivered in the first second of an FVC manoeuvre (Miller 2005).

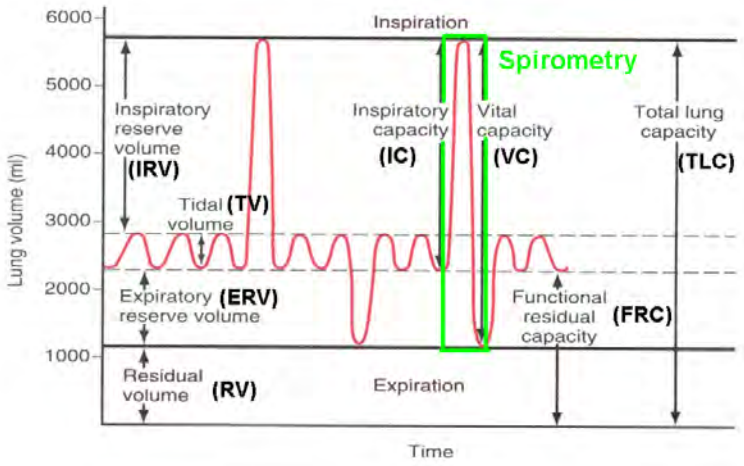

Figure 2.13: Simple spirometry expressed as volume VS time. In a simple spirometry the patient employs all the needed time to inhale and exhale all the possible air from the lungs.

Figure 2.14 shows the graphics of volume VS time, flow and volume VS time and flow VS volume in a spirometry.

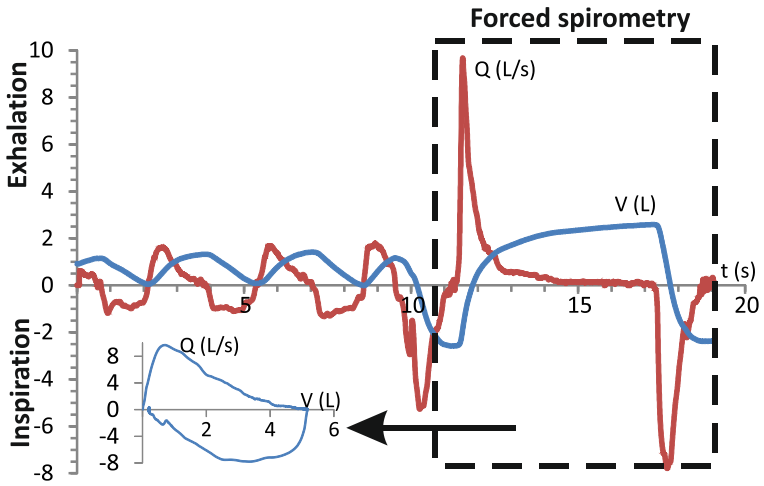

Figure 2.14: Forced spirometry expressed as flow and volume VS time and as flow VS volume (marked with an arrow). In the forced spirometry, the patient is asked to make an expiration and then an inspiration as forcefully and completely as possible.

2.4.3. Minimal requirements and recommendations

To be valid, a spirometry should fulfil a number of requirements.

- From a technical point of view, it is necessary to use equipment that meets the standards set by scientific organizations (SEPAR, ATS, ERS).
- The realization manoeuvre should meet the next requirements:
  - Abrupt onset and expulsion continued until reaching zero flow (less than 25 *mL/s*), encouraging the patient to reach the maximum flow.
  - The expiration time has to be at least of 6 seconds.
  - There shouldn't be an abrupt decrease of the flow at the end of the expiration.
  - The quality of the realization must be proven through the graphic analysis of the spirometry. This is essential to detect failures on its realization and to know if the manoeuvre has been correct.
  - They are necessary at least two manoeuvres with a variability of the FVC and FEV_1 less of 5% or 200 *mL*.

It is recommendable to inform the patient to avoid the use of bronchodilator medication the day before of the realization of the spirometry. The use of beta-2-adrenergic medication should be avoided in the 6 hours prior to spirometry. And theophylline and derivatives should be avoided in the 12 hours prior to spirometry (García de Vinuesa 2010).

2.4.4. Interpretation

The employed parameters in spirometry are:

- Forced Vital Capacity (FVC): is the maximal volume of air exhaled with maximally forced effort from a maximal inspiration, i.e. vital capacity performed with a maximally forced expiratory effort, expressed in litres at body temperature and ambient pressure saturated with water vapour (BTPS) (Miller 2005).

- Forced expiratory volume at first second (FEV_1): is the maximal volume of air exhaled in the first second of a forced expiration from a position of full inspiration, expressed in litres at BTPS (Miller 2005).
- Relation FEV_1/FVC: is the percentage relationship between FEV_1 and FVC.
- Forced expiratory flow 25-75 (FEF 25-75%): is the relation between the expelled volume between the 25 and 75% of the FVC, and the time employed in expelling it.
- Peak expiratory flow (PEF): is the maximum flow obtained during the forced expiration.

The spirometry results must be expressed in a numerical and graphic way. For the numerical results, usually are employed three plots of information: in the first one, the reference values are shown; the second one shows the patient's values; and the last one shows the percentage relationship of the measured values between the reference values. The reference values employed in spirometry may vary because of sex, age, size, race and weight of the patient (García de Vinuesa 2010).

For the graphic representation, the flow/volume curve is the best option (Figure 2.15). It provides more detail for the initial portion (first second) of the FVC manoeuvre. Since this portion of the manoeuvre, particularly the PEF, is correlated with the pleural pressure during the manoeuvre, the flow/volume display is useful to assess the magnitude of effort during the initial portions of the manoeuvre (Miller 2005).

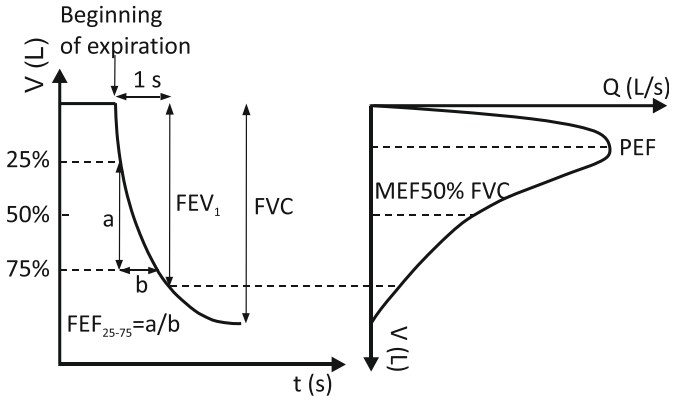

Figure 2.15: Transformation of a forced spirometry graphic from volume - time to flow - volume. The flow - volume representation is the one mainly used in clinical practice.

In Figure 2.16 a normal spirometry is shown. These percentages are important for the diagnosis of certain respiratory diseases, but for the monitoring of the patients the most important parameters are the patient's values and their variation in time.

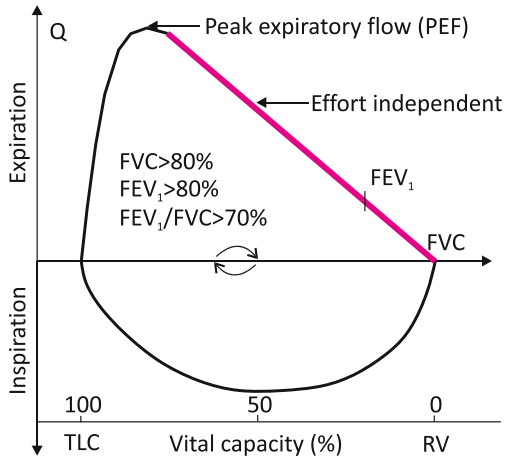

Figure 2.16: Representation of flow VS volume in a forced spirometry. The upper curve represents the expiratory manoeuvre, where its first portion (peak flow) is effort dependent, but the rest of the expiratory curve is effort independent. The lower curve represents the inspiratory manoeuvre.

The spirometry values are considered pathologic when they are below of certain values:

- For the FVC and FEV1, when they are below the 80% of the normal values
- For the FEV1/FVC, when the relationship is below 70%
- And for the FEF25-75%, when it is below the 60% of the normal values

2.4.5. Clinical applications

The forced spirometry analysis allows establishing the existence of a ventilatory alteration, and classifies it in different groups: obstructive, non-obstructive, mixed, and central airway obstruction.

Obstructive ventilatory alteration: it is produced in respiratory diseases associated with airflow limitation, either caused by increased resistance of the airways, as is the case of Chronic Obstructive Pulmonary Disease (COPD) or asthma, or by decreased lung elastic recoil, as occurs in emphysema, or a combination of both. The spirometric graphic (Figure 2.17) in these cases has a decreased maximum peak and fall delay.

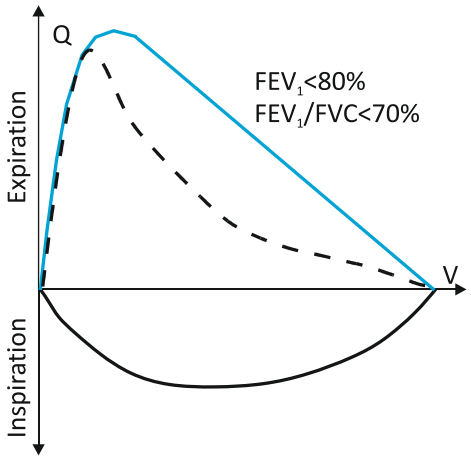

Figure 2.17: Obstructive spirometry, where the relationship between FEV1 and FVC is less than 0.7. The solid line shows the expected expiratory curve.

FEV1 is diminished, and FEV1/FVC is under 70%. FVC can be normal or slightly diminished. According to the intensity of the alteration the obstruction degree is established (Table 2.2).

Obstruction degree	FEV1
Slight	>65%
Moderate	50-64%
Severe	35-49%
Very severe	<35%

Table 2.2: Obstruction degree according to SEPAR's guidelines for forced spirometry

This work will be focused in the obstructive respiratory diseases.

Non obstructive ventilatory alteration: it is produced in respiratory diseases that have in common a decreased lung volume due to alterations in the lung parenchyma, the rib cage or the respiratory muscles and their innervation. The spirometry shows an overall decrease of the curves with a normal morphology (Figure 2.18).

FVC and FEV1 are diminished and FEV1/FVC is usually increased.

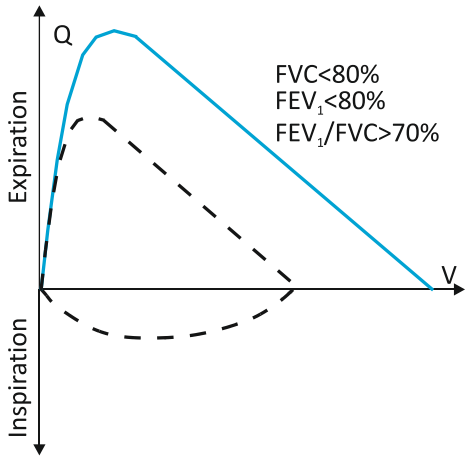

Figure 2.18: Non obstructive forced spirometry. Both FVC and FEV1 are under the 80% of the predicted values, but the relationship between them remains normal (>0.7). The solid line shows the expected expiratory curve.

Mixed ventilatory alteration: there are mixed characteristics from the two previous diseases (Figure 2.19).

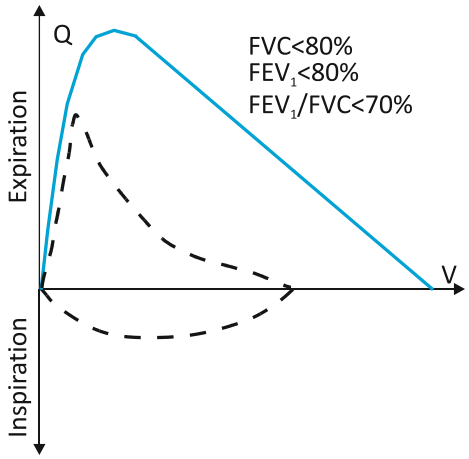

Figure 2.19: FVC and FEV1 are under the 80% of the predicted values, and also the relationship between is less than 0.7. The solid line shows the expected expiratory curve.

Central airway obstruction: a flattening of the expiratory curve (intrathoracic obstruction), or the inspiratory curve (extrathoracic obstruction) can be observed (Figure 2.20) (García de Vinuesa 2010).

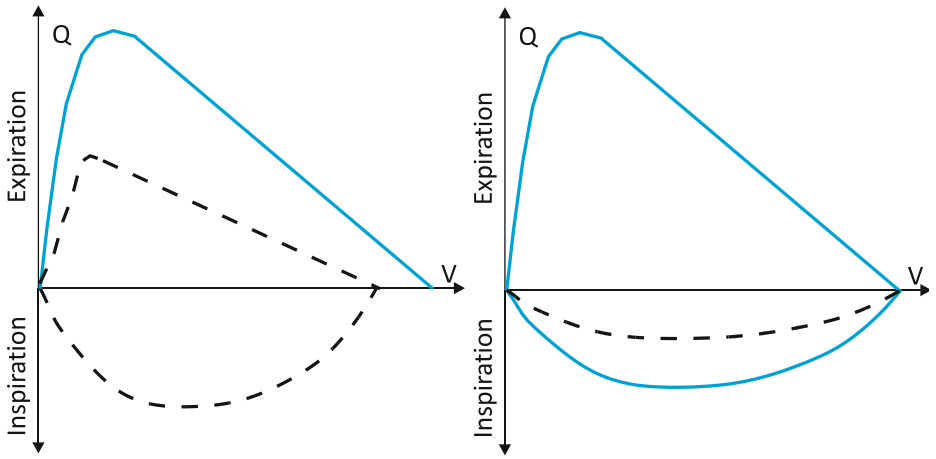

Figure 2.20: The left picture represents an intrathoracic obstruction (for example, in a patient with tracheal stenosis), where a flattening of the expiratory curve can be observed. The right picture represents an extrathoracic obstruction (for example in vocal cords dysfunction), with a flattening of the inspiratory curve. The solid lines represent the expected expiratory and inspiratory curves.

2.5. Obstructive lung diseases

Lung diseases with an obstructive diagnosis are, basically, COPD (Chronic Obstructive Pulmonary Disease), and asthma, although other diseases and entities as tumours can also hinder the air flow. Its obstructive pattern can be easily detected in the forced spirometry, as it was previously described, but they usually need more complex tests to distinguish between them. However, their fluid dynamic features are quite different.

COPD is a preventable and treatable disease that is often associated with other systemic abnormalities. It is characterized by the presence of chronic obstruction of the airways, poorly reversible and usually progressive, associated with an abnormal inflammatory response mainly against tobacco' smoke; but also continued exposure to products from the combustion of biomass in closed environments has also been associated with COPD. This chronic inflammatory response may induce parenchymal tissue destruction (resulting in emphysema), and disrupt the normal repair and

defence mechanisms (resulting in small airway fibrosis). These pathological changes lead to air trapping and progressive airflow limitation, and, in turn, to breathlessness and other characteristic symptoms of COPD (GOLD 2013). Also, the homozygous deficiency of alpha-1-antitrypsin is associated with early emphysema in smokers (Grupo de trabajo GesEPOC 2012). COPD is the fourth leading cause of death in the world, and it represents an important public health challenge (GOLD 2013).

The pathological lesions found in patients with COPD have been described in detail in several works, and can be classified mainly into two groups: those that primarily affect to the lung elastic recoil (called emphysema) and other group that mainly affects the restrictive properties of flow in bronchi and bronchioles (called airway diseases).

In ideal conditions an expert pathologist can accurately estimate the degree of airway obstruction from a comprehensive quantitative assessment of the diseased lung. However, as it is easy to imagine, this situation is only possible in cases where a pneumonectomy or autopsy has been performed, which makes it a not very useful method in clinical practice for the assessment of obstruction. The physiologist assessment of the disease's severity in the individual case can differ greatly from the pathologist. These differences reflect an incomplete understanding of the basic pathophysiology of COPD, as well as important methodological problems arising from the study of such a complex organ, both structurally and functionally, as is the lung.

Emphysema is defined as an impairment of lung tissue characterized by an abnormal enlargement of the airspaces located distal to the terminal bronchioles (i.e., corresponding to the respiratory bronchioles, alveolar ducts and alveoli), accompanied by the destruction of their walls, with no evidence of a clear fibrosis. Emphysema can be centroacinar/centrilobular, or panacinar/panlobular.

In centroacinar or centrilobular emphysema there are enlarged and not separated air spaces, which usually have a diameter between 1 and 10 mm, and which tend to be more evident in the upper lobes. Microscopically, these lesions can be observed in the proximal portions of the respiratory bronchiole (remember that this is the first portion of the airways where alveoli begin to appear). Alveolar structures of the distal acini are usually well preserved, although the largest lesions of centroacinar emphysema can obliterate much of the acini (Niewoehner 2008).

In panacinar or panlobular emphysema the whole lung is more uniformly affected. It is manifested as a diffuse and subtle increase in air spaces, which will measure millimetres or centimetres. In the most severe cases it may even form large bullae in the lungs. Microscopically, alveolar ducts show diffuse enlargement and the adjacent alveoli are erased to the point where it is not possible to distinguish the different

alveolar units. Panacinar emphysema diffusely affects all the regions of the lungs, and sometimes, especially if it is associated with α -1- antitrypsin deficit, it may have predominance in the lung bases.

The term “chronic bronchitis” has been employed extensively with multiple meanings. Strictly speaking, this is an inflammatory disorder affecting the bronchus, but it also is used to define a clinical condition characterized by excessive mucus secretion in the bronchial tree, and which is manifested clinically by chronic and productive cough. It was once thought that the excess of mucus had a role in the development of airflow obstruction, but it has been demonstrated that it is not related with the obstruction. Measurements of airway calibre made in lungs obtained at autopsy and surgical interventions show that the internal calibre of the airways is reduced in COPD patients compared to healthy subjects. Furthermore, in COPD patients, the bronchial walls are abnormally thickened due to an abnormal growth of epithelial elements, smooth muscle and connective tissue elements. The abnormally thickened walls of the airways can assume a greater functional significance at lower lung volumes, because the peripheral airways decrease in length and diameter when the lung has no air inside (i.e., in FRC) (Niewoehner 2008).

In patients with respiratory diseases the central airways (the ones that have >2 *mm* of internal diameter) have a significant increase in the size of the mucus secreting glands and also an increase in the number of goblet cells, which clinically is manifested as an hypersecretion of mucus, which in turn determines a local inflammatory response that will perpetuate this situation (Figure 2.21). Affectation of the peripheral airways (the ones with an internal diameter <2 *mm*) is the main responsible for airflow obstruction. It produces the apparition of peribronchiolar fibrosis, distortion, narrowing and obliteration of the airways, and the appearance of mucus plugs, which will condition the airway limitation (Sala 2007).

COPD must be suspected in every middle-aged patient with chronic cough, chronic expectoration, progressive dyspnoea, and a history of exposure to the risk factors previously described. To confirm the diagnosis a forced spirometry is essential, which will show a non-reversible obstruction (FEV_1/FVC <70%) after the administration of, at least, 4 inhalations of 100 μg of salbutamol (Fernández 2010). For an early diagnosis of this disease is recommended to perform a spirometry in every smoker or ex-smoker over 35 years old, and repeat it every 2 years if it remains normal (Grupo de trabajo GesEPOC 2012).

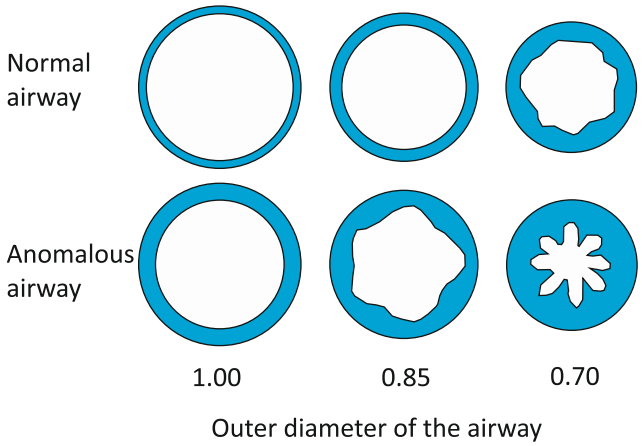

Figure 2.21: The outer diameter of the airway decreases as the lung volume becomes smaller. As the volume of the airway walls remains constant, the wall becomes thicker at lower pulmonary volumes, with a disproportionate decrease of the internal diameter of the airway. Abnormally thick walls, as happens in COPD, may exaggerate this effect.

Asthma is a heterogeneous condition. Its natural history includes acute episodic deterioration (exacerbations) against a background of chronic persistent inflammation and/or structural changes that may be associated with persistent symptoms and reduced lung function. The exposure to trigger factors combines with the underlying phenotype, the degree of hyper responsiveness and of airflow obstruction, and the severity of airway inflammation to cause wide variability in the manifestations of asthma in individual patients (American Thoracic Society and European Respiratory Society Task Force on asthma 2009). Asthma can be defined as a chronic inflammatory disease of the airways, whose pathogenesis involves various cells and inflammation mediators, conditioned in part by genetic factors, and which courses with bronchial hyper responsiveness and a variable obstruction, that can be totally or partially reversible, either by drug action or spontaneously (GEMA 2009).

Based on the definition of asthma, spirometry is one of the fundamental measures for asthma control, and is essential for its diagnosis. It provides an objective and highly reproducible measure of airflow limitation caused by smooth muscle contraction or structural changes. The main spirometric parameters relevant to asthma are FEV_1, FVC, FEV_1/FVC ratio, bronchodilator (BD) responsiveness (the change in FEV_1 after inhaling a bronchodilator), and post-BD spirometry (American Thoracic Society and European Respiratory Society Task Force on asthma 2009).

Figure 2.22 shows the diagnostic algorithm for asthma, based on the recommendation of the GEMA guide (2009).

The distinctive attribute between COPD and asthma is the chronic quality of the first. A nearly normal pulmonary function can be observed in asthma patients after a bronchodilator treatment.

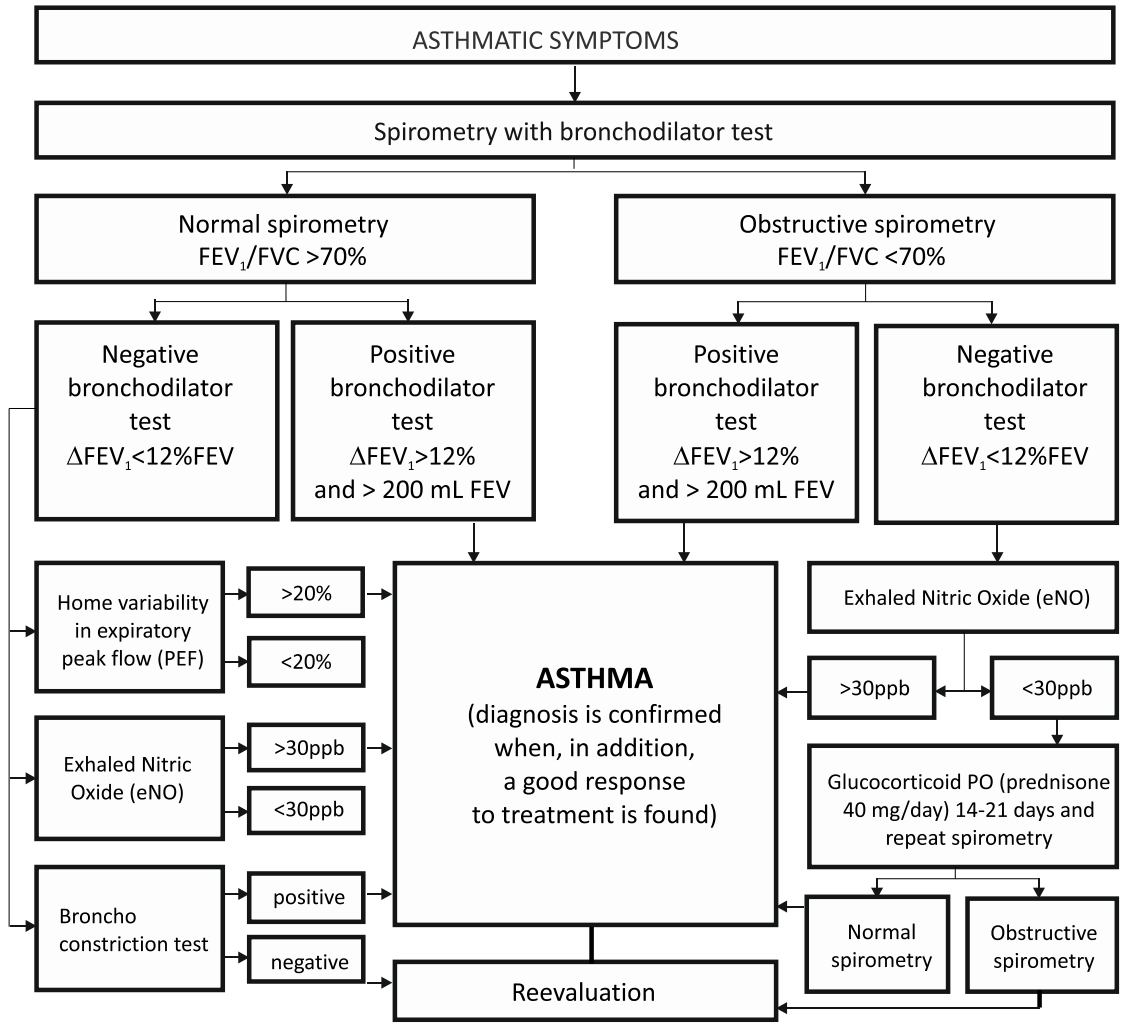

Figure 2.22: diagnostic algorithm for asthma, based on the recommendation of the GEMA guide (2009).

The effects of COPD on pulmonary function are:

- Appearance of airflow limitation, which is manifested as a fall in FEV_1 on spirometry.
- Appearance of lung hyperinflation (because the elastic recoil pressure is decreased by the alteration of the architecture of the lung), which is manifested as an increase in TLC in lung volumes.

- Appearance of air trapping, defined as an increase of VR when measuring lung volumes.

Pulmonary hyperinflation is the main result of airflow limitation. It is defined by the increase of FRC above reference values for a given individual. Dynamic hyperinflation occurs when the duration of expiration is insufficient for lung emptying to reach the level of RV. This happens mainly in two situations: when the expiratory airflow is limited (if the airway resistance is increased), and when the expiratory time is shortened (for example in patients with tachypnea, -increased respiratory rate-) (Sala 2007).

The main fluid dynamic effect in chronic bronchitis is produced by the section reduction of the airways, mainly due to chronic inflammation. The pressure loss increases and the flow rate decreases, mainly during the first second, when air velocity is the highest. As the global airways section increases going down the bronchial tree, is to be expected that the obstruction of the lower order branches is the most significant part of the phenomena. As the flow can be considered laminar, at least in the less severe phase of the illness, the pressure loss should be more or less proportional to the flow rate. The presence of an obstruction originated by a tumour, on the other hand, can be considered as a singular pressure loss, which is influenced by the square of the flow rate.

The respiratory obstruction generated by emphysema has a completely different source: the pressure driving the flow during the expiratory manoeuvre is due to the elastic lung recoil; in emphysema, the loss of elastic tissue elements reduces this pressure, hampering the lungs deflation.

Several works have demonstrated the complexity of the pulmonary flow. Zhang and Kleinstreuer (2008) elaborated a symmetric branching model and found that the unsteady typical flow of normal breath led to different flow features than in the steady state case, being greater during high frequency ventilation. Luo et al. (2007) investigated the effect of COPD on particle deposition in the upper lung airways for a symmetric four-generation model. Yang et al. (2006) worked with a three-generation airway model for both healthy and COPD cases, and found that the velocity profile entering the segments has great influence on flow patterns and pressure drop.

2.6. Lung models

The basic objective of the experimental and numerical studies of the air flow in the lungs is to deepen into the knowledge of the gas exchange (O_2 and CO_2) and particle deposition, to optimize the application of pharmaceutical aerosols for lung diseases. These are non-stationary phenomena due to the complexity of the airway geometry, the existence of interactions between air, water, and solids, and the presence of cellular mechanics and heat transfer, as it has been reviewed in the previous subsections. This means that the velocity, density, pressure and temperature change over time. Not all the phenomena occurring in the lung airways can be simulated. In fact, for the performance of experimental and numerical works is necessary to establish a number of simplifications, such as considering the flow to be isothermal (that always has the same temperature), or the inhaled particles to be spherical.

The first models of aerosol deposition in the lungs were based on very simple pulmonary morphologies. They used a small number of breathing conditions and a limited range of particle sizes, and were usually models confined to an area of the respiratory tract instead of models of the entire respiratory tract. In addition, they were limited to aerosols generated in industrial settings, like mining.

The first mathematic model for particle deposition was done in 1935 by Findeisen. This author, basing his study on the anatomical knowledge of the '30s, divided the respiratory tract into only 9 generations, reaching alveolar ducts and sacs. This model assumed a series of dimensions, flow speeds, transit times, and types of ramification for each generation, and several formulas were established in order to calculate the particle deposition in each generation according to the 3 basic mechanisms of deposition: impaction, sedimentation, and diffusion. Figure 2.23 shows the bronchial tree scheme proposed by Findeisen.

The main limitations of this model are that the airways above the trachea were not contemplated, and the anatomic simplicity of the used lower airway model. However, this pioneering model established the basic rules for the development of other later models.

Another significant model was developed by Landhal in 1950, which added two new compartments to Findeisen's model: mouth and pharynx. Later, Beekmans presented a new model in 1965, in which the 3 basic deposition mechanisms were assumed, and an attempt of improvement was made by correcting the dimensions of the airway caused

by its expansion during inspiration. In addition, it considered the role of the mix between tidal and residual volume in the three last generations of the airway. In this model, Beekmans established equal inspiratory and expiratory times, and after every phase he established a pause in which the deposition was produced by diffusion and sedimentation.

Lungenteile	Verzweigungsfaktor	Anzahl	Innerer Durchmesser cm	Länge cm	Gesamtquerschnitt qcm	Störungsgeschwindigkeiten * cm/sec	Durchströmungszeiten sec
A Trachea	1	1	1,3	11,0	1,3	150	0,07
B Hauptbronchien . . .	2	2	0,75	6,5	1,1	180	0,04
C Bronchien 1. Ordnung	6	12	0,4	3,0	1,5	130	0,02
D Bronchien 2. Ordnung	8	100	0,2	1,5	3,1	65	0,02
E Bronchien 3. Ordnung	8	770	0,15	0,5	14	14	0,04
F Bronchioli terminales .	70	$5{,}4 \cdot 10^4$	0,06	0,3	150	1,3	0,22
G Bronchioli respiratorii	2	$1{,}1 \cdot 10^5$	0,05	0,15	220	0,9	0,17
H Ductuli alveolarii .	240	$2{,}6 \cdot 10^7$	0,02	0,02	8200	0,025	0,82
I Sacculi alveolarii . .	2	$5{,}2 \cdot 10^7$	0,03	0,03	(147 000) **	etwa 0	1,2

* Für 200 ccm/sec Ventilationsgeschwindigkeit.
** Gesamtoberfläche der kugelförmigen Sacculi alveolarii.

Figure 2.23: Bronchial tree scheme proposed by Findeisen in 1935.

A more anatomically detailed model of the airways was published by Davies (1961), which divided the airways into 15 generations, starting in the mouth and ending in the alveolar sacs. Nevertheless, this was not the main model used to develop a furtherer mathematical model for the calculation of particle deposition.

The most commonly used anatomical model was developed by Weibel in 1963. In this model, the ways of bifurcation are indicated, designating the trachea as the first airway (order 0) and presuming that each airway leads to two branches (regular dichotomy). Weibel described a minimum of 23 airway generations up to the alveolar ducts (Figure 2.24).

Alternative approaches based on Weibel's morphology have been proposed by some research groups in order to enhance the description of the lungs. Among them, it must be mentioned the work by Horsfield and Cumming (1968), who introduced some asymmetries in the model, as the diameter of the airways and the branching angles; or the morphology developed by Hammersley and Olson (1992) which is suitable for the smaller airways, between generations 6 to 12.

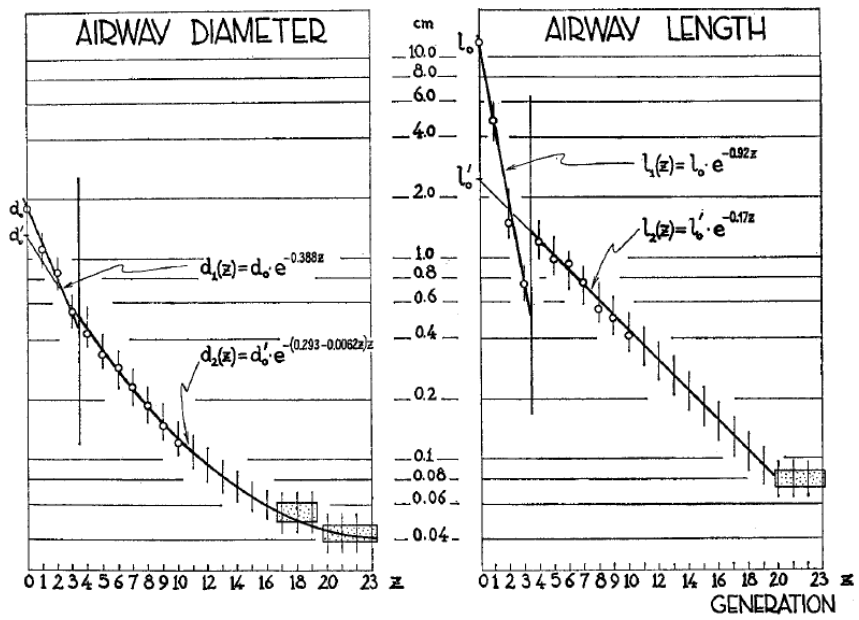

Figure 2.24: Average diameter and length of the different airway segments referred to an adult lung, proposed by Weibel.

Besides these theoretical studies, there were investigated detailed mathematical descriptions by Sauret et al. (1999), Hegedus et al. (2004), and Schmidt et al. (2004), which proposed high-resolution models of morphologically realistic airways up to the fifth generation. Figure 2.25 shows the structure of the geometry of an asymmetric realistic bifurcation.

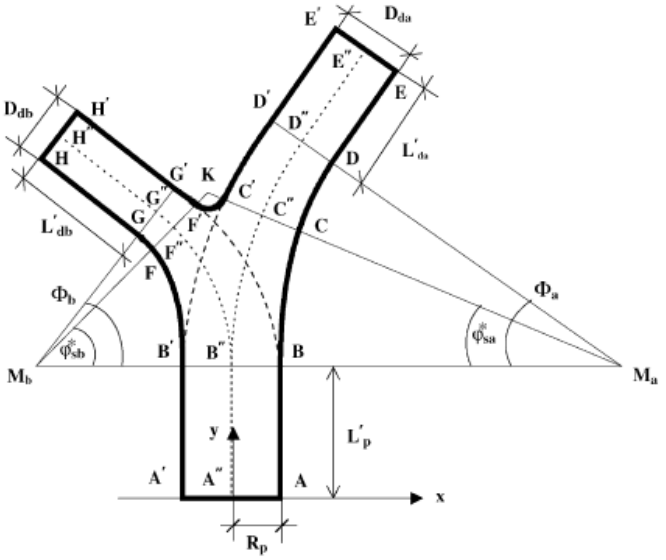

Figure 2.25: Geometry of a realistic bifurcation (Hegedus model).

In this line, algorithmic techniques were also proposed by Kitaoka et al. (1999) and Tawhai and Burrowes (2003) in order to describe the geometry of the lower airways.

Current studies are based predominantly in Computational Fluid Dynamics (CFD). The increasing power of computers and its lower price has allowed the advance of this technique, in which the Navier-Stokes equations are solved in the domain under study.

Few studies to date have attempted to simulate the flow in the whole airways or even throughout the conducting airways. It can be deduced from the basic morphology of Weibel (1963) that the number of paths for the airflow in the airways is equal to 2 to the power of 23, i.e. more than 16 million of individual flow segments. A computational resolution of the complete flow at all scales with an adequate accuracy would require a mesh size of the order of several billions of elements, making it impossible to simulate.

A first approach to this problem was made by Nowak et al. (2003). In this paper, the authors used several series of increasingly smaller models of the airways, in each of which it is applied an entry boundary condition obtained from the simulation of the section immediately above. The branching and azimuthal angles were assumed to be 60° and 90° (Figure 2.26).

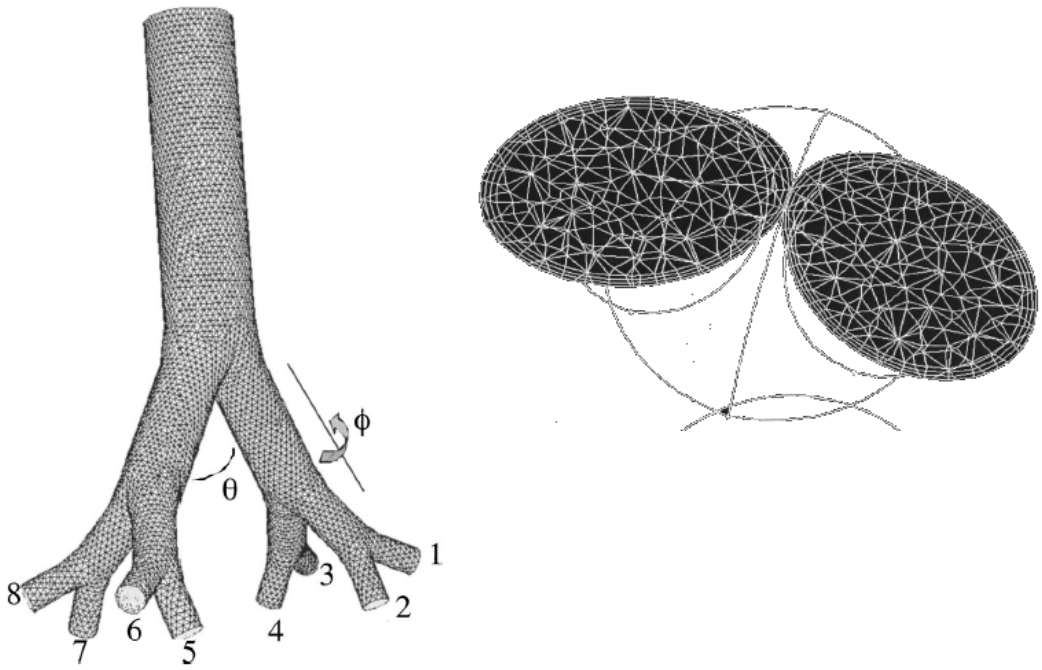

Figure 2.26: Nowak model, being 60° and 90° the branching and azimuthal angles.

One of the difficulties that arise in this type of sequential procedure is that the output boundary condition at the end of each section should be prescribed before running the calculations. The results obtained by the authors suggested that a constant pressure condition is appropriate, although it should be noted that only the inhalation cycle was investigated.

A similar methodology was applied by Zhang et al. (2008) in order to investigate the deposition of micro particles in a numerical model developed up to generation 16. Figure 2.27 depicts typical airflow structures in some selected parallel and serial triple bifurcation units. The tracheobronchial tree is constructed from symmetric triple-bifurcation units which follow Weibel's configuration. Figure 2.27 shows schematically how the tracheobronchial region can be replicated by adjustable triple bifurcation units which are repeated in series and in parallel. Specifically, outflow conditions from an oral airway model were imported as inlet conditions for the first level B1-B3.4, which at their outlets (generation G3.1, G3.3, etc.) are then adjusted ''in series'' to become inlet conditions for the next-level ''paralleled'' (B4.1-B6.4, B4.3-B6.12, etc.), and so on.

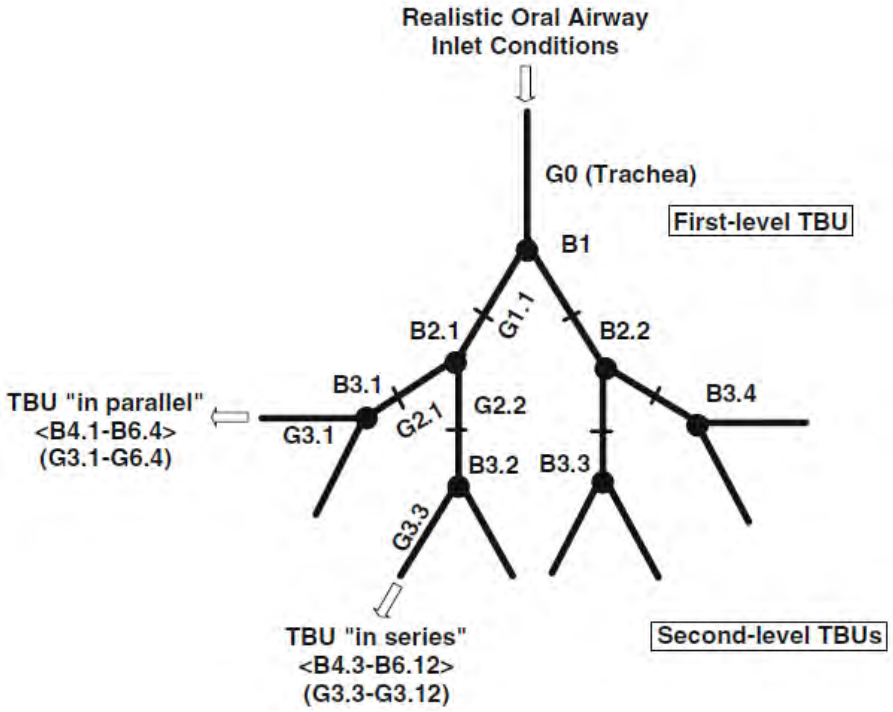

Figure 2.27: Schematic of triple bifurcation units in Zhang model (2008).

Although both studies represented a significant advance for the simulation of airflow in the lungs, this sequential procedure does not allow a full flow coupling at all scales.

Due to the fact that the airflow behavior in the human lung is very complex, a proper numerical investigation would require a simulation method which can provide a real solution to the airflow across the whole lung network. Thus, since the full flow resolution across the pulmonary tree goes far beyond the current computational capabilities, the most recent researches usually opt for the partial resolution of the airway geometry. This means that only a portion of the airways is modeled, by imposing identical conditions to those areas that are not modeled. This approach is used in the work of Gemci et al. (2008) for a human lung model based on the model of Schmidt (2004). The geometry in Gemci's work is a 17 generation model (Figure 2.28) that only includes 1,453 bronchi, in contrast to 2 to the power of 17 bronchi (131,072) for a fully developed model of the conducting airways. The boundary condition imposed on the unresolved regions was constant pressure. The results showed that the pressure drop through all the predicted geometry was 30% less than the value obtained in the experimental study of Hyatt and Wilcox (1963). The reason given by the authors to explain this discrepancy is that the mesh used in the calculations (which had about 6.7 million cells) was not fine enough to ensure independent results.

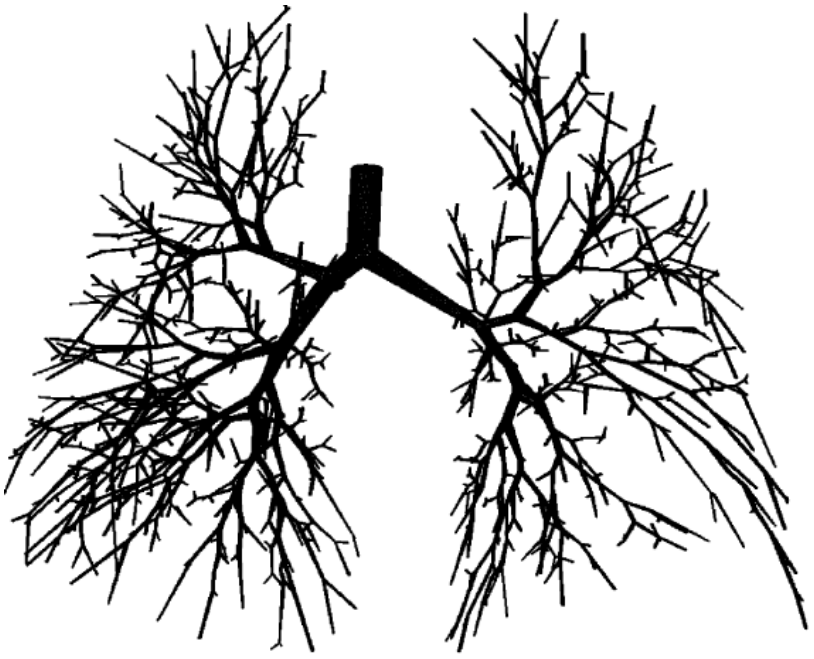

Figure 2.28: View of the generated mesh of 17 generations of pulmonary airways (1,453 bronchi) with 6.744x10^6 cells based on abstracted topological graph data from Schmidt.

More recently, Walters and Luke (2010) presented a new methodology to simulate large scale regions of the human airways (up to the 12th generation) by means of a statistical description. This methodology is based on a finite number of flow paths fully resolved in order to provide a detailed description of the entire small-scale flow field. The results presented by the authors showed excellent agreement in generations 4 to 12. In addition, this approach significantly reduced the computational costs. Figure 2.29 shows the virtual geometry created by stochastic coupling of unresolved boundary conditions. The real 4-path geometry is shown in figure 2.29*a* and the virtual geometry in 2.29*b*.

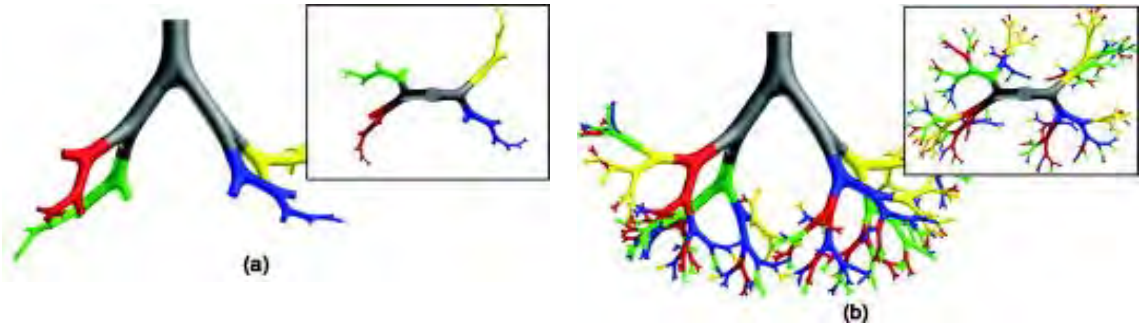

Figure 2.29: a) Four-path geometry developed up to generation 12 in Walters' model b) Fully developed geometry of the model.

On a furtherer investigation (Walters and Luke, 2011), the authors used a similar method in order to investigate the deposition of particles in the airways. This work presents two aspects that can be improved: first, the simulations were performed in the state of equilibrium, not taking into account the recommendations given in Zhang (2004) about the inherent nature of the airflow, and more importantly, the simulations by Walters and Luke only studied the inhalation phase of the breathing cycle.

There are many other later theoretical studies about the behavior of flow in the airways (Adler 2007, Ball 2008 I & II, Grosse 2007, Theunissen 2008, Yang 2006 I & II, Zhang 2011). These studies have generally been focused on isolated sections of the lung, such as the trachea and first generations of the airways or the alveolar ducts and sacs.

In figure 2.30 it is described the Zhang model (Zhang 2011) containing the first three generations of the airways.

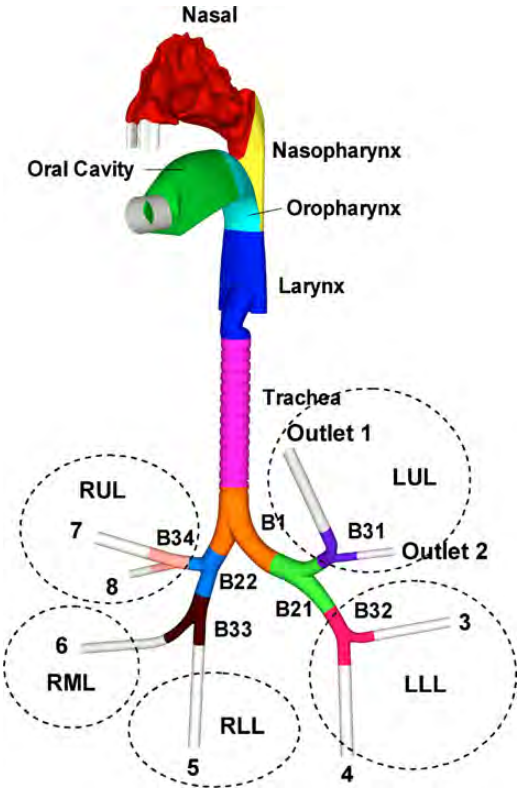

Figure 2.30: Airway model (Zhang 2011) comprising the nasal and oral cavities, nasopharynx, oropharynx, larynx, trachea and the first three generations of bronchia.

Figure 2.31 shows a simulation of the air velocity at the alveolar zone (Kleinstreuer, 2010).

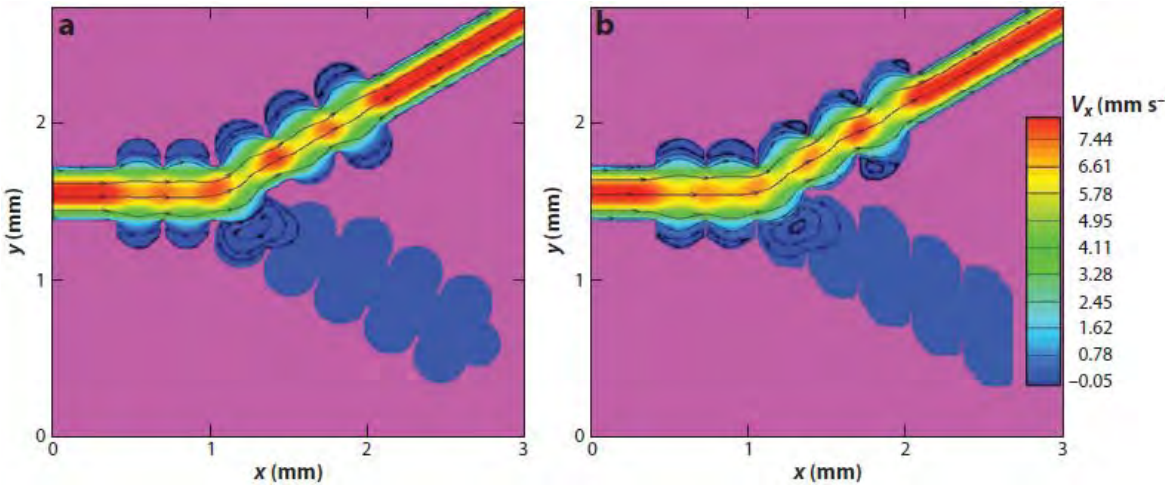

Figure 2.31: Air velocity at alveoli.

To our knowledge, the use of CFD in Spain to study the airways has only been performed at the Universidad Autónoma of Madrid (Castro 2003) and the Universidad of Valladolid (Quispe 2010), although in these cases it was limited to the upper airways. Figure 2.32 shows flow streamlines and velocity contours in the nose and its passage to the pharynx in Castro's model (Castro 2003).

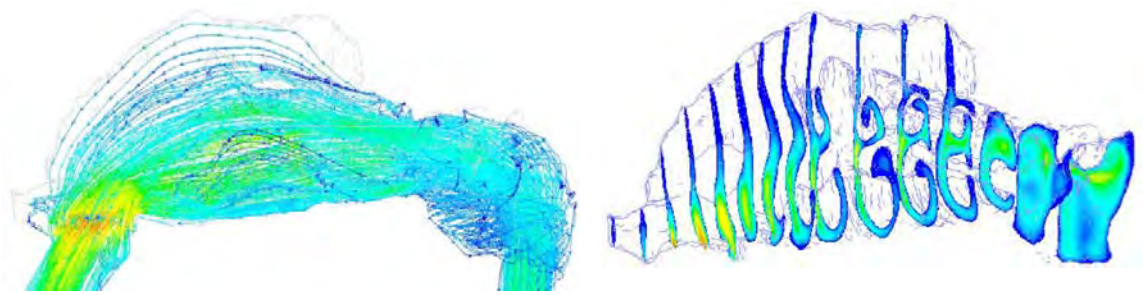

Figure 2.32: Flow streamlines and velocity contours in the nose and its passage to the pharynx (Castro 2003).

2.7. Conclusions

It can be inferred from the background given in this section that there are two major challenges that must be investigated in order to obtain a valid numerical model that can be used to investigate the airflow in the human airway:

- The models developed to date are only extended to the end of the conducting airways, excluding the respiratory zone. Therefore, it would be desirable to generate a model of the lung up to the generation 23.

- The expiratory phase in the above models is still far from being correctly simulated. This is because the flow field during exhalation is significantly more complex than during inhalation, because of the convergence of flow streams at each bifurcation, from two smaller segments onto a segment of greater diameter. This phase of respiration requires a thorough research on the most appropriate boundary conditions to be imposed on the unresolved flow paths in order to obtain a realistic description of the flow at the bifurcations.

CHAPTER 3
Model development

3.1. Morphological bases

For the elaboration of the three-dimensional airway model it has been chosen to follow the one proposed by Kitaoka et al (1999) supplemented with Weibel's model (1963).

The classic model of Weibel indicates the bifurcation modes. It designs the trachea as the first airway (order 0). This model assumes that each airway generates two new branches (regular dichotomy). So the left and right main bronchi are order 1 and so on. There are at least 23 airway generations until the alveolar sacs.

According to this model, there is one order 0 generation (because $2^0 = 1$), 2 airways of order 1 ($2^1 = 2$), 4 airways of order 2 ($2^2 = 4$)… Therefore there are 2^{23} airways or order 23; thereby, the number of airways increases in an exponential way up to a total of 8,388,608. Figure 3.1 shows a scheme of these airways.

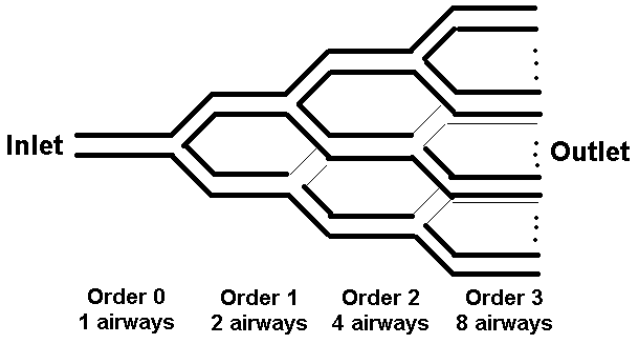

Figure 3.1: Airway scheme of a model with dichotomous branching. The entrance (corresponding to the trachea) corresponds to the generation of order 0. It gives rise to two order 1 branches, which divide into four order 2 branches, etc.

The diameter of each ramification diminishes according to the formula $d_Z = d_0 \cdot 2^{-Z/3}$, being *z* the generation order and *d* the diameter. This relationship is maintained up to the generation 16 (conducting zone). From generation 17 to 23 there are little changes in the dimensions of the airway, because they are more or less alveolized (transitional and respiratory zone). Figure 3.2 shows this idealized model of Weibel, with the airway/area relationship.

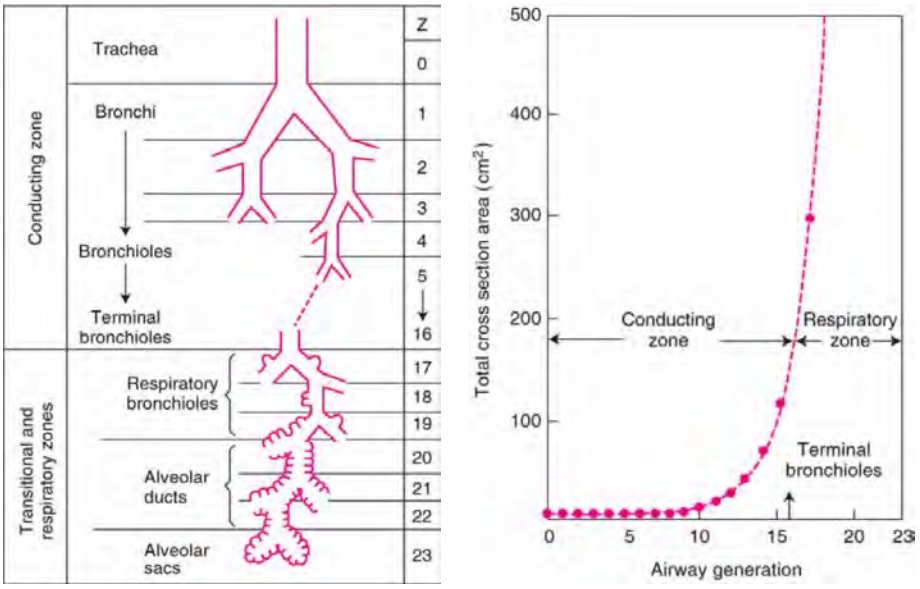

Figure 3.2: Weibel's one-dimensional model. In the left image, the different order branches and their correspondence to the bronchial tree anatomy are shown. In the right image it is shown the relationship between the airway generation and its total cross section area.

In Weibel's model it wasn't taken into account the spatial disposition of the branches; therefore it is considered a model that only allows modelling the lung function in one dimension.

Kitaoka et al. achieved the design of a realist three dimensional model of the lung, elaborated through nine basic rules. Those rules are the following:

- Rule 1: Branching is dichotomous.
- Rule 2: The parent branch and its two daughter branches lie in the same plane, called the branching plane.
- Rule 3: The volumetric flow rate through the parent branch is conserved after branching; that is, the sum of the flows in the daughter branches is equal to the flow in the parent branch.
- Rule 4: The region supplied by a parent branch is divided into two daughter regions by a plane called the "space-dividing plane." The space-dividing plane is perpendicular to the branching plane and extends out to the border of the parent region. There is a supplementary rule (rule 4a) for correcting the space division scheme whenever the shape of the region requires it.
- Rule 5: The flow-dividing ratio "*r*" is set to be equal to the volume-dividing ratio, defined as the ratio of the volume of the smaller daughter region to that of its parent. Figure 3.3 shows a picture with those rules.

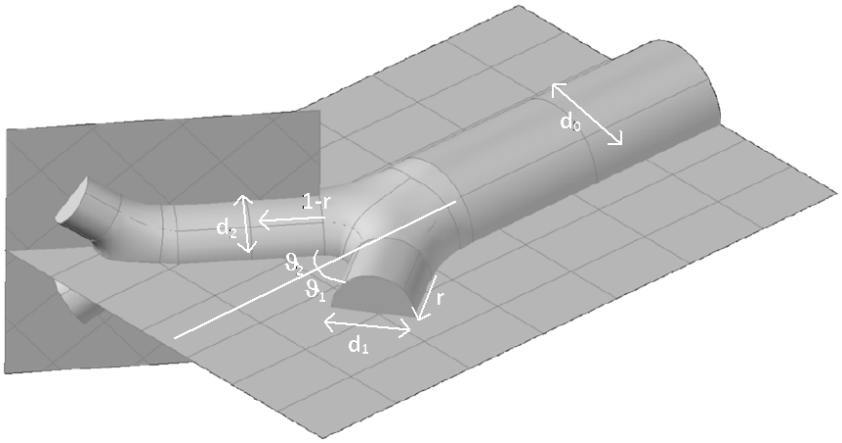

Figure 3.3: The space-dividing plane designates the region supplied by each daughter region. The flow-dividing ratio "r" must be equal to the volume-dividing ratio.

- Rule 6: Diameters and branching angles of the two daughter branches are determined by substituting *r* from rule 5 into next equations.

With no symmetry:

$$\left.\begin{array}{c} d_1 = d_0\, r^{\frac{1}{n}} \\ d_2 = d_0\,(1-r)^{1/n} \end{array}\right\} \quad d_0^n = d_1^n + d_2^n$$

$$cos\theta_1 = \frac{1 + r^{4/n} - (1-r)^{4/n}}{2r^{2/n}};\ cos\theta_2 = \frac{1 - r^{4/n} + (1-r)^{4/n}}{2(1-r)^{2/n}} \tag{3.1}$$

With symmetry:

$$\theta_1 = \theta_2; r = 1/2;\ d_1 = d_2 = d_0\, 2^{-1/n}$$

$$cos\theta = 2^{\left(\frac{2}{n}-1\right)} \tag{3.2}$$

being:

- *d*: airway diameter
- subindex 0: mother branch
- subindexes 1 and 2: daughter branches
- *n*: constant called diametrical exponent (for laminar flow its value is 3 and for turbulent flow is 2.6).

There is a supplementary rule (rule 6a) for correcting the branching angle according to the shape of the daughter region.

- Rule 7: The length of each daughter branch has assigned a value that is three times its diameter. There is a supplementary rule (7a) for correcting the length according to the shape of the region.
- Rule 8: If branching continues in a given direction, the daughter branch becomes the new parent branch, and the associated branching plane is set perpendicular to the branching plane of the old parent. The angle between the two successive branching planes is called the "rotation angle of the branching plane." There is a supplementary rule (8a) for correcting the rotation angle according to the shape of the region.
- Rule 9: The branching process in a given direction stops whenever the flow rate becomes less than a specified threshold or the branch extends beyond its own region.

These recommendations were followed for the development of the model up to the conductive airway (16^{th} generation). It wasn`t developed from the 17^{th} generation to the end because at this level the airways start to be alveolized. The development of the geometry of the alveolar units is much more complex and is beyond the scope of this work.

If these recommendations are followed up to generation 16, the resulting model looks like shown in Figure 3.4.

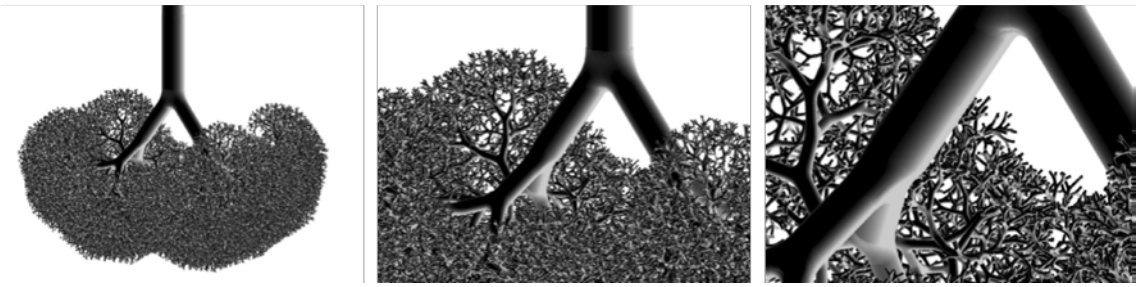

Figure 3.4: Complete morphology of the lung, developed from the trachea up to the end of the conducting zone (generation 16). The numerical simulation in this model, with a total of 65,536 branches, it is not affordable.

With a total of 2^{16} branches (65,536 branches), the numerical simulation on it would be simply unaffordable, so a procedure is required to simplify the model, but preserving the entire lung function.

A way to simplify the model consists in developing it through a single pathway. When the trachea divides into the two main bronchi, the model will continue through the right main bronchus and the pathway through the left main bronchus will be

truncated. When the right main bronchus bifurcates into the right upper bronchus and the intermediate bronchus, the model will continue through the intermediate bronchus and the upper right bronchus will be truncated, and so on. To simulate the entire lung in spite of having a single pathway, it is necessary to impose the conditions in the developed branch to its homologous truncated one. That is, what happens in the intermediate bronchus it is imposed to the right upper bronchus. And what happens in main right bronchus it is imposed to the main left bronchus. This kind of model has been researched and developed by various investigators (Walters *et al* 2010 & 2012, Longest 2012), and it has proven to be effective for the simulation of the entire lung, saving time and computational costs.

Another simplification of this model is not taking in consideration the changes in the airway diameter in function of the respiratory cycle phase.

3.2. Lung geometry

The development of the geometry of this airway model will be explained in the next two subsections.

3.2.1. Lower airways

The geometry of a typical human lung was developed with the commercial code Ansys Gambit 2.4.6. This model comprises the generations 0 to 16, belonging to the conducting zone. The transitional and respiratory zones were excluded. The geometry of the bifurcations in the bronchioles at all the generations is created by a similar procedure.

The diameter *d* and the length *l* of the different branches were deduced from the relations proposed by Weibel (1963) and Kitaoka (1999):

$$d = 0.018^{-0.388\,n} \text{ if } n \leq 3$$
$$d = 0.013^{-(0.2929-0.00624\,n)\,n} \text{ if } n > 3 \quad (3.3)$$

$$\mathrm{l} = 0.012^{-0.92\,n} \text{ if } n \leq 3$$
$$\mathrm{l} = 0.025^{-0.17\,n} \text{ if } n > 3 \quad (3.4)$$

A summary of the main geometric dimensions in the branches is presented in Table 3.1.

Gen	Diameter (m)	Length (m)	Branches (m^2)	Total (m^2)
0	1.800000E-02	1.200000E-01	2.5447E-04	2.5447E-04
1	1.221142E-02	4.782228E-02	1.1712E-04	2.3424E-04
2	8.284380E-03	2.485314E-02	5.3903E-05	2.1561E-04
3	5.620225E-03	1.686068E-02	2.4808E-05	1.9847E-04
4	4.451270E-03	1.266542E-02	1.5562E-05	2.4899E-04
5	3.512926E-03	1.068537E-02	9.6923E-06	3.1015E-04
6	2.807205E-03	9.014874E-03	6.1893E-06	3.9611E-04
7	2.271429E-03	7.605532E-03	4.0522E-06	5.1868E-04
8	1.860991E-03	6.416519E-03	2.7201E-06	6.9634E-04
9	1.543866E-03	5.413392E-03	1.8720E-06	9.5847E-04
10	1.296864E-03	4.567088E-03	1.3209E-06	1.3526E-03
11	1.103061E-03	3.853092E-03	9.5563E-07	1.9571E-03
12	9.500025E-04	3.250718E-03	7.0883E-07	2.9033E-03
13	8.284568E-04	2.742516E-03	5.3905E-07	4.4159E-03
14	7.315347E-04	2.313764E-03	4.2030E-07	6.8862E-03
15	6.540636E-04	1.952042E-03	3.3599E-07	1.1010E-02
16	5.921409E-04	1.646869E-03	2.7538E-07	1.8048E-02

Table 3.1: geometric dimensions of the lung branches from generation 0 (the trachea) up to generation 16 (the end of the respiratory conducting zone).

First of all, three circles are created corresponding to: the diameter of the high-order generation, the diameter of the low-order generation, and an intermediate diameter between them (Figure 3.5). Also, secondary surfaces are created in the plane containing the circles and in the perpendicular plane.

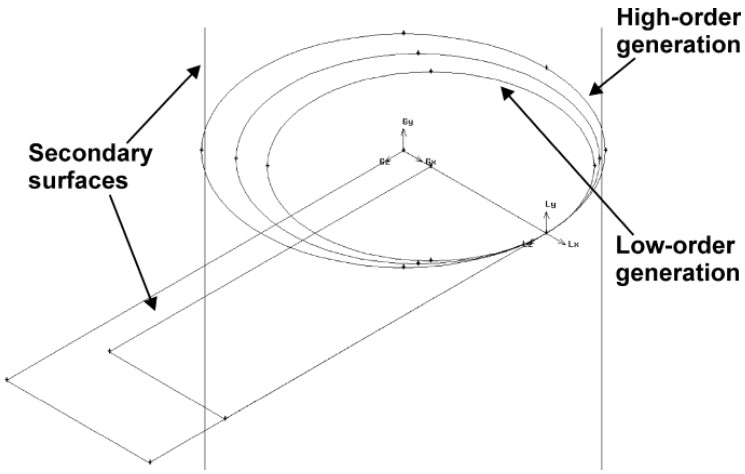

Figure 3.5: Diameters of a branch at the bifurcation.

As seen, the circles are split in 4 arches in order to create the front, back, and lateral boundaries of the volume, as will be explained later. The major edge of one of the secondary surfaces is extruded a length *L* to generate an axis of rotation (Figure 3.6). The path in the bronchiole from the high-order to the low-order generation is prescribed by rotating the intermediate circle and the smaller circle round the axis at an angle of β/2 and β respectively. The remaining secondary surfaces are rotated at an angle of β round the axis too. The parameter β was set to 35° based on the guidelines given by Weibel (1963) and Kitaoka (1999).

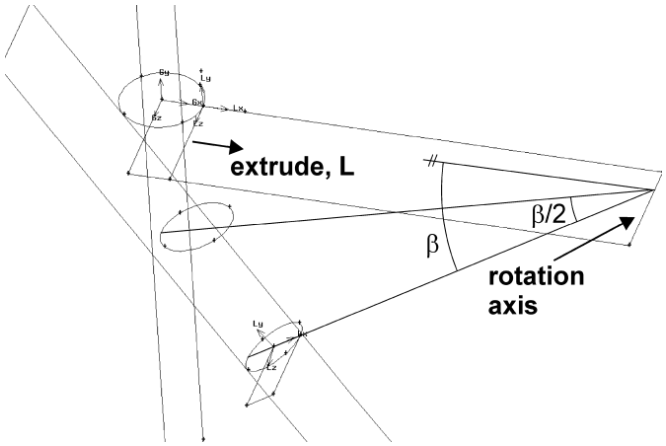

Figure 3.6: Path in the bronchiole from the high-order to the low-order generation.

The parameter *L* was adjusted from the others. Its value is variable, depending on the number of branch where bifurcation takes place (Figure 3.7).

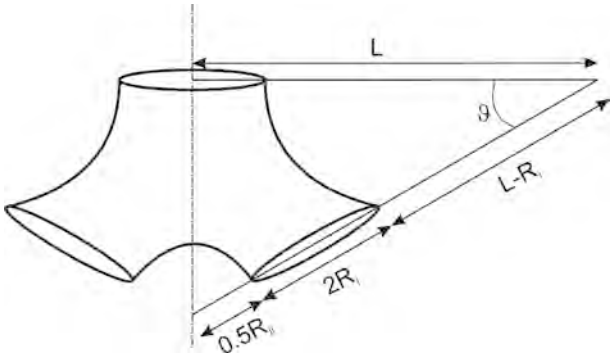

Figure 3.7: Geometrical relations between the variables.

The lateral surfaces of the bronchiole were generated by means of the arches of the circles and a symmetry condition. The right-hand lateral surface is created by joining the top and bottom arches with two additional curves generated by a 3-point arc (see Figure 3.8).

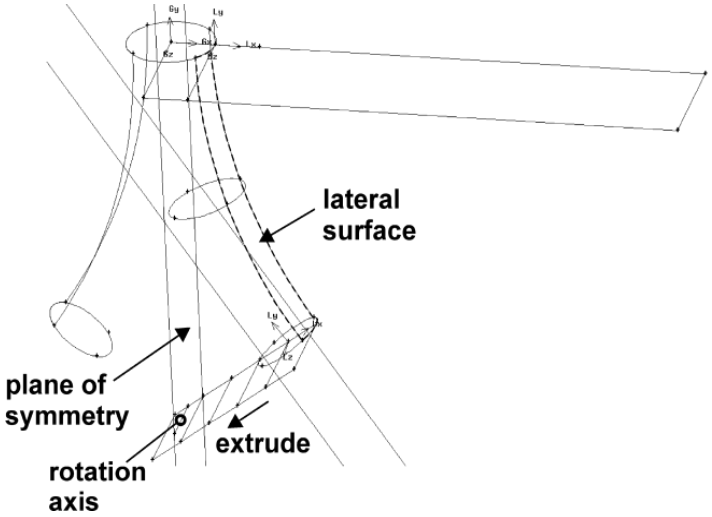

Figure 3.8: Generation of the lateral surfaces in the bronchiole.

This lateral surface, together with the bottom circle, is reflected with respect to the secondary vertical plane (plane of symmetry) in order to create the left-hand lateral surface, as shown in Figure 3.8. Besides, the secondary surface that lies in the plane of the bottom circle is extruded until intersecting the plane of symmetry. The intersection originates a second axis of rotation that will be used to create the bottom surface of the bronchiole.

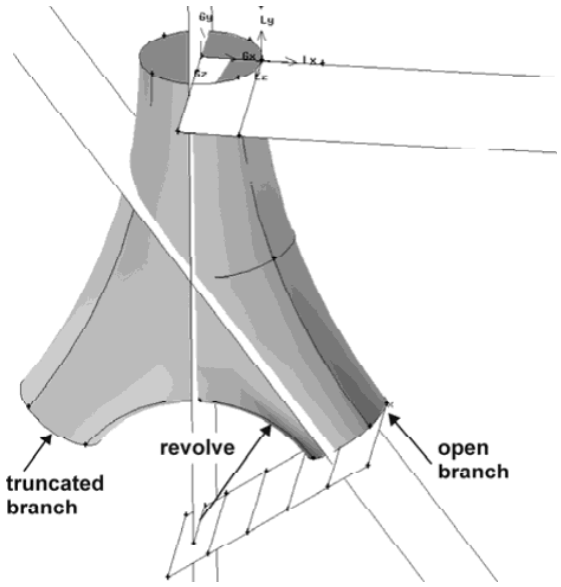

Figure 3.9: Geometry of the bifurcation.

The inner arch of the bottom circle is revolved with respect to the axis indicated in the previous paragraph until joining with its symmetrical arch. All the surfaces are now available so the volume of the bronchiole can be generated. The result of these operations is seen in Figure 3.9.

As explained before, the main purpose of the investigation is to develop a numerical model of the lung as realistic as possible while avoiding prohibitive computational costs. To achieve this, the remaining morphology of the lung will be developed along only one of the two possible branches in each bronchiole (one branch will be considered as “truncated”).

The last step in the creation of the morphology is to generate the geometry of the active (open) branch. This is done by extruding the circle that prescribes the diameter of the low order generation a specific length *l* (Figure 3.10).

The secondary surface that lies in the plane on this circle is then moved to the plane located at the end of the extrusion. This surface, together with the secondary surface that contains the axis of the cylinder generated in the extrusion, is rotated 90° with respect to the local axis indicated in the figure according to the models described by Weibel (1963) and Kitaoka (1999).

The geometry of the lung can be further developed up to reaching the respiratory zone (up to generation 16) if the procedure described so far is repeated systematically.

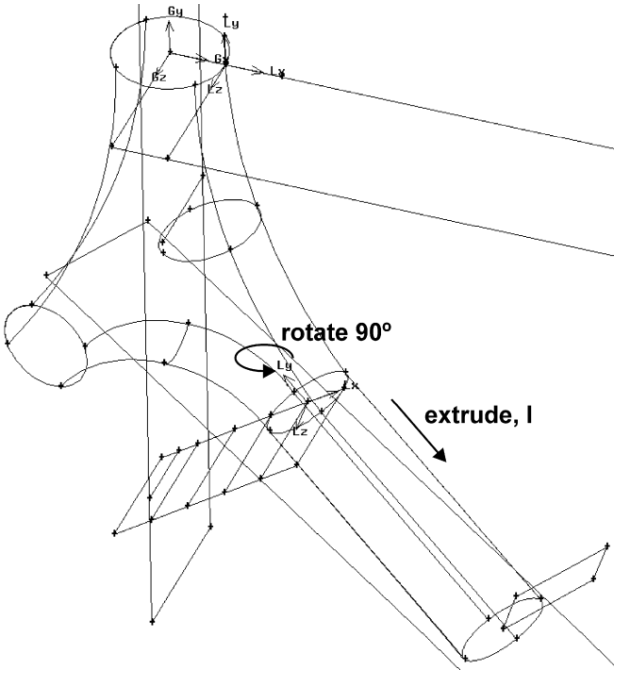

Figure 3.10: Generation of the open branch.

The numerical model of the lung is shown in Figure 3.11; also, this figure presents a detail of the lower generations. A series of additional surfaces were created in the branches for data analysis purposes.

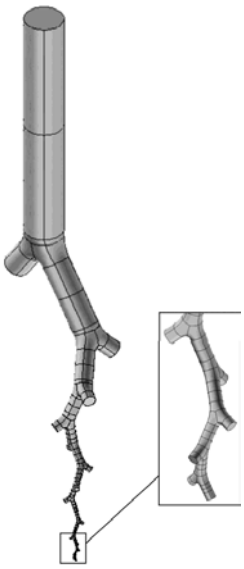

Figure 3.11: Developed numerical model of the lower airways, with a close-up of the lower generations. The complete morphology of the airways can be generated from the

numerical model by imposing symmetry at each of the truncated branches.

The complete morphology of the lung can be generated from the numerical model. This is done by imposing symmetry at each of the truncated branches.

The entire lung was presented in Figure 3.4 for showing purposes only; of course, the numerical simulation of this complete morphology would be simply unaffordable.

3.2.2. Upper airways

Once constructed the lower airways, the next step is to complete the model by adding the nose, mouth, larynx, and pharynx.

The nose (Figure 3.12) is a simplified model of the one used in Castro (2003). The model was constructed using seven cross surfaces obtained by CT, whose perimeter has served to support the construction of the longitudinal surface.

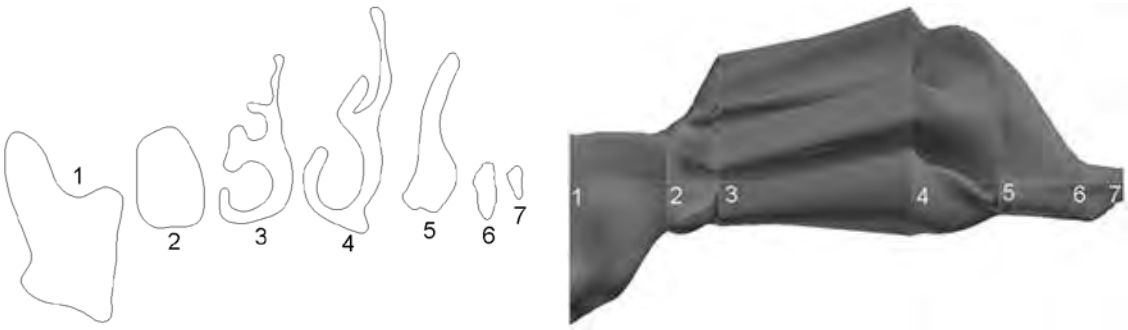

Figure 3.12: Geometry of the nose, based in the model developed by Castro in 2003. In the left image are represented several coronal cuts at certain parts of the nose model, indicated in the right image. The perimeter of the coronal cuts allowed the construction of the longitudinal surfaces.

The mouth (Figure 3.13) and throat (Figure 3.14) are a reproduction of the Stapleton model (2000).

The construction of the mouth has followed the same steps as with the nose.

Figure 3.13: Geometry of the mouth. In the left image are represented several coronal cuts at certain parts of the mouth model, indicated in the right image.

The throat geometry is more complicated because its three inputs (two nasal passages –the choanae- and the mouth passage –the fauces-) have to transform into a single conduct (the pharynx) whose output is the trachea. Inside this conduct it is located the epiglottis, a cartilage separating the trachea from the esophagus, which must be taken into account.

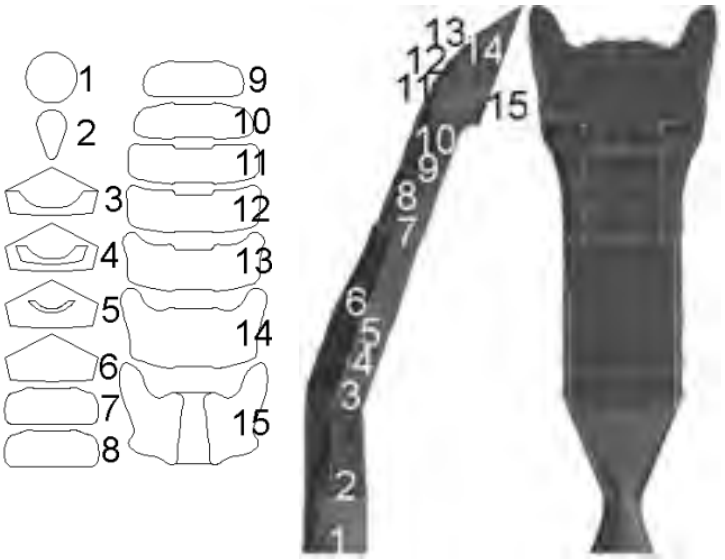

Figure 3.14: Geometry of the pharynx. In the left image are represented several coronal cuts at certain parts of the model, indicated in the right image. The perimeter of the coronal cuts allowed the construction of the longitudinal surfaces.

The entire model, composed by the nose, mouth, pharynx and lower airways, is presented in Figure 3.15.

Figure 3.15: Complete tested model, comprising the nose, mouth, pharyngeal region and lower airways, with a single path fully developed up to generation 16.

3.3. Numerical model

Once realized the geometry, the next step is the creation of the numerical model in which are going to be solved the flow equations.

3.3.1. Meshing

First, the mesh will be made, choosing the appropriate cell type. This is a very important step since an improper meshing can lead to invalid results. Calculation parameters and boundary conditions will be elected, making a sensitivity analysis of the mesh. The model of the lung was meshed with tetrahedral cells (Figure 3.16) due

to their better adaptation to complex geometries. The size of the tetrahedrons varies between 4.45×10^{-1} mm^3 and 5.45×10^{-4} mm^3.

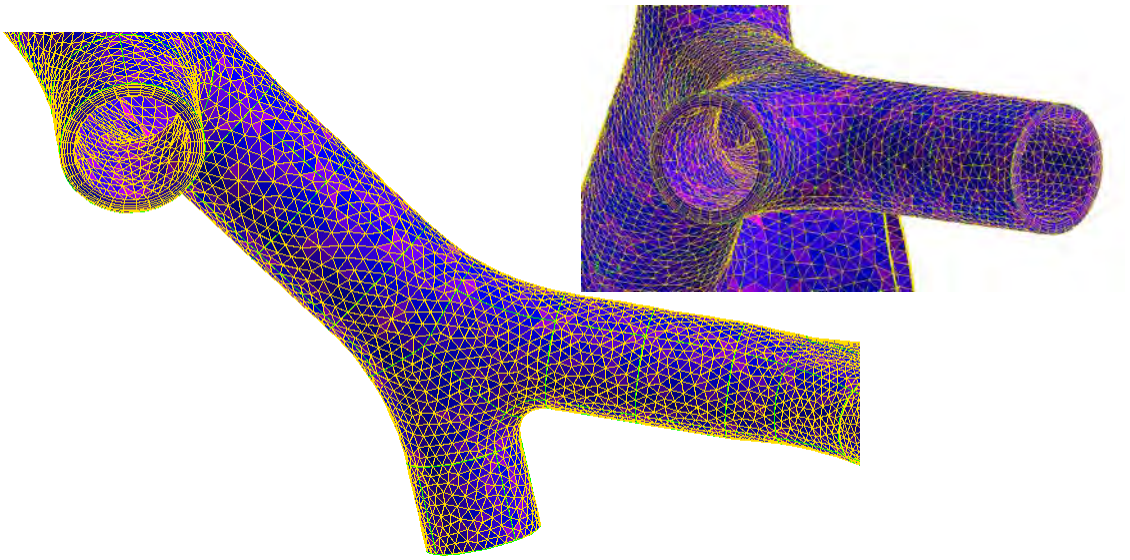

Figure 3.16: Surface meshes at some branches; it can be observed its tetrahedral shape. In the close-up a detail of the boundary layer mesh is shown.

A boundary layer mesh was built before meshing the volumes in order to obtain a better description of the boundary layer in the numerical calculations. The laminar flow is characterized by an orderly movement of the fluid's particles, with well-defined streamlines and paths. In the case of a cylindrical pipe (with a circular cross section, as is the case of conducting airways) the laminar flow has a parabolic velocity profile, being the velocity zero at the walls of the duct and maximum at its center, and equal to twice the average velocity (Figure 3.17).

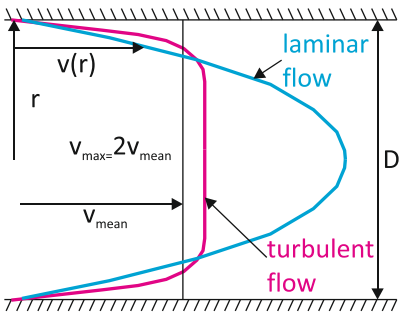

Figure 3.17: Velocity profile in a laminar flow, where velocity is zero at the wall of the duct and it is maximum at its centre, and equal to twice the average velocity. Also the average velocity profile in a turbulent flow is shown.

In this case, the fluid in movement has well-defined "sheets", each one moving at its own speed and “touching” the close sheets, but without mixing with the other ones. Therefore major changes in the fluid velocity occur in the proximity of the duct wall, so it is in this area where it is interesting to have a greater number of cells for a better description of the fluid’s motion.

A detail of the boundary layer mesh in one truncated branch is presented in Figure 3.16; in this case, only the cells in the boundary layer are made visible.

3.3.2. Flow equations

The equations that describe a fluid in movement can be deduced from the mass and momentum conservation laws. Applying these conservation laws to a fluid element, the Navier-Stokes equations are obtained. The equations for incompressible flows of Newtonian fluids are:

Continuity:

$$\nabla \cdot \vec{v} = 0 \tag{3.5}$$

Momentum:

$$\rho \frac{d\vec{v}}{dt} = -\nabla p + \rho \vec{g} + \mu \nabla^2 \vec{v} \tag{3.6}$$

where:

- ρ: density
- μ: dynamic viscosity of the fluid.

If these equations are solved it is possible to know the properties of a fluid: pressure and velocity. These equations can only be solved in an analytical way in problems with simple geometry and boundary conditions, as they are fully closed for fluids with known properties, but cannot be solved in a general sense primarily due to their nonlinearity, embodied in the convection terms Even in these cases, the solution obtained by the analytical procedure must consider the flow as laminar, even if it is

turbulent. In fact, habitually the flows are turbulent and in these cases the equations must be solved by means of numerical methods, with the help of the computer, and employing models of turbulence, which make the procedure even more complicated.

To understand in which consists the turbulence it can be useful some typical examples. When a tap is opened just a little bit, the water flows smooth and cleanly. This flow is called laminar. If the tap is totally opened, the flow no longer looks transparent and it is turbulent (Figure 3.18). The same can be observed in a cigarettes' smoke when it is lightened in calmed air. When it goes out of the cigar, the flow is laminar, but later it becomes wavy and diffuses.

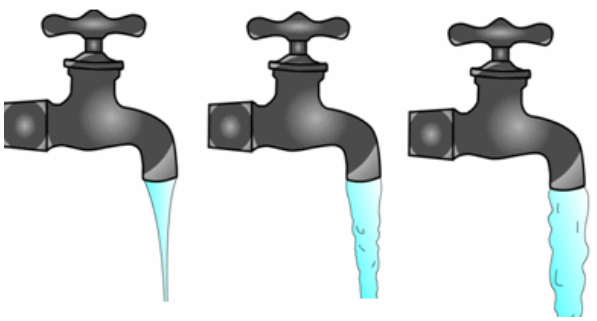

Figure 3.18: Laminar and turbulent flow in the water jet of a tap. At first the flow is laminar, but then it becomes turbulent.

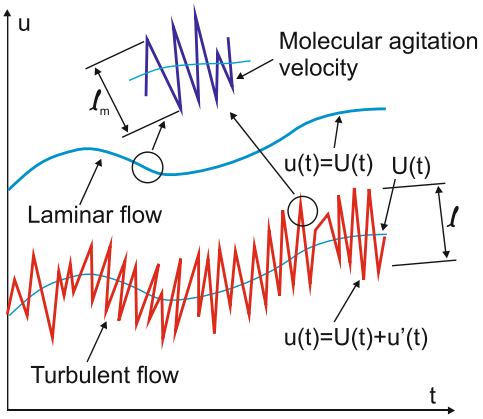

Figure 3.19: Differences between laminar and turbulent flow.

The turbulence can be defined as an intrinsic instability phenomenon of the flow, which causes the fluid to have a chaotic behaviour. Eddies occur more or less randomly around the mean direction of the movement. This happens when the velocity of a fluid exceeds a specific threshold, below which the viscous forces dampen chaotic behaviour (Figure 3.19).

To determine if a flow is turbulent or not it is employed the Reynolds number. This number indicates the relationship between the inertial forces and the viscous forces of the flow.

$$Re = \frac{\rho v D}{\mu} \tag{3.7}$$

where:

- ρ: density

- μ: dynamic viscosity
- v: velocity of the fluid
- D: duct diameter

Practically all the fluid flows that interest scientists and engineers are turbulent ones; turbulence is the rule, not the exception, in fluid dynamics. Richard Feynman, a Nobel Prize in physics, called turbulence "the most important unsolved problem of classical physics". And the British meteorologist Lewis F. Richardson described it in verse:

Big whorls have little whorls,
which feed on their velocity,
and little whorls have lesser whorls,
and so on to viscosity.

The eddies, also called vortices, that characterize the turbulent flow, are of many different sizes. These vortices appear and disappear without continuity solution: the bigger eddies break into smaller ones, those into even smaller others, and so on. When eddies become small enough they dissipate as heat because of their viscosity.

Turbulence appears when the Reynolds number exceeds a certain value (between 400 and 2,000). Turbulence is a desirable phenomenon in many occasions. For example, when using an inhalator device, turbulence improves the mixing of the drug introduced in the airflow, and makes it go deeper in the lungs. An example of this would be the Turbuhaler™ device.

Returning to the Navier-Stokes equations, they are a mathematical adequate representation of the flow, even for the turbulent ones. However, the resolution of these equations calculating the turbulent flow with the maximum detail as possible requires realizing a temporal discretization (because of the variations of the fluid's condition over time) and a very detailed mesh that in the practice is unfeasible.

Usually the most interesting facts to study in the air at the airways are the effects of turbulence on the mean values of the velocity and pressure. For this, the equations don't calculate the movement of all eddies. They calculate the movement of the bigger eddies and then are employed models of turbulence to estimate the effect of the smaller eddies on the bigger ones (Figure 3.20).

Nowadays many turbulence models are employed, varying in their complexity. Some of them are:

- Zero equations: mixing length
- One equation: Spalart-Almaras
- Two equations:

- o k-ε (k-epsilon) with several variants: standard, RNG, realizable
- o k-ω (k-omega) also with several variants: Wilcox's, Wilcox's modified, SST (shear stress transport) and Near-wall treatment
- o ASM (algebraic stress model)

- Seven equations: Reynolds stress

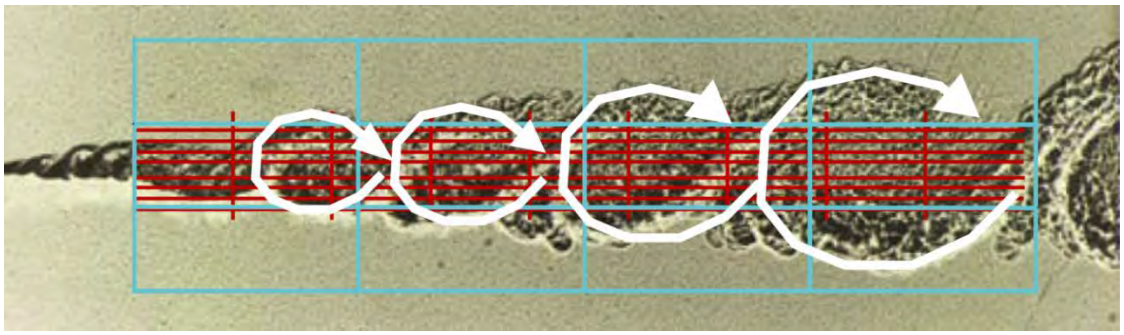

Figure 3.20: Different sizes of vortices and meshing in a turbulent flow.

Since the flow in the human airways is both laminar and turbulent, with transition zones, the turbulence model chosen for this work is the SST k-ω, which is best suited to these conditions. While the standard k-ω turbulence model performs better than k-ε in the near wall region, it is worse in the far field; this is the reason why the shear stress transport formulation (SST k-ω variant) has been selected, since it is a combination of both. The SST k-ω model is a hybrid model which solves the near-wall region with k- ω turbulence model and the region far from the wall with a k-ε one. The use of k- ω model in the near-wall region aims at improving its performance in this region (Versteeg and Malalasekera, 2007).

Summarizing these observations about the turbulence, it can be explained that the validity of the numerical simulations depends largely on the turbulence modelling, which still doesn't have perfect models for its resolution.

3.3.3. Solution parameters

The movement of the fluids and the particles can be analysed by means of two descriptions, called Eulerian (named after the Swiss mathematician L. Euler, 1707 -

1783) and Lagrangian (in honour of the French mathematician J.L. Lagrange, 1736-1813). These two descriptions are based on the fact that a movement is described by two different physical laws that represent the same phenomenon. In the Eulerian description, a point is studied, knowing at any given time the properties of the particles which are in that moment in that specific point. This description is the used for the study of the fluid flow. The other description, the Lagrangian, studies the position at any given time of a certain particle, being more appropriate for the study of the movement of solids. Thus, for this work the Euler method will be used to study the air, and the Lagrangian method will be used to study the inhaled particles.

The numerical calculations were solved with the commercial code Ansys Fluent 6.3.26. This code was used to solve the unsteady Reynolds-averaged Navier-Stokes equations (URANS) by the finite volume method, converting them from differential equations into their numerical analogues (Eulerian method). The solver was set to pressure-based and implicit with an absolute formulation for the velocity fields. The discretization of the spatial and temporal derivatives in the equations was carried out by means of second-order schemes. The discretization of the pressure was standard. The SIMPLE (Semi-Implicit Method for Pressure Linked Equations -Patankar 1980-) algorithm was imposed to resolve the coupling between pressure and velocity fields. Turbulent closure was established with the SST k-ω model and Transitional Flows.

3.3.4. Truncated branches conditions

The truncated branches in the airways need a special boundary condition because the same conditions that were imposed at the inlet and outlet of the model cannot be applied. This special condition must represent faithfully the effect of the removed airways. Figure 3.21a shows the behaviour of the air velocity at various sections of the airways.

The figure 3.21b illustrates the same property but in the used airway model. It has been tested using three different boundary conditions, pressure, flow and velocity, in both modes, inspiration and expiration. In all three cases is needed to put at the cross section of the truncated branches the same conditions that the symmetrical section of the complete branch has.

It is known that in any straight tube with a fully developed laminar flow the speed is not constant, being greatest at the centre and zero at the walls of the lungs, as it was previously explained. In every cross section of the numerical model, only the mean value of variables (pressure, flow and velocity) can be obtained. However, the property that best represents the characteristics of the air flow is the velocity at each point of the cross section (velocity profile), as shown in Figure 3.21a and b. Therefore, it is necessary to build a user-defined function to can do this.

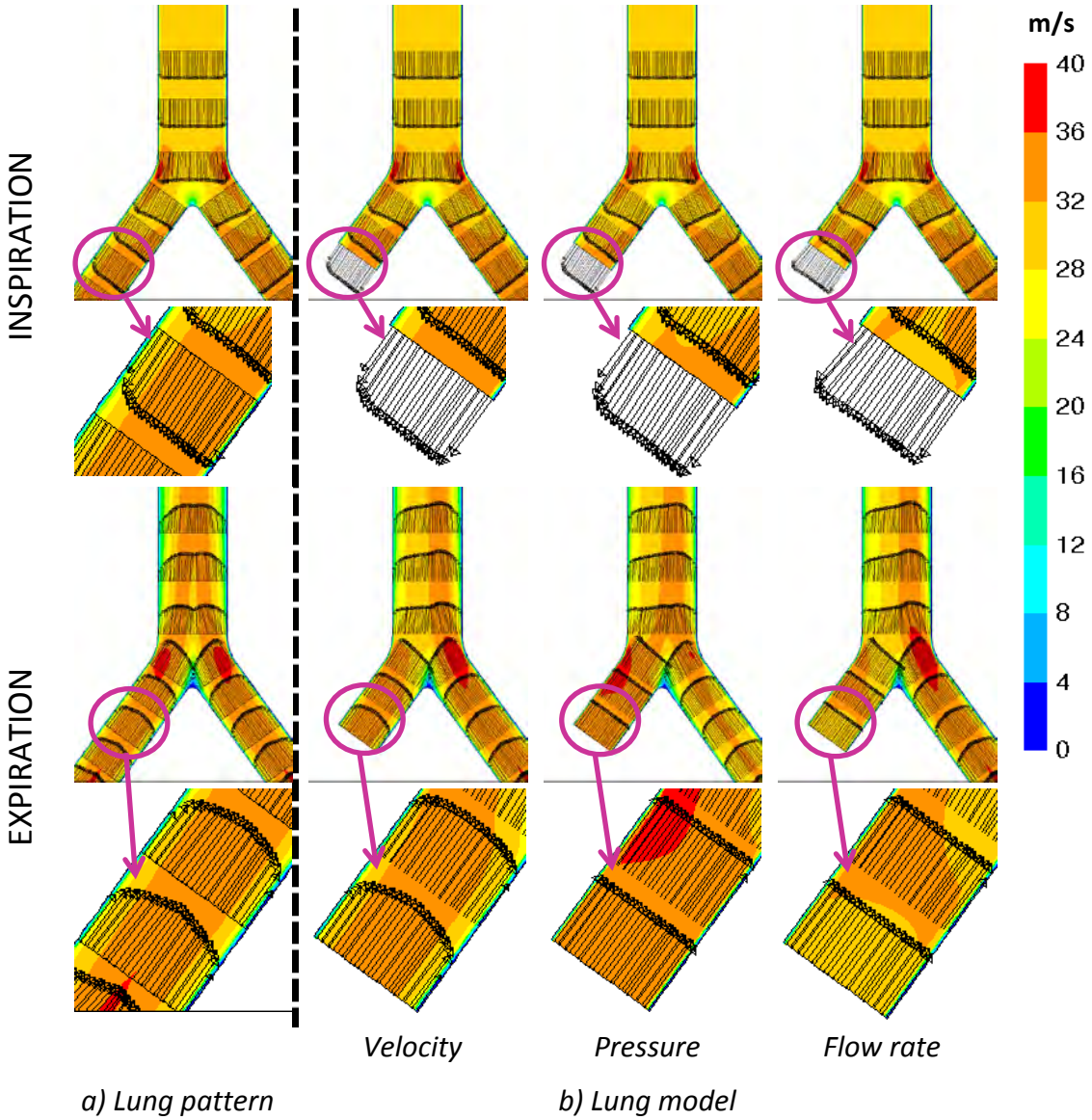

Figure 3.21: Representation of the lung model boundary conditions: velocity, pressure and flow rate. It can be observed that velocity profile is the property that best represents the characteristics of the airflow, especially in the expiration.

The user-defined function was used to impose a symmetric operation of the two branches at each bronchiole. This UDF obtains the velocity profile at each open branch (either in inhalation or exhalation) from the calculations and prescribes the same profile in the corresponding truncated branch (Figure 3.22). This methodology is repeated iteratively until achieving convergence in the flow field.

A detailed description of this UDF (about 400 lines long) can be read in Appendix B.

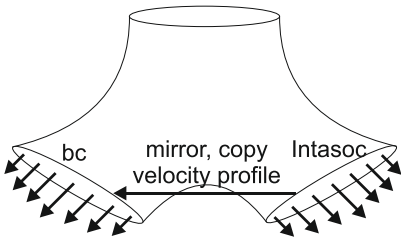

Figure 3.22: The same velocity profile, obtained from the opened branch, is prescribed in the truncated branch by means of a user-defined function.

3.3.5. Boundary conditions

Figure 3.23 shows the lung model. It is necessary to introduce in the program what is each surface: which one is the inlet (the beginning of the trachea, marked in the Figure 3.23), which ones are the outlets (the truncated branches, marked in black in the same figure) and which ones are the walls of the airways (the lateral surface of the ducts).

It is also necessary to indicate what will be the volume filled by the fluid, which in this case is air.

The fluid can't go through the airway walls, being the velocity zero at the wall.

The boundary conditions of the model have to be as realistic as possible. During the respiratory cycle, the entrance to the mouth is at atmospheric pressure while in the bronchioles, during inspiration, the pressure must be negative, and then positive at expiration.

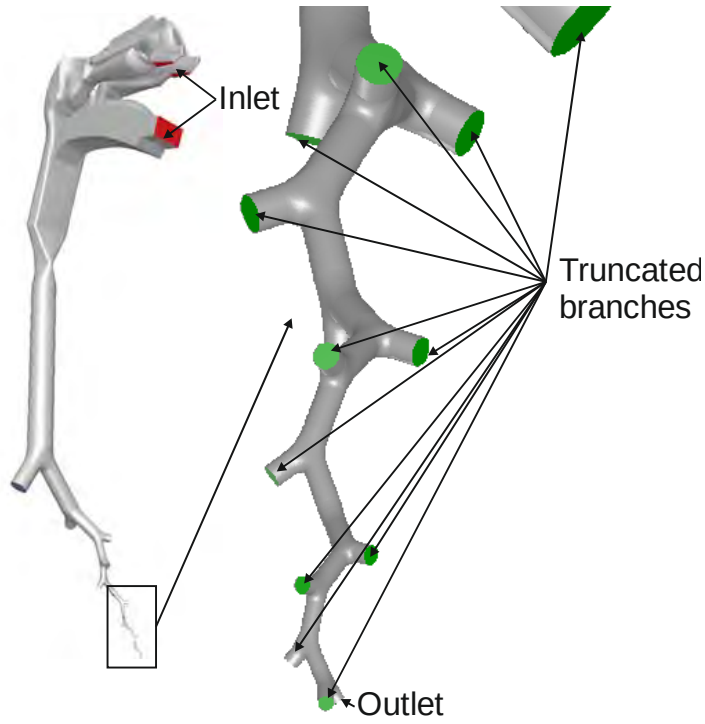

Figure 3.23: Lung model surfaces. The outlets are the truncated branches, in the bronchioles.

3.3.6. Calculation

The conditions imposed were a specific volume flow rate at the mouth and a constant gauge pressure at the lowest generation.

The flow rates simulated for inspiration are 15, 30, 50, 75 and 100 *L/min*, corresponding to breathing conditions between sedentary and heavy-activity. The flow rates 30 and 75 *L/min* are used also in exhalation mode.

The following step is to set up the conditions for the termination of the program. This is an iterative method, so the code starts the calculations with an approximate solution (this initial value must be also introduced, and generally is set to 0), moving at each iteration closer to the real solution. The process ends when the difference in results between one iteration and the previous one is less than 10^{-5} (so convergence has occurred). The code is programed to perform a certain number of iterations. If these

termination criteria are met, the simulation stops, and if they are not met, the code performs all the programmed iterations. If the code still doesn't reach the convergence, it can be set to perform even more iterations. During the process of calculating the screen shows a graph of the evolution of residues between consecutive iterations (Figure 3.24).

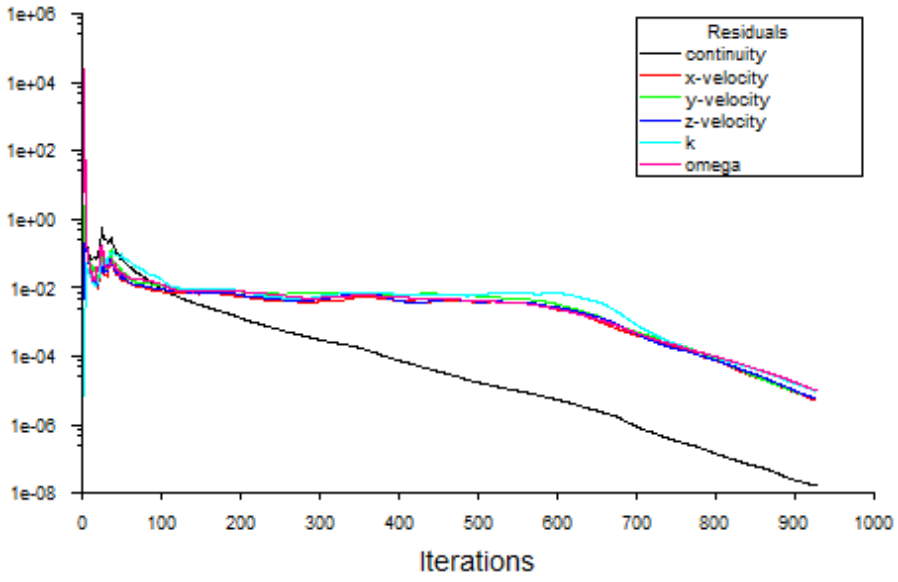

Figure 3.24: Evolution of the residues between consecutive iterations.

3.3.7. Meshing sensitivity

A grid dependence analysis was carried out before performing the final calculations. For this purpose, three additional grids of size $0.7x10^6$, $2x10^6$ and $4x10^6$ cells were built in order to check the change in the magnitude of two reference variables as a function of the number of cells. Due to a fixed flow rate which is imposed at the trachea, the reference variable chosen was the static pressure at the lowest generation. It was observed that the typical variations predicted were below 2.5% (when compared to the results for the finest grid) excluding the coarsest mesh. So the $1x10^6$ mesh was chosen, as the results obtained were similar with the $4x10^6$ mesh and its computational time is significantly lower (Figure 3.25).

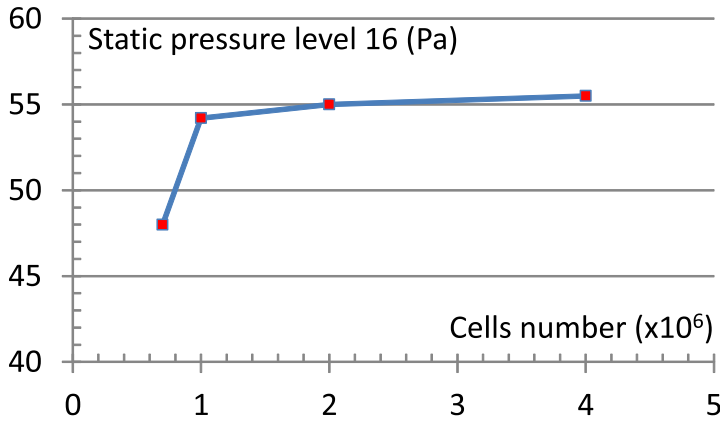

Figure 3.25: Results of the independence test. The variations predicted for the static pressure at G16 were below 2.5% between the $1x10^6$ and the $4x10^6$ meshes, so the first one was chosen to decrease computational costs.

3.4. Results

The contours of the instantaneous static pressure during exhalation are shown in Figure 3.26. As observed, the magnitude of the pressure diminishes while ascending from the lowest generation to the trachea, where a magnitude of zero pressure is reached (i.e. atmospheric conditions). Also, it is noted that regions of negative pressure are predicted at the bifurcations of the bronchioles above the 4^{th} generation. The symmetry of the pressure field at the bifurcations can be observed.

The instantaneous absolute velocity field during exhalation is shown in Figure 3.27 for generations between 2 and 7; also, a detail of this field at the lower generations is also presented. In general, it can be said that the flow shows a predominant component of the velocity in the axial direction.

Velocity and pressure drop were determined over the entire conductive area. As expected, the velocity increases in the first three levels of the airways as the total cross-sectional area of the lung decreases (see previous table 3.1), and then it gradually decreases in the next levels, since the total cross-sectional area of the lung is globally increasing.

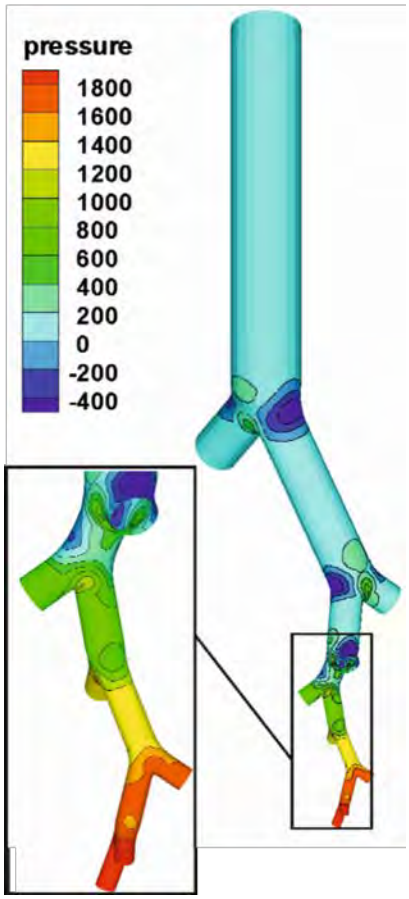

Figure 3.26: Contours of the instantaneous static pressure (Pa) during exhalation. The symmetry of the pressure field at the bifurcations can be observed. Regions of negative pressure are predicted at the bifurcations of the bronchioles above the 4th generation.

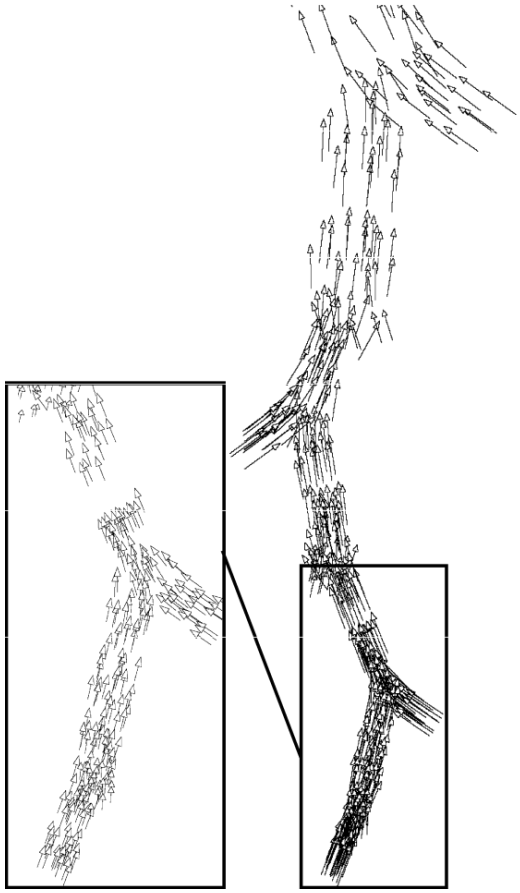

Figure 3.27: Velocity vector field during exhalation at generations 2-7 with a detail of the lower ones.

The pressure decreases as the air flows through the airways, with a greater drop in the first 3 levels because the velocity is higher in that area (Figure 3.28). These results agree with those existing in the literature (Hofmann et al, 1989, Sbirlea-Apiou, 2007 and Gemci, 2008).

More details about the behavior of the flow from the inlet to the first branches in the lung are shown in the figures 3.29 to 3.33. For a better understanding, only some of the streamlines are shown.

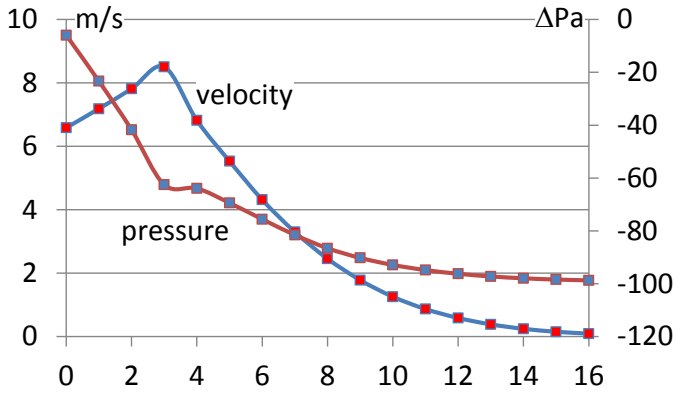

Figure 3.28: Velocity magnitude (m/s) and pressure drop (Pa) in the pulmonary branches for heavy-activity (100 L/min)

In the irregular areas, the flow tends to convolve. An illustration of this occurs in the nose, palate, pharynx and epiglottis. Greater details of the flow in the nose and pharynx are shown in Figure 3.30.

On the other hand, in the areas of more or less regular geometry, the stream lines pass almost parallel to each other. This is perfectly observed in the lung airways (Figures 3.31 to 3.33).

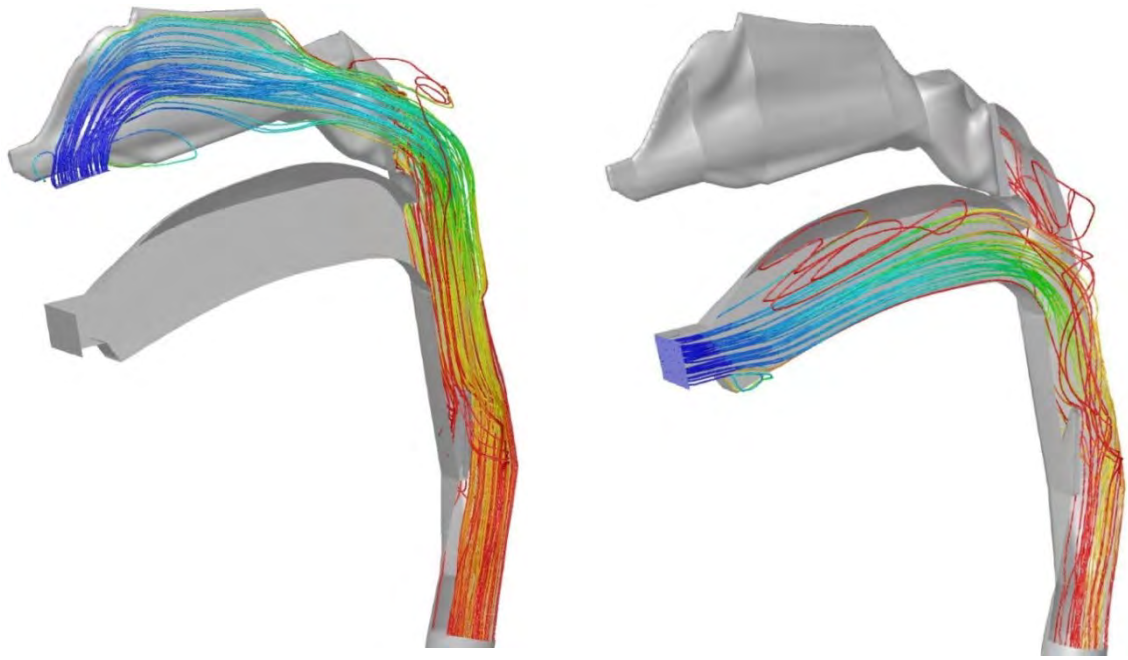

Figure 3.29: Stream lines coming from the inlet: nose at left and mouth at right.

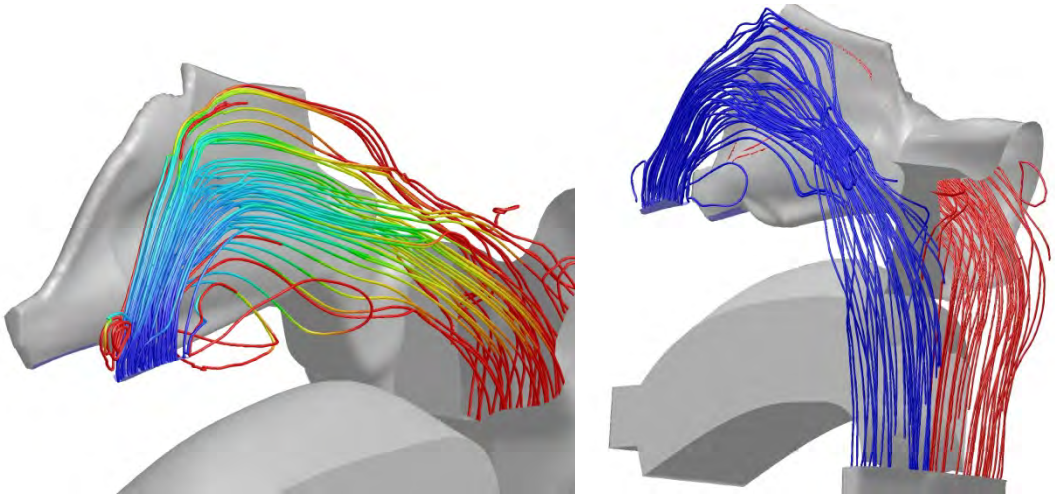

Figure 3.30: A detailed of the stream lines coming from the nose. It can be observed how they tend to convolve in the irregular areas.

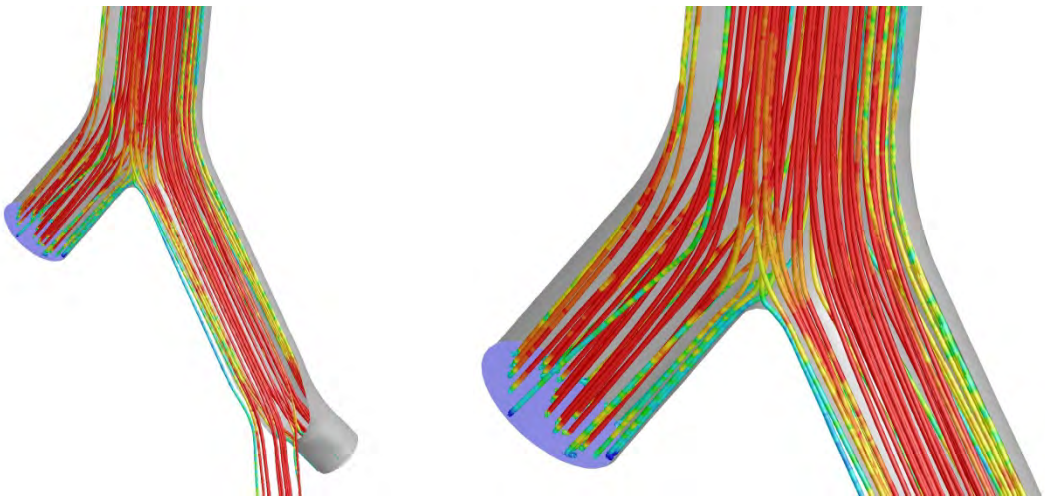

Figure 3.31: Stream lines in the truncated branch and the conductive airway. In the lower airways, as they have a regular geometry, the stream lines are almost parallel to each other.

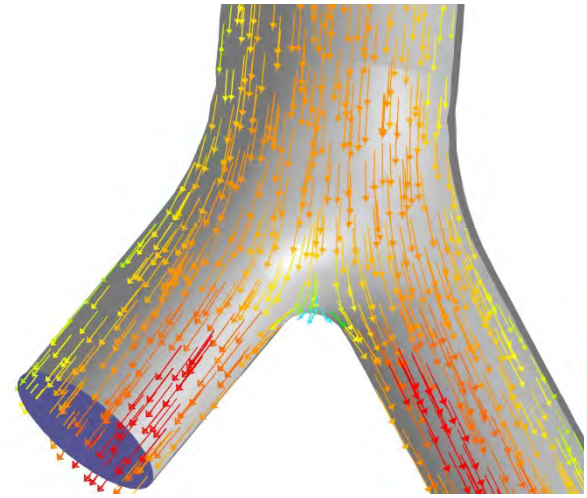

Figure 3.32: Velocity vectors in a bifurcation of the lower airways.

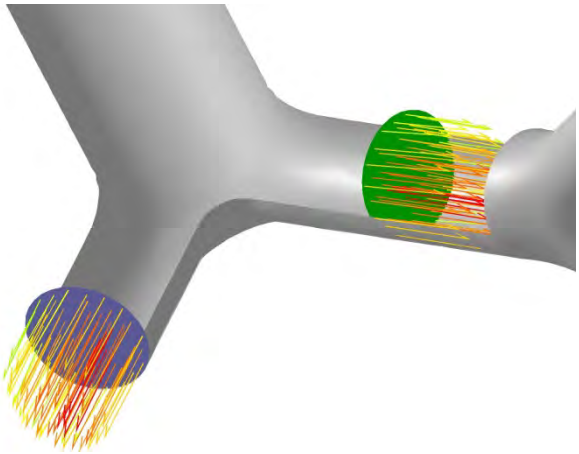

Figure 3.33: Velocity vectors in the exit of the truncated branch (marked in blue colour) and its symmetrical face in the opened airway (marked in green colour).

CHAPTER 4
Fluid dynamic characteristics of COPD

4.1. Introduction

The numerical model of the human airways developed in the previous chapter will be employed to simulate the fluid dynamic characteristics of different obstructive pulmonary diseases. As seen in Chapter 2, COPD is diagnosed by means of forced spirometry, so it is necessary to have experimental data for its simulation. These data (volume and flow rate) will be obtained from tests of individuals without obstructive pulmonary diseases. Subsequently, these data will be processed in the model to obtain the pressure-volume and pressure-time relations at the end of the smaller bronchioles studied.

The variables obtained will be used as boundary conditions to simulate the developed model. Since in the a spirometry the flow rate, volume and pressure variables change over time, it becomes necessary to place unsteady variable as boundary conditions.

4.2. Forced spirometry tests

The spirometer employed was the CPFS/D USB model, with MedGraphics preVent™ pneumotachometer, with BREEZESUITE™ diagnostic software (Medical Graphics Corporation 2004, 350 Oak Grove Parkway, St. Paul, Minnesota 55127-8599).

The spirometer features are:

- Flow Range: ± 18 *L/s* (± 1080 *L/min*)
- Resolution: 8.64 *mL/s*
- Accuracy: ± 3% or 50 *mL*, whichever is greater
- Deadspace: 39 *mL*
- Resistance: <1.20 $cmH_20/(L/s)$ a 12 *L/s*

Figure 4.1: The spirometer employed in the tests (marked in the box) with the computer used as data output.

The spirometer requires daily calibration and it must also be calibrated after each cleaning or disinfecting, or if an unexpected problem is detected. In addition to the calibration procedures incorporated into the device by the manufacturer, the spirometer should be calibrated by applying external signals. For this, a calibration syringe with a volume of 3 *L* is used (Figure 4.2). The syringe is emptied several times with different pulses (simulating high, medium and low flows) to check if the flow reading shows regular measurements.

Figure 4.2: Syringe with a volume of 3 L employed for calibrating the spirometer.

The option to obtain the time by time data was chosen. An ASCII file was generated with two data rows, time (*s*) and flow rate (*L/s*), from each spirometry performed.

A series of forced spirometry tests of individuals without obstructive pulmonary diseases were performed to obtain data under realistic conditions. The individuals

were 5 caucasian males, with ages between 40 and 60 years old, and each of them performed 3 different tests to achieve reproducible results. The spirometry that best matched the ERS quality criteria was chosen, being represented in Figure 4.3 the relationship between flow rate and time. From all data of this spirometry, the portion corresponding to the manoeuvre of the forced spirometry itself corresponded to the data obtained between second 11.32 and second 19.09.

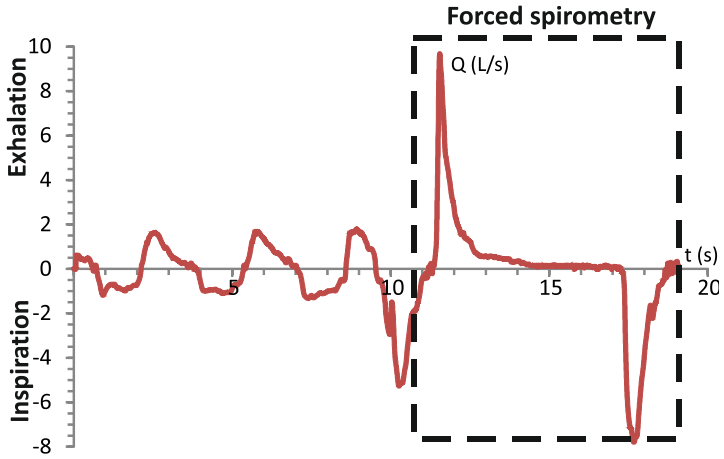

Figure 4.3: Relationship between flow rate and time from the chosen spirometry. In the box is remarked the portion corresponding to the forced spirometry manoeuvre.

The relations between volume-time and flow rate-volume are shown in Figures 4.4 and 4.5.

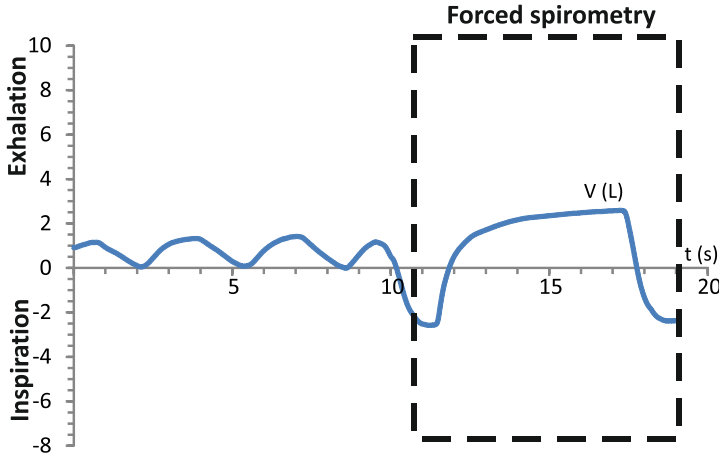

Figure 4.4: Relationship between volume and time in the chosen spirometry. Again, in the box is remarked the portion corresponding to the forced spirometry manoeuvre.

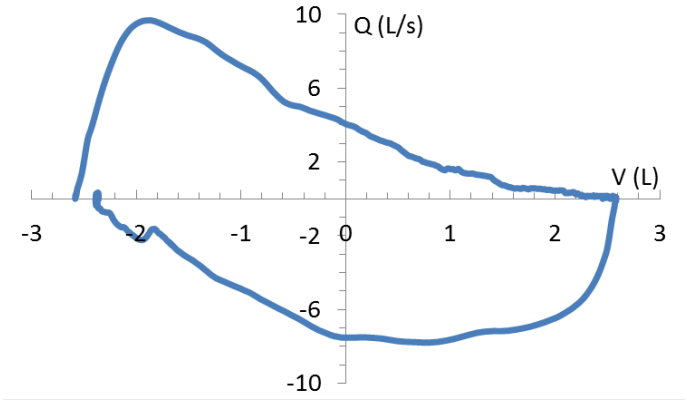

Figure 4.5: Relationship between flow rate and volume just in the forced spirometry manoeuvre. This graphic is the most used in clinical practice for the interpretation of the forced spirometry.

The maximum value obtained was 9.67 L/s, being 2.51 L/s the root mean square. The maximum error (3%) was 290 mL/s and the mean was 50 mL/s.

To obtain these values, previous results need to be integrated (Table 4.1) according to the formula 4.1.

$$V = \int_{11.32}^{19.09} Q\, dt$$

$$V = \sum_{i}^{i=n} \left[V_{i-1} + \frac{(Q_{i-1} + Q_i)}{2} * (t_i + t_{i-1}) \right] \quad (4.1)$$

t	Q	V	t	Q	V	t	Q	V	t	Q	V
s	L/s	L	s	L/s	L	s	L/s	L	s	L/s	L
0.00	0.00	0.00	0.21	9.18	0.50	1.28	0.90	4.06	6.33	-7.85	3.49
0.03	0.20	0.00	0.22	9.57	0.60	1.70	0.51	4.36	6.37	-7.83	3.18
0.07	0.50	0.02	0.23	9.67	0.69	2.85	0.24	4.79	6.43	-7.70	2.71
0.11	1.00	0.05	0.24	9.52	0.79	6.00	0.00	5.17	6.53	-6.80	1.99
0.12	1.25	0.06	0.30	8.11	1.32	6.03	-0.41	5.16	6.70	-4.40	1.04
0.13	1.70	0.07	0.37	6.23	1.82	6.05	-0.84	5.15	6.90	-2.31	0.36
0.14	2.40	0.09	0.47	4.65	2.36	6.08	-2.77	5.10	7.10	-0.62	0.07
0.16	4.30	0.16	0.60	3.33	2.88	6.13	-5.39	4.89	7.33	0.00	0.00

0.18	6.30	0.27	0.80	1.94	3.41	6.18	-6.55	4.59
0.20	8.40	0.41	1.00	1.40	3.74	6.28	-7.70	3.88

Table 4.1: Values obtained by integration according to the formula 4.1

4.3. Simulated spirometry

The forced spirometry allows obtaining these data at the mouth of the individual. What is intended to do in this work is to put these conditions in the inlet of the model (the mouth), in addition to the known atmospheric pressure, to obtain them in the rest of model.

First of all, it is necessary to simplify the spirometry. The amplitude of the original spirometry was 7.77 seconds, ranging from second 11.32 to second 19.09, with 777 points. Figure 4.6a shows the flow rate VS time curve in the original forced spirometry. For calculation purposes it was necessary to simplify the number of points and adjust the curve. As observed in the figure, the rate of change of the flow rate is very dependent on the time interval considered. In consequence, the points are closer together when the change in flow is larger (Figure 4.6b).

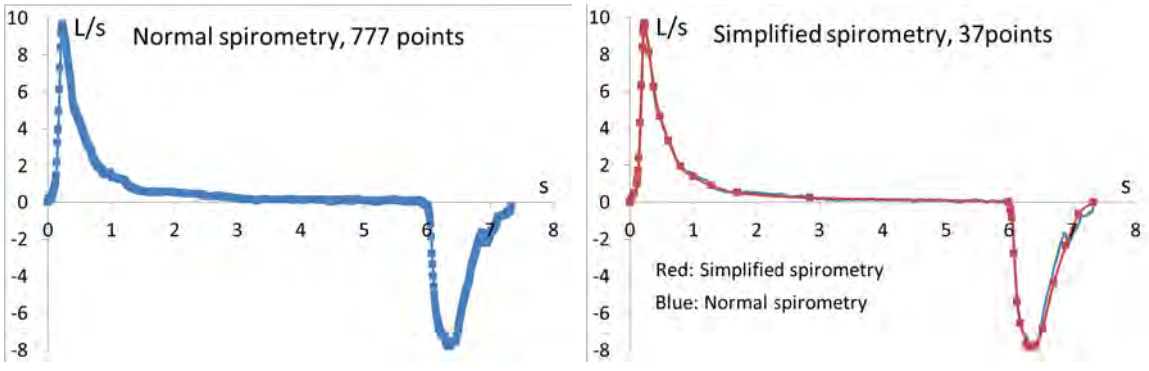

a) *b)*

Figure 4.6: Figure a) shows the original spirometry flow rate VS time curve, composed by 777 points. Figure b) shows the simplified curve, composed by 37 points. Both curves can be perfectly overlapped.

By default, the code Ansys Fluent has no prepared functions to simulate time-dependent variables, so it is necessary to prepare this special type of function using a user-defined function (UDF). The temporal evolution of the volume and flow rate will be imposed at the inlet boundary during the calculations by means of the UDF.

Due to non-uniformity of the breathing cycle, this UDF must include a subroutine to adapt the magnitude of the time step to a defined rate of change (adaptive time step). Instead of using a constant time step, a constant flow rate step is used, from which the time step is obtained. The number of steps to tour the spirometry is indicated, and the UDF determines otherwise the constant flow rate variation and the variable time step.

Figure 4.7 illustrates this, being the left sketch the option with constant time step (variable flow rate step) and the right sketch the option with constant flow rate step (variable time step).

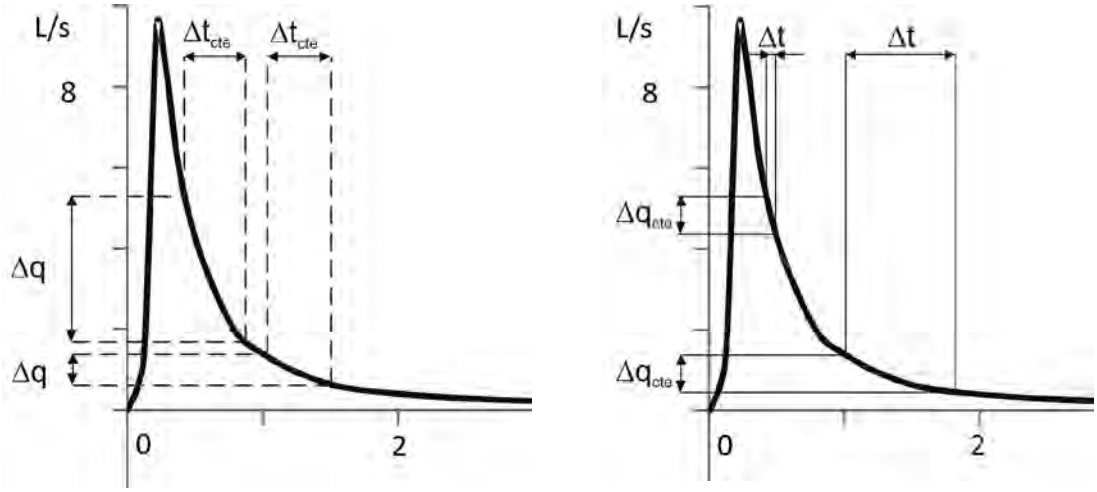

Figure 4.7: The left sketch shows the option with constant time step (variable flow rate step), being the right sketch the option with constant flow rate step (variable time step).

To reproduce the same conditions as in a real spirometry, the boundary values imposed were a flow rate varying along time at the mouth, a static pressure in the inhalation cycle and a total pressure (sum of static and dynamic pressures) in the exhalation at the lowest generation (Figure 4.8).

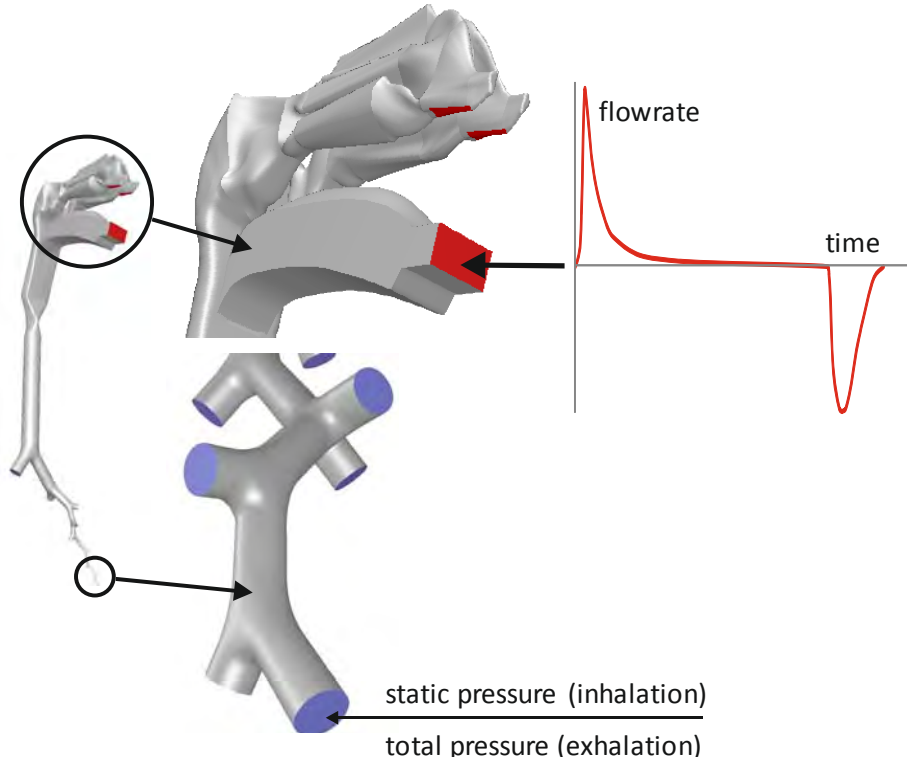

Figure 4.8: Boundary conditions imposed: flow rate varying along time at the mouth, static pressure in the inhalation cycle and total pressure in the exhalation at the lowest generation.

The UDF automatically changes the conditions in inhalation to exhalation. The complete UDF is shown in Appendix C.

The convergence criterion established was to reduce the scaled residuals for all the variables below 10^{-5}. The number of used steps was 1,000 being 1,400 the maximum of iterations required in order to assure the convergence of the results at each time step. With these values, the time required for each simulation was 5 days working in parallel on a computer with an i-7 processor of 8 cores.

One variable not obtained in a real spirometry and that the simulation can obtain is the static pressure at the lowest generation (G16) of lung. Figure 4.9 shows this value compared with the inlet boundary condition used (unsteady flow rate obtained from the chosen forced spirometry test). The obtained numerical result looks like correct because the tendency of the curve of the static pressure at G16 is similar to the flow rate curve. The flow in the mouth depends on the pressure at the lowest generation, as explained in subsection 2.1.3.1. If the pressure increases, the flow rate also increases. At the exhalation phase pressure is positive, while in the inhalation phase pressure becomes negative.

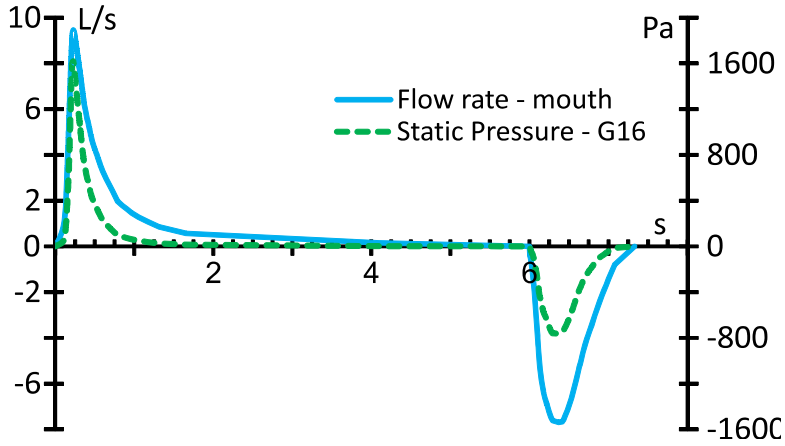

Figure 4.9: Unsteady flow rate imposed at the mouth in the simulation, and static pressure obtained in the lowest generation (G16).

One way to check if this simulation was correctly done is to repeat the test, but in this case the obtained unsteady pressure will be to put as inlet boundary condition at the lowest generation (G16). In the following section this procedure will be developed.

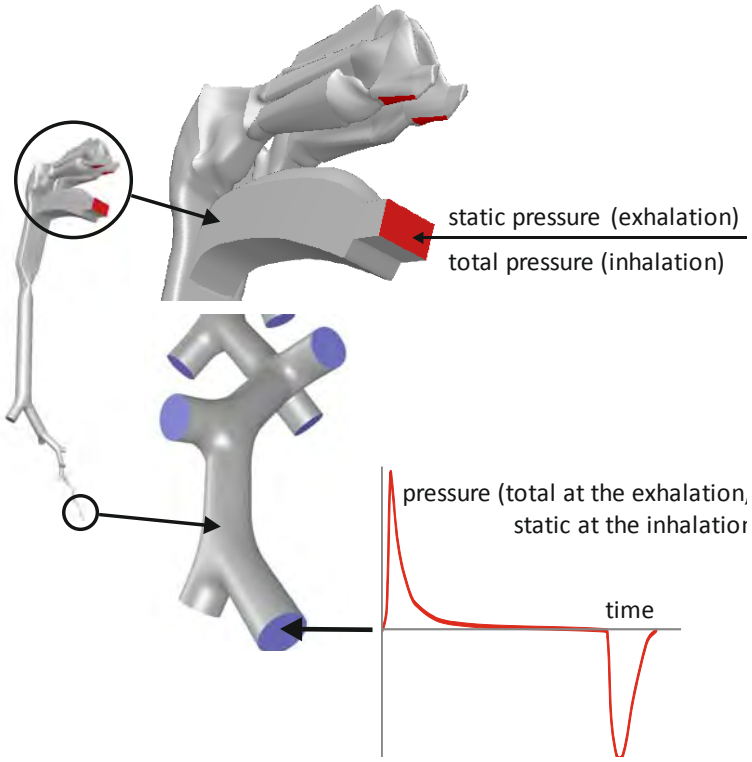

Figure 4.10: Boundary conditions imposed at the checking test: a known static or total pressure varying along time is imposed at the lowest generation, and a static pressure on the exhalation cycle and a total pressure on the inhalation cycle are imposed at the mouth.

4.4. Checking of the simulation

Figure 4.10 shows the new boundary conditions employed to check the previous test. A known static or total pressure (sum of static and dynamic pressures) varying along time is imposed at the lowest generation, and at the mouth the conditions are a static pressure on the exhalation cycle and a total pressure on the inhalation cycle.

The same steps as when spirometry was simulated will be repeated. If the results were correct, the same variables in both cases must have equal values.

In Figure 4.11, the velocity at the mouth with the obtained output velocity and the original spirometric values are represented. The results agree quite well.

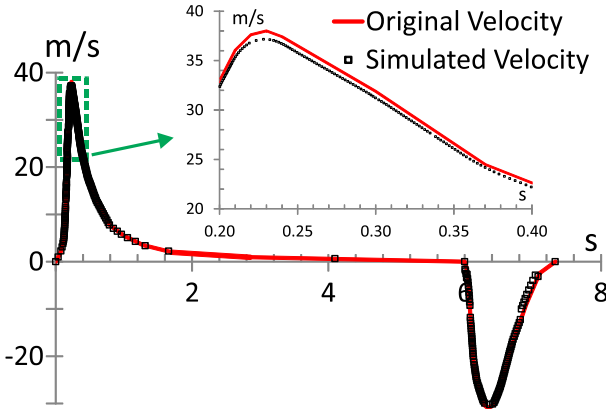

Figure 4.11: Real and simulated velocities at the mouth. Both results are in agreement. A close-up of the initial portion of the curves is shown.

The maximum velocity occurs at time 0.23 s, being 38.02 m/s the value obtained experimentally and 37.04 m/s the simulated value. Therefore, the maximum error is less than 2.6%.

4.5. COPD simulations

Once verified the correct functioning of the lung model in healthy people, it will be evaluated how it works in diseased lungs.

To simulate COPD conditions (chronic bronchitis and emphysema) the unsteady static and total pressure obtained in the past step is imposed at the lowest generation (G16), whereas a gauge pressure is established at the mouth. In the case of chronic bronchitis, in accordance with the comments in paragraph 2.5 and the represented in Figure 2.19, the diameter of the airway was decreased, whereas in the case of emphysema, a branch of order 3 was closed, which is equivalent to having 1/8 of inoperable lung.

Varying the geometry and the unsteady boundary conditions, the analysis of the obtained results allows the characterization of the particular fluid dynamic phenomenon of each disease and how it is perceived in the tests.

4.5.1. Emphysema

Actually, as was previously explained, closing a third order branch is not a physiological emphysema, which is impossible to simulate with accuracy in this model lacking alveoli. The occlusion of a branch of third level allows knowing what globally happens with pulmonary flows when having an inoperable lung part, but certainly this doesn't allow studying the fluid dynamic characteristics of emphysema. This occlusion is equivalent to having 1/8 of inoperable lung.

The simulation conditions are the same as in a normal lung, a static pressure varying along time at the lowest generation and a static pressure on the inhalation cycle and a total pressure on the exhalation at the mouth.

Figure 4.12 shows the pathlines and the velocity vectors in the first 3 branches at a given moment of the expiratory flow in the emphysematous model.

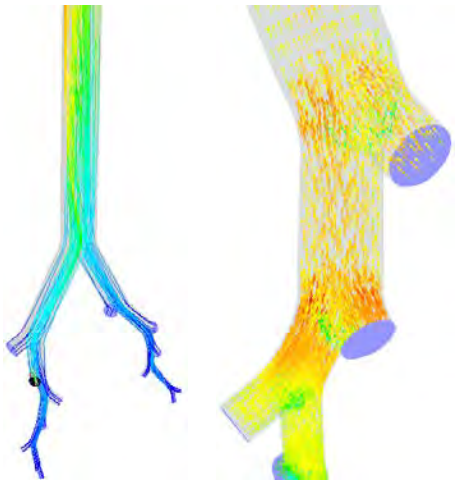

Figure 4.12: Pathlines in two branches of the emphysematous model and velocity vectors in the first 3 branches at a given moment of the expiratory flow.

For the same flow conditions, Figure 4.13 shows the contours of velocity in cross sections of different branches, in clockwise sense. In general, the flow is axisymmetric, with predominant axial component of velocity.

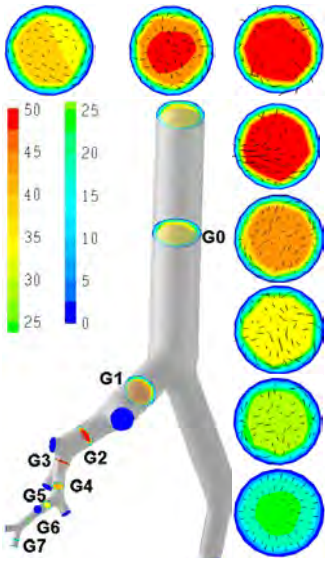

Figure 4.13: contours of velocity in cross sections of different branches shown in clockwise sense. It can be observed that the flow is axisymmetric, with a predominant axial component of velocity.

To check the accuracy of the model, a set of variables will be analysed. First, the evolution of the flow rate (Figure 4.14) is compared in both models: normal lung and emphysematous lung.

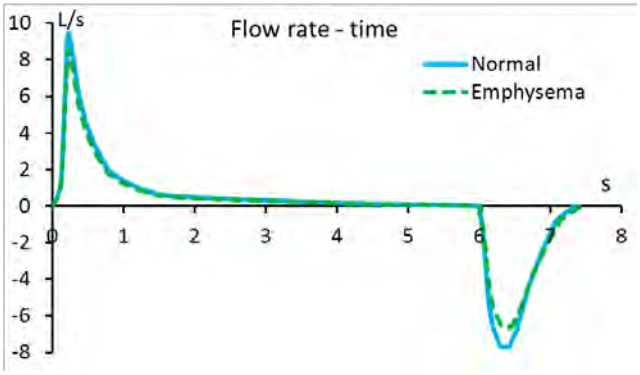

Figure 4.14: Flow rate magnitude in a normal lung and with emphysema.

In this approach, the conditions imposed to simulate emphysema correspond to mild conditions. The simulation captures these situations, with results similar to the ones expected to obtain by means of the forced spirometry.

The next results are shown as graphics of flow rate versus volume (Figure 4.15) and volume versus time (Figure 4.16) in both lung models, normal and emphysematous.

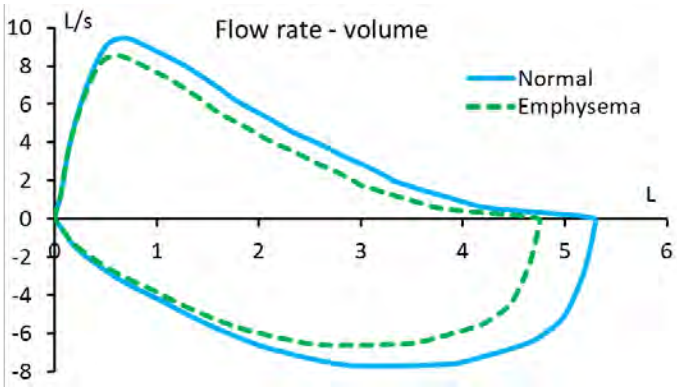

Figure 4.15: Flow rate versus volume. In dashed line is shown the curve corresponding to the normal lung model, and in solid line the curve corresponding to the emphysematous lung model.

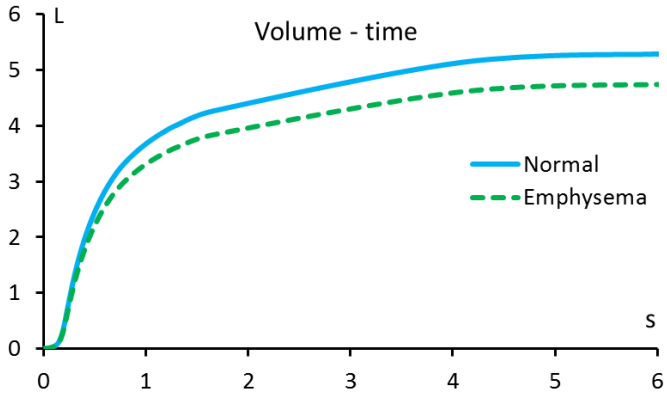

Figure 4.16: Volume versus time. In dashed line is shown the curve corresponding to the normal lung model, and in solid line the curve corresponding to the emphysematous lung model.

From these data it can be obtained the most used parameters in clinical studies (FVC, Forced Vital Capacity; FEV_1, Forced Expiratory Volume in first second; FEF_{25-75}, Forced Expiratory Flow at 25% point to the 75% point of Forced Vital Capacity; PEF, Peak Expiratory Flow). Figure 4.17 and table 4.2 show these parameters.

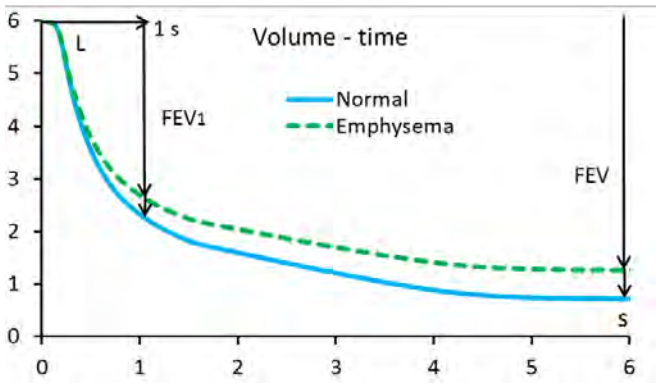

Figure 4.17: Volume versus time. In dashed line is shown the curve corresponding to the normal lung model, and in solid line the curve corresponding to the emphysematous lung model.

	Healthy	Emphysema
FVC (*L*)	5,29	4.74
FEV_1 (*L*)	3,69	3.29
FEV_1/FVC (%)	72,68	69.34
PEF (*L/s*)	9.46	8.54

Table 4.2: The obtained results of FEV, FEV_1, FEV_1/FVC and PEF in the original forcedspirometry and the obtained spirometry for emphysema are shown

4.5.2. Chronic bronchitis

To simulate the effect of the chronic bronchitis, the diameter of the airway was decreased a 90%. The same steps that were previously explained, with the same representation of variables, will be followed with a lung with bronchitis.

Similar results to a lung with emphysema are obtained, as is expected also in clinical practice.

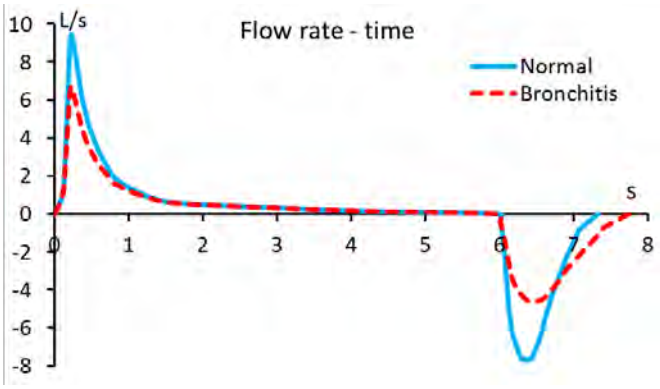

Figure 4.18: Flow rate magnitude in a normal lung and with chronic bronchitis. In dashed line is shown the curve corresponding to the normal lung model, and in solid line the curve corresponding to the bronchitic lung model.

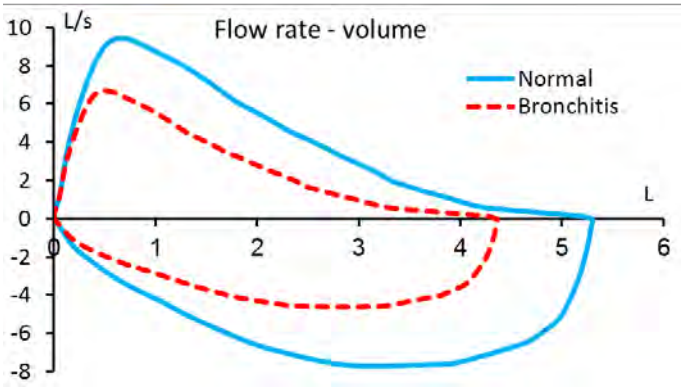

Figure 4.19: Flow rate versus volume. In dashed line is shown the curve corresponding to the normal lung model, and in solid line the curve corresponding to the bronchitic lung model.

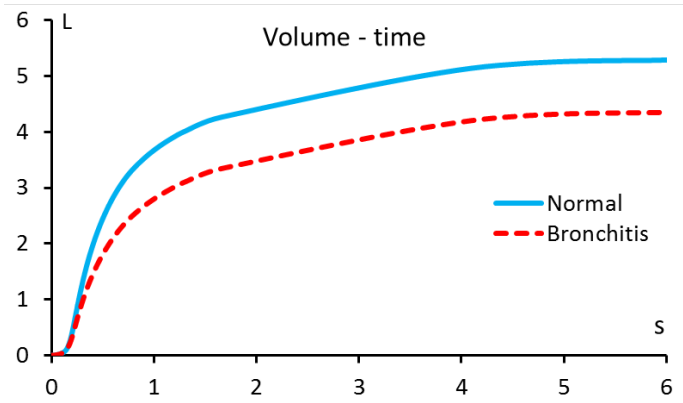

Figure 4.20: Volume versus time. In dashed line is shown the curve corresponding to the normal lung model, and in solid line the curve corresponding to the bronchitic lung model.

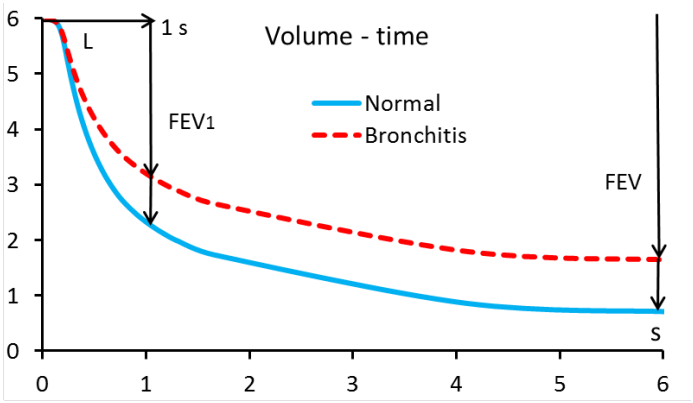

Figure 4.21: Volume versus time. In dashed line is shown the curve corresponding to the normal lung model and in solid line the curve corresponding to the bronchitic lung model.

	Healthy	Chronic bronchitis
FVC (*L*)	5,29	4,35
FEV_1 (*L*)	3,69	2,81
FEV_1/FVC (%)	72,68	64,56
PEF (*L/s*)	9,46	6,7

Table 4.3: The obtained results of FEV, FEV_1, FEV_1/FVC and PEF in the original forced spirometry and the obtained spirometry for chronic bronchitis are shown

4.6. Conclusions

It is possible to simulate with accuracy obstructive lung diseases in this model, with results that are very similar to the ones expected to obtain in a classic forced spirometry. The obstructive diseases globally affect the whole lung, but employing this single path airway model they can be properly simulated with low computational costs. The main handicap of this model is that the simulation of lung emphysema may not be as accurate as desirable, as it lacks alveoli. However, the results obtained by closing a third order branch allow knowing what globally happens with pulmonary flows when having an inoperable lung part. An advantage of this model is that it allows obtaining information about the static pressure at the lowest generation (G16) of lungs, which is not available in a forced spirometry.

CHAPTER 5
Particle deposition

5.1. Introduction

At rest or doing light exercise, most people breathe through the nose. With heavy exercises, since the resistance through the mouth is less than through the nose, there is a tendency to breathe through the mouth. For this reason, inhalation of aerosol drugs is oral. Inhaled medication is the basis of treatment of patients with COPD. It is recognized that a great amount of the inhaled drug is going to be trapped in the mouth and oropharyngeal region. Therefore, it is crucial to understand the factors that affect the deposition of particles in the lungs in order to improve the mechanisms of drug delivery for the treatment of lung diseases. Nowadays, the techniques of Computational Fluid Dynamics (CFD) allow studying this phenomenon without need of complex laboratory experiments. Particle deposition data in humans are limited, and the available ones show great variability among them.

In this chapter, the results of particle simulations in a model of human airways are presented. Different influences on the particle deposition are discussed.

5.2. Discrete phase model

The particulate flow is an important part of two-phase flows in which the fluid (gas or liquid) and the particles (solid, liquid or gaseous) are treated as two distinct phases. This type of flow is found in the airways. The geometric properties of the particles (their size and distribution) influence the dynamic behaviour of these flows.

Dispersed phase flow is the one in which the particle motion is controlled by fluid forces (drag, lift, etc.). By contrast, a dense phase flow is dominated by collisions between particles.

Coupling is known as the phenomenon of transfer of mass, momentum and energy. For values of volume fraction of the dispersed phase lesser than 10^{-6}, the particles

have no significant effect on the turbulence, being called this phenomenon one-way coupling. This is the case of particles entering into the airways. For values of volume fraction of dispersed phase between 10^{-6} and 10^{-3}, the particles affect the turbulence, being called two-way coupling. Figure 5.1 shows a map of regimes of interactions between the volume fraction of particles and fluid turbulence suggested by Elghobashi (1994).

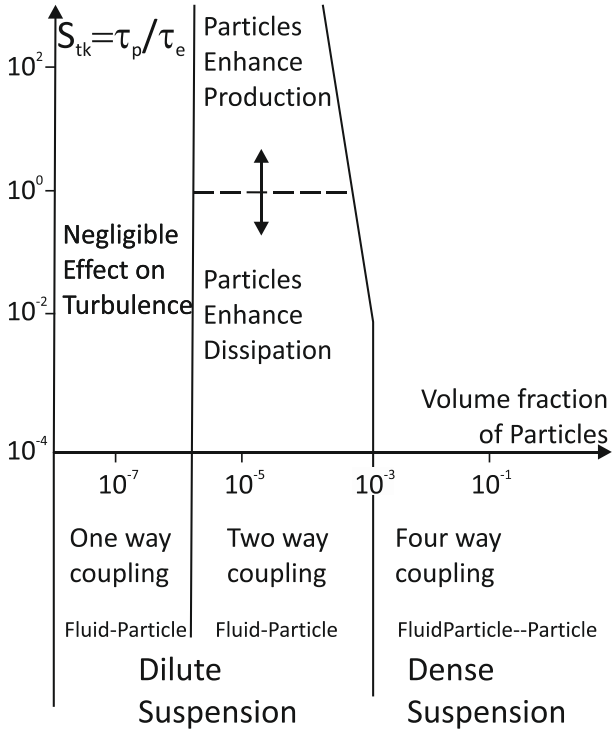

Figure 5.1: Map of regimes of interactions between particles and turbulence proposed by Elghobashi in 1994.

The particle response time (τ_p) and the residence time of large eddy (τ_e) are:

$$\tau_p = \frac{\rho_p d^2}{18\,\mu};\ \tau_e = \frac{l}{u} \tag{5.1}$$

being:

- ρ_p: particle density
- μ: fluid dynamic viscosity
- ℓ: length scale
- u: fluid velocity

The coefficient between τ_p and τ_e is the Stokes number (S_{tk}). When the value of this number is below 1, particles tend to follow the flow without depositing. On the contrary, particles tend to deposit due to the lung morphology and the flow characteristics (Zhang and Kleinstreuer, 2002). Grgic et al (2004) suggest that obtaining the Deposition Fraction as a function of Stokes and Reynolds numbers (S_{tk} x $Re^{0.37}$) improves the characterization of oral particle deposition.

The two most widely methods used for mathematical modelling of two-phase flows are Eulerian and Lagrangian. In the Eulerian approach, the particles are treated as a second fluid that behaves as a continuous model, and the equations are developed for the average properties of the particles. The Lagrangian approach is useful when the particulate phase is so small that the description of the behaviour of particles in a continuous model is not feasible. Since for each particle is calculated the velocity and trace, this approach is most suitable for the discrete nature of the particle motion. However, to obtain statistical averages with reasonable accuracy, a large number of particles must be tracked.

This approach is called Discrete Phase Model (DPM), which follows the movement of individual particles. The trajectory of each particle is calculated over a number of steps while passing through the fluid domain. Being known each particle properties (mass and size) at each step, the resultant of the forces acting on it can be calculated. The particle trace is determined by integrating the entire domain.

Unlike the continuous phase (Eulerian approach), which moves across cells, the DPM follows the particles (Lagrangian approach), having each particle its own coordinates. For the calculation of the trace, the inertial, drag and gravity forces are taken into account, both in steady and unsteady flows.

To include the effect of turbulence in the particle dispersion, the stochastic particle and cloud tracking models can be used. Figure 5.2 shows a sketch of these models.

- Stochastic tracking model: it takes into account local variations in the flow properties (temperature, velocity and species concentration), requires a large number of stochastic attempts to achieve a statistically significant sample (depending on the density of the mesh), and its use is recommended in complex geometries.
- Particle cloud model: it uses statistical methods to follow the turbulent dispersion of particles on an average trace, calculating this trace from the set of averaged equations of motion for the particles represented in the cloud, and particle distribution within the cloud follows the Gaussian density function probability.

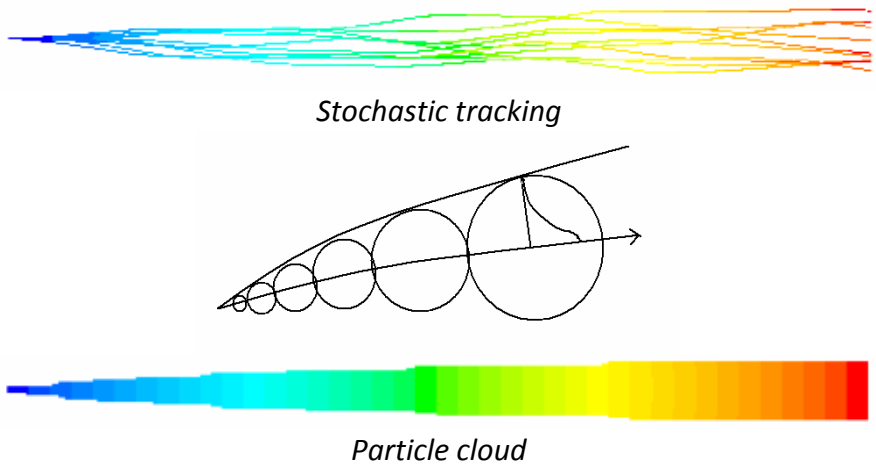

Figure 5.2: Stochastic tracking and Particle cloud models.

The particles are considered as inert, although the model supports more complex cases, where particles may evaporate or burn.

The volume fraction of particles entering the airway is typically of a lower order than 10^{-6} so the model of one-way coupling is taken, in which the movement of the particles has no effect on the movement of fluid, so there is not interaction between them.

Brownian motion, caused by the collision of the air molecules, is considered to have no influence on the particles trace if they have a MMAD greater than 0.1 μm. Drag force is the dominant force because the particles density is much higher than the fluid density. Typically, the density of particles is close to the density of water, which is 1,000 kg/m^3 as opposed to $1.2\ kg/m^3$ for the air.

5.3. Configuration

The boundary conditions are the same as described in the previous chapter except that with the discrete phase model the model walls are going to trap the particles that collide with them.

Particles are introduced by means of an injection type called surface, specifying the particle properties and velocity. The particles must be introduced from a surface close to the entrance of the model (0.1 *mm*) and not near its walls (0.5 *mm*) to avoid the immediate deposition. Robinson (2006) found that 50,000 particles are necessary to minimize random variation in the deposition efficiency predictions due to the randomness of the particle position profile.

Deposition is determined by summing up the "trapped" particles. This occurs when their centre of mass touch the wall. The program Ansys Fluent also reports the number of incomplete, aborted, or unable to be tracked particles. These numbers can be minimized by adjusting various input parameters.

The main physiological factors determining the particle deposition are the respiratory rate (number of breaths per minute) and tidal volume (volume inhaled in one breath). Their product is called respiratory minute volume. Both the respiratory rate and tidal volume depend on the physical activity of the individual.

The flow rates tested were 15, 30 and 75 *L/min*, which are equivalent to different respiratory rhythms, varying from light activity to heavy exercise.

The seeding conditions of the particles were:

- Inert material density: 1,000 kg/m^3
- Particle size: 1 μm, 5 μm, 10 μm, 15 μm and 20 μm
- Velocity: the same as air
- Density: 0.5%
- Number of injected particles: 98,658

5.4. Oral inhalation

The first thing to take into consideration is the input of particles in the mouth to see if there is any predominant direction. For the flow rates and particle sizes indicated above, several angles, between 0° and 70° (Figure 5.3) in increments of 10°, have been tested, as being shown in Figure 5.4.

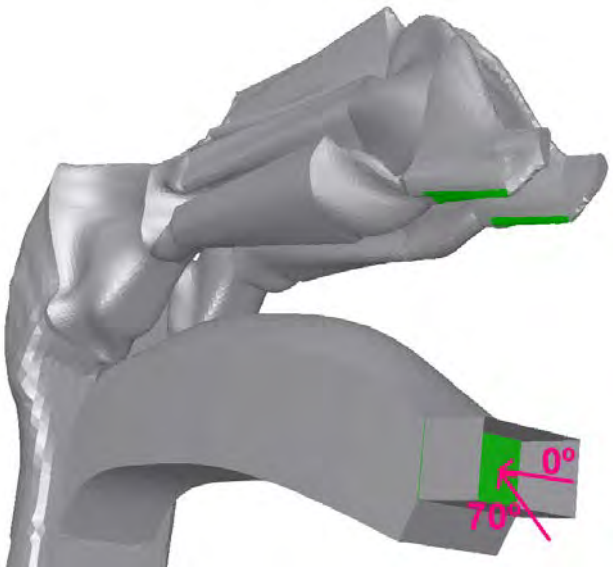

Figure 5.3: Model of the nose and mouth, in which the injection surfaces in the mouth (marked in white colour) and tested angles (between 0° and 70°, in increments of 10°) are shown.

Two definitions can be employed for the trapped particles: Deposition Efficiency (DE) and Deposition Fraction (DF). DE represents the mass ratio between the trapped particles in a certain area and the particles entering that area. DF is the mass ratio between the trapped particles in an area and the total of particles entering the mouth into the lungs. In the case shown in Figure 5.4, both definitions are the same, as the mouth is the first portion of the respiratory system.

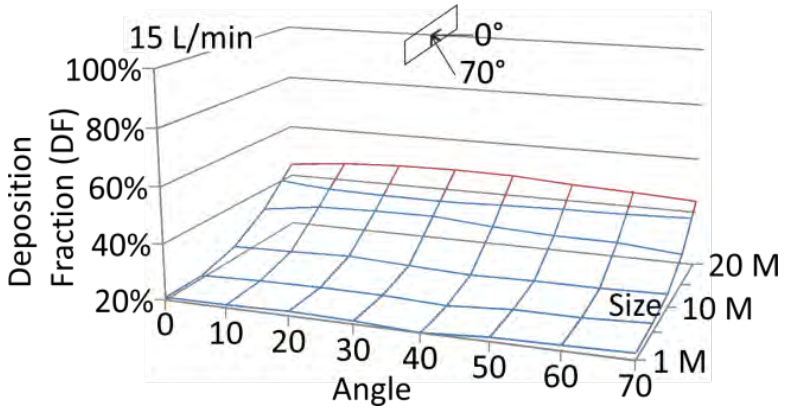

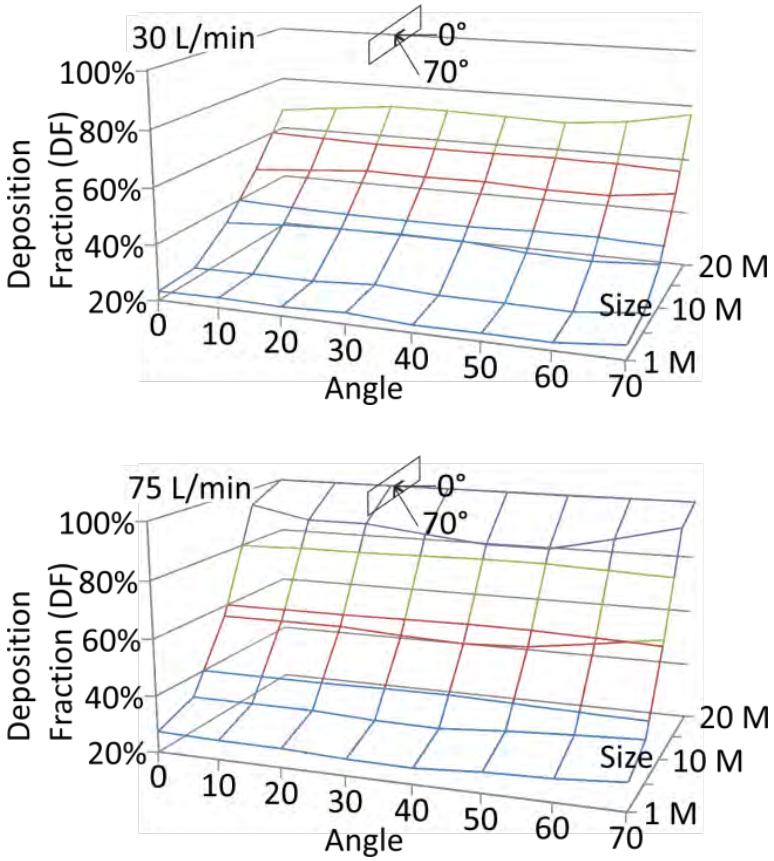

Figure 5.4: Deposition Fraction (DF) of particles in the oropharyngeal region in function of the inlet angle, for several sizes and flow rates. It can be observed that the main factors that modify the DF in the oropharyngeal region are the flow rate and particle size, but not the inlet angle.

It was found that the angle at which the particles are placed in the mouth does not change the pattern of particle deposition, because the particles are dragged by the air as the patient inhales (in the case of a dry powder inhaler or when inhaling from a holding chamber), following the curvature of the mouth in every case. It can be observed that the main factors that modify the DF in the oropharyngeal region are the flow rate and particle size.

According to the previous figures, the use of inhalers with particles larger than 10 μm and flow rates over 30 *L/min* must be avoided, because the percentage of particles deposited before reaching the lung is greater than 50%.

The next figures show the concentration of particles, in kg/m^2, settled on the duct walls. The red colour means “high concentration” of settled particles on the wall, and the blue colour means absence of settled particles.

For the case of 75 *L/min* and particle size of 15 μm, about 60% of particles are deposited in the oropharyngeal region, and also between the tongue and palate area. A detail of the pattern of deposition is shown in Figure 5.5. For angles close to 0°, the particles are predominantly deposited in the tongue and the back wall of the pharynx. As the angle increases, the particles tend to be deposited in the palate (more than in the tongue) and also, in a lesser degree, in the back wall of the pharynx.

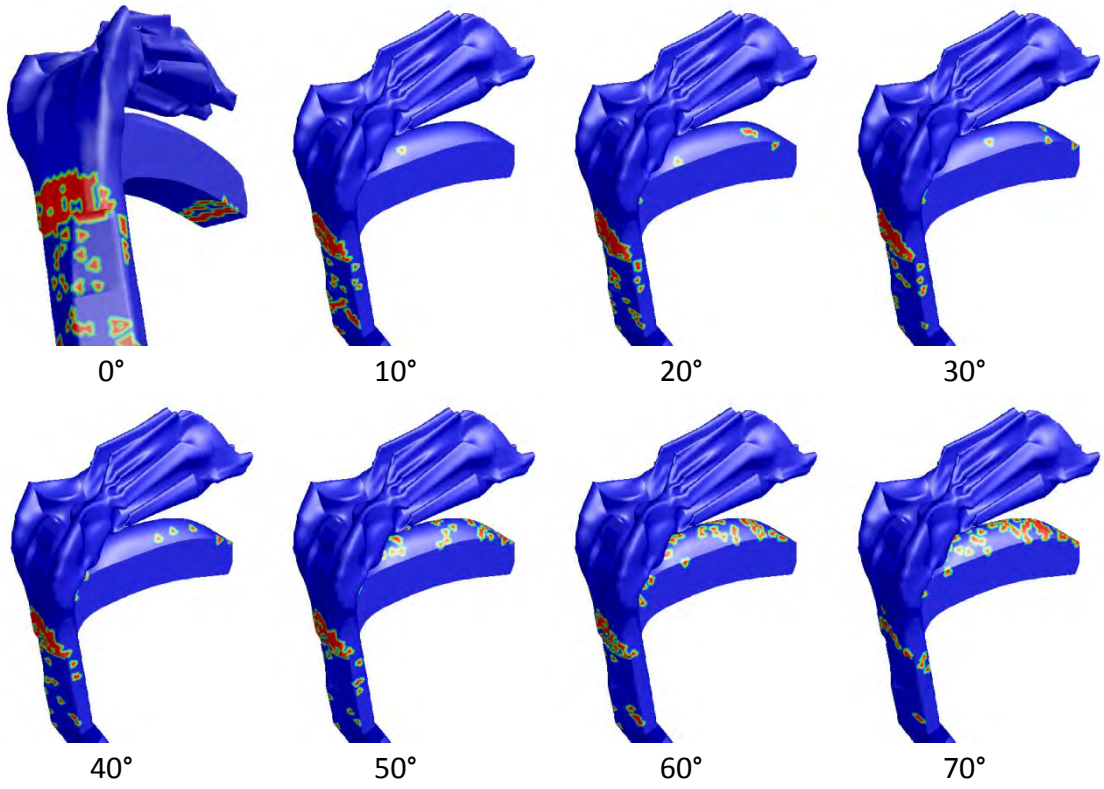

Figure 5.5: Oropharyngeal deposition pattern, with a flow rate of 75 L/min, particle diameter of 15 μm, and inlet angles from 0° to 70°, varying in 10° each. The main deposition spots are the back wall of the pharynx, the tongue (for angles close to 0°) and the palate (for angles close to 70°).

Figures 5.6 to 5.8 show the oropharyngeal particle deposition when entering particles from the mouth, at the same inlet angle (set at 0°) and particle size (15 μm), using three different flow rates: 15, 30 and 75 *L/min*. It can be observed how as the flow rate increases, the deposited particles in the tongue and oropharyngeal region also increase.

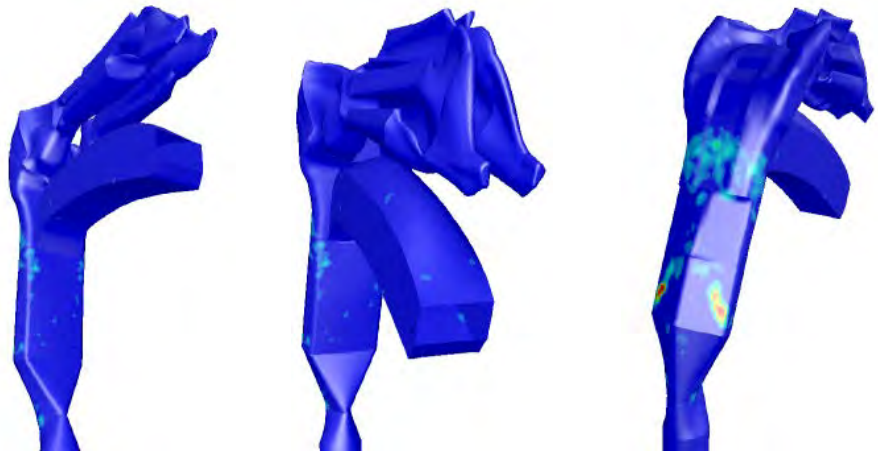

Figure 5.6: Different views of the oropharyngeal deposition pattern, entering particles (diameter 15 μm) by the mouth with a flow rate of 15 L/min, and at a 0° angle.

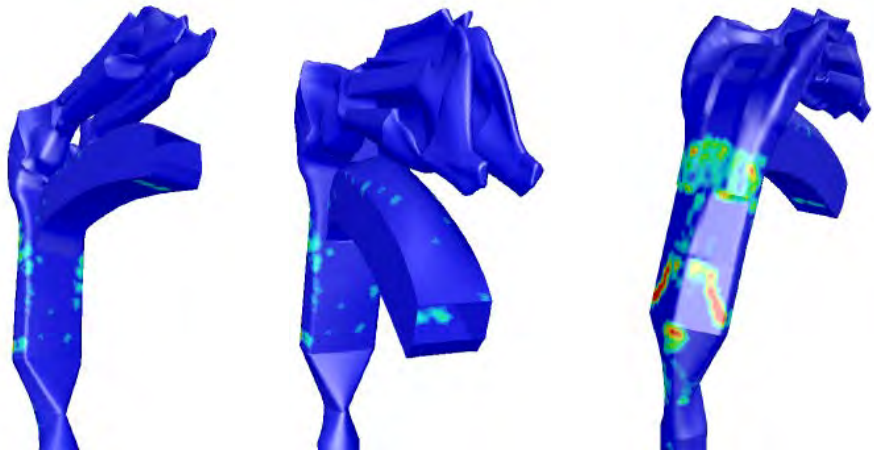

Figure 5.7: Different views of the oropharyngeal deposition pattern, entering particles (diameter 15 μm) by the mouth with a flow rate of 30 L/min, and at a 0° angle.

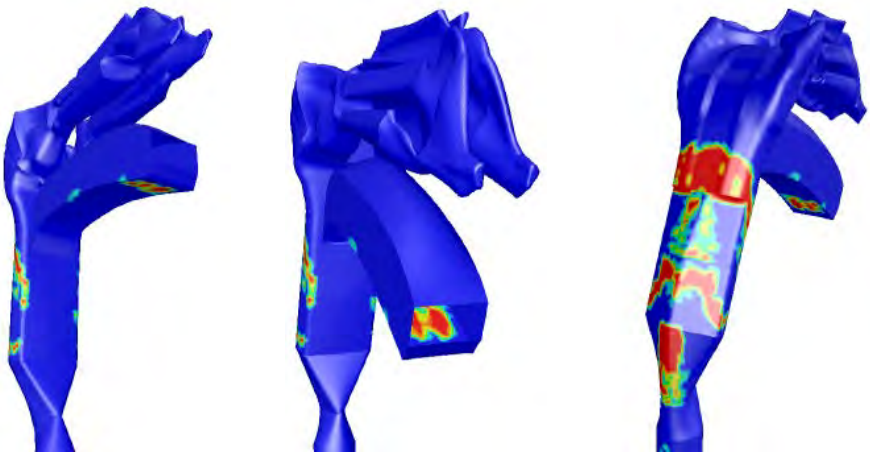

Figure 5.8: Different views of the oropharyngeal deposition pattern, entering particles (diameter 15 μm) by the mouth with a flow rate of 75 L/min, and at a 0° angle.

The main conclusion of this set of simulations is that inhalation from dry powder inhalers or holding chambers with flow rates over 30 *L/min*, and especially over 75 *L/min*, must be avoided, because the percentage of particles deposited in the mouth and oropharyngeal region before reaching the lungs is greater than 50%. Patients must be trained to inhale from these devices with the minimal possible flow rates, to enhance the entrance to the peripheral airways of the inhaled drugs. The angle at which these devices are introduced in the mouth doesn't affect the deposition fraction of the inhaled drug, as the particles are carried by the air as the patient inhales, following the curvature of the mouth. The inhalation directly from metered dose inhalers must be investigated, as the inhaled drug exits the device propelled at high velocities, and then is carried by the air that the patient inhales.

5.5. Nasal inhalation

The inhalation of drugs is performed through the mouth, while the respiration is mainly performed through the nose. The inhalation of particles through the nose is important in the case of environments with high levels of air pollutants.

Figures 5.10 to 5.12 represent the same conditions employed in the previous example, but in this case the particles were inhaled through the nose.

It can be observed how as the flow rate increases, there is a change in the deposited particles from the back wall of the pharynx to the nose, due to its complex morphology designed to filter the particles and avoid their entrance to the lower airways.

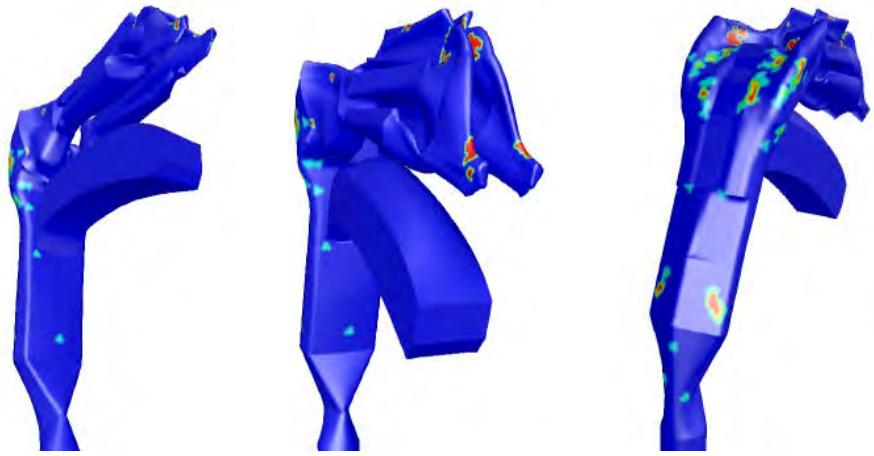

Figure 5.10: Different views of the oropharyngeal deposition pattern, entering particles (diameter 15 μm) by the nose with a flow rate of 15 L/min.

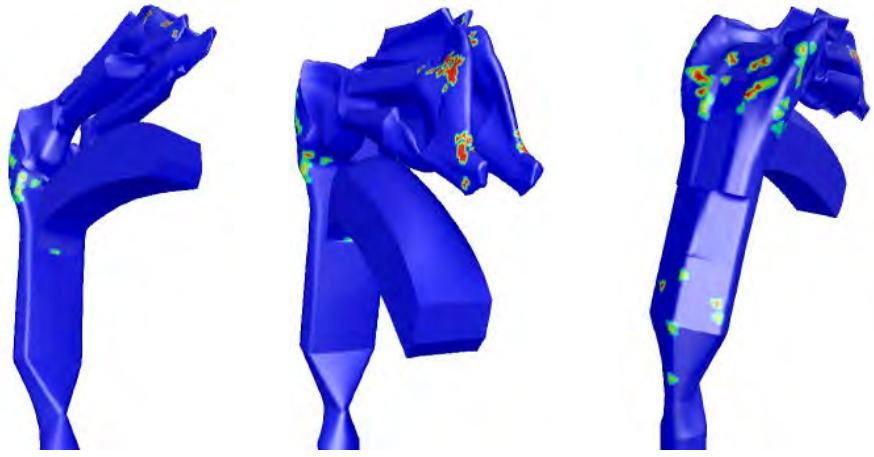

Figure 5.11: Different views of the oropharyngeal deposition pattern, entering particles (diameter 15 μm) by the nose with a flow rate of 30 L/min.

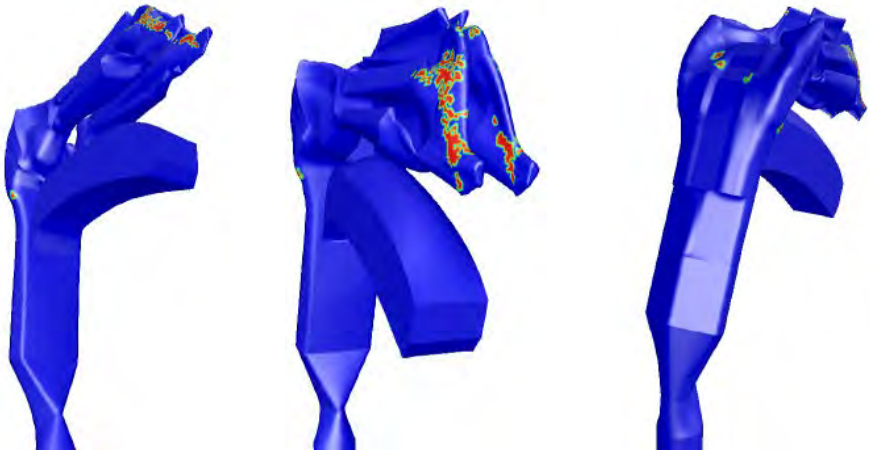

Figure 5.12: Different views of the oropharyngeal deposition pattern, entering particles (diameter 15 μm) by the nose with a flow rate of 75 L/min.

5.6. Particles in the lungs

Once it is verified that the model works in the upper airways, the next step is the introduction of particles in the whole lungs to obtain the pattern of particle deposition in the different branches of the lower airways.

The boundary conditions used in these tests were described in section 5.3. In this case the range of particles goes from 1 μm to 20 μm. The particles are introduced by means of the previously described injection surface located 0.1 *mm* below the entrance to the trachea.

Figure 5.14 shows the obtained results, also comparing them with the ones obtained in the simulation of oral deposition. It can be observed how as the flow rate and the particle size increase, the particles tend to be trapped in the first generations of the airways (especially in generations 1 to 5).

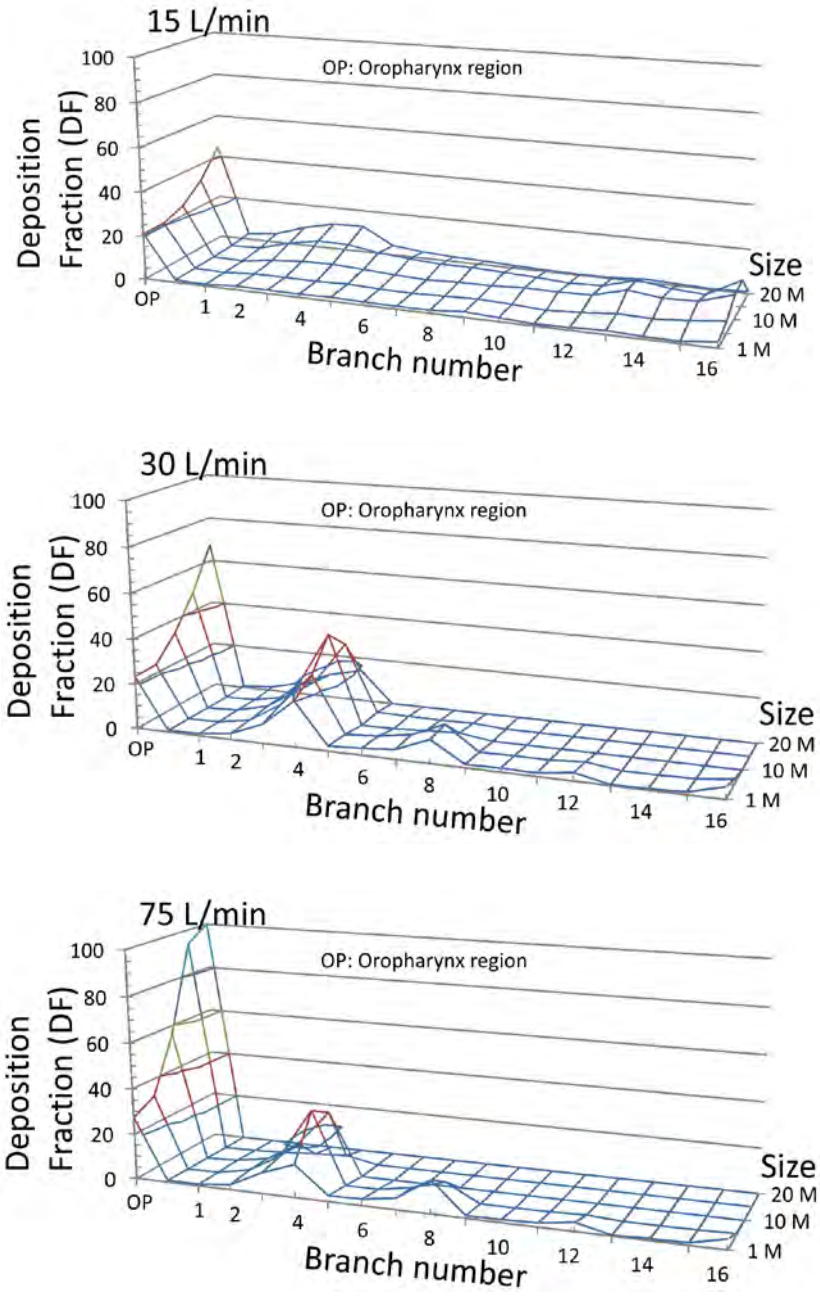

Figure 5.14: Deposition Fraction (DF) of particles in the airway for several sizes and flow rates. As the flow rate increases, the particles tend to be trapped in the oropharyngeal region and the first generations of the lower airways. The same happens when increasing the particle size.

5.7. Discussion

These results agree with the ones obtained by Conway *et al.* (2012), shown in figure 5.15. Conway *et al.* investigated the aerosol deposition in the respiratory tract of healthy human subjects employing 2D and 3D imaging methods. The conditions of the experimental tests were:

- Tidal volume: 1,000 *mL*
- Inhalation time: 3.33 *s*
- Particles: 5.76 μm (mass median diameter)

These conditions correspond to a mean flow rate of 18 *L/min*. The CFD results obtained in the simulations of our work correspond to a flow rate of 15 *L/min* with a particles size of 5 μm up to generation 16 of the airways. The observed difference may be due mainly to the numerical model used in the lung, but it can also be influenced by the parameters used, but in general terms, both results show the same tendency.

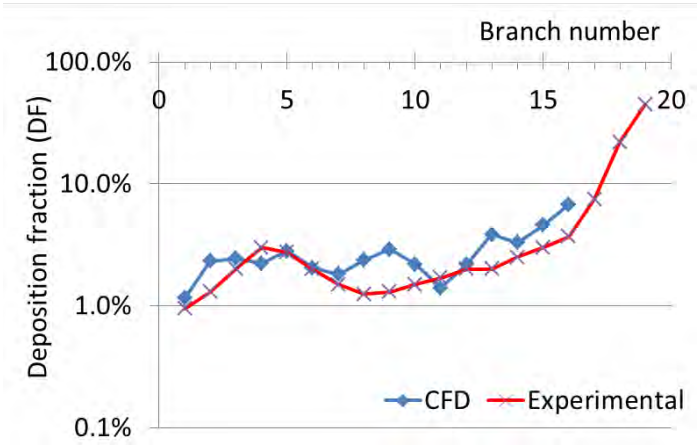

Figure 5.15: Comparison of the deposition fraction, for a 15 L/min flow rate, obtained in the experimental work of Conway et al. (2012) and the CFD simulations realized in this chapter.

In general terms, it can be affirmed that CFD is a good tool for studying the deposition of inhaled particles in the human airways, avoiding complex laboratory tests that require exposing volunteers to tests with radiation.

CHAPTER 6
Model customization

6.1. Introduction

As it has been explained in previous chapters, the deposition of an aerosolized drug in a greater or lesser extent, in central or peripheral airways, can be achieved by modifying the particle size of the drug or/and the inspiratory flow of the patient. It is difficult to predict the particle deposition because the calibre and anatomy of the airways in each patient may vary, but generally it can be accepted that particles with a diameter of 5-10 microns are deposited predominantly in the oropharynx and large airways, and particles between 1 and 5 microns are deposited in greater amounts in the small airways and alveoli.

Bronchoconstriction, inflammation and the impairment of the airway architecture are other factors that will alter particle deposition. These phenomena can appear in several diseases such as COPD, cystic fibrosis or bronchiectasis. The down-gauging of the airways causes increased air speed, which produces a higher degree of turbulence in areas in which the flow should be laminar. Moreover, the obstruction in some airways causes the air to be directed predominantly toward unobstructed areas, obtaining a higher drug deposition therein, while the main objective is to have a high level of drug deposition preferentially in the areas affected by the obstruction.

These peculiarities of certain pathologies, and even of each patient, make it interesting to have in clinical practice a method that allows the individualization of aerosolized therapies. It must not be the same to treat an asthmatic patient, where the main interest is to have a peripheral deposition of salbutamol, than treating a COPD patient, in which it would be more effective to obtain a central deposition of ipratropium bromide, just to cite two examples. One way to achieve a greater individualization of treatments would be modelling an exclusive airway model of each patient.

6.2. Techniques and limitations

In hospitals there is available an increasing number of powerful scanners with high resolution images and software that allows three-dimensional reconstruction of the bronchial tree. These images are an important source of data for later building a model that allows the analysis of flow and particle deposition by CFD techniques. The possibilities of computerized tomography (CT) for the study of the airways are undervalued.

Although currently in the Hospital Universitario Central of Asturias is not available the equipment necessary to obtain all the data needed to perform each patient's individualized airway model, it has been possible to obtain new and promising images of the airways. In figures 6.1 to 6.6 there are shown some examples.

Figure 6.1: Three-dimensional reconstruction of the thoracic CT of a 57 year old male diagnosed of COPD.

Figure 6.2: The same image after proceeding to retire part of the lung parenchyma.

Figure 6.3: Reconstruction after retiring almost all the lung parenchyma.

Figure 6.4: 3D reconstruction of the thoracic CT of 16 year old male with no

pulmonary injuries (frontal view).

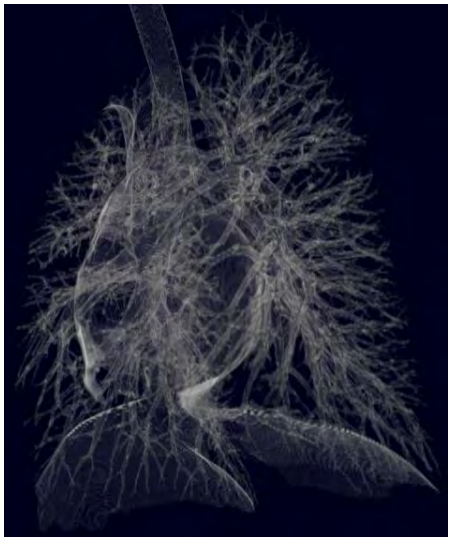

Figure 6.5: The same image in an oblique view.

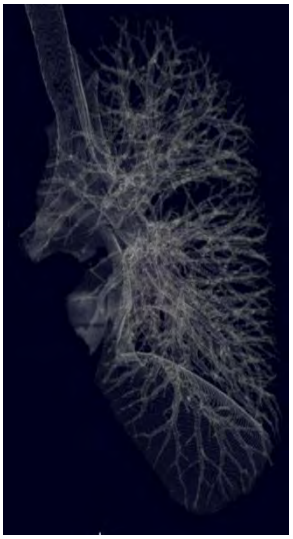

Figure 6.6: The same image in a lateral view.

An example of customized airway model of a patient is provided in the work of De Backer et al. (2007), in which a model for CFD simulation was performed from the thoracic CT of a 79 years old woman with COPD and congenital hypoplasia of the right main bronchus (Figure 6.7).

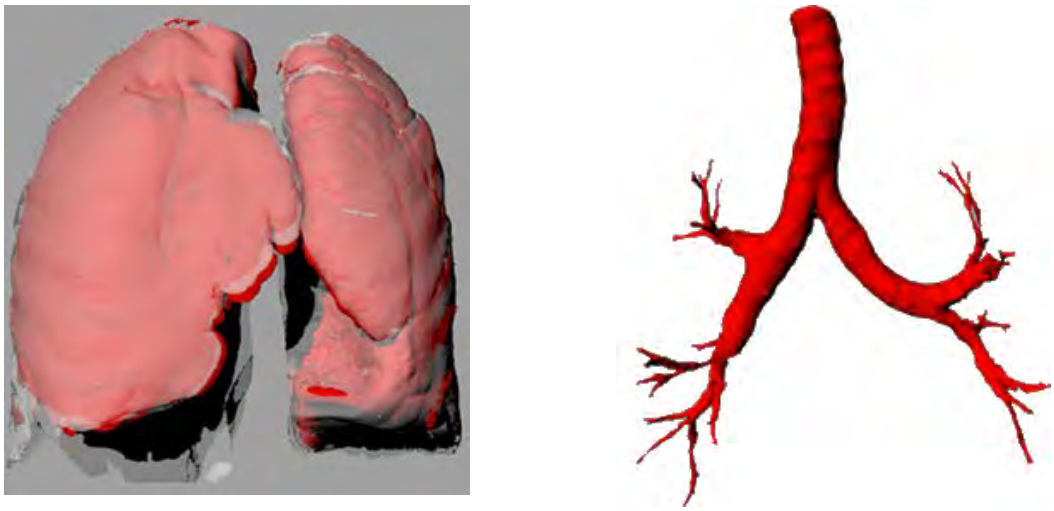

Figure 6.7: Lung volumes of a 79 years old woman with COPD and congenital hypoplasia of the right main bronchus, shown at functional residual capacity (FRC, red) and total lung capacity (TLC, transparent); and reconstructed airway model at FRC.

In this work, the model was validated by the subsequent performance of a ventilation gammagraphy. However particle deposition was not studied to be able to offer the patient a personalized treatment.

The deposition of particles in the airways simulated by CFD can validated in vivo by performing imaging tests using a radiolabeled aerosol. However these complex techniques are available in a small number of centres. Nowadays, the most commonly used techniques for determining the distribution of inhaled drugs are gammagraphy and single photon emission computed tomography (SPECT) in three dimensions (3D), although other techniques, such as positron emission tomography (PET) and magnetic resonance imaging (MRI), are gaining importance. These techniques are used in combination with drugs or radioactively marked molecules (Dolovich 2004).

The isotope usually used in gammagraphy and 3D SPECT is technetium-99m (^{99m}Tc), which is associated with the drug being studied without being part of it. Gammagraphy provides lung images in 2 dimensions (2D), and it has frequently been used to compare the effectiveness of aerosol lung deposition using different inhalation devices, as well as the effects of different respiratory and lung disease parameters on the deposition. The distribution of the drug is generally studied according to areas of interest, comparing the apical and basal regions, or central and peripheral distributions.

SPECT can obtain accumulative 2D images of the thorax of the patient, which gives more precise images in order to evaluate drug deposition patterns in the lungs. However, this is not possible if there is no unabsorbable direct radioactive marker available for the drug being studied. It is useful, on the other hand, for the study of variables that are secondary to the inhalation of medication, such as pulmonary perfusion and ventilation, mucociliary clearance or pulmonary epithelial permeability.

In the case of PET, the markers used are usually carbon, fluoride, nitrogen, and oxygen, which are atoms that make up any organic molecule, and it is therefore simpler to mark the drug being studied. The markers that are most commonly used are ^{11}C and ^{18}F. The images obtained by PET can be divided into areas that are either more central or more peripheral and correlated with the degree of radioactivity detected and, therefore, with the dose of drug deposited in each region (Dolovich 2004).

This research opens a very interesting and practical field of clinical experimentation. In the absence of a "gold standard" process to validate the theoretical model of pulmonary particle deposition, the proposal to develop in the future is the adaptation of the model mathematically developed in this study with bronchial images obtained from high resolution computerized tomography (HRCT). The quantification of the

different bronchial divisions up to peripheral areas, combined with the knowledge of the exact number of divisions and their morphology, attributable to the underlying pathology, allows the adaption to each patient of the most effective inspiratory flow and particle size to be used to achieve a more efficient lung deposition of aerosolized drugs.

6.3. Enhancement of the model development

An important feature of the human lung is its asymmetrical morphology, so the model was modified from the original symmetrical geometry to an asymmetrical one. The bronchial tree is divided into three zones, trachea (level 0), intralobular bronchi (levels 1-3) and bronchioles (levels 4-16). In the first two zones, the diameters of the branches and branching angles would be obtained from CT images to be as realistic as possible, and these data will be used for the construction of the improved model. The two daughter branches of the same parent branch have not only different diameters and lengths but also different spatial angles. In the table 6.1 are the magnitudes used in this model, taken from Raabe et al (1976).

The lung geometry after level 3 follows the models developed by Weibel (1963), Horsfield (1968) and Kitaoka (1999), with dichotomous and symmetric divisions. The truncated geometry is created by removing the 50% of the airway paths in each generation.

The resulting model, after the trachea, consists of eight individual flow paths: right upper (2 paths), right middle (1 path), right lower (1 path), left upper (2 paths) and left lower (2 paths). Figure 6.8 shows the built model.

Once built the model, the following steps will be to study:

- Again, the aerodynamic behaviour using spirometry.
- Two new situations in COPD: bronchitis and emphysema.
- Particle deposition in the model.

Branch	Diameter (mm)	Length (mm)	In-plane branching half angle (degree)	Out-of-plane spatial angle (degree)
R1	12.49	22.00	35	0
R2U	8.21	15.60	63	25
R3	10.01	26.00	15	25
R4	7.50	11.27	18	60
R5	4.80	10.81	33	60
R6	5.85	21.00	61	5
R7	7.20	8.00	15	5
L1	13.50	50.00	73	0
L2	9.00	11.00	44	15
L3	8.44	16.00	48	15
L4	7.88	9.70	28	0
L5	6.02	9.70	70	0
L6	4.80	10.81	25	35
L7	7.50	11.27	65	35

Table 6.1: Magnitudes employed in the new and enhanced airway model for the first three generations of the airways, taken from Raabe et al (1976)

The first two steps were performed as previously explained in chapter 4 (Fluid dynamic characteristics of COPD), obtaining similar results. Once it is verified again that the model properly works, the next step is proceeding to introduce particles in it. The seeding conditions of the particles were:

- Inert material density: 1,000 kg/m^3
- Particle size: 1 μm, 5 μm, 10 μm and 15 μm
- Velocity: the same as air
- Density: 0.5%
- Number of injected particles: 98,658

The particles are introduced by means of an injection surface located 0.1 *mm* below the entrance to the trachea.

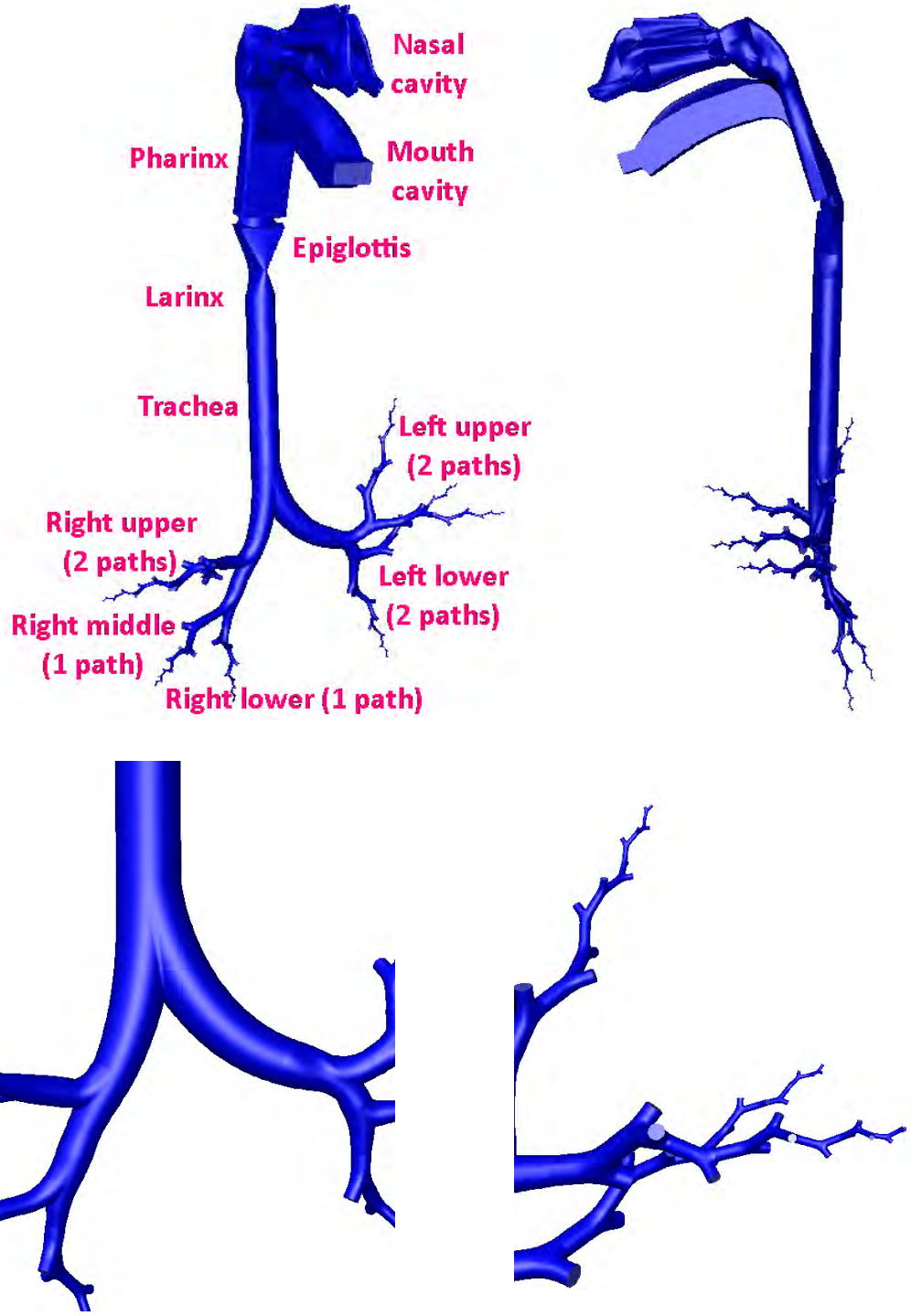

Figure 6.8: Numerical model with 8 complete paths developed up to generation 16. In the left upper image a frontal image of the complete model is shown. In the right upper image it can be observed from a lateral view. Both lower images show close-ups of the central and peripheral airways of the model.

Figure 6.9 shows the obtained results. It can be observed how as the flow rate and the particle size increase, the particles tend to be trapped in the oropharyngeal region and the first generations of the airways.

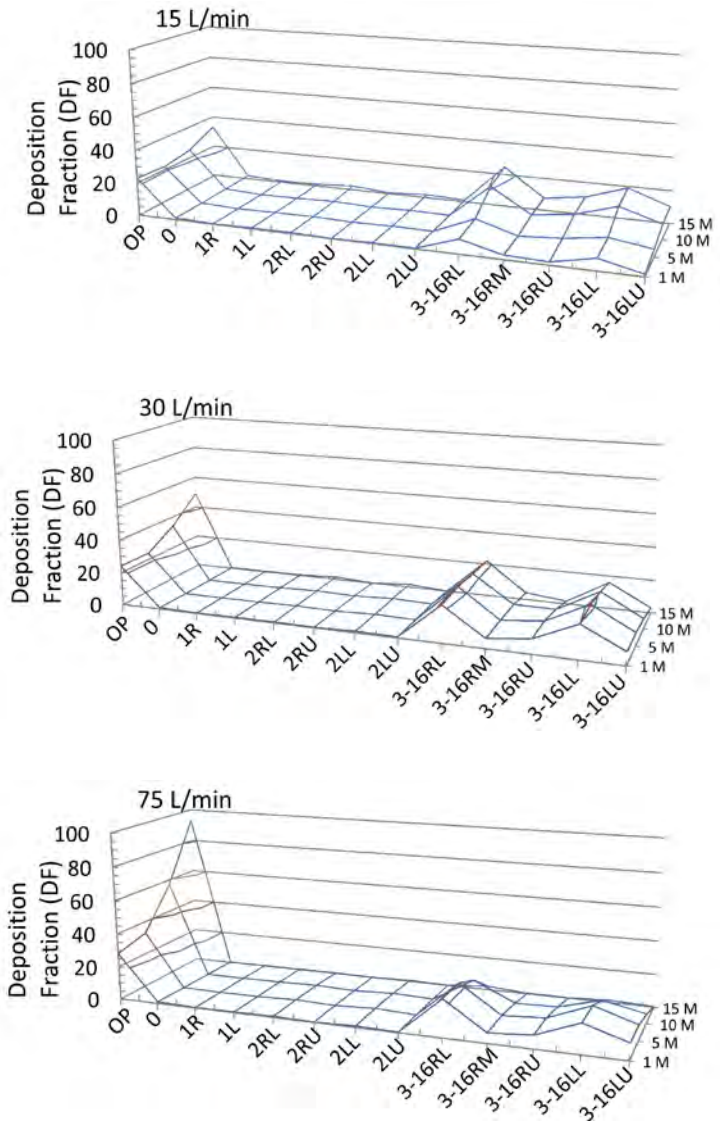

Figure 6.9: Deposition Fraction (DF) of particles in the airway for several sizes and flow rates. OP: oropharynx, 0: trachea, 1R: main right bronchus, 1L: main left bronchus, 2RL: right lower intralobar bronchus, 2RU: right upper intralobar bronchus, 2LL: left lower intralobar bronchus, 2LU: left upper intralobar bronchus, 3-16RL: right lower bronchioles from generation 3 to 16, 3-16RM: right medium bronchioles from generation 3 to 16, 3-16RU: right upper bronchioles from generation 3 to 16, 3-16 LL: left lower bronchioles from generation 3 to 16, 3-16 LU: left upper bronchioles from generations 3 to 16.

As the flow rate increases, the particles tend to be trapped in the oropharyngeal region and the first generations of the lower airways. The same happens when increasing the

particle size.

The obtained results are written in table 6.2 in conjunction with the mentioned in the previous chapter (Conway, 2012) for the same conditions (Tidal volume 1,000 *mL*, Inhalation time 3.33 *s*, Particles 5.76 μm).

	Deposition fraction (%)				
	Right Lung	Left Lung	Trachea	Total thoracic	Extrathoracic
Experimental 18 L/min	38.83	31.20	4.77	74.80	22.70
CFD 15 L/min	40.24	28.84	0.40	69.48	24.00
CFD 30 L/min	37.33	28.92	0.60	66.85	33.00

Table 6.2: Comparison of the deposition fraction between CFD and experimental results

Like the one airway model, the enhanced five airways model reproduces in a right way the flow and particle deposition.

CHAPTER 7
Conclusions and future works

7.1. Conclusions

1. The development of a realistic three-dimensional model of human airways is possible when using images obtained by computerized tomography of the chest to develop the anatomy of the central airways, and mathematical models for the geometry of the peripheral airways to the end of the conducting airway (16^{th} generation of the airways).
2. It is possible to apply computational fluid dynamics (CFD) techniques to study the physiology of respiration, employing the three-dimensional model of the airways previously developed.
3. However, the computational costs for a completely developed airway model are very high and unaffordable, so they are necessary strategies to simplify the calculations, such as using a model partially developed: 8 airway paths are developed up to the sixteenth generation of the airway, and the rest remain truncated. The boundary conditions of the developed branches are applied to the truncated ones by means of a user-defined function (UDF).
4. This model, once developed, allows studying quite accurately the fluid dynamic characteristics of obstructive diseases such as chronic bronchitis or emphysema. This method is more accurate in the case of chronic bronchitis. In the case of emphysema, this model lacking alveoli provides results that are just an approximation to reality.
5. Whit this model it is also possible to study the deposition of inhaled particles in the lung , proving that:
    a. Slow breathing with a low flow (e.g. at rest) causes the particles to go further through the airways, reaching more peripheral lung areas, as gravitational force predominates over the particles. Conversely, high flow breathing (e.g. during exercise) causes the particles to be retained in the oropharyngeal region and the first bronchial tree generations, due to the inertial force that makes impaction behavior to predominate.
    b. The smaller the particles are, the further they will get through the airways. If their size is increased, also the gravitational force increases, which causes the particles to deposit on the walls of the airway.
    c. The angle at which the particles are placed in the mouth (for example inhaling from a dry powder inhaler) does not change the pattern of particle

deposition, because the particles are dragged by the air as the patient inhales, following the curvature of the mouth in every case. So the oropharyngeal deposition is only affected by the flow rate and particle size.

d. Summarizing, to optimize the deposition of an inhaled drug in the lungs, it must be formulated with particles with a MMAD not greater than 5 μm, and it must be avoided to be inhaled with flows higher than 30 *L/min*.

7.2. Conclusiones

1. Es posible elaborar un modelo tridimensional realista de la vía aérea humana usando imágenes del tórax obtenidas mediante tomografía computarizada para desarrollar la anatomía de las vías aéreas centrales (aproximadamente hasta la tercera o cuarta generación), y modelos matemáticos para desarrollar la geometría de las vías aéreas periféricas hasta el final de la vía aérea de conducción (16ª generación).
2. Es posible aplicar las técnicas de dinámica de fluidos computacional (CFD) para estudiar la fisiología de la respiración, empleando para ello el modelo tridimensional de la vía aérea humana previamente desarrollado.
3. Sin embargo, los costes computacionales necesarios para la simulación en un modelo completamente desarrollado de la vía aérea son excesivamente elevados e inasumibles, por lo que son necesarias estrategias para simplificar los cálculos, como por ejemplo emplear un modelo parcialmente desarrollado: únicamente 8 ramales de la vía aérea son desarrollados hasta la decimosexta generación, permaneciendo el resto truncados. Las condiciones de contorno de los ramales desarrollados se aplican a los ramales truncados a través de una función definida por el usuario (UDF).
4. Este modelo permite estudiar de forma suficientemente exacta las características de la dinámica de flujo en las enfermedades pulmonares obstructivas, como la bronquitis crónica y el enfisema pulmonar. Este método es más adecuado para el estudio de la bronquitis crónica. En el enfisema, este modelo carente de alveolos, proporciona resultados que son sólo una aproximación a la realidad.
5. Con este modelo es también posible estudiar el depósito de partículas inhaladas en los pulmones, demostrando que:
    a. La respiración lenta con caudales bajos (como por ejemplo en reposo) hace que las partículas penetren más profundamente en las vías aéreas,

alcanzando regiones del pulmón más periféricas, ya que la fuerza predominante sobre las partículas es la gravitacional. Por el contario, la respiración agitada y con caudales elevados (como en el ejercicio) provoca que las partículas tiendan a quedar atrapadas en la región orofaríngea y en las primeras generaciones de la vía aérea, debido a la fuerza inercial que hace que predomine el comportamiento de choque sobre las partículas.

b. Cuanto más pequeñas sean las partículas inhaladas, más profundamente van a penetrar en las vías aéreas. Al aumentar su tamaño, también se incrementa el efecto de la fuerza gravitacional, provocando que las partículas tiendan a depositarse en las paredes de las vías aéreas.
c. El ángulo en el que las partículas son introducidas en la boca (como por ejemplo al inhalar desde un dispositivo de polvo) no modifica el patrón de depósito de las partículas, puesto que éstas son arrastradas por el aire que el paciente inhala, siguiendo la curvatura de la boca en todos los casos. Por lo tanto, el depósito orofaríngeo sólo se ve afectado por el caudal de flujo y el tamaño de las partículas inhaladas.
d. En resumen, para optimizar el paso de un fármaco inhalado a los pulmones, éste debe de estar compuesto por partículas con un DMMA no superior a 5 μm, y debe evitar ser inhalado con flujos superiores a 30 *L/min*.

7.3.Final reflexions and future works

The highlight of this work is its multidisciplinary character. Computational fluid dynamics is a technique that has been used in the last two decades, but mostly focused on aerospace industry or for the design of new prototype of cars. Timidly, in the last years it has been applied to medicine, but, as demonstrated in the last CFD papers and in the content of the abstracts of the main CFD conferences, almost always applied to the study of circulatory dynamics. Its application to the study of respiratory pathology and to the study of the deposition of inhaled particles in the airways is a great novelty. As noted in the chapters of this thesis, very few groups have investigated a correct way to simulate the lungs, and generally using designs that assume simplifications which make not possible the comparison with a real lung. Furthermore, in Spain, this is a completely new field of investigation. There are only two preceding works to this thesis in which CFD is applied to the study of the respiratory tract, but in both cases, limited to the upper airways. This work is the first

one in Spain to unify this knowledge applied to all the conducting airways, and the results have proven to be consistent with the current knowledge of the subject, obtained through laboratory measurements using more complex methods and not as accurate as CFD.

Another aspect of this work that must be taken in consideration is that it opens a new route to the individualization of treatment for various respiratory diseases. Having available in clinical practice a model of the airways which allows knowing the exact patterns of deposition of inhaled drugs, and which is easily adaptable to each patient based on CT images already available from this patient (or easily obtainable performing a HRCT, which requires much less radiation than conventional CT), allows obtaining individualized treatment plans for the patients, according to their anatomical and functional characteristics and the requirements for their disease. It is not the same treating asthma, in which, because of the distribution of target receptors, is interesting to achieve a uniform deposition of the drug across the whole airways, but also in the most peripheral areas of the lung (adrenergic β2 receptors are located in high density in the airway epithelium between the main bronchi and terminal bronchioles), than treating COPD , where the target receptors (muscarinic M3), are mainly found in the submucosal glands and lymph nodes, and in a lesser degree in the smooth muscle of the airways and in alveolar walls. Therefore, in COPD it must be achieved a more central deposition of the drugs.

Until now, the methods available in clinical practice to study the deposition of inhaled drugs required realizing multiple examinations to the patient after inhaling a radiopharmaceutical drug under strict laboratory conditions. Furthermore, these examinations often require exposing the patient radiation doses that should not be neglected. These difficulties have relegated these methods of study just to the field of research. CFD has been demonstrated to obtain consistent results with these complex experiments, without subjecting the patient to unnecessary examinations, so it is a tool that should be taken into consideration for clinical practice.

However CFD techniques also have limitations. Elaborating adapted models to each patient initially requires several days of work, although, the exploration of new ways to simplify their development, as the use of partially developed models with a limited number of branches of the airways, has allowed to gradually reduce the modeling and simulating times. Also, it must be remembered that the success in the use of CFD techniques primarily lies in having staff with sufficient experience and knowledge in its handling.

In future works, alveoli will be added to the model. Firstly, it will be generated and investigated a model for a single alveolus. The key point of this simulation is that

alveoli are deformable elements affected by expansion and contraction processes. An improved model of the respiratory zone will be generated in a second step. To accomplish this, it will be used a single airway developed between generations 18 and 23, obtained from the previously created bronchial tree model. A set of alveoli will be included in this airway in order to obtain a more accurate description of the flow field of the respiratory zone of the lungs. The simulations on the model of the bronchial tree, including alveoli in the respiratory zone, provide valuable information on the relationship between the volume of the alveoli and the respiratory airflow. Moreover, this model could be used to provide a reasonable estimation of the alveolar pressure.

This study opens a completely new field for the understanding of the mechanisms influencing the deposition of inhaled drugs in the lungs, and could be the basis for future works on an integrated model linking CFD simulations of particle deposition with models of dissolution and absorption of drugs. Also, inhalation of pollutants will be simulated following the same procedure as for the aerosolized drug deposition. The only relevant difference, besides the size and morphology of the particles, is the fact that contaminants are continuously inhaled while the drugs are administered on a small time interval.

The main goal of this project is to have a tool in medical practice that allows the personalization of inhaled drugs, to help the patients with lung diseases to improve its deposition in the lungs. In some selected patients (for example with altered airway structure –lung resections, bronchial dysplasia…-) a high resolution computerized tomography (HRTC) can be performed to obtain detailed images of their airway anatomy to personalize even more the CFD model. HRCT allows obtaining high quality images of the lungs employing lower doses of radiation than in common thoracic CT.

Another advantage of this model is that it allows obtaining more information than the initially provided by tests as PET or SPECT. SPECT can obtain accumulative 2D images of the thorax of the patient to evaluate drug deposition patterns in the lungs. The images obtained by PET can be divided into areas that are either more central or more peripheral and correlated with the degree of radioactivity detected and, therefore, with the dose of drug deposited in each region. Both tests allow estimating the dose of the inhaled drug deposited in the lungs, but in an imprecisely way, dividing the lungs in central or peripheral regions, in upper or lower zones, etc., but they don’t allow knowing with precision in which airways the drug is deposited. The three-dimensional model of the human airways developed for this work, and in which each airway generation is identified by a colour code, can be divided into layers superimposable to the SPECT images, allowing estimating at which level of the airways is deposited the inhaled drug. This method allows maximizing the information obtained by SPECT.

Figures 7.1 and 7.2 show the fully developed airway model divided into layers at different levels of the thorax.

Just to remark once again the relevance of this work, the U.S. Food and Drug Administration (FDA) announced in 2012 a research project in with the main objective was to develop a CFD model of inhaled medication that may account for product characteristics and the physiological parameters of inhaled drugs on the total and regional deposition in the lungs. This project was funded with $250,000.

Summarizing, this thesis intends to leave an open door to future research on this subject, providing the basis to start applying computational fluid dynamics to respiratory medicine.

7.4. Reflexiones finales y trabajos futuros

Lo más destacable del presente trabajo es su carácter multidisciplinar. La dinámica de fluidos computacional es una técnica que ya lleva años desarrollándose, pero casi siempre centrada en el entorno de la industria aeroespacial o en el diseño de nuevos prototipos de coches. Tímidamente, en los últimos años ha ido despuntando aplicada a la medicina, pero tal y como demuestran las últimas publicaciones de trabajos y el contenido de los resúmenes de los principales congresos de CFD, casi siempre aplicada al estudio de la dinámica circulatoria. Su aplicación al estudio de las patologías pulmonares y al depósito de partículas inhaladas en la vía respiratoria supone una gran novedad. Como se ha señalado en los capítulos de esta tesis, son muy pocos los grupos que han investigado una manera correcta de simular los pulmones, empleando diseños que generalmente asumen simplificaciones que no los hacen comparables a un pulmón real. Además, en España, éste es un campo aun totalmente novedoso. Únicamente existen dos trabajos precedentes a esta tesis en los que se aplique la CFD al estudio de las vías respiratorias, pero en ambos casos circunscrito a la vía respiratoria superior. Este trabajo es el primero en España que trata de aunar los conocimientos aplicados a toda la vía aérea de conducción, y sus resultados han demostrado ser concordantes con el conocimiento actual del tema obtenido a través de mediciones en laboratorio empleando métodos mucho más complejos y no tan precisos.

Otro aspecto a destacar de este trabajo es que abre una nueva vía a la individualización de los tratamientos para las distintas patologías respiratorias. El disponer en la práctica clínica de un modelo de la vía aérea que permite conocer con exactitud patrones de depósito de fármacos inhalados, y que es fácilmente adaptable a cada paciente basándose en imágenes en TC que ya se dispongan de ese paciente (o que pueden obtenerse fácilmente realizando un TCAR, que requiere de mucha menos radiación que un TC convencional), permite establecer planes de tratamiento individualizados para los pacientes, acordes con sus características anatómicas y funcionales y los requerimientos para su enfermedad. No es lo mismo tratar el asma, en el que por la distribución de los receptores diana interesa tener un depósito uniforme del fármaco en toda la vía aérea, pero con gran interés en que llegue a las zonas más periféricas del pulmón (los receptores adrenérgicos β2 se encuentran en alta densidad en el epitelio de la vía aérea comprendida entre bronquios principales y bronquiolos terminales), que tratar la EPOC, en la que los receptores diana son los muscarínicos M3, que se encuentran principalmente en las glándulas submucosas y ganglios del pulmón, y en menor proporción en músculo liso de las vías aéreas, nervios y pared alveolar. Por lo tanto en esta patología interesaría un depósito más central del fármaco.

Hasta la actualidad los únicos métodos disponibles en la práctica clínica para estudiar el depósito de fármacos inhalados requerían someter al paciente a múltiples exploraciones tras haber inhalado en estrictas condiciones de laboratorio un radiofármaco. Además, estas exploraciones usualmente requieren exponer al paciente a dosis de radiación que no deben ser desdeñadas. Todo esto hace que estos métodos de estudio queden relegados únicamente al ámbito de la investigación. La CFD ha demostrado obtener resultados concordantes a estos complejos estudios sin necesidad de someter al paciente a exploraciones innecesarias, por lo que es una herramienta que debe ser tenida en consideración para la práctica clínica.

No obstante las técnicas de CFD también presentan limitaciones. El elaborar un modelo adaptado a cada paciente requiere inicialmente de varios días de trabajo, aunque según se han ido explorando nuevos métodos para simplificar su desarrollo, como el empleo de modelos parcialmente desarrollados a través de una serie de ramales de la vía aérea, ha ido permitiendo reducir paulatinamente los tiempos de modelado y simulación. Además, hay que recordar que el éxito en el uso de las técnicas de CFD reside fundamentalmente en disponer de personal con suficiente experiencia y conocimientos en su manejo.

Otra ventaja de este modelo es que permite obtener más información de la que proporcionan inicialmente pruebas como el PET o el SPECT. El SPECT permite obtener imágenes bidimensionales acumulativas del tórax para evaluar el patrón de depósito

del fármaco administrado al paciente. Las imágenes obtenidas en el PET pueden ser divididas en zonas centrales o periféricas y correlacionadas con el grado de radioactividad detectado, y por tanto con la dosis de fármaco depositada en cada región. Ambos métodos permiten estimar la cantidad de fármaco depositado en el pulmón de manera poco precisa, dividiendo en pulmón en zonas más centrales o periféricas, en zonas superiores e inferiores, etc., pero no permiten conocer con exactitud en qué vías respiratorias está depositado. El modelo tridimensional de las vías aéreas desarrollado para este trabajo, y en el que cada generación de la vía aérea está identificada por un código de color, puede dividirse en capas superponibles a las imágenes del SPECT, permitiendo estimar a qué nivel se encuentra depositado el fármaco. De este modo, permitiría maximizar la información obtenida por el SPECT.

Las imágenes 7.1 y 7.2 muestran el modelo completamente desarrollado, y dividido en capas a distintas alturas del tórax.

Para remarcar una vez más la relevancia de este trabajo, la Administración de Comida y Fármacos de Estados Unidos (FDA por sus siglas en inglés, Food and Drug Administration) anunció en 2012 un proyecto de investigación en el que el principal objetivo era desarrollar un modelo de CFD para medicación inhalada que permitiese conocer las características y los parámetros fisiológicos que rigen el depósito de los fármacos. Este proyecto fue financiado con 250,000$.

En resumen, este trabajo pretende dejar abiertas las puertas a futuras investigaciones en el tema, proporcionando las bases para iniciarse en la aplicación de la dinámica de fluidos computacional a la neumología.

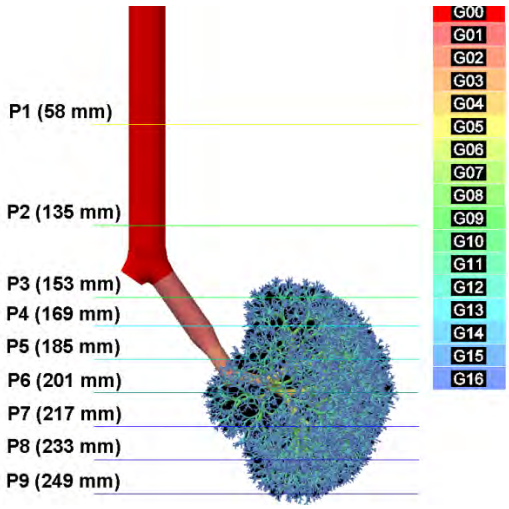

Figure 7.1: Fully developed airway model divided into 9 transversal sections (P1-P9). The different branches are represented in a range of colours.

Figura 7.1: Modelo complete de la vía aérea dividido en 9 secciones a diferentes Alturas (P1-P9). Las diferentes generaciones de la vía aérea están identificadas con colores.

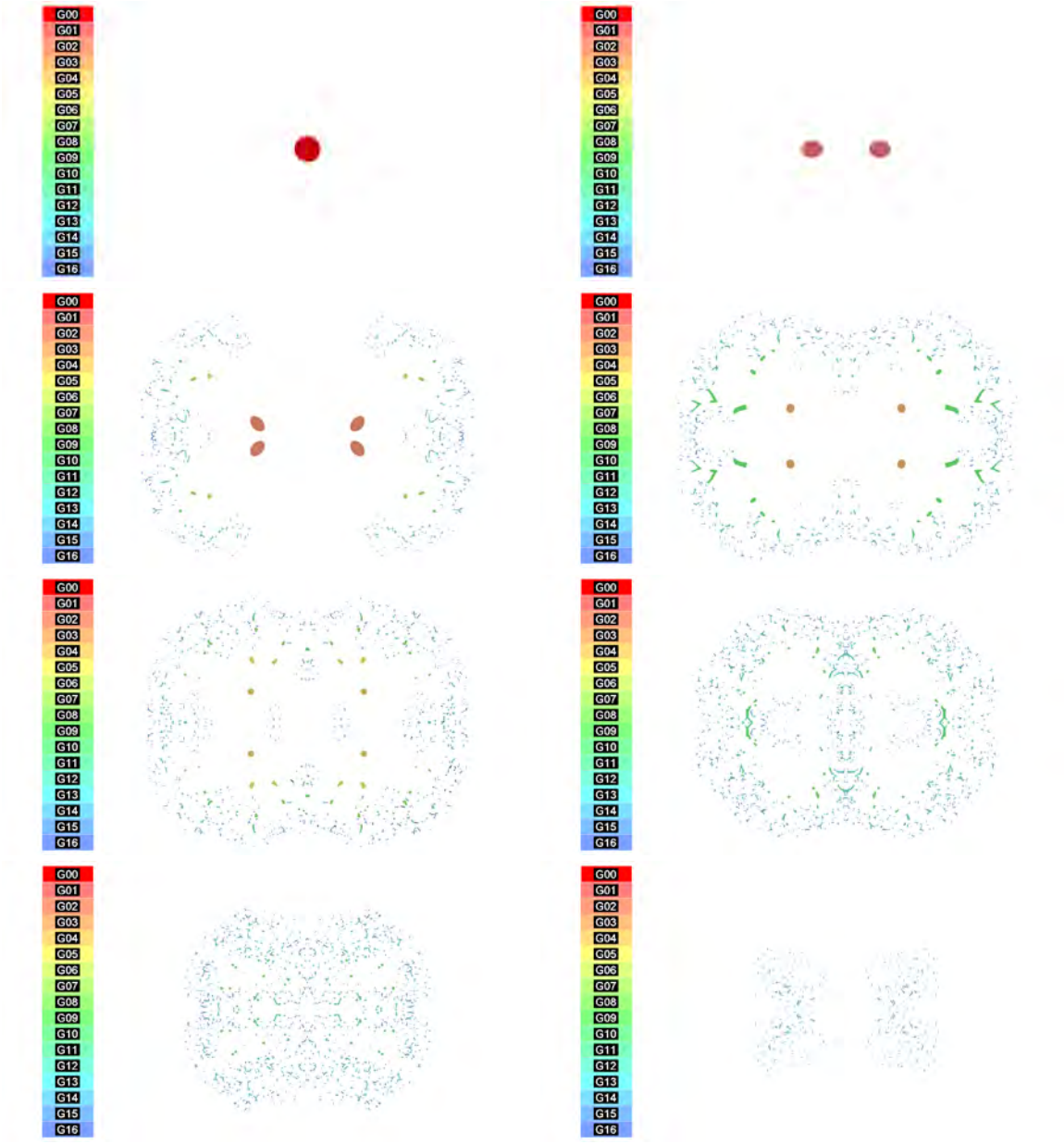

Figure 7.2: Representation of 8 of de 9 transversal sections (P2-P9). The identification of each branch in these sections is done through the colour scale.

Figure 7.2: Representación de 8 de las 9 secciones transversales del modelo (P2-P9). Puede identificarse cada generación de la vía aérea mediante la escala de colores.

References

Adler K and Brucker C. Dynamic flow in a realistic model of the upper human lung airways. Exp. Fluids. 2007; 43:411–23.

Aerosols. In: United States Pharmacopeia. Webcom Limited: Toronto, 2006: 2617-2636

Agustí A GN, Función pulmonar aplicada: puntos clave. Mosby/Doyma Libros, 1995, Barcelona.

Altiere RJ and Thompson DC, Physiology and Pharmacology of the Airways. In: Inhalation Aerosols, 2d Edition, Informa Healthcare (2007).

Altshuler B, Yarmus L and Palmes ED. Aerosols deposition in the human respiratory tract. Arch Environ Health 1957; 15:292-303

American Thoracic Society and European Respiratory Society Task Force on asthma. An official American Thoracic Society/European Respiratory Society Statement: Asthma control and exacerbations. Am J Respir Crit Care Med 2009; 180:59-99

Ansys Fluent version 6.3.26, 2006, 10 Cavendish Court, Lebanon, NH03766.

Ansys Gambit version 2.4.6, 2006, 10 Cavendish Court, Lebanon, NH03766.

Aránguez E, Ordóñez JM, Serrano J, Aragonés N, Fernández-Patier R, Gandarillas a, Galán I. Contaminantes atmosférico y su vigilancia. Rev esp salud pública 1999; 73: 123-132

Ashworth HL, Wilson CG, Sims EE, Wotton PK and Hardy JG. Delivery of propellant soluble drug from a metered dose inhaler. Thorax 1991; 46: 245-247

Ball CG, Uddin M and Pollard A. High resolution turbulence modelling of airflow in an idealised human extrathoracic airway. Comput Fluids 2008; 37:943–64

Ball CG, Uddin M and Pollard A. Mean flow structures inside the human upper airway. Flow Turbul Combust 2008; 81:155–88

Baird C. Compuestos químicos que destruyen el ozono. In: Domenech X. Química ambiental. 2nd ed. Spain: Reverté; 2001. p 63-75

Baird C. El efecto invernadero y el calentamiento global. In: Domenech X. Química ambiental. 2nd ed. Spain: Reverté; 2001. p 179-225

Basbaum CB and Finkbeiner WE. Mucus-secreting cells of the airways. In: Massaro D, ed. Lung Cell Biology. New York: Marcel Dekker, 1989: 37-39

Beekmans JM. The deposition of aerosols in the respiratory tract. Can J Physiol Pharmacol 1965; 43: 157-172

Böhm GM. Air pollution and lung cancer. Cancer Detect Prev 1982; 5(4): 371-374

Brain DD. Free cells in the lungs- some aspects of their role, quantitation and regulatory. Arch Int Med 1970; 126: 477-487

Burton, R. T., Isaacs, K. K., Fleming, J. S. and Martonen, T. B. Computer Reconstruction of a Human Lung Boundary Model From Magnetic Resonance Images. Respiratory Care 2004; 49(2):180-185.

Camps PWL. A note on the inhalation treatment of asthma. Guy´s Hosp Report 1929; 79: 496-498

Castairs J, Nimmo A and Barnes P. Autoradiographic visualization of beta-adrenoceptor subtypes in a human lung. Am Rev Respir Dis 1985; 132: 451-547.

Castro-Ruiz Pilar. Análisis computarizado del flujo aéreo en cavidad nasal. Tesis Doctoral. Universidad Autónoma de Madrid. 2003.

Cates CJ and Rowe BH. Holding chambers versus nebulisers for beta-agonist treatment of acute asthma (Cochrane review). The Cochrane Library. Oxford: Update Software 2001; 3

Chan TL, Lippinann M, Cohen VR and Schlesinger RB. Effect of electrostatic charges on particle deposition in a hollow cast of the human larynx tracheobronchial tree. J Aerosol Sci 1978; 9:463–475.

Chan HK and Chew NYK. Novel alternative methods for the delivery of drugs for the treatment of asthma. Adv Drug Del Rev 2003; 55: 793-805

Concessio NM, VanOort NM, Knowles MR and Hickey AJ. Pharmaceutical dry powder aerosols: correlation of powder properties with dose delivery and implications for pharmacodynamics effect. Pharmaceut Res 1999; 16: 828-834

Conway J, Fleming J, Majoral C, Katz I, Perchet D, Peebles Ch, Tossici-Bolt L, Collier L, Caillibotte G, Pichelin M, Sauret-Jackson V, Martonen T, Apiou-Sbirlea G, Muellinger B, Kroneberg Ph, Gleske J, Scheuch G, Texereau J, Martin A, Montesantos S and Bennett M. Controlled, parametric, individualized, 2-D and 3-D imaging measurements of aerosol deposition in the respiratory tract of healthy human subjects for model validation, Journal of Aerosol Science 2012 Oct; 52: 1–17.

Cordasco EM and Van Ordstrand HS. Air pollution and COPD. Postgrad Med 1977 Jul; 62 (1): 124-127

Daniels T, Mills N, Whitaker P. Nebuliser systems for drug delivery in cystic fibrosis. Cochrane Database of Systematic Reviews 2013 Issue 4. Art. No: CD007639.

Davies CN. A formalized anatomy of the human respiratory tract. In: Davies CN, ed. Inhaled Particles and Vapours. Oxford: Pergamon Press, 1961: 82-87

Davis DL, Bell ML and Fletcher T. A look back at the London smog of 1952 and the half century since. Environ Health Perspect 2002 Dec; 110 (12): A734-735.

De Backer J, Vos W, Gorlé C, Germonpré P, Partoens B, Wuyts F, Parizel P and De Backer W. Flow analyses in the lower airways: Patient-specific model and boundary conditions. Medical Engineering & Physics 2008; 30: 872–879

De Backer JW, Vos WG, Vinchurkar SC, Claes R, Drollmann A, Wulfrank D, Parizel PM, Germonpré P and De Backer W., Validation of computational fluid dynamics in CT-based airway models with SPECT/CT. Radiology. 2010 Dec; 257(3):854-62.

Dolovich M, Ruffin RE, Roberts R and Newhouse MT. Optimal delivery of aerosols from metered dose inhalers. Chest 1981; 80 (Suppl 6): s911-s915

Dolovich M and Labiris R. Imaging drug delivery and drug responses in the lung. Proc Am Thorac Soc 2004; 1(4): 329-37

Elghobashi SE and Abou-Arab WT. On predicting particle-laden turbulent flows. Applied Science Research 1994, 52:309–329.

European Lung Foundation. Efectos sobre la salud de la contaminación del aire exterior [Internet]. Sheffield: European Lung Foundation; [cited 2013 Oct 28]; [about 2 screens]. Avalaible from: http://www.es.european-lung-foundation.org/17443-efectos -sobre-la-salud-de-la-contaminacion-del-aire-exterior.htm.

Fadl A, Wang J and Zhang Z. Metered-dose inhaler efficiency enhancement: a case study and novel design. Inhal Toxicol. 2010 Jun; 22(7):601-9

Fernández J, Marín F, García JM. Enfermedad pulmonar obstructiva crónica (EPOC). Tratamiento del paciente estable. In: Soto Campos JG. Manual de diagnóstico y terapéutica en neumología. Madrid: Ergon; 2010. p. 321-331

Findeisen W. Uber das Absetzen kleiner, in der Luft suspendierter Teilchen in der menschlichen Lunge bei der Atmung. Arch Ges Physiol 1935; 236: 367-379

Folkesson HG, Matthey MA, Westrom BR, Kim KJ, Karlsson BW and Hastings RH. Alveolar epithelial clearance of protein. J Appl Physiol 1996; 80: 1431-1445

Freitas RK and Schröder W. Numerical investigation of the three-dimensional flow in a human lung model. Journal of Biomechanics 2008; 41:2446–2457.

Fresconi FE and Prasad AK. Secondary velocity fields in the conducting airways of the human lung. J. Biomech. Eng. Trans. 2007; ASME 129:722–32.

Gabrio BJ, Stein SW and Velasquez DJ. A new method to evaluate plume characteristics of hidrofluoroalkane and chlorofluorocarbon metered dose inhalers. Int J Pharm 1999; 186: 3-12

Gail D and Lenfant JCM. Cells of the lung: neology and clinical implications. Am Rev Respir Dis 1983; 127: 366-387

García de Vinuesa Broncano G, García de Vinuesa Calvo G. Exploración funcional respiratoria: aplicación clínica. In: Soto Campos JG. Manual de diagnóstico y terapéutica en neumología. Madrid: Ergon; 2010. p. 73-88

García Río F, Prados Sánchez C, Villamar León J and Álvarez-Sala Walter R. Aerosoles, inhaladores, nebulizadores y humidificadores. Bases teóricas y aplicaciones prácticas de la aerosolterapia y de la ventiloterapia. Medicine 1997; 7:1779-1785

Gea J. Aspectos estructurales y mecánicos del pulmón. In: Casan P, García F, Gea J. Fisiología y biología respiratorias. Madrid (Spain): Ergon; 2007. p 23-29

Gemci T, Ponyavin V, Chen Y, Chen H and Collins R. Computational model of airflow in upper 17 generations of human respiratory tract. J. Biomech. 2008; 41:2047–54.

Giner J, Basualdo LV, Casan P, Hernández C, Macián V, Martínez I et al. Normativa sobre la utilización de fármacos inhalados. Arch Bronconeumol 2000; 36:34-43

Global Statregy for the diagnosis, management and prevention of COPD, Global initiative for Chronic Obstructive Lung Disease (GOLD) 2013. Avalaible from: http://www.gold copd.org

Grgic B, Finlay WH, Burnell PKP, Heenan AF. In vitro intersubject and intrasubject deposition measurements in realistic mouth–throat geometries. Journal of Aerosol Science 2004, 35(8), 1025–1040.

Grosse S, Schroder W, Klaas M, Klockner A and Roggenkamp J. Time resolved analysis of steady and oscillating flow in the upper human airways. Exp. Fluids. 2007; 42:955–970.

Grupo de trabajo de GesEPOC. Guía de práctica clínica para el diagnóstico y tratamiento de pacientes con Enfermedad Pulmonar Obstructiva Crónica (EPOC) – Guía española de la EPOC (GesEPOC). Arch bronconeumol 2012, 48(supl 1):2-58

Guía Española para el Manejo del Asma (GEMA 2009). Arch Bronconeumol 2009; 45(7):1-35. http://www.gemasma.com.

Hammersley, J. and Olson, D. Physical Models of the Smaller Pulmonary Airways. J Appl Physiol 1992; 72(6):2402-2414.

Hegedüs, Cs. J., Balásházy, I., and Farkas, Á. Detailed Mathematical Description of the Geometry of Airway Bifurcations. Respiratory physiology & neurobiology 2004; 141(1):99-114.

Heyder J. Particle transport onto human airway surfaces. Eur J Respir Dis 1982; 63 (Suppl 119):29-50

Hickey AJ and Crowder TM. Next generation dry powder inhalation delivery systems. En: Hickey AJ, editor. Inhalation aerosols. Physical and biological basis for therapy. 2nd ed. New York: Informa Healthcare USA; 2007: 445-460

Hofmann W, Martonen TB and Graham RC. Predicted deposition of nonhygroscopic aerosols in the human lung as a function of subject age. J Aerosol Med 1989; 2:49–68.

Horsfield, K., and Cumming, G. Morphology of the Bronchial Tree in Man. J Appl Physiol 1968, 24(3):373-383.

Horsfield K. The relation between the structure and function in the airways of the lung. Brit J Dis Chest. 1974; 68:145-160.

Hyatt, R. E. and Wilcox, R. E. The Pressure-Flow Relationship of the Intrathoracic Airways in Man. Journal of clinical investigation 1963; 42:29-39.

Inthavong K, Choi LT, Tu J, Ding S and Thien F., Micron particle deposition in a tracheobronchial airway model under different breathing conditions. Medical Engineering & Physics 2010 Dec; 32(10):1198-212.

Jackson WF. Nebulised budesonide therapy in asthma. A scientific and practical review. Lund: Astra Draco AB; 1995

Johnson M, Newman S, Bloom R, Talaee N and Clarke S. Delivery of albuterol and ipratropium bromide from two nebulizer systems in chronic stable asthma. Chest 1989; 96(1): 6-10

Kitaoka H, Takaki R and Suki B. A three-dimensional model of the human tree. J. Applied Physiology 1999; 87:2207-2217.

Keller R. Air pollution and lung diseases in adults. Soz Praventivmed 1986; 31(1):12-15

Kleinstreuer C, Shi H and Zhang Z. Computational analyses of a pressurized metered dose inhaler and a new drug-aerosol targeting methodology. J Aerosol Med 2007 Fall; 20(3):294-309.

Kleinstreuer C, Zhang Z and Donohue JF. Targeted drug-aerosol delivery in the human respiratory system. Annu Rev Biomed Eng 2008; 10:195-220

Kleinstreuer C, Shi H and Zhang Z. Airflow and Particle Transport in the Human Annual Review of Fluid Mechanics 2010, Vol. 42: 301-334

Labiris N and Dolovich M. Pulmonary drug delivery. Part I: Physiological factors affecting therapeutic effectiveness of aerosolized medications. Br J Clin Pharmacol 2003; 56:588-599.

Labiris N and Dolovich M. Pulmonary drug delivery. Part II: The role of inhalant delivery devices and drug formulations in therapeutic effectiveness of aerosolized medications. Br J Clin Pharmacol 2003; 56:600-612.

Landahl HD. On the removal of air-borne droplets by the human respiratory tract: 1. The lung. Bull Math Biophys. 1950; 12:43–51.

Lange CF and Finlay WH. Overcoming the adverse effect of humidity in aerosol delivery via pressurized metered-dose inhalers during mechanical ventilation. Am J Respir Crit Care Med 2000; 161(5):1614-8

Leach C. Targeting inhaled steroids. Int J Clin Pract Suppl 1998; 96:23-27

Leach CL. Relevance of radiolabeled steroid inhalation studies to clinical outcomes. J Aerosol Med 1998; 11(suppl 1):S29-S34

Leach CL, Bethke TD, Boudreau RJ, Hasselquist BE, Drollman A, Davidson P, et al. Two-dimensional and three-dimensional imaging show ciclesonide has high lung deposition and peripheral distribution: a nonrandomized study in healthy volunteers. J Aerosol Med 2006; 19:117-126

Lippmann M, Yeates DB and Albert RE. Deposition, retention and clearance of inhaled particles. Br J Ind Med 1980; 37(4):337–362

Liu, Y., So, R. M. C. and Zhang, C. H. Modeling the Bifurcating Flow in a Human Lung Airway. Journal of Biomechanics 2002; 35(4):465-473.

Longest PW, McLeskey JT and Hindle M. Characterization of nanoaerosol size change during enhanced condensational growth. Aerosol Sci Technol 2010; 44:473–483.

Longest PW and Hindle M. Numerical model to characterize the size increase of combination drug and hygroscopic excipient nanoparticle aerosols. Aerosol Sci Technol 2011; 45(7):884–899

Longest PW, Tian G, Delvadia R, Hindle M. Development of a stochastic individual path (SIP) model for predicting the deposition of pharmaceutical aerosols: effects of turbulence, polydisperse aerosol size, and evaluation of multiple lung lobes. Aerosol Sci Technol 2012; 46:12, 1271-1285

Lourenco RV and Cotromanes E. Clinical aerosols. I. Characterization of aerosols and their diagnostic uses. Arch Intern Med 1982; 142:2163-2172

Luo, H. Y., Liu, Y., and Yang, X. L. Particle deposition in obstructed airways. J. Biomech 2007; 40(14):3096–3104.

Ma, B. and Lutchen, K. R. An anatomically based hybrid computational model of the human lung and its application to low frequency oscillatory mechanics. Annals of Biomedical Engineering 2006; 34(11):1691-1704.

Mak J and Barnes P, Autoradiographic visualization of muscarinic receptor subtypes in human and guinea pig lung. Am Rev Respir Dis 1990; 141:1559-1568.

Martínez-Martínez BE and Salgado-Aguilar G. Aerosolterapia. Neumol Cir Torax 2003; 62(1):24-28

Martonen TB. Analytical model of hygroscopic particle behavior in human airways. Bull Math Biol 1982; 44:425–442.

Martonen TB. The behavior of cigarette smoke in human airways. Am Ind Hyg Assoc J. 1992; 53:6–15.

Martonen TB. Mathematical model for the selective deposition of inhaled pharmaceuticals. J Pharm Sci 1993; 82:1191–1199.

Martonen TB and Katz I. Deposition patterns of polydisperse aerosols within human lungs. J Aerosol Med 1993; 6:251–274.

Martonen T and Katz I. Deposition patterns of aerosolized drugs within human lungs: effect of ventilatory parameters. Pharm Res 1993; 10:871–878.

Martonen TB and Katz I. Inter-related effects of morphology and ventilation on drug deposition patterns. STP Pharm Sci. 1994; 4:11–18.

Martonen, T.B., Schroeter, J.D. and Fleming, J.S. 3D in silico modeling of the human respiratory system for inhaled drug delivery and imaging analysis Journal of Pharmaceutical Sciences 2007; 96(3):603-617,

Martonen TB, Zhang Z and Lessmann R. Fluid dynamics of the human larynx and upper tracheobronchial airways. Aerosol Sci Technol 1993; 19:133–156.

McKee DJ. Tropospheric ozone: human health and agricultural impacts. Boca Ratón. Lewis Publishers; 1993.

Mercer TT. Production of therapeutic aerosols; principles and techniques. Chest 1981; 80 (suppl):818-820

Miller MR, Hankinson J, Brusasco V, Burgos F, Casaburi R, Coates A *et al.* Standardisation of spirometry. Eur respire J 2005; 26:319-338

Moin P, Kim J. Tackling Turbulence with Supercomputers. Scientific American 1997; 276(1):62-68

Montesantos S, Katz I, Fleming J, Majoral C, Pichelin M, Dubau C, Piednoir B, Conway J, Texerau J and Caillibotte G. Airway morphology from high resolution computed tomography in healthy subjects and patients with moderate persistent asthma. Anat Rec 2013 Jun; 296: 852–866

Muir DCF, Sweetland K and Love RG. Inhaled aerosol boluses in man. In: Walton WH, ed. Inhaled Particles 111. Sheffield, U.K.: Gresham Press. 1971; 81–90.

Mylavarapu G, Murugappan S, Mihaescu M, Kalra M, Khosla S and Gutmark E, Validation of computational fluid dynamics methodology used for human upper airway flow simulations. Journal of biomechanics 2009; 42(10):1553-1559.

Neher JO and Koenig JQ. Health effects of outdoor air pollution. Am Fam Physician 1994 May 1; 49(6): 1397-1404, 1407-1408.

Newhouse M, Sanchís J and Bienenstock J. Lung defense mechanisms. N Engl J Med 1976; 295:990-998

Newhouse MT and Kennedy A. Condensation due to rapid, large temperature (t) changes impairs aerosol dispersion from Turbuhaler (T). Am J Respir Cell Mol Biol 2000; 161:A35

Newman SP, Pavia D, Moren F, Sheahan NF and Clarke SW. Deposition of pressurized aerosols in the human respiratory tract. Thorax 1981; 36:52-55

Newman SP and Clarke SW. Therapeutic aerosols 1- physical and practical considerations. Thorax 1983; 38:881-886

Newman SP. Aerosol deposition considerations in inhalation therapy. Chest 1985; 88(Suppl): 152s-160s

Newman SP, Weisz AWB, Talaee N and Clarke SW. Improvement of drug delivery with breath actuated pressurized aerosol for patients with poor inhaler technique. Thorax 1991; 46:712-716

Newman SP. A comparison of lung deposition patterns between different asthma inhalers. J Aerosol Med 1995; (suppl 3):S21-S26

Niewoehner DE. Relacione entre la estructura y la función: fisiopatología de la obstrucción al flujo aéreo. In: Stockley R, Rennard S, Rabe K, Celli B. Enfermedad pulmonar obstructiva crónica. Massachussets (E stados Unidos): Blackwell Publishing Ltd; 2008. p 3-19

Nowak, N., Kadake, P. P. and Annapragada, A. V. Computational Fluid Dynamics Simulation of Airflow and Aerosol Deposition in Human Lungs. Annals of Biomedical Engineering 2003; 31(4):374-390

O'Callaghan C and Barry PW. The science of nebulized drug delivery. Thorax 1997; 52(suppl 2):s31-s44

Patankar, SV. Numerical Heat Transfer and Fluid Flow. Hemisphere, Washington D.C., 1980

Prime D, Atkins PJ, Slater A and Sumby B. Review of dry powder inhaler. Adv Drug Del Rev 1997; 26:51-58

Pritchard JN. Particle growth in the airways and the influence of airflow. En: Newman SP, Morén F, Crompton GK, editores. A new concept in inhalation therapy. Bussum: Medicom; 1987. p3-24

Querol, X. Calidad del aire, partículas en suspensión y metales. Rev Esp Salud Pública 2008; 82:447-454.

Quispe Apaclla César, 2010. Estudio del flujo de aire a través de las fosas nasales en la inspiración y espiración, considerando el intercambio de calor existente. Tesis Doctoral. Universidad de Valladolid.

Rau JL. The inhalation of drugs: advantages and problems. Respir Care 2005; 50(3):367-382

Raabe, O. G.,Yeh, H. C., Schum, G. M. and Phalen, R. F. Tracheobronchial geometry: Human, dog, rat, hamster (LF-53) 1976. Albuquerque, NM: Lovelace Foundation for Medical Education and Research.

Robinson, R. J., Oldham, M. J., Clinkenbeard, R. E., and Rai, P. Experimental and numerical analysis of a 7 generation human replica tracheobronchial model. Ann. Biomed. Eng. 2006, 34(3):373–383

Rouvière H., Delmas A. Estructuras anatómicas de los aparatos digestivo y respiratorio contenidas en la cabeza y el cuello. En: Götzens V, coordinador. Anatomía humana descriptiva, topográfica y funcional. Tomo I. Cabeza y cuello. 10ª edición. Barcelona: Masson; 2002. p. 388-462

Sala E, Agustí A. EPOC. In: Casan P, García F, Gea J. Fisiología y biología respiratorias. Madrid (Spain): Ergon; 2007. p 389-416

Sandeau J, Katz I, Fodil R, Louis B, Apiou-Sbirlea G, Caillibotte G and Isabey D. CFD simulation of particle deposition in a reconstructed human oral extrathoracic airway for air and helium–oxygen mixtures. Journal of Aerosol Science 2010 March; 41(3):281–294

Satir P and Sleigh MA. The physiology of cilia and mucociliary interactions. Ann Rev Physiol 1990; 52:137-155

Sauret, V., Goatman, K. A., Fleming, J. S., and Bailey, A. G. Semi-Automated Tabulation of the 3D Topology and Morphology of Branching Networks Using CT: Application to the Airway Tree. Phys Med Biol 1999; 44(7):1625-1638.

Sbirlea-Apiou G, Katz I, Caillibotte G, Martonen T and Yang Y. Deposition mechanics of pharmaceutical particles in human airways. En: Hickey AJ, editor. Inhalation aerosols. Physical and biological basis for therapy. 2nd ed. New York: Informa Healthcare USA; 2007: 1-30

Scheuch G and Stahlhofen W. Particle deposition of inhaled aerosol boluses in the upper human airways. J Aerosol Med 1988; 1:29–36.

Schmidt, A., Zidowitz, S., Kriete, A., Denhard, T., Krass, S., and Pietgen, H.-O. A Digital Reference Model of the Human Bronchial Tree. Computerized medical imaging and graphics 2004; 28(4):203-211.

Sera, T., Fujioka, H., Yokota, H., Makinouchi, A., Himeno, R., Schroter, R. C. and Tanishita, K. Three-Dimensional Visualization and Morphometry of Small Airways From Microfocal X-Ray Computed Tomography. Journal of Biomechanics 2003; 36(11):1587-1594.

Sevilla-Sánchez D, Soy-Muner D and Soler-Porcar N. Utilidad de los macrólidos como antiinflamatorios en las enfermedades respiratorias. Arch Bronconeumol 2010; 46:244-54

Stapelton KW, Guentsch E, Hoskinson MK, Finlay WH. On the suitability of the κ-ε turbulence modeling for aerosol deposition in the mouth and throat: a comparison with experiment. J Aerosol Sci 31: 739–749, 2000

Summers QA. Inhaled drugs and the lung. Clin Exp Allergy 1991; 21:259-268

Taburet AM. and Schmit B. Pharmacokinetic optimization of asthma treatment. Clin Pharmacokinet 1994; 26:396-418

Tawhai, M. H., and Burrowes, K. S. Developing Integrative Computational Models of Pulmonary Structure. Anatomical record 2003; 275B(1):207-218.

Terzano C and Colombo P. State of the art and new perspectives on dry powder inhalers. Eur Rev Med Pharmacol Sci 1999; 3:247-254

Theunissen R and Riethmuller ML. Particle image velocimetry in lung bifurcation models. In Particle Image Velocimetry: New Developments and Recent Applications, ed. A Schroder, CE Willert. 2008; pp. 73–101. Berlin: Springer.

Versteeg, HK and Malalasekera, W. An Introduction to Computational Fluid Dynamics, 2007. Harlow: Pearson

Virchow JC, Kroegel C and Matthys H. Antiasthma drug delivery: what is on the horizon? Clin Pharmacokinetic 1994; 27:85-93

Walters, D.K. and Luke, W. H. A Method for Three-Dimensional Navier-Stokes Simulations of Large-Scale Regions of the Human Lung Airway. Journal of Fluids Engineering 2010; 132(5): 01-1 to 01-8.

Walters, D.K. and Luke, W.H. Computational Fluid Dynamics Simulations of Particle Deposition in Large-Scale, Multi-Generational Lung Models. ASME Journal of Biomechanical Engineering 2011; vol 133, No. 011003.

Walters, D.K., Burgreen, G.W., Lavallee, D.M., Thompson, D.S., and Hester, R.L. Efficient, Physiologically Realistic Lung Airflow Simulations. IEEE Transactions in Biomedical Engineering 2011; 58(10):3016-3019.

Walters, D.K., Burgreen, G.W., Hester, R.L., Thompson, D.S., Lavallee, D.M., Pruett, W.A. and Ford-Green, J. Simulations of Cyclic Breathing in the Conducting Zone of the Human Lung. ASME Paper 2012, No. FEDSM2012-72474.

Weibel, E. R. Morphometry of the human lung. Springer-Verlag, 1963.

World Health Organization. Sulphur oxides and suspended particulate matter. Environ health criteria 8. Geneve: World Health Organization; 1979.

World Health Organization. Air quality guidelines for Europe. Who regional ublications. European series No 23. Copenhagen, 1987.

Yang XL. Respiratory flow in obstructed airways. J Biomech 2006; 39:2743–2751

Yang, X. L., Liu, Y., So, R. M. C., and Yang, J. M. The Effect of Inlet Velocity Profile on the Bifurcation COPD Airway Flow. Comput Biol Med 2006; 36(2):181–194.

Zhang, Z., Kleinstreuer, C. and Kim, C. Flow Structure and Particle Transport in a Triple Bifurcation Airway Model. Journal of Fluids Engineering 2001; 123(2):320-330.

Zhang, Z. and Kleinstreuer, C. Transient Airflow Structures and Particle Transport in a Sequentially Branching Lung Airway Model. Physics of Fluids 2002; 14(2):862-880.

Zhang, Z., and Kleinstreuer, C. Airflow structures and nano-particle deposition in a human upper airway model. Journal of computational physics 2004; 198(1):178-210.

Zhang, Z., Kleinstreuer, C., Donohue, J. F. and Kim, C. S. Comparison of micro- and nano-size particle depositions in a human upper airway model. Journal of Aerosol Science 2005, 36, 211.

Zhang Z, Kleinstreuer C and Kim CS. Airflow and nanoparticle deposition in a 16-generation tracheobronchial airway model. Ann Biomed Eng 2008; 36:2095–2110

Zhang Z, Kleinstreuer C and Kim CS. Comparison of analytical and CFD models with regard to micron particle deposition in a human 16-generation tracheobronchial airway model. J Aerosol Sci 2009; 40:16–28

Zhang, Z., and Kleinstreuer, C. Computational analysis of airflow and nano particle deposition in a combined nasal–oral–tracheobronchial airway model. Journal of Aerosol Science 2011; 42:174–194.

APPENDICES

APPENDIX A
Published articles related to the thesis

RESEARCH PUBLICATIONS

- Fernández Tena A, Casan Clarà P. *Deposition of Inhaled Particles in the Lungs*. Arch Bronconeumol. 2012; 48 (7): 240-246. Impact Factor 1,372

- Ana F. Tena, Pere Casan, Alfonso Marcos, Raúl Barrio, Jorge Parrondo. *A methodology for geometry generation of the lower conductive zone of the lung airways and simulation by intermediate boundary conditions*. Proceedings of Fluids Engineering Summer Meeting, FEDSM2012-72419, pp. 847-854; 8 pages DOI:10.1115/ FEDSM2012-72419

- A. F. Tena, P. Casan, J. Fernández, C. Ferrera, A. Marcos. *Characterization of particle deposition in a lung model using an individual path*. EPJ Web of Conferences, 45 01079 (2013), DOI: 10.1051/epjconf/34501079.

- Ana Fernández Tena, A. Marcos, A. I. Enríquez, R. Guzmán, H. Jiménez, L. Vigil, P. Casan. *Modelo tridimensional de la vía aérea para la simulación del depósito de partículas inhaladas*. Archivos de Bronconeumología, Junio 2012, Núm. Esp. Congreso - Vol. 48 (1 - 296). Impact Factor 1,372

- Ana Fernández Tena, Joaquín Fernández Francos, Miguel Ariza Prota, Ana Isabel Enríquez Rodríguez, Francisco Julián López González, Pere Casan Clarà. *Simulación del depósito de partículas inhaladas en la vía aérea.* Archivos de Bronconeumología, Junio 2013, Núm. Esp. Congreso - Vol. 49 (1-313). Impact Factor 1,372

CONFERENCE PUBLICATIONS

INTERNATIONAL CONFERENCES

TITLE: Fluid dynamic analysis of the deposition particles in the first branches of the lung airways using a three dimensional CFD model
AUTHORS: Ana F. Tena, Pere Casan, Alfonso Marcos, Raúl Barrio, Eduardo Blanco
CONFERENCE: 4th International Congress on Energy and Environment Engineering and Management
PLACE: Mérida, Badajoz **YEAR**: 2011

TITLE: Analysis of the fluid dynamic characteristics of the obstructive pulmonary diseases using a three-dimensional CFD model of the upper conductive zone of the lung airways
AUTHORS: Ana F. Tena, Pere Casan, Alfonso Marcos, Raúl Barrio, Eduardo Blanco
CONFERENCE: ECCOMAS Thematic International Conference on Simulation and Modeling of Biological Flows (SIMBIO 2011)
PLACE: Bruselas, Bélgica **YEAR:** 2011

TITLE: Nueva metodología para la generación de la geometría de la zona conductiva inferior de las vías respiratorias del pulmón
AUTHORS: Alfonso Carlos Marcos, Alberto Marcos, Ana F. Tena, Pere Casan, Raúl Barrio
CONFERENCE: XVI Congreso Internacional de Ingeniería de Proyectos
PLACE: Valencia **YEAR:** 2012

TITLE: Numerical simulation of the nano particle deposition using a three-dimensional model of lung airways
AUTHORS: Ana F. Tena, Pere Casan, Joaquín Fernández, Alfonso Marcos, Raúl Barrio
CONFERENCE: The 15th International Conference on Fluid Flow Technologies (CMFF'12)
PLACE: Budapest, Hungría **YEAR:** 2012

TITLE: Fluid dynamics characterization on handling nebulizers
AUTHORS: Ana F. Tena, Pere Casan, Joaquín Fernández, Eduardo Blanco, Keith Walters
CONFERENCE: 5th International Congress on Energy, Environment Engineering and Management
PLACE: Lisboa, Portugal **YEAR:** 2013

TITLE: Simulation of particle deposition in the human airways
AUTHORS: Ana F. Tena, Joaquín Fernández, Francisco Rodríguez, Pere Casan,
CONFERENCE: ERS (European Respiratory Society) 2013 Annual Congress
PLACE: Barcelona **YEAR**: 2013

NATIONAL CONFERENCES

TITLE: Modelo tridimensional de la vía aérea para la simulación del depósito de partículas inhaladas
AUTHORS: Ana Fernández Tena, A. Marcos, A. I. Enríquez, R. Guzmán, H. Jiménez, L. Vigil, P. Casan
CONFERENCE: 45 congreso SEPAR.
PLACE: Madrid **YEAR:** 2012

TITLE: Simulación del depósito de partículas inhaladas en la vía aérea
AUTHORS: Ana Fernández Tena, Joaquín Fernández Francos, Miguel Ariza Prota, Ana Isabel Enríquez Rodríguez, Francisco Julián López González, Pere Casan Clará
CONFERENCE: 46 congreso SEPAR
PLACE: Oviedo **YEAR:** 2013

TITLE: Estimación del depósito orofaríngeo de fármacos administrados mediante inhaladores de polvo
AUTHORS: Ana Fernández Tena, Joaquín Fernández Francos, Ana Isabel Enríquez Rodríguez, Rosirys Mercedes Guzmán Taveras, Pere Casan Clarà
CONFERENCE: 19 congreso ASTURPAR
PLACE: Oviedo **YEAR:** 2014

Some of them are shown on the following pages

EPJ Web of Conferences **45**, 01079 (2013)
DOI: 10.1051/epjconf/20134501079

Characterization of particle deposition in a lung model using an individual path

A. F. Tena[1], P. Casan[1], J. Fernández[2a], C. Ferrera[2], A. Marcos[2]

[1]Instituto Nacional de Silicosis. Dr Bellmunt s/n. 33006 Oviedo, Spain.
[2]Universidad de Extremadura. Avda de Elvas s/n, 06006 Badajoz, Spain.

Abstract. Suspended particles can cause a wide range of chronic respiratory illnesses such as asthma and chronic obstructive pulmonary diseases, as well as worsening heart conditions and other conditions. To know the particle depositions in realistic models of the human respiratory system is fundamental to prevent these diseases. The main objective of this work is to study the lung deposition of inhaled particles through a numerical model using UDF (User Defined Function) to impose the boundary conditions in the truncated airways. For each generation, this UDF puts the values of velocity profile of the flow path to symmetrical truncated outlet. The flow rates tested were 10, 30 and 60 *ℓ/min*, with a range of particles between 0.1 *μm* and 20 *μm*.

1 Introduction

One of main health problems to the urban population is the exposure to air pollution. Suspended particles (made up of soot, smoke, dust and liquid droplets) can cause a wide range of chronic respiratory illnesses such as asthma and chronic obstructive pulmonary diseases, as well as worsening heart conditions and other conditions. To know the particle depositions in realistic models of the human respiratory system is fundamental to prevent these diseases, and this is the objective of this work.

Following the model developed by Weibel [1], a 3D numerical model of the bronchial tree has been developed from the trachea to the sixteenth level bronchioles. It has been discretized with a mesh of about one million cells. The Navier-Stokes equations have been solved with a commercial CFD finite volume code (Ansys Fluent). Other authors [2 and 3] have developed similar models, also using an individual path. In order to obtain reasonable results from a truncated model, it is necessary to apply physiologically realistic boundary conditions at these truncated outlets.

This work is part of a broader, which tries to model the airflow in the lung with all their characteristics: unsteady flow, inhalation and exhalation of particles, common diseases (asthma, bronchitis, etc.). A first step was [4] the construction and simulation of a particular 7-level model, using a single way to study the unsteady flow that occurs during the execution of a spirometry test. A second step [5] was to study the lung deposition of inhaled particles through a numerical model. A third step, the main objective of this work, is to study the lung deposition of inhaled particles through a numerical model by means of UDF (User Defined Function) to impose the boundary conditions in the truncated airways. For each generation, this UDF puts the values of the velocity profile of the flow path to symmetrical truncated outlet. The flow rates tested were 10, 30 and 60 *ℓ/min*, which are equivalent to the different respiratory rhythms. The particle size used ranged between 0.1 *μm* and 20 *μm*, being introduced by means of an injection type called surface, specifying particle properties and velocity.

2 Methodology

The numerical model of the nasal cavity and nasopharynx was obtained from a 30-year-old woman by means of CT images [6]. The throat reproduces the model written in [7]. The geometry follows the models developed by Weibel [1] and Kitoaka et al [8]. The 3D numerical model has been made with the commercial code Ansys Gambit© [9].

The trachea has a length of 12 *cm* and a diameter of 1.8 *cm*. The bifurcation angle was set to 35º according to the guidelines given in [1, 8]. The geometry of the bifurcations in the bronchus at all the generations is created by a similar procedure. The diameter *d* and the length *ℓ*, deduced from the relations proposed by Kitaoka (levels 1, 2 and 3) and Weibel (rest of levels), are:

2a: ffrancos@unex.es

Article available at http://www.epj-conferences.org or http://dx.doi.org/10.1051/epjconf/20134501079

$$\begin{cases} d = 0.018\exp(-0.388\,n) & \text{if } n \le 3 \\ d = 0.013\exp\left[-(0.2929 - 0.00624\,n)\,n\right] & \text{if } n > 3 \end{cases} \quad (2)$$

$$\begin{cases} l = 0.12\exp(-0.92\,n) & \text{if } n \le 3 \\ l = 0.025\exp(-0.17\,n) & \text{if } n > 3 \end{cases} \quad (3)$$

Half lung is presented in Figure 1. The numerical simulation of this complete morphology is simply unavoidable because the lung until level 16 has 65536 branches (Table 1).

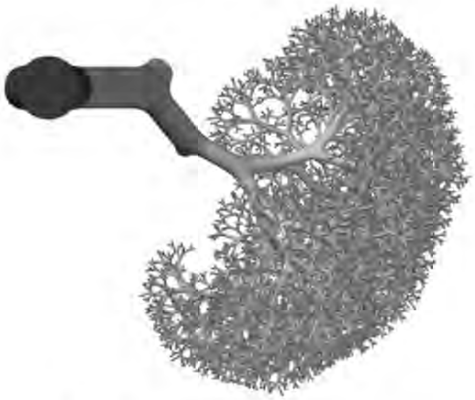

Fig 1. Complete morphology of the lung

Table 1. Main parameters of the branches

n	branche	diameter (mm)	length (mm)	branche (mm^2)	total (mm^2)
0	1	18.00	120.00	254.47	254
1	2	12.21	47.82	117.12	234
2	4	8.28	24.85	53.90	216
3	8	5.62	16.86	24.81	198
4	16	4.45	12.67	15.56	249
5	32	3.51	10.69	9.69	310
6	64	2.81	9.01	6.19	396
7	128	2.27	7.61	4.05	519
8	256	1.86	6.42	2.72	696
9	512	1.54	5.41	1.87	958
10	1024	1.30	4.57	1.32	1353
11	2048	1.10	3.85	0.96	1957
12	4096	0.95	3.25	0.71	2903
13	8192	0.83	2.74	0.54	4416
14	16384	0.73	2.31	0.42	6886
15	32768	0.65	1.95	0.34	11010
16	65536	0.59	1.65	0.28	18048

Figure 2 shows a global image of the model. The complete morphology of the lung can be generated from this model by imposing symmetry at each of the branches.

Fig 2. Numerical model geometry

3 Numerical model

A boundary layer mesh was built before meshing the volumes in order to obtain a better description of the boundary layer in the numerical calculations. The lung was meshed with tetrahedral cells due to their better adaptation to complex geometries, reducing its size while descending from the high-order to the low-order generations. The size of the tetrahedrons was consistent with the size of the boundary layer cells. The volume of the cells ranges between $2.96\text{x}10^{-12}$ and $2.01\text{x}10^{-10}$ m^3. The maximum equiangle skew was restricted to 0.6 for 97.60% of the cells in the mesh. Figure 3 shows a detail of the mesh generated.

The total number of cells used to begin the simulations was about 10^6, though other meshes of different size ($2\text{x}10^6$ and $4\text{x}10^6$) were generated in order to investigate the dependence of the numerical predictions. As can be seen in Figure 4, the variation observed in the outlet static pressure rate when considering different mesh sizes is not very significant. If one compares 1,000,000 and 2,000,000 cells models with the 4,000,000 cells model, the relative deviation is 1.77% and 1.04% respectively.

Fig 3. Detail of the mesh (nose and level 16th of the lung)

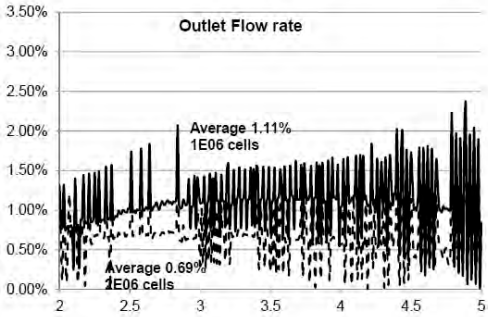

Fig 4. Results of the independence tests

The numerical simulations were performed with the code Ansys Fluent© [10]. This code was used to solve the full steady 3D Reynolds-averaged Navier-Stokes equations by the finite volume method. The fluid used in the calculations was air. The velocities will vary between 0.65 and 3.93 *m/s* at the trachea, so the Reynolds number is between 840 and 5050. The flow was considered as incompressible and turbulent. To effectively address both laminar and turbulent flow conditions, the model used for turbulent closure was the SST k-omega together with the transitional flows option to enable a low-Reynolds-number correction to the turbulent viscosity. This model provides a good approximation to transitional flows because the value of ω does not reach the zero value as the laminar flow limit is approached. Furthermore, the turbulence is simulated all the way to the viscous sublayer, avoiding the use of standard wall functions, which are inaccurate for transitional flows. The pressure-velocity coupling was established by means of the SIMPLE algorithm. Second-order upwind discretizations were used for the convection terms and central difference discretizations were established for the diffusion terms. The $y+$ values at all wall boundaries were maintained on the order of approximately 2 or less. This model has already been tested in the first step of this broad work [4].

A specific volume flow rate at the nose and a constant gauge pressure at the lowest generation were imposed as the boundary conditions. An additional user-defined function was used to impose a symmetric operation of the two branches at each bronchus. A detailed description of this UDF (which is about 400 lines long) is beyond the scope of this article. This UDF obtains the velocity profile at each open branch from the calculations and prescribes the same profile in the corresponding truncated branch. This methodology is repeated iteratively until achieving convergence in the flow field. Convergence was accepted with criteria of 0.00001 residuals for continuity and each velocity component in the momentum equation. Convergence required about 1,100 iterations and approximately 15 min CPU time in a cluster with 8 cores.

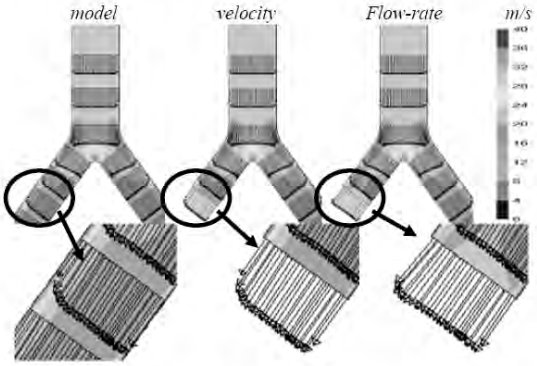

Fig 5. Outlet boundary conditions (velocity and flowrate)

Figure 5 shows a sample of this UDF. On the left there is a bifurcation in normal conditions, with uncut branches, showing the normal profile of the velocity field. On the middle is shown a bifurcation with the left branch truncated, using as boundary condition the velocity profile of the open branch and, on the right, the same but with the uniform flow-rate.

The particle trajectory equation can either be solved with the momentum and energy equations for the continuum flow (coupled) or after the momentum and energy equations have converged (uncoupled). The coupled option allows particles to interact with the flow fluid and affect the flow solution. In this case, the uncoupled option was chosen.

Once the static simulation finished, the Discrete Phase Model (DPM) was switched on to predict the trajectory

of discrete phase particles. To study particle deposition, the Lagrangian approach was used; particle trajectories were calculated within the steady flow fields of interest as a post processing step. Forces on the particles of interest include drag, pressure gradient, gravity, lift, and Brownian motion. To model the effects of turbulent fluctuations on particle motion, a random walk method was employed. The tracking parameters used were 50,000 for the "maximum number steps" and 5 for the "step length factor".

Particles were introduced by means of an injection type called surface, specifying particle properties and velocity. Robinson [11] founded that 50.000 particles are necessary to minimize random variation in the deposition efficiency predictions due to the randomness of the particle position profile.

Deposition was determined by summing up the "trapped" fate particles, which occurs when their centre of mass touches the wall. Fluent reported the number of incomplete, aborted, or unable to be tracked particles. These numbers could be minimized by adjusting various input parameters

4 Results

The flow rates tested were 10, 30, and 60 *ℓ/min*, which are equivalent to different respiratory rhythms. The seeding conditions of the particles were:

- Inert material density: 1.000 kg/m^3.
- Particle size: 0.1 *μm*, 0.5 *μm*, 1 *μm*, 2 *μm*, 5 *μm*, 10 *μm* and 20 *μm*.
- Velocity: the same that air.
- Density 0.5%.
- Number of injected particles: 50.058.

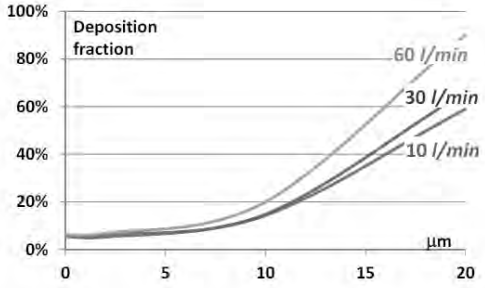

Fig 6. Relationship between particle size and lung deposition. Numerical results.

The regional deposition of particles can be quantified in terms of the deposition fraction (DF), defined as the mass ratio of deposited particles in a specific region to the particles entering the lung. Here (figure 6) is the ratio of the particles trapped in the first seven levels and entering the lung. These results agree with Dolovich [12] except in the range of particles between 0.1 and 2 *microns*, where numerical values are greater than those obtained experimentally.

Figures 7 and 8 show the concentration of the particles (kg/m^2) settled on the duct walls for a flow rate of 60 *ℓ/min* and for a size of 5 *μm*. Red colour means high concentration of settled particles on the wall, and blue colour means absence of settled particles.

Fig 7. Particles concentration (kg/m^2).

Fig 8. Particles concentration (kg/m^2).

As can be seen, most of the particles is retained in the nose and in the junction of the larynx and trachea, where the epiglottis.

The rest of particles travel through the lung. It can be seen how the UDF placed on truncated branches allows the exit of the particles, working the lung as if he had all the branches. According to the designed UDF, it can be said that the particle satisfies the task assigned, allowing to simulate the lung by means of an individual path.

5 Conclusions

This paper has explored a general methodology to simulate a model of a human lung. It has developed a complete and realistic model of the lower conductive zone of the lung (generations 0 to 16). Thais can be simulated within reasonable computational times. The operation of the 'truncated' airway is included in the simulations by means of a user-defined function. This function was used to: 1) obtain the velocity profile at each 'active' (open) branch, and 2) prescribe this profile in the truncated branch. This was useful to simulate the operation of the truncated branches at each bronchiole.

The distribution of particles in the lung airways depends of its size. Small particles are distributed more uniformly than bigger particles, which follow the mean flow. The main objective of this work, to study the particle deposition from the mouth to the level 16 using a mixture of particles of different sizes has been achieved. Due to the high number of branches (131,072), it is necessary to work with a single pathway, so the boundary conditions applied in the truncated branches are very important. It can be concluded that the numerical model presented in this paper and the user-defined function routine included to account for the operation of the truncated branches can be satisfactory used to simulate the real operation of a human lung over the entire breathing cycle. This model provided a realistic description of the operation of the lung while avoiding too large computational costs.

Our future efforts will focus in the simulation of several pulmonary diseases (bronchitis, emphysema, etc.).

Acknowledgements

The authors gratefully acknowledge the financial support provided by Gobierno de Extremadura and FEDER under project GR10047 and also by Ministerio de Economía y Competitividad under project DPI 2010-21103-C04-04

References

1. E R Weibel, Morphometry of the human lung, Springer-Verlag (1963)
2. G Tian, P W Longest, G Su and M Hindle, Characterization of Respiratory Drug Delivery with Enhanced Condensational Growth using an Individual Path Model of the Entire Tracheobronchial Airways, Annals of Biomedical Engineering, 2011, Volume 39, Number 3, Pages 1136-1153.
3. D K Walters and W H. Luke, A Method for Three-Dimensional Navier--Stokes Simulations of Large-Scale Regions of the Human Lung Airway, J. Fluids Eng. 132, 051101 (2010).
4. A F Tena, P Casan, A Marcos, R Barrio, E Blanco. Analisys of the fluid dynamic characteristics of the obstructive pulmonary diseases using a three-dimensional CFD model of the upper conductive zone of the lung airways. Proceedings of the SIMBIO 2011, Brussels, (Belgique), 2011.
5. A F Tena, P Casan, J Fernáz, A Marcos, R Barrio. Numerical simulation of the nano particle deposition using a three-dimensional model of lung airways. Conference on Modelling Fluid Flow (CMFF'12), Budapest, Hungary, 2012.
6. P Castro-Ruiz F, Castro-Ruiz, A. Costas-López, C. Cenjor-Español. Computational fluid dynamics simulations of the airflow in the human nasal cavity. Acta Otorrinolaringol Esp 2005; 56: 403-410.
7. M Brouns, S T. Jayaraju1, C Lacor, J De Mey, M Noppen, W Vincken, and S Verbanck. Tracheal stenosis: a flow dynamics study. Journal of Applied Physiology March 2007 vol. 102 no. 3 1178-1184.
8. H Kitaoka H, R Takaki, B Suki. A three-dimensional model of the human tree. *J. Applied Physiology. 1999; 87: 2207-2217.*
9. *Gambit version 2.4.6,* 2006. ©ANSYS Inc.
10. *Fluent version 6.3.26,* 2006. ©ANSYS Inc.
11. Robinson, R. J., Oldham, M. J., Clinkenbeard, R. E., and Rai, P. 2006. Experimental and nu-merical analysis of a 7 generation human rep-lica tracheobronchial model. Ann. Biomed. Eng. 34(3):373–383.
12. Dolovich MB, Newhouse MT. Aerosols. *Generation, methods of administration, and therapeutic applications in asthma. In Allergy. Principles and practice*, 4th edn, eds Middleton E Jr, Reed CE, Ellis EF, Adkinson NF Jr, Yunginger JW, Busse WW. St Louis: Mosby Year Book, Inc., 1993; 712–739.

P1275 An application of electronic nose technology for diagnosis of Alzheimer's disease
A. R. Koczulla, M. Gold, A. Hattesohl, D. Lubbe, D. Mengel, S. Schmid, B. Tackenberg, J. Rieke, S. Maddula, J. I. Baumbach, J. Michelis, J. Alferink, M. Heneka, W. Oertel, F. Jessen, S. Janciauskiene, C. Vogelmeier, R. Dodel, J. P. Bach (Marburg, Giessen, Dortmund, Bonn, Münster, Hanover, Germany)

HALL 1-40 SESSION 112 12:50 - 14:40

Thematic Poster Session: Airway calibre, airway challenge and assessment of oxygenation

Chairs: K. Sylvester (Cambridge, United Kingdom), D. Ionita (Bucharest, Romania), C. Hernandez (Barcelona, Spain), A. Houtkooper (Ten Helder, the Netherlands)

P1276 Early bronchial asthma diagnosis with electrical impedance spirometry
V. Mishlanov, A. Zuev, T. Ustiantzeva (Perm, Russian Federation)

P1277 Repeatability and reproducibility of impulse oscillometry and body plethysmography in healthy, asthmatic and COPD subjects
N. Vanjare, S. Rasam, S. Bhosale, Y. Gupta, S. Salvi, R. Kodgule (Pune, India)

P1278 Comparison of the sensitivity and specificity of the methacholine challenge test and exercise test for the diagnosis of asthma in athletes
T. Molostova, M. Mustafina, A. Cherniak, Z. Naumenko, L. Shogenova, Z. Aisanov (Moscow, Russian Federation)

P1279 Redihaler with filter mouthpiece versus NebuChamber with inhalation valve
E. Ruberg, I. Steenbruggen, S. Uil, H. Grotjohan (Zwolle, the Netherlands)

P1280 Validity of the forced expiratory flow 25-75 for identification of bronchial hyperresponsiveness in a pulmonary function laboratory
R. Q. Yolanda, C. M. Jorge, G. G. Rosa, V. E. Julio, R. M. T. Rosa María, P. M. Luis (Madrid, Spain)

P1281 Simulation of particle deposition in the human airways
A. Fernandez Tena, J. Fernandez Francos, F. Rodriguez Jerez, P. Casan Clara (Oviedo, Badajoz, Spain)

P1282 Analysis of impulse oscillometry data of chronic obstructive pulmonary diseae patients in community health care center, Ho Chi Minh City, Vietnam
T. T. L. Le, X. T. Tran, N.N.M. To, N.T.D. Do, T. S. Nguyen, Q. D. K. Truong, V.T. Vo, T.K.T. Tran (Ho Chi Minh, Vietnam)

P1283 Specificity and sensitivity of mannitol challenge testing for asthma in young adults from the Western Australian Pregnancy (Raine study) Cohort
E. White, G. Hall, E. Hollams, N. DeKlerk, Z. Hantos, P. Holt (Perth, Australia; Szeged, Hungary)

P1284 Relationship the impulse oscillometry parameters and the lung damage in idiopathic pulmonary fibrosis patients
E. Semenova, M. Kameneva, A. Tishkov, V. Trofimov, L. Novikova (Saint-Petersburg, Russian Federation)

P1285 The DLNO/DLCO ratio is not dependent on breath holding time in healthy subjects
I. van der Lee, S. Dijkman, F. Krouwels (Hoofddorp, the Netherlands)

P1286 Severity classification of DSP in COPD
M. Rutter, K. Sylvester (Cambridge, United Kingdom)

P1287 Influence of ASC correction on specific airway resistance using the body box
W. Put, C. van der Grinten (Maastricht, the Netherlands)

P1288 Accuracy of 2 types of pulse oximeters in cardio pulmonary exercise testing
J. Makonga-Braaksma, R. v Winkoop-Ruitenberg, P. Dalinghaus (Amersfoort, the Netherlands)

P1289 How frequent are unusual types of ventilatory impairment (mixed and nonspecific)? Analysis of over 10,000 patients data
P. Boros, M. Martusewicz-Boros, S. Wesolowski (Warsaw, Poland)

P1290 The FEV_1/TLC ratio: Can it differentiate between normal subjects and patients with airflow obstruction and restrictive ventilatory defects - a preliminary analysis?
A. Kendrick (Bristol, United Kingdom)

P1291 Determining why patients with idiopathic pulmonary fibrosis (IPF) have difficulty performing gas transfer
M. Bryce, K. Oates, G. Chivers, H. Parfrey (Cambridge, United Kingdom)

P1292 Measurements of carbon monoxide (CO) in exhaled air and calculation of alveolar-capillary membrane diffusion capacity
E. Babarskov, E. Stepanov, Y. Shulagin, A. Cherniak, Z. Aisanov, A. Chuchalin (Moscow, Russian Federation)

P1293 Surveying the practice of arterialised earlobe capillary blood gas sampling amongst respiratory specialists practitioners
J. Young, K. Sylvester, J. Fuld (Cambridge, United Kingdom)

P1294 Reliability of the elastic and mechanical properties of esophageal balloon catheters
S. Walterspacher, L. Isaak, J. Gutmann, H. J. Kabitz, S. Schumann (Freiburg, Germany)

P1281

Simulation of particle deposition in the human airways

Ana Fernandez Tena[1], Joaquin Fernandez Francos[2], Francisco Rodriguez Jerez[1], Pere Casan Clara[1].

[1]Respiratory Medicine, Instituto Nacional De Silicosis (Hospital Universitario Central De Asturias), Oviedo, Spain; [2]Mechanical Engineering, Universidad De Extremadura, Badajoz, Spain

Objective: To study the airway deposition of inhaled particles, using a numerical model of fluid dynamics.

Methods: A 3D model of the airways has been developed, from mouth up to terminal bronchioles. A simulation code of Computational Fluid Dynamics (CFD) has been used, which simulates the air movement in the model, and the trajectory of inhaled particles, according to their velocity and size. Different airflows have been simulated: 10, 30 and 80 l/min, with 3 particle sizes: 5 nm, 0.5 µm and 20 µm. When a particle collides with the airway wall, it is trapped there. This code calculates the percentage of particles trapped in the different anatomical parts of the model.

Results: In figure1, red color in the airways represents areas with a high concentration of trapped particles, whereas the blue color spots are areas without trapped particles. The number of trapped particles in the pharynx is higher as the bigger the particles are and the higher the airflow is. When the particles are small and the airflow is low, the particles tend to be trapped in more distal regions.

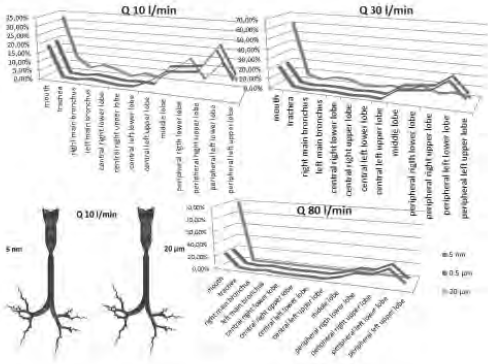

Conclusions:

1. It's possible to develop a realistic computer model to simulate the breath and the deposition of inhaled particles, employing CFD codes.
2. Pharynx is the area where the most part of the particles are going to be trapped.
3. It is possible to improve the deposition of inhaled particles in more distal areas breathing with a low airflow and using inhalers with a small particle size.

P1282

Analysis of impulse oscillometry data of chronic obstructive pulmonary diseae patients in community health care center, Ho Chi Minh City, Vietnam

Xuan Tan Tran[1], Quang Dang Khoa Truong[1], Thi Sen Nguyen[2], Thi Tuyet Lan Le[2].

[1]Biomedical Department, International University - Vietnam National University, Ho Chi Minh, Viet Nam; [2]Physiological Department, Ho Chi Minh City Medicine and Pharmacy University, Ho Chi Minh, Viet Nam

Background: Impulse oscillometry system is a non-invasive method to access the oscillatory mechanics of the respiratory system. The aim of this study was to analyze the accuracy of the impulse oscillometry parameters in diagnosis of COPD, and investigate which IOS parameters are related to airflow obstruction in COPD patients in Community Health Care Center in Ho Chi Minh City, Vietnam.

Methods: The study contain thirty COPD patients and thirty-two healthy people, whole of them are greater than 40 years, were recruited in Community Health Care Center (CHAC), Ho Chi Minh city, Vietnam. IOS measurements (R5, R20, X5, X20, AX & Fres), and Spirometry (FEV1, FVC) were performed. Pearson or

Arch Bronconeumol. 2012;48(7):240–246

ARCHIVOS DE BRONCONEUMOLOGIA

www.archbronconeumol.org

Review

Deposition of Inhaled Particles in the Lungs☆

Ana Fernández Tena, Pere Casan Clarà*

Instituto Nacional de Silicosis, Hospital Universitario Central de Asturias, Facultad de Medicina, Universidad de Oviedo, Oviedo, Spain

ARTICLE INFO

Article history:
Received 26 January 2012
Accepted 1 February 2012
Available online 26 May 2012

Keywords:
Aerosol
Lung deposition
Inhalers

ABSTRACT

Inhaled medication is the first-line treatment of diseases such as asthma or chronic obstructive pulmonary disease. Its effectiveness is related to the amount of drug deposited beyond the oropharyngeal region, the place where the deposit occurs and its distribution (uniform or not). It is also important to consider the size of the inhaled particles, the breathing conditions, the geometry of the airways, and the mucociliary clearance mechanisms.

Currently, mathematical models are being applied to describe the deposition of inhaled drugs based on the size of the particles, the inspiratory flow, and the anatomical distribution of the bronchial tree. The deposition of particles in the small airways gets maximum attention from pharmaceutical companies and is of great interest as it is related with a better control in patients receiving these drugs.

Depósito pulmonar de partículas inhaladas

Palabras clave:
Aerosol
Depósito pulmonar
Inhaladores

RESUMEN

La medicación inhalada constituye el tratamiento de primera línea de enfermedades como el asma o la enfermedad pulmonar obstructiva crónica. Su efectividad está en relación con la cantidad de fármaco que logre depositarse más allá de la región orofaríngea, con el lugar en que se produzca el depósito y con la distribución uniforme o no del mismo. Otros factores trascendentes son el tamaño de las partículas inhaladas, las condiciones de respiración, la geometría de las vías aéreas y los mecanismos de aclaramiento mucociliar.

Actualmente se están aplicando modelos matemáticos que permiten describir el depósito de fármacos inhalados a partir del tamaño de las moléculas, el flujo inspiratorio y la distribución anatómica del árbol bronquial. El depósito de partículas en las vías aéreas pequeñas recibe la máxima atención de las empresas farmacéuticas y es del máximo interés para poder controlar mejor a los pacientes que reciben estos fármacos.

Introduction

The air that we breathe contains more than just nitrogen and oxygen. In addition, there are thought to be small concentrations of other gases (ozone, hydrogen, krypton, argon) and a variable quantity of water vapor depending on the environment in which we find ourselves. We do not know if this is all, although we fear that it is not. What we call "air" also contains enormous quantities of suspended particles, solid as well as liquid, organic and inorganic, bacteria, viruses, antigens, particles that can be more elemental, volatile or solid, simple or combined. All these elements make up the exterior environment where we breathe and live.

Our lungs are tremendous sponges of blood that also act as enormous filters that purify the air we breathe. By the time the oxygen and nitrogen molecules are deposited in the alveoli, we could say that they are practically free of the majority of these "contaminants" and that these local and general defense systems are quite effective during many, many years. This, of course, is true as long as we have taken care not to deliberately deteriorate our lungs by smoking.

The respiratory tract is especially designed, both anatomically and functionally, so that air can reach the most distal areas of the lungs in the cleanest possible condition. Nasal hairs, nasal turbinates, vocal chords, the cilia of the bronchial epithelium, the sneeze and cough reflexes, etc., all contribute to this filtering process. And, on most occasions it is properly done. But human beings are full of paradoxes: an efficient system, designed to avoid certain

☆ Please cite this article as: Fernández Tena A, Casan Clarà P. Depósito pulmonar de partículas inhaladas. Arch Bronconeumol. 2012;48:240–6.

* Corresponding author.
E-mail address: pcasan@ins.es (P. Casan Clarà).

1579-2129/$ – see front matter

particles from penetrating into the lungs, is at the same time used to intentionally deposit drugs in the airways and even for these to reach the alveoli in the best possible condition. It is thus necessary to get around the defense systems by evading reflex arcs, mucus layers, ciliary movements, etc., so that, with the inspiratory flow, the molecules that can improve diseases are deposited in the lungs. A system that evolved over time in order to filter and clean the air should be dodged in order to deposit other substances that we deliberately want to reach the inside of the organism. Without a doubt, an understanding of anatomy, airway function and the laws of physics that govern flow dynamics, size, shape, and the number of inhaled particles will contribute to the development of this area of expertise. This area is so close to our specialty and has generated great interest, especially for the development of new methods to administer medication.

Factors That Affect the Deposition of Aerosolized Drugs

Particle Size and Shape

The size and shape of particles are primordial factors that condition their deposition in the lungs. The size is defined by what is called the mass median aerodynamic diameter (MMAD) or diameter of a particle of mass equal to the average particle diameter of a population, meaning the diameter of a particle in which 50% of the aerosol mass is greater and the other 50% is smaller.[1] Depending on their size and shape, the particles can be deposited by means of four mechanisms:

- *Impaction.* This is the physical phenomenon by which the particles of an aerosol tend to continue on a trajectory when they travel through the airway, instead of conforming to the curves of the respiratory tract.[2] Particles with enough momentum (product of the mass and velocity) are affected by centrifugal force at the points where the airflow suddenly changes direction, colliding with the airway wall. This mainly happens in the first 10 bronchial generations, where the air speed is high and the flow is turbulent.[3] This phenomenon mainly affects particles larger than 10 μm, which are mostly retained in the oropharyngeal region, especially if the drug is administered by dry powder inhalers (DPI) or metered-dose inhalers (MDI).[4]
- *Interception.* This is mainly the case of fibers, which, due to their elongated shape, are deposited as soon as they contact the airway wall.
- *Sedimentation.* This is the physical phenomenon by which particles with sufficient mass are deposited due to the force of gravity when they remain in the airway for a sufficient length of time. This predominates in the last 5 bronchial generations, where the air speed is slow and the residence time is therefore longer.[3]
- *Suspension.* This is the phenomenon by which the particles of an aerosol move erratically from one place to another in the airways. This happens as a consequence of the Brownian diffusion of particles with an MMAD smaller than 0.5 μm when they reach the alveolar spaces, where the air speed is practically zero. These particles are generally not deposited and they are expelled once again upon exhalation.

The particles of aerosolized drugs usually have a uniform shape and are symmetrical on several planes. They rarely are smaller than 1 μm, and therefore the predominating mechanisms are impaction and sedimentation.[5]

It can generally be considered that particles with an MMAD higher than 10 μm are deposited in the oropharynx, those measuring between 5 and 10 μm in the central airways and those from 0.5 to 5 μm in the small airways and alveoli. Therefore, for topical respiratory treatment it is best to use particles with an MMAD between 0.5 and 5 μm. This is what is known as the breathable fraction of an aerosol.[6]

Airflow Velocity

Because particles are transported through the airway by an air current, their trajectories are affected by its characteristics. The air flow in the lungs is determined by the tidal volume and respiratory rate. Sbirlea-Apiou et al.[7] demonstrated that in the first four generations of the airway, the deposition increases for any size particle as the inspiratory flow increases. However, the opposite is true in the last generations of the airway, where the deposition of particles is inversely proportional to this flow. This is due to that fact that the increased inspiratory flow reduces the residence time of the particles in the airway, therefore the effects of the severity and of the Brownian movement will be quite lower. Obviously, a minimal inspiratory flow is necessary to drag the particles toward the interior of the bronchial tree.

Airway Geometry

The probabilities of particle deposition by impaction increase when the particles themselves are larger, the inspiratory airflow is greater, the angle separating the two branches is wider and the airway is narrower.[8]

In pathologies such as chronic bronchitis or asthma, which may alter the lung architecture with the appearance of bronchoconstriction, inflammation or secretion accumulation, the deposition of aerosolized drugs is modified. The smaller caliber of the airway increases air speed, producing turbulence in places where the flow is usually laminar. The airway obstruction also means that the air tends to be displaced toward unobstructed areas, and therefore the drug will also tend to be deposited mostly in healthy areas of the lung.[9]

Degree of Humidity

The particles of aerosolized drugs can be hygroscopic to a greater or lesser extent. Hygroscopicity is the property of some substances to absorb and exhale humidity depending on the setting in which they are found. This means that they can get larger or smaller in size upon entering into the airway, with the consequent modification in the deposition pattern compared to what was initially expected. The diameter that a particle reaches after hygroscopic growth depends on its initial diameter, the intrinsic properties of the particle, and the environmental conditions in the airways. The mole fraction of water vapor contained in the airway has been demonstrated to be an important factor related with the increase in the MMAD of the aerosol particles.[10] In general, it is considered that hygroscopic growth does not have much of an effect in particles with MMAD less than 0.1 μm; meanwhile it is very intense in particles with MMAD larger than 0.5 μm.[11]

The hygroscopicity of molecules can be used to try to favor the deposition of inhaled drugs. Studies have been developed in which an aerosol was administered with a submicrometric or nanometric MMAD in order to reduce extrathoracic loss, taking advantage of later growth due to hygroscopicity, which enabled the particles to be retained within the lungs.[12,13]

Mechanisms for Mucociliary Clearance

Once deposited in the airways, the particles can be carried by the mucociliary system, degraded or absorbed into the systemic circulation or the lymph ducts.[9] The first of these mechanisms is

found in the conducting airways (from the trachea to the terminal bronchioles), which have ciliated epithelium that are covered by two layers of mucus: a low-viscosity periciliary layer, or sol, and a thicker layer that covers the former, or gel. This biphasic layer of mucus protects the epithelium from dehydration, helping to humidify the air and providing a protective barrier by trapping inhaled particles.[14] The insoluble particles are trapped by the gel and they are moved toward the pharyngolaryngeal region by the movements of the ciliated epithelium, where it is either coughed up or swallowed.[15,16] The clearance speed depends on the number of ciliated cells and the cilia beat frequency, and it may be affected by factors that influence the function of the cilia or the quantity or quality of the mucus. In cystic fibrosis (CF), for example, very thick mucus is produced that does not correctly move along with the cilia. This is due to a mutation in the gene that codes the CFTR receptor, which regulates the passage of the chloride ion through the surface of the epithelial cells.[17]

The soluble particles are eliminated by absorptive mechanisms. The liposoluble molecules cross the respiratory epithelium by passive transport; the hydrosoluble molecules can cross the epithelial barrier either through the intercellular spaces or by active transport (by mechanisms of endocytosis and exocytosis).[18] Once in the submucosal region, the particles can enter the systemic circulation, bronchial circulation or lymphatic system.[9] The particles that are deposited in the alveoli can be devoured and eliminated by the alveolar macrophages if they are insoluble particles (non-absorptive mechanism)[19]; if they are soluble, they can be absorbed into the systemic circulation.[20]

Optimal Locations for Drug Deposition in the Treatment of Some Respiratory Diseases

The administration of inhaled drugs presents a series of advantages over systemic administration, making it preferable for the treatment of local diseases. High doses of a drug may be administered and rapidly absorbed through the epithelium of the airways, meaning that the inhaled administration enables a drug to act quickly, while minimizing systemic side effects. If, however, an aerosolized drug is deposited at a suboptimal dose or in a region of the lung that is not affected by the pathology to be treated, the effectiveness of the treatment will be compromised.[21] The receptors for β2 adrenergic agonists (salbutamol, terbutaline) and M3 muscarinic receptor antagonists (ipratropium bromide) are not uniformly distributed throughout the lung. More than 90% of the β receptors are located in the alveolar walls, and specifically there is a high density of β2 receptors located in the epithelium of the airway between the main bronchi and the terminal bronchioles.[22] There is a high density of M3 receptors in the submucosal glands and lung lymph nodes, while there is a lower proportion in the smooth muscle of the airways, in the nerves that innervate the bronchi and in the alveolar wall.[23] The location of these receptors in the lung suggests that ipratropium bromide should be deposited in the conducting airways in order to reach a greater effectiveness; meanwhile, salbutamol should be deposited more peripherally (in the middle and small airways) to produce an adequate therapeutic effect. In the case of inhaled corticoids, the treatment seems to be more beneficial when more of the drug is dispersed throughout the lungs, as inflammatory cells such as eosinophils, lymphocytes, and macrophages are present throughout the respiratory tract and alveoli in asthma patients.[24,25] The optimal location for the deposition of aerosolized antibiotics depends on the disease to be treated. In the case of CF, there is chronic colonization by *Pseudomonas aeruginosa*, which tends to grow in the lumen of the airways, with a limited invasion of the pulmonary parenchyma. The infection starts in the bronchioles and moves toward more proximal airways[26]; therefore, the ideal place for deposition of inhaled antibiotics would be throughout all the conducting airways. Mucus accumulations in certain areas can impede the antibiotics being deposited in regions behind the obstruction, which are presumably the most infected areas, and the effectiveness of the treatment is therefore compromised.[9,27]

Devices for the Administration of Inhaled Drugs

The treatment of respiratory infections with inhaled steam has been traditionally done for as long as anyone can remember. In 1828, Schneider and Waltz developed an atomizer for mineral water sprays, but it was also used as an inhaler. The first portable inhaler was created in 1856 by Sales-Giron, a physician at a spa. It consisted of a manual liquid atomizer that enabled patients to administer inhaled balsamic infusions at home. The discovery of adrenalin in 1901 by Takamine and Aldrich, and its inhaled administration for the first time in 1929,[28] initiated the search for and administration of new inhaled drugs, leading to improvements in the devices for their administration.[29]

The devices currently used for the administration of inhaled drugs can be divided into three types: nebulizers, metered-dose inhalers, and dry powder inhalers.

Nebulizers

There are basically two types of nebulizers: jet and ultrasonic. Jet nebulizers are based on the Bernouilli effect, according to which a compressed gas that passes through a narrow orifice creates a low-pressure area upon exiting. If at this low-pressure point we connect a tube that has a thin layer of liquid, the low pressure will cause this liquid to be aspirated in small droplets. Ultrasonic nebulizers use piezoelectric crystals that vibrate at a high frequency within the nebulizing chamber, transmitting the vibratory energy to the liquid that is in contact with it, converting said liquid into an aerosol.[30] Jet nebulizers can generally aerosolize most drug solutions, and ultrasonic nebulizers may not be effective if viscous suspensions or solutions are used.[31]

Nebulizers can administer high doses of medication in patients who are not able to coordinate or cooperate and they are able to administer several substances mixed together in one same solution. The minimal inspiratory flow needed for the aerosol produced by a nebulizer to reach the lungs is 6–8 l/min.[2] However, there are high amounts of drug lost as much of the medication is retained in the nebulizer dead-space, or it is lost in the room air during expiration. It has been estimated that only 10% of the dose that is initially placed in the nebulizer will be effectively deposited in the lungs.[32] The large droplets are deposited in the oropharynx, while the droplets are too small to penetrate in the lungs and are once again expelled during expiration.

Pulmonary deposition may be increased by modifying the patient's way of inhaling. Most patients inhale by using circulating volume. If the patient takes a deep breath and holds it in, the quantity of medication retained in the lungs may increase 14%–17%.[8] Probably the most practical way to modify the deposition pattern is to reduce the size of the droplets that are generated. This can be done with ultrasonic nebulizers by making the piezoelectric crystal vibrate at a greater frequency; doing so with jet nebulizers can increase the compressed gas flow.[33]

Metered-dose Inhalers

Metered dose inhalers (MDI) are devices used to administer aerosolized drugs that emit a fixed dose of medication with each pulse. They have a metallic chamber containing a suspension or

solution of the drug with a liquid propellant that, at room temperature and atmospheric pressure, turns to its gaseous phase. A key piece in this system is the dosage valve, which releases at each pulse a controlled, reproducible dose of medication. The drug is released at a high speed (at more than 30 m/s through the mouthpiece) and in the form of particles with an MMAD of between 2 and 4 μm.[34] MDI have a series of advantages, such as their small size (making them easy to handle), the exactness of the dosage, the possibility to fit them to spacer chambers, the fact that they do not require high flows to be inhaled and their low cost in general. Their main drawbacks are the difficulty inherent in synchronizing activation–inhalation and the low dose that reaches the lungs, which has been estimated at approximately 10%–20% of the dose emitted.[35,36] The high release speed and the large size of the particles generated mean that more than half of these impacts in the oropharyngeal region.[36] Another drawback of MDI is the possible variation in the dose released at each pulse if the device is not correctly shaken.[34]

In the past, the propellant used was chlorofluorocarbons (CFC), but due to their harmful effects on the ozone layer, they have been banned by the United Nations. The substitute currently used in MDI are hydrofluoroalkanes (HFA).[37] HFA transform into their gaseous state at a higher temperature than CFC,[38] reducing the cold freon effect, which is the interruption of breathing when the particles impact against the back wall of the oropharynx. There are currently on the market MDI-HFA with salbutamol, fluticasone, beclomethasone, anticholinergics, and the combination of salmeterol–fluticasone.[34] The development of MDI with HFA has also been able to reduce the size of the aerosol droplets and, therefore, improve the lung deposition of the drug. In the case of beclomethasone–HFA, with an MMAD of 1.1 μm, it has been demonstrated that up to 56% of the initial dose is deposited.[39–41]

The optimal conditions for the inhalation of an aerosol using an MDI are to start breathing from functional residual capacity, activating at that moment the inhaler, inhale using an inspiratory flow less than 60 l/min and follow the inspiration with 10 s of apnea.[42] This method increases deposition by sedimentation in the more peripheral areas of the airway. The minimal inspiratory flow necessary for its use is approximately 20 l/min.[2]

One way to avoid the lack of coordination between the patient and the device are to use inhalation chambers that fit on the mouthpiece of the MDI. The aerosol goes into the chamber and the particles that are too big impact against its wall and are retained there, while the smaller particles remain in suspension within the chamber until they are inhaled by the patient. In addition, the space that the chamber provides between the MDI and the mouth of the patient allows the aerosol to lose speed, reducing impaction against the oropharynx. In this manner, local adverse effects are reduced and the lung deposition of the drug is increased.[43] It has been demonstrated that MDI used with inhalation chambers are as effective as nebulizers in the treatment of acute asthma attacks.[44]

Furthermore, with the aim of avoiding a lack of coordinated activation and inhalation, new MDI have been developed that automatically release the medication when the patient inhales, such as Autohaler® and Easybreath®; these devices have been shown to improve the lung deposition of drugs in patients for whom coordination is difficult.[45] In addition, they require less inspiratory flow than conventional MDI, at around 18–30 l/min, which makes them more adequate for patients with physical limitations, children and the elderly.[34,46]

Dry Powder Inhalers

Dry powder inhalers (DPI) were designed with the aim to eliminate the inherent coordination difficulties of MDI. They administer individual doses of drugs in a powder form contained in capsules that should be broken open before their administration (unidose systems), or in blisters that move around in a device or have powder reservoirs (multidose systems).

Other advantages of DPI are that they do not require propellants for their administration, which makes them more respectful of the environment, and many of them have an indicator of the doses remaining. The main drawbacks are that patients perceive to a lesser degree the drug entering the airway, which may complicate treatment compliance, and its price is generally higher than that of MDI. DPI should be stored in a dry setting, as humidity favors the agglomeration of the powder that can obstruct the inhalation system.[37]

The dose that reaches the lungs is similar to MDI, and less than 20% of the initial dose actually reaches the lungs. It has been demonstrated that if the inhalation technique is correct, there is no difference between the administration of a drug by means of DPI or MDI.[47] The use of low inspiratory flow, humidity, and changes in temperature are all factors that have been shown to worsen the lung deposition of medications with DPI.[48]

In the case of DPI, the "aerosol" is produced by the inspiratory effort of the patient.[47] An inspiratory flow of at least 30 l/min is necessary for the powder medication to become dispersed and reach the lungs, which may be difficult to be done in the elderly, children or patients with severe respiratory disorder.[49] The air is directed toward the container with loose powder, which generally consists of particles that are too large to penetrate the airway due to the formation of powder agglomerations or to the presence of large-sized particles that transport the drug, such as lactose. The dispersion of the powder into particles that enter into the inhaled fraction is produced by the formation of turbulent airflows inside the powder container, which break the powder agglomerations up into smaller-sized particles and separate the transport particles from the drug.[50] The particles that are generated have a final MMAD that ranges from 1 to 2 μm.[51,52] Every DPI has a different airflow resistance that determines the inspiratory effort necessary to disperse the powder. The greater the resistance of the device, the more difficult it is to generate the inspiratory effort, but at the same time the deposition of the drug in the lungs is greater.[53,54]

Methods for Studying the Lung Deposition of Particles

The first models of aerosol deposition in the lungs were based on very simple pulmonary morphologies. They used a small number of breathing conditions and a limited range of particle sizes, and were usually models confined to an area of the respiratory tract instead of models of the entire respiratory tract. In addition, they were limited to aerosols generated in industrial settings, like mining.

The first mathematic model of particle deposition was done in 1935 by Findeisen. This author, basing his study on the anatomical understanding of the age, divided the respiratory tract into only 9 generations, reaching the alveolar sacs and ducts. This model assumed a series of dimensions, flow speeds, transit times, and types of ramification for each generation, and formulas were established in order to calculate the particle deposition in each generation according to the 3 basic mechanisms of deposition: impaction, sedimentation, and diffusion. The main limitations of this model are that the airways above the trachea were not contemplated, and the anatomic simplicity of the lower airway model used. However, this pioneering model established the basic norms for the development of other later models.[55]

Another significant model was that by Landhal in 1950, which added two new compartments to the Findeisen model: the mouth and pharynx.[56] Later, Beekmans presented a new model in 1965, in which the 3 basic deposition mechanisms were assumed, and an attempt was made at correcting the dimensions of the airway

caused by its expansion during inspiration. In addition, it considered the role of the mix between tidal and residual volume in the three last generations of the airway. In this model, Beekmans established equal inspiratory and expiratory times, and after every phase he established a pause in which the deposition was produced by diffusion and sedimentation.[57]

A more anatomically detailed model of the airways was published by Davies: including 15 generations, it starting in the mouth and ending in the alveolar sacs. Nevertheless, this was not the basis used to develop a mathematical model calculating particle deposition.[58] The most commonly used anatomical model was the Weibel model. In this model, the ways of bifurcation are indicated, designating the trachea as the first airway (order 0) and presuming that each airway leads to two branches (regular dichotomy). Weibel described a minimum of 23 bronchial generations up to the alveolar ducts.[59]

There are many other later theoretical studies about the behavior of flow in the airways.[60–69] These studies have generally been focused on isolated sections of the lung, such as the trachea and the first generations of the airway or the alveolar ducts and sacs. Currently, the predominating studies are based on computational fluid dynamics (CFD). CFD is a technique that tries to use computers to simulate the movement of fluids and to resolve the mathematic equations governing their movement (Navier–Stokes equations). In this way, the behavior of a fluid and the particles that travel in it can be simulated. By means of CFD it is possible to develop a model of the airways, with any desired degree of detail, in order to simulate the behavior of air and the aerosol particles within it (Figs. 1 and 2).[70] Thoracic computed tomography (CT) images of a patient may be used to develop a personalized model and to check the deposition of inhaled drugs in that patient.[71]

At the same time these mathematical models were arising, numerous experimental models about particle deposition were developed, including those by Drinker, Brown, Patterson, etc.,[72–74] whose results generally did not differ from the mathematical models. These experimental studies generally calculated total aerosol deposition by measuring the quantity that entered and exited the respiratory tract.[75]

Nowadays, the most commonly used techniques for determining the distribution of inhaled drugs are gammagraphy and single photon emission computed tomography (SPECT) in 3 dimensions (3D), although other techniques, such as positron emission tomography (PET) and magnetic resonance imaging (MRI), are gaining importance. These techniques are used in combination with drugs or radioactively marked molecules.[76]

The isotope usually used in gammagraphy and in 3D SPETC is technetium-99m (^{99m}Tc), which is associated with the drug being studied without being part of it. Gammagraphy provides lung images in 2 dimensions (2D), and it has frequently been used to compare the effectiveness of aerosol lung deposition using different inhalation devices, as well as the effects of different respiratory and lung disease parameters on the deposition. The distribution of the drug is generally studied according to areas of interest, meaning comparing the apical and basal regions, or central and peripheral distributions.[76]

SPECT can obtain accumulative 2D images of the thorax of the patient, which gives more precise images in order to evaluate drug deposition patterns in the lungs. However, this is not possible if there is no unabsorbable direct radioactive marker available for the drug being studied. It is useful, on the other hand, for the study of variables that are secondary to the inhalation of medication, such as pulmonary perfusion and ventilation, mucociliary clearance or pulmonary epithelial permeability.[76]

In the case of PET, the markers used are usually carbon, fluoride, nitrogen, and oxygen, which are atoms that make up any organic molecule, and it is therefore simpler to mark the drug being studied. The markers that are most commonly used are C^{11} and F^{18}. The images obtained by PET can be divided into areas that are either more central or more peripheral and correlated with the degree of radioactivity detected and, therefore, with the dose of drug deposited in each region.[76]

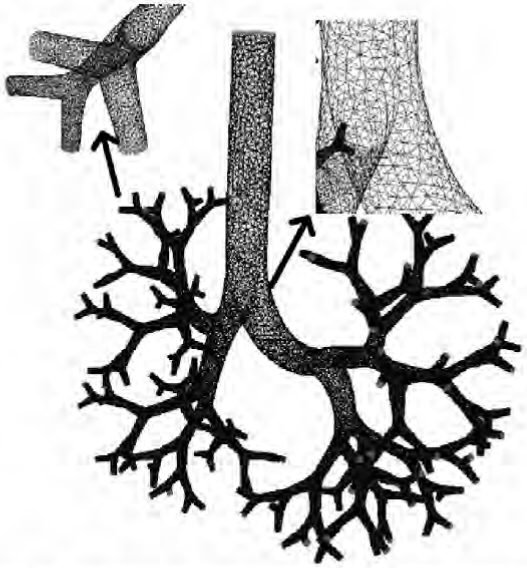

Fig. 1. Theoretical model of the human airway up until the seventh generation used to calculate computational fluid dynamics (CFD). It can be observed that it is made up of multiple cells in the shape of a tetrahedron, inside each of which the CFD program calculated the air behavior.

Discussion

Inhaled medication is the first line of treatment in disease such as asthma or COPD. Laboratories continuously study new inhalation devices that would provide better drug deposition in the lungs. In order for an aerosolized drug to be effective, an adequate quantity of it should be able to be deposited beyond the oropharyngeal region. The location of the deposition (central or peripheral airways) and the uniform or non-uniform distribution of the inhaled drug also play an important role in its effectiveness.

The effect of aerosol therapies depends on the dose deposited as well as its distribution in the lungs. If an aerosol is deposited at a suboptimal dose or in a region of the lung that is not affected by the pathology being treated, the efficacy of the treatment will be compromised.

Factors such as the size of the aerosol particles, breathing conditions, the geometry of the airways or mucociliary clearance mechanisms play a fundamental role in the lung deposition of aerosolized drugs.

These peculiarities of each individual make it necessary to have available in clinical practice some type method that would be able to personalize aerosolized therapies. One way to achieve more personalized treatment would be to create airway models that are exclusive for each patient using CFD techniques. Hospitals now have more powerful, high-resolution scanners and software that create three-dimensional reconstructions of the bronchial tree. These images would be an important data source for the construction of a model that would provide flow and particle deposition

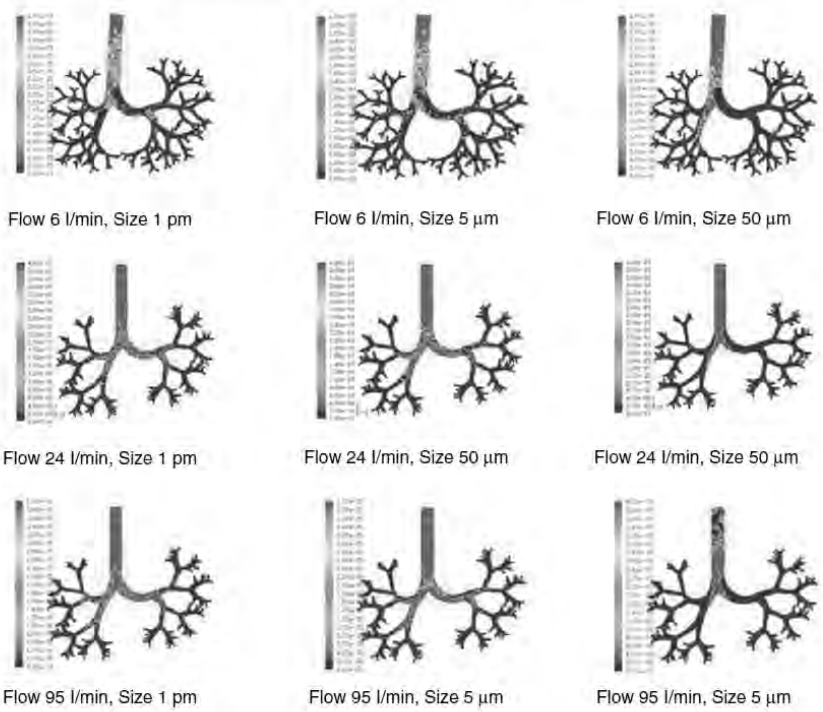

Fig. 2. Results of the simulation with computational fluid dynamics (CFD) of particle behavior at different sizes (1 pm, 5 µm, and 50 µm), which are dragged by flows of 6, 24, and 95 l/min. The red areas indicate a high density of trapped particles. It can be observed that, as the size of the particle and flow increase, more particles tend to become trapped in more central regions of the airway due to impaction.

analysis using CFD techniques. The possibilities of CT for studying the airway are underestimated.

In this current phase of our knowledge and understanding, these mathematical models, calculated by applying CFD techniques with information from HRCT, should be compared and evaluated with the classic approach provided by gammagraphy images or PET. We believe that the application of these hypothetical models will enable drug deposition to be studied and new inhalation devices to be designed that contribute toward the improved health state of our patients. In any event, a good source of "inspiration" could be the way in which smoker patients inhale.

Conflict of Interests

The authors declare having no conflict of interests.

References

1. Pritchard JN. Particle growth in the airways and the influence of airflow. In: Newman SP, Morén F, Crompton GK, editors. A new concept in inhalation therapy. Bussum: Medicom; 1987. p. 3–24.
2. Newhouse M, Sanchis J, Bienenstock J. Lung defense mechanisms. N Engl J Med. 1976;295:990–8.
3. Lourenco RV, Cotromanes E. Clinical aerosols. I. Characterization of aerosols and their diagnostic uses. Arch Intern Med. 1982;142:2163–72.
4. Heyder J. Particle transport onto human airway surfaces. Eur J Respir Dis. 1982;63 Suppl. 119:29–50.
5. Aerosols. United States Pharmacopeia. Toronto: Webcom Limited; 2006. p. 2617–36.
6. Jackson WF. Nebulised budesonide therapy in asthma. A scientific and practical review. Lund: Astra Draco AB; 1995.
7. Sbirlea-Apiou G, Katz I, Caillibotte G, Martonen T, Yang Y. Deposition mechanics of pharmaceutical particles in human airways. In: Hickey AJ, editor. Inhalation aerosols. Physical and biological basis for therapy. 2nd ed. New York: Informa Healthcare USA; 2007. p. 1–30.
8. Newman SP. Aerosol deposition considerations in inhalation therapy. Chest. 1985;88 Suppl.:152s–60s.
9. Lippmann M, Yeates DB, Albert RE. Deposition, retention and clearance of inhaled particles. Br J Ind Med. 1980;37:337–62.
10. Lange CF, Finlay WH. Overcoming the adverse effect of humidity in aerosol delivery via pressurized metered-dose inhalers during mechanical ventilation. Am J Respir Crit Care Med. 2000;161:1614–8.
11. García Río F, Prados Sánchez C, Villamar León J, Álvarez-Sala Walter R. Aerosoles, inhaladores, nebulizadores y humidificadores. Bases teóricas y aplicaciones prácticas de la aerosolterapia y de la ventiloterapia. Medicine. 1997;7:1779–85.
12. Longest PW, McLeskey JT, Hindle M. Characterization of nanoaerosol size change during enhanced condensational growth. Aerosol Sci Technol. 2010;44:473–83.
13. Longest PW, Hindle M. Numerical model to characterize the size increase of combination drug and hygroscopic excipient nanoparticle aerosols. Aerosol Sci Technol. 2011;45:884–99.
14. Basbaum CB, Finkbeiner WE. Mucus-secreting cells of the airways. In: Massaro D, editor. Lung cell biology. New York: Marcel Dekker; 1989. p. 37–9.
15. Gail DB, Lenfant JCM. Cells of the lung: neology and clinical implications. Am Rev Respir Dis. 1983;127:366–87.
16. Satir P, Sleigh MA. The physiology of cilia and mucociliary interactions. Annu Rev Physiol. 1990;52:137–55.
17. Sevilla-Sánchez D, Soy-Muner D, Soler-Porcar N. Utilidad de los macrólidos como antiinflamatorios en las enfermedades respiratorias. Arch Bronconeumol. 2010;46:244–54.
18. Summers QA. Inhaled drugs and the lung. Clin Exp Allergy. 1991;21:259–68.
19. Brain DD. Free cells in the lungs — some aspects of their role, quantitation and regulatory. Arch Int Med. 1970;126:477–87.
20. Folkesson HG, Matthey MA, Westrom BR, Kim KJ, Karlsson BW, Hastings RH. Alveolar epithelial clearance of protein. J Appl Physiol. 1996;80:1431–45.
21. Labiris N, Dolovich M. Pulmonary drug delivery. Part I: Physiological factors affecting therapeutic effectiveness of aerosolized medications. Br J Clin Pharmacol. 2003;56:588–99.
22. Castairs JR, Nimmo AJ, Barnes PJ. Autoradiographic visualization of beta-adrenoceptor subtypes in human lung. Am Rev Respir Dis. 1985;132:541–7.
23. Mak JCW, Barnes PJ. Autoradiographic visualization of muscarinic receptor subtypes in human and guinea pig lung. Am Rev Respir Dis. 1990;141:1559–68.
24. Kraft M, Djukanovic R, Wilson S, Holgate ST, Martin RJ. Alveolar tissue inflammation in asthma. Am J Respir Crit Care Med. 1996;154:1505–10.

25. Carroll N, Cooke C, James A. The distribution of eosinophils and lymphocytes in the large and small airways of asthmatics. Eur Respir J. 1997;10:292–300.
26. Davies PB, Drumm M, Konstan MW. Cystic fibrosis. Am J Respir Crit Care Med. 1996:154:1229–56.
27. Anderson PJ, Blanchard JD, Brain JD, Feldman HA, McNamara JJ, Heyder J. Effect of cystic fibrosis on inhaled aerosol boluses. Am Rev Respir Dis. 1989;140:1317–24.
28. Camps PWL. A note on the inhalation treatment of asthma. Guy's Hosp Rep. 1929;79:496–8.
29. Rau JL. The inhalation of drugs: advantages and problems. Respir Care. 2005;50:367–82.
30. Martínez-Martínez BE, Salgado-Aguilar G. Aerosolterapia. Neumol Cir Torax. 2003;62:24–8.
31. Newman SP. A comparison of lung deposition patterns between different asthma inhalers. J Aerosol Med. 1995;8 Suppl. 3:S21–6.
32. O'Callaghan C, Barry PW. The science of nebulized drug delivery. Thorax. 1997;52 Suppl. 2:s31–44.
33. Mercer TT. Production of therapeutic aerosols; principles and techniques. Chest. 1981;80 Suppl.:818–20.
34. Altshuler B, Yarmus L, Palmes ED. Aerosols deposition in the human respiratory tract. Arch Environ Health. 1957;15:292–303.
35. Newman SP, Clarke SW. Therapeutic aerosols 1 — physical and practical considerations. Thorax. 1983;38:881–6.
36. Newman SP, Pavia D, Moren F, Sheahan NF, Clarke SW. Deposition of pressurized aerosols in the human respiratory tract. Thorax. 1981;36:52–5.
37. Labiris N, Dolovich M. Pulmonary drug delivery. Part II: The role of inhalant delivery de-vices and drug formulations in therapeutic effectiveness of aerosolized medications. Br J Clin Pharmacol. 2003;56:600–12.
38. Gabrio BJ, Stein SW, Velasquez DJ. A new method to evaluate plume characteristics of hydrofluoroalkane and chlorofluorocarbon metered dose inhalers. Int J Pharm. 1999;186:3–12.
39. Leach C. Targeting inhaled steroids. Int J Clin Pract Suppl. 1998;96:23–7.
40. Leach CL. Relevance of radiolabeled steroid inhalation studies to clinical outcomes. J Aerosol Med. 1998;11 Suppl. 1:S29–34.
41. Leach CL, Bethke TD, Boudreau RJ, Hasselquist BE, Drollman A, Davidson P, et al. Two-dimensional and three-dimensional imaging show ciclesonide has high lung deposition and peripheral distribution: a nonrandomized study in healthy volunteers. J Aerosol Med. 2006;19:117–26.
42. Dolovich M, Ruffin RE, Roberts R, Newhouse MT. Optimal delivery of aerosols from metered dose inhalers. Chest. 1981;80 Suppl. 6:s911–5.
43. Ashworth HL, Wilson CG, Sims EE, Wotton PK, Hardy JG. Delivery of propellant soluble drug from a metered dose inhaler. Thorax. 1991;46:245–7.
44. Cates CJ, Rowe BH. Holding chambers versus nebulisers for beta-agonist treatment of acute asthma (Cochrane review). In: The Cochrane Library. Oxford: Update Software; 2001. p. 3.
45. Newman SP, Weisz AWB, Talaee N, Clarke SW. Improvement of drug delivery with breath actuated pressurized aerosol for patients with poor inhaler technique. Thorax. 1991;46:712–6.
46. Giner J, Basualdo LV, Casan P, Hernández C, Macián V, Martínez I, et al. Normativa sobre la utilización de fármacos inhalados. Arch Bronconeumol. 2000;36:34–43.
47. Taburet AM, Schmit B. Pharmacokinetic optimization of asthma treatment. Clin Pharmacokinet. 1994;26:396–418.
48. Newhouse MT, Kennedy A. Condensation due to rapid, large temperature (t) changes impairs aerosol dispersion from Turbuhaler (T). Am J Respir Cell Mol Biol. 2000;161:A35.
49. Virchow JC, Kroegel C, Matthys H. Antiasthma drug delivery: what is on the horizon. Clin Pharmacokinet. 1994;27:85–93.
50. Concessio NM, VanOort NM, Knowles MR, Hickey AJ. Pharmaceutical dry powder aerosols: correlation of powder properties with dose delivery and implications for pharmacodynamics effect. Pharm Res. 1999;16:828–34.
51. Terzano C, Colombo P. State of the art and new perspectives on dry powder inhalers. Eur Rev Med Pharmacol Sci. 1999;3:247–54.
52. Hickey AJ, Crowder TM. Next generation dry powder inhalation delivery systems. In: Hickey AJ, editor. Inhalation aerosols. Physical and biological basis for therapy. 2nd ed. New York: Informa Healthcare USA; 2007. p. 445–60.
53. Chan HK, Chew NYK. Novel alternative methods for the delivery of drugs for the treatment of asthma. Adv Drug Del Rev. 2003;55:793–805.
54. Prime D, Atkins PJ, Slater A, Sumby B. Review of dry powder inhaler. Adv Drug Deliv Rev. 1997;26:51–8.
55. Findeisen W. Uber das Absetzen kleiner, in der Luft suspendierter Teilchen in der menschlichen Lunge bei der Atmung. Arch Ges Physiol. 1935;236:367–79.
56. Landahl HD. On the removal of air-borne droplets by the human respiratory tract: 1. The lung. Bull Math Biophys. 1950;12:43–51.
57. Beekmans JM. The deposition of aerosols in the respiratory tract. Can J Physiol Pharmacol. 1965;43:157–72.
58. Davies CN. A formalized anatomy of the human respiratory tract. In: Davies CN, editor. Inhaled particles and vapours. Oxford: Pergamon Press; 1961. p. 82–7.
59. Weibel ER. Morphometry of the human lung. Berlin: Springer-Verlag; 1963.
60. Adler K, Brucker C. Dynamic flow in a realistic model of the upper human lung airways. Exp Fluids. 2007;43:411–23.
61. Ball CG, Uddin M, Pollard A. High resolution turbulence modelling of airflow in an ideal-ised human extrathoracic airway. Comput Fluids. 2008;37:943–64.
62. Ball CG, Uddin M, Pollard A. Mean flow structures inside the human upper airway. Flow Turbul Combust. 2008;81:155–88.
63. Fresconi FE, Prasad AK. Secondary velocity fields in the conducting airways of the human lung. J Biomech Eng Trans ASME. 2007;129:722–32.
64. Gemci T, Ponyavin V, Chen Y, Chen H, Collins R. Computational model of airflow in upper 17 generations of human respiratory tract. J Biomech. 2008;41:2047–54.
65. Grosse S, Schroder W, Klaas M, Klockner A, Roggenkamp J. Time resolved analysis of steady and oscillating flow in the upper human airways. Exp Fluids. 2007;42:955–70.
66. Theunissen R, Riethmuller ML. Particle image velocimetry in lung bifurcation models. In: Schroder A, Willert CE, editors. Particle image velocimetry: new developments and recent applications. Berlin: Springer; 2008. p. 73–101.
67. Yang XL. Respiratory flow in obstructed airways. J Biomech. 2006;39:2743–51.
68. Zhang Z, Kleinstreuer C, Kim CS. Airflow and nanoparticle deposition in a 16-generation tracheobronchial airway model. Ann Biomed Eng. 2008;36:2095–110.
69. Zhang Z, Kleinstreuer C, Kim CS. Comparison of analytical and CFD models with regard to micron particle deposition in a human 16-generation tracheobronchial airway model. J Aerosol Sci. 2009;40:16–28.
70. Tena AF, Casan P, Marcos A, Barrio R, Blanco E. Analysis of the fluid dynamic characteristics of the obstructive pulmonary diseases using a three-dimensional CFD model of the upper conductive-zone of the lung airways. In: Proceedings of the ECCOMAS thematic international conference on simulation and modeling of biological flows. 2011.
71. De Backer J, Vos W, Gorl'e C, Germonpr'e P, Partoens B, Wuyts F, et al. Flow analyses in the lower airways: patient-specific model and boundary conditions. Med Eng Phys. 2008;30:872–9.
72. Drinker P, Thompson RM, Finn JL. Quantitative measurements of the inhalation, retention and exhalation of dust and fumes by man. I. Concentration of 50 to 450 mg per cubic meter. J Ind Hyg Toxicol. 1928;10:13–25.
73. Browns CE. Quantitative measurements of the inhalation, retention and exhalation of dusts and fumes by man. II. Concentration below 50 mg per cubic meter. J Ind Hyg Toxicol. 1931;13:285–91.
74. Van Wijk AM, Pattterson HS. The percentage of particles of different sizes removed from dust-laden air by breathing. J Ind Hyg Toxicol. 1940;22:31–5.
75. Swift D, Asgharian B, Kimbell JS. Use of mathematical aerosol deposition models in predicting the distribution of inhaled therapeutic aerosols. In: Hickey AJ, editor. Inhalation aerosols. Physical and biological basis for therapy. 2nd ed. New York: Informa Healthcare USA; 2007. p. 55–82.
76. Dolovich M, Labiris R. Imaging drug delivery and drug responses in the lung. Proc Am Thorac Soc. 2004;1:329–37.

Proceedings of the ASME 2012 Fluids Engineering Summer Meeting
FEDSM2012
July 8-12, 2012, Rio Grande, Puerto Rico

FEDSM2012-72419

A METHODOLOGY FOR GEOMETRY GENERATION OF THE LOWER CONDUCTIVE ZONE OF THE LUNG AIRWAYS AND SIMULATION BY INTERMEDIATE BOUNDARY CONDITIONS

Ana F Tena
Instituto Nacional de Silicosis
Oviedo, Asturias, Spain

Pere Casan
Instituto Nacional de Silicosis
Oviedo, Asturias, Spain

Raúl Barrio
Universidad de Oviedo
Gijón, Asturias, Spain

Alfonso Marcos
Universidad de Extremadura
Badajoz, Extremadura, Spain

Jorge Parrondo
Universidad de Oviedo
Gijón, Asturias, Spain

ABSTRACT

This paper presents a general methodology for the development and simulation of a human lung between scales 0-16. The methodology is based on the simulation of only one of the two possible branches at each bronchiole. The operation of the truncated branches is included by means of a user-defined function. This function prescribes the velocity profile calculated for the active branches in the truncated ones in order to make the hydraulic losses equal between them. This procedure was tested between 0 and 7th generation by imposing the time profile of a real forced spirometry test in the trachea as boundary condition. The test showed a very good agreement between the numerical predictions and the spirometry data.

INTRODUCTION

The morphology of the human lung consists of a series of dichotomous bifurcations that result in a complex branching network [1, 2]. Several idealized descriptions of this morphology have been proposed in the technical literature in order to generate relative simple geometries than can be used to resolve the flow with a proper CFD code.

However, the simulation of the entire lung excluding the alveolar region (generations 0-16) is still beyond the actual computational capacities, so that typical calculations are carried out by means of: 1) simulations up to a specific generation only [3-5], sometimes including 1D transmission models of the small-scale airways [6]; 2) sequential simulation of subsections [6-8] that, unfortunately, does not allow for the simultaneous coupling of the flow at all scales; and 3) the resolution of a reduced number of flow paths with proper boundary conditions or stochastic approaches [9, 10]. Furthermore, these simulations usually impose constant pressure or constant mass flow boundary conditions that have been found to produce reasonable results during inhalation only, since the flow in the exhalation cycle is substantially more complex.

This article explores a general methodology to create and simulate a model of the human lung from the trachea to the alveolar region (generations 0-16). The methodology, based on the morphologies proposed by Weibel [11] and Kitaoka [12], pays special attention to the divisions at each bronchiole. The main objective of the investigation is to develop a simplified morphology of the lung, which could be used to resolve the flow at all scales simultaneously, while avoiding prohibitive mesh sizes and computational times. We use the symmetry of the model at each bronchiole to calculate the flow only along one of the two possible branches in the bifurcation. The velocity profile calculated in the active branch is imposed to the truncated branch as boundary condition by means of an external user-defined function (UDF).

This procedure was successful for both the inhalation and the exhalation cycle and avoids imposing a constant mass flow that would result in a non-realistic constant velocity profile. The numerical solver used in the present work is the commercial code Fluent® [13]. This code is applied to resolve the unsteady Reynolds-averaged Navier-Stokes equations (URANS) together with the RNG k-epsilon model for turbulent closure.

NOMENCLATURE

A	area, m^2
d	branch diameter, m
L, l	length, length of the branch, m
n	order of the branch, (0 to 16)
p	static pressure, Pa
Q	volume flow rate, l/s
t	time, s
v	velocity, m/s
β	angle, °

NUMERICAL MODEL OF THE LUNG

The morphology of a typical human lung was developed with the commercial code Gambit® [14]. The geometry is based on the models proposed by Weibel [11] and Kitaoka [12], comprising the generations 0 to 16 thus excluding the upper conductive zone to the trachea and the alveolar region.

The geometry of the bifurcations in the bronchioles at all the generations is created by a similar procedure. First of all, three circles are created corresponding to: the diameter of the high-order generation, the diameter of the low-order generation, and an intermediate diameter between them (Fig. 1). Also, secondary surfaces are created in the plane containing the circles and in the perpendicular plane.

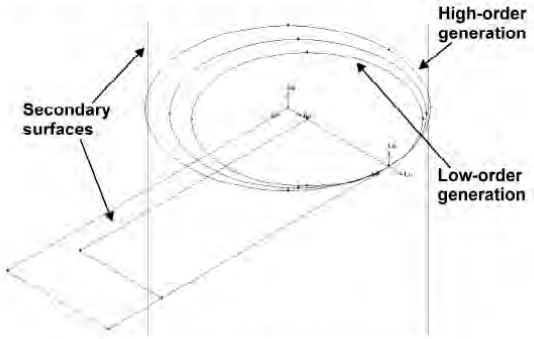

FIG. 1 DIAMETERS IN THE BIFURCATION.

As seen, the circles are split in 4 arches in order to create the front, back, and lateral boundaries of the volume, as explained later. The major edge of one of the secondary surfaces is extruded a length **L** to generate an axis of rotation (Fig. 2). The path in the bronchiole from the high-order to the low-order generation is prescribed by rotating the intermediate circle and the smaller circle round the axis an angle of **β/2** and **β** respectively. The remaining secondary surfaces are rotated an angle of **β** round the axis too. The parameters **L** and **β** were set to 0.1 m and 35° respectively based on the guidelines given in [11, 12].

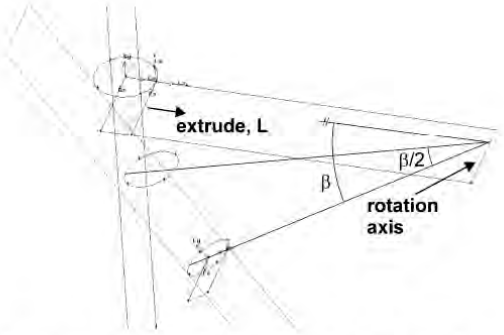

FIG. 2 PATH IN THE BRONCHIOLE FROM THE HIGH-ORDER TO THE LOW-ORDER GENERATION.

The lateral surfaces of the bronchiole were generated by means of the arches of the circles and a symmetry condition. The right-hand lateral surface is created by joining the top and bottom arches with two additional curves generated by a 3-point arc (see Fig. 3). This lateral surface, together with the bottom circle, is reflected with respect to the secondary vertical plane (plane of symmetry) in order to create the left-hand lateral surface, as shown in Fig. 3. Besides, the secondary surface that lies in the plane of the bottom circle is extruded until intersecting the plane of symmetry. The intersection originates a second axis of rotation that will be used to create the bottom surface of the bronchiole.

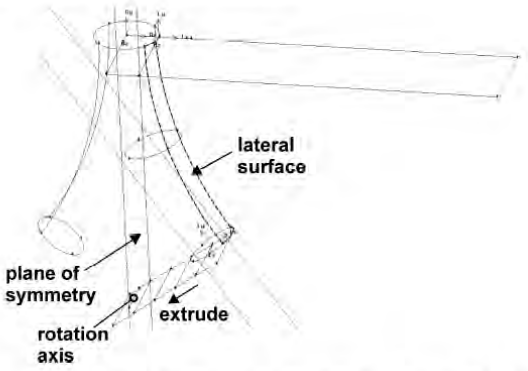

FIG.3 GENERATION OF THE LATERAL SURFACES IN THE BRONCHIOLE.

The inner arch of the bottom circle is revolved with respect to the axis indicated in the previous paragraph until joining with its symmetrical arch (Fig. 4). All the surfaces are now available so that the volume of the bronchiole can be generated. The result of these operations is seen in Fig. 4.

As explained in the introduction, the main purpose of the investigation is to develop a numerical model of the lung as realistic as possible while avoiding prohibitive computational costs. To achieve this, the remaining morphology of the lung will be developed along only one of the two possible branches in each bronchiole (one branch will be considered as 'truncated').

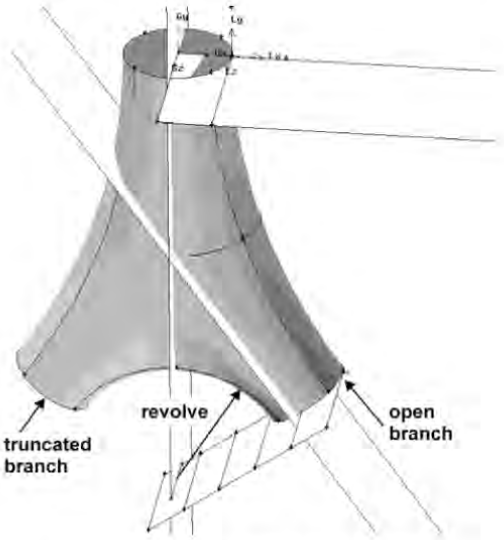

FIG. 4 GEOMETRY OF THE BIFURCATION.

The last step in the creation of the morphology is to generate the geometry of the active (open) branch. This is done by extruding the circle that prescribes the diameter of the low-order generation a specific length **l** (Fig. 5). The secondary surface that lies in the plane on this circle is then moved to the plane located at the end of the extrusion. This surface, together with the secondary surface that contains the axis of the cylinder generated in the extrusion, is rotated 90° with respect to the local axis indicated in the figure according to the models described in [11, 12].

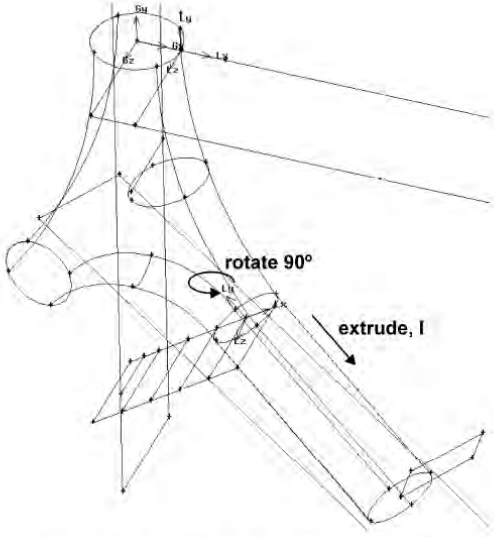

FIG. 5 GENERATION OF THE OPEN BRANCH.

The geometry of the lung can be further developed up to reaching the alveolar region (generation 16) if the procedure described so far is repeated systematically. The numerical model of the lung is shown in Fig. 6; also, this figure presents a detail of the lower generations. A series of additional surfaces were created in the branches for data analysis purposes.

The complete morphology of the lung can be generated from the numerical model of Fig. 6. This is done by imposing symmetry at each of the truncated branches. The entire lung is presented in Fig. 7 for showing purposes only; of course, the numerical simulation of this complete morphology would be simply unavoidable.

A summary of the main geometric dimensions in the branches is presented in Table 1. The diameter **d** and the length **l** were deduced from the relations proposed by Weibel and Kitaoka [11, 12]:

$$\begin{cases} d = 0.018\exp(-0.388\,n) & \text{if } n \le 3 \\ d = 0.013\exp\left[-(0.2929 - 0.00624\,n)\,n\right] & \text{if } n > 3 \end{cases} \quad (1)$$

$$\begin{cases} l = 0.12\exp(-0.92\,n) & \text{if } n \le 3 \\ l = 0.025\exp(-0.17\,n) & \text{if } n > 3 \end{cases} \quad (2)$$

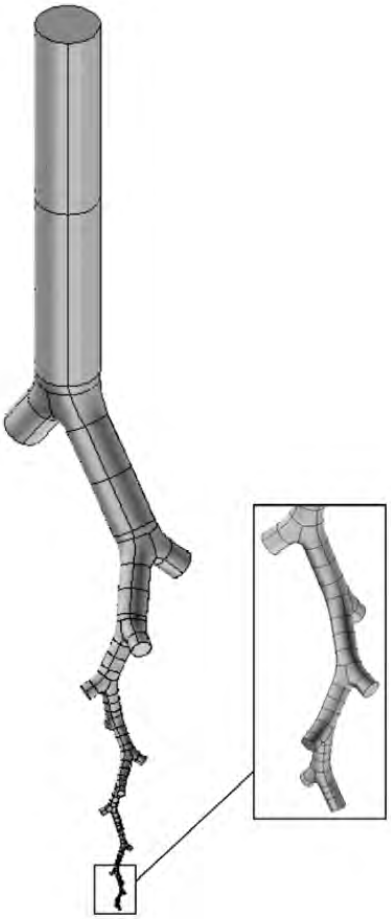

FIG. 6 NUMERICAL MODEL OF THE LUNG.

TABLE 1 MAIN PARAMETERS OF THE BRANCHES.

n	Branches	d (m)	l (m)	A (m^2)
0	1	0.01800	0.12000	2.545E-04
1	2	0.01221	0.04782	1.171E-04
2	4	0.00828	0.02485	5.390E-05
3	8	0.00562	0.01686	2.481E-05
4	16	0.00445	0.01267	1.556E-05
5	32	0.00351	0.01069	9.692E-06
6	64	0.00281	0.00901	6.189E-06
7	128	0.00227	0.00761	4.052E-06
8	256	0.00186	0.00642	2.720E-06
9	512	0.00154	0.00541	1.872E-06
10	1024	0.00130	0.00457	1.321E-06
11	2048	0.00110	0.00385	9.556E-07
12	4096	0.00095	0.00325	7.088E-07
13	8192	0.00083	0.00274	5.391E-07
14	16384	0.00073	0.00231	4.203E-07
15	32768	0.00065	0.00195	3.360E-07
16	65536	0.00059	0.00165	2.754E-07
17	131072	0.00054	0.00139	2.314E-07

The model of the lung was meshed with tetrahedral cells due to their better adaptation to complex geometries. The size of the tetrahedrons diminishes while descending from the high-order to the low-order generations. A boundary layer mesh was built before meshing the volumes in order to obtain a better description of the boundary layer in the numerical calculations. The size of the tetrahedrons was consistent with the size of the boundary layer cells. The total size of the grid is about 10^6 cells. A quality analysis of the mesh showed a very satisfactory result, indicating a magnitude of the equisize skew that was below 0.6 for 98% of the cells in the mesh.

Figure 8 shows an example of the surface mesh at some branches. Besides, a detail of the boundary layer mesh in one truncated branch is presented; in this case, only the cells in the boundary layer are made visible in the figure.

FIG. 7 COMPLETE MORPHOLOGY OF THE LUNG.

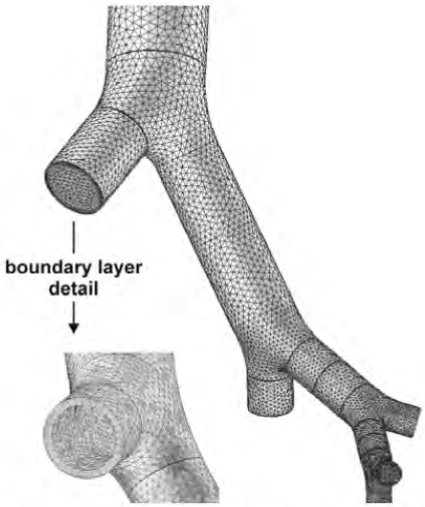

FIG. 8 EXAMPLE OF THE SURFACE MESHES AT SOME BRANCHES. A DETAIL OF THE BOUNDARY LAYER MESH IN A TRUNCATED BRANCH IS ALSO SHOWN.

A grid dependence analysis was carried out before performing the final calculations. For this purpose, two additional grids of size $2 \cdot 10^6$ and $4 \cdot 10^6$ cells were built in order to check the change in the magnitude of two reference variables as a function of the number of cells. The reference variables chosen were the static pressure and the volume flow rate at the lowest generation. It was observed that the typical variations predicted were below 1.5% (when compared to the results for the fine grid) even for the coarse mesh.

CALCULATION METHODOLOGY

The numerical calculations were resolved with the commercial code Fluent® [13]. This code was used to solve the unsteady Reynolds-averaged Navier-Stokes equations (URANS) by the finite volume method.

The solver was set to pressure-based and implicit with an absolute formulation for the velocity fields. The discretization of the spatial and temporal derivatives in the equations was carried out by means of second-order schemes. The discretization of the pressure was standard. The SIMPLE algorithm was imposed to resolve the coupling between pressure and velocity fields. Turbulent closure was established with the RNG k-epsilon model and enhanced wall treatment to resolve the flow field close to the walls.

The boundary conditions imposed during the inhalation cycle were a specific volume flow rate at the trachea and a constant gauge pressure at the lowest generation. In contrast, a specific volume flow rate at the bottom of the lung and a zero gauge pressure at the trachea were prescribed during exhalation. An additional simulation of the exhalation cycle was carried out by imposing at the lowest generation the time profile of the static pressure obtained in the previous simulation. This was done in order to check the consistency of the numerical predictions, as explained in the following section.

A law of variation along time for the volume flow rate at the trachea was used to carry out the unsteady calculations. This law was obtained by means of a forced spirometry test of one of the authors (see Fig. 9). The temporal evolution of the volume flow rate was imposed at the inlet boundary during the calculations by means of an external user-defined function (UDF). As observed in Fig. 9, the rate of change of the volume flow rate is very dependent on the time interval considered. In consequence, the UDF included a subroutine to adapt the magnitude of the time step to this rate of change (adaptive time step). To achieve this, the original spirometry function was split into a series of intervals, each with a specific magnitude of the time step (adjusted data in Fig. 9), with the purpose of reducing the computational time needed for the calculations. The number of time steps used to simulate the entire breathing cycle was set to 37.

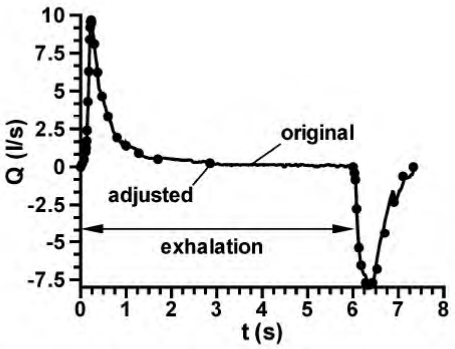

FIG. 9 ORIGINAL AND ADJUSTED LAW FOR THE FORCED SPIROMETRY TESTS.

An additional user-defined function was used to impose a symmetric operation of the two branches at each bronchiole. This UDF obtains the velocity profile at each open branch (either in inhalation or exhalation) from the calculations and prescribes the same profile in the corresponding truncated branch. A detailed description of this UDF (which is about 400 lines long) is beyond the scope of this article. This methodology is repeated iteratively at each time step until achieving convergence in the flow field. Preliminary tests showed that a maximum of 100 iterations were required in order to assure the convergence of the results at each time step. The convergence criterion established was to reduce the scaled

residuals for all the variables below $8 \cdot 10^{-5}$. About 5 complete breathing cycles were required to achieve a periodic unsteady solution.

PRELIMINARY RESULTS

Although the numerical model of the lung was developed from generations 0 to16, preliminary calculations including up to the 7th generation were performed first in order to check the procedure described in the previous section. Therefore, the results presented in this section of the paper are only for generations between 0 and 7.

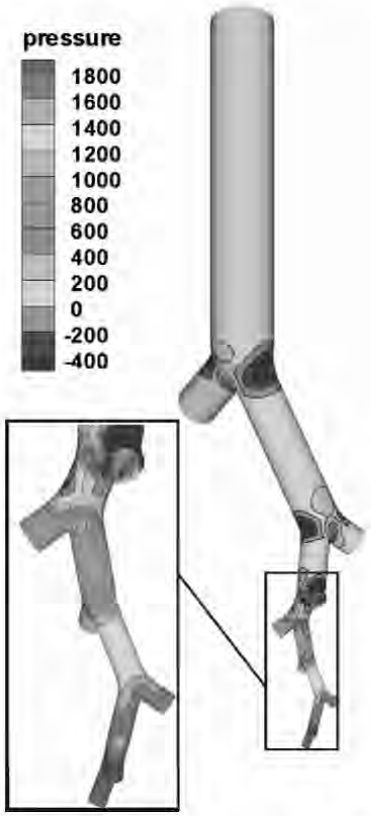

FIG. 10 CONTOURS OF THE INSTANTANEOUS STATIC PRESSURE [PA] ALONG THE BRANCHES DURING EXHALATION. A DETAIL OF THE LOWER GENERATIONS IS ALSO SHOWN.

The contours of the instantaneous static pressure during exhalation are shown in Fig. 10. As observed, the magnitude of the pressure diminishes while ascending from the lowest generation to the trachea, where a magnitude of zero pressure is reached (i.e. atmospheric conditions). Also, it is noted that regions of negative pressure are predicted at the bifurcations of the bronchioles above the 4th generation. The symmetry of the pressure field at the bifurcations can be observed in Fig. 10.

The instantaneous absolute velocity field during exhalation is shown in Fig. 11 for generations between 2 and 7; also, a detail of this field at the lower generations is also presented. In general, it can be said that the flow is axisymmetric and shows a predominant component of the velocity in the axial direction.

The time distribution of the instantaneous static pressure at the lowest generation (g7) during the entire breathing cycle is presented in Fig. 12. As explained in the previous section, this result was obtained by prescribing the adjusted spirometry of Fig. 9 at the trachea.

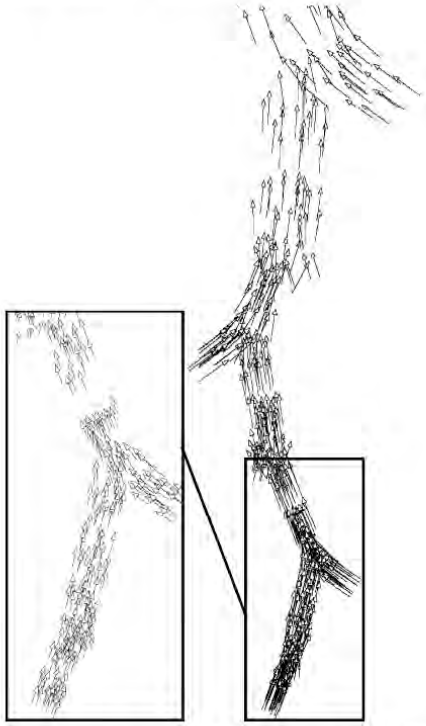

FIG. 11 VELOCITY VECTOR FIELD DURING EXHALATION AT GENERATIONS 2-7 WITH A DETAIL OF THE LOWER ONES.

The results of Fig. 12 show an increasing static pressure during the exhalation cycle up to a maximum magnitude at the same time where the volume flow rate (Fig. 9) is maximum. Similarly, it is observed that the static pressure in generation 7 decreases to negative values during inhalation and reaches a minimum magnitude when the inlet volume flow is maximum in absolute value.

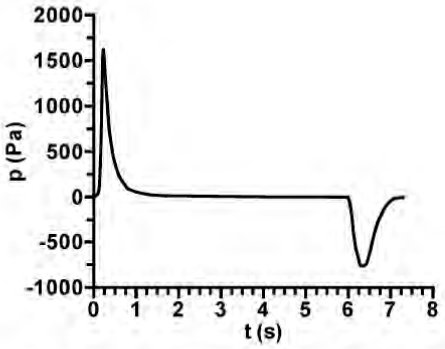

Fig. 12 TIME DISTRIBUTION OF THE INSTANTANEOUS STATIC PRESSURE AT GENERATION 7.

A final simulation was performed in order to check the consistency of the numerical predictions. For this purpose, the time profile of the static pressure obtained during exhalation (Fig. 12) was imposed at generation 7 as inlet boundary condition. If the calculation procedure were correct, the time profile of the volume flow rate (or, similarly, of the outlet velocity) predicted at the trachea should be equal to the original spirometry of Fig. 9.

The result of this test is presented in Fig. 13. As seen, the degree of agreement between the numerical calculation and the real spirometry is very satisfactory, showing a very close correspondence between both velocity profiles. This indicates that the numerical model developed and the UDF procedure described can be used to properly simulate the operation of a real lung.

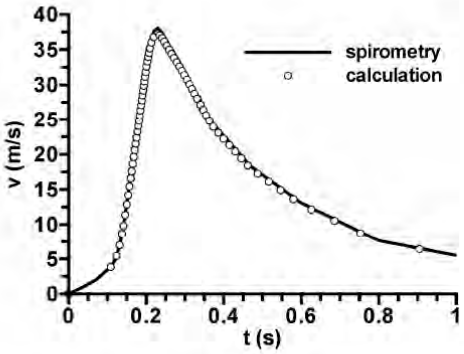

FIG. 13 COMPARISON BETWEEN REAL SPIROMETRY AND CALCULATION (BASED ON PRESSURE BOUNDARY CONDITION) DURING THE EXHALATION CYCLE.

CONCLUSIONS

This paper has explored a general methodology to simulate a model of a human lung. The main goal of the investigation was to develop a complete and realistic model of the lower conductive zone of the lung (generations 0 to 16) that can be simulated within reasonable computational times.

For this purpose, the path along only one airway at each bronchiole was generated and simulated. The operation of the 'truncated' airway is included in the simulations by means of a user-defined function. This function was used to: 1) obtain the velocity profile at each 'active' (open) branch, and 2) prescribe this profile in the truncated branch. This was useful to simulate the operation of the truncated branches at each bronchiole.

Preliminary tests were carried out until generation 7 in order to check this procedure. The time profile of a real forced spirometry test was imposed as boundary condition in the trachea by means of an additional user-defined function, showing a satisfactory prediction of the general flow field in the lung. Also, the consistency of the numerical calculations was tested by prescribing the time profile of the static pressure obtained during exhalation as inlet boundary condition at generation 7. It was observed that the outlet velocity profile predicted at the trachea was almost the same as the one obtained in the spirometry.

Therefore, it can be concluded that the numerical model presented in this paper and the user-defined function routine included to account for the operation of the truncated branches can be satisfactory used to simulate the real operation of a human lung over the entire breathing cycle. This model provided a realistic description of the operation of the lung while avoiding too large computational costs. Our future efforts will focus in the simulation of the entire flow field in the lung (until generation 16) and also in the study of several pulmonary diseases (bronchitis, emphysema, etc.) and particle deposition by discrete phase modeling.

ACKNOWLEDGMENTS

The authors gratefully acknowledge the financial support of Junta de Extremadura and FEDER under Project GR10047 and also of Ministerio de Ciencia e Innovación under Project DPI 2010-21103-C04-04.

REFERENCES

[1] Sera, T., Fujioka, H., Yokota, H., Makinouchi, A., Himeno, R., Schroter, R. C., Tanishita, K., 2003, "Three-Dimensional Visualization and Morphometry of Small Airways From Microfocal X-Ray Computed Tomography". *Journal of Biomechanics*, **36**(11), pp. 1587-1594.

[2] Burton, R. T., Isaacs, K. K., Fleming, J. S., Martonen, T. B., 2004, "Computer Reconstruction of a Human Lung Boundary Model From Magnetic Resonance Images". *Respiratory Care*, **49**(2), pp. 180-185.

[3] Zhang., Z., Kleinstreuer, C., Kim, C., 2001, "Flow Structure and Particle Transport in a Triple Bifurcation Airway Model". *Journal of Fluids Engineering*, **123**(2), pp. 320-330.

[4] Zhang, Z., Kleinstreuer, C., 2002, "Transient Airflow Structures and Particle Transport in a Sequentially Branching Lung Airway Model". *Physics of Fluids*, **14**(2), pp. 862-880.

[5] Liu, Y., So, R. M. C., Zhang, C. H., 2002, "Modeling the Bifurcating Flow in a Human Lung Airway". *Journal of Biomechanics*, **35**(4), pp. 465-473.

[6] Ma, B., Lutchen, K. R., 2006, "An Anatomically Based Hybrid Computational Model of the Human Lung and Its Application to Low Frequency Oscillatory Mechanics". *Annals of Biomedical Engineering*, **34**(11), pp. 1691-1704.

[7] Nowak, N., Kadake, P. P., Annapragada, A. V., 2003, "Computational Fluid Dynamics Simulation of Airflow and Aerosol Deposition in Human Lungs". *Annals of Biomedical Engineering*, **31**(4), pp. 374-390.

[8] Zhang, Z., Kleinstreuer, C., Kim, C. S., 2008, "Airflow and Nanoparticle Deposition in a 16-Generation Tracheobronchial Airway Model". *Annals of Biomedical Engineering*, **36**(12), pp. 2095-2110.

[9] Gemci, T., Ponyavin, V., Chen, Y., Chen, H., Collins, R., 2008, "Computational Model of Airflow in Upper 17 Generations of Human Respiratory Tract". *Journal of Biomechanics*, **41**(9), pp. 2047-2054.

[10] Walters, D. K., Luke, W. H., 2010, "A Method for Three-Dimensional Navier-Stokes Simulations of Large-Scale Regions of the Human Lung Airway". *Journal of Fluids Engineering*, **132**(5), 01-1 to 01-8.

[11] Weibel, E. R. *Morphometry of the human lung*. Springer-Verlag, 1963.

[12] Kitaoka, H., Takaki, R., Suki, B., 1999, "A Three Dimensional Model of the Human Airway Tree". *Journal of Applied Physiology*, **87**(6), pp. 2207-2217.

[13] Fluent® version 6.3.26, 2006, ©ANSYS Inc. All Rights Reserved.

[14] Gambit® version 2.4.6, 2006, ©ANSYS Inc. All Rights Reserved.

Conference on Modelling Fluid Flow (CMFF'12)
The 15th International Conference on Fluid Flow Technologies
Budapest, Hungary, September 4-7, 2012

NUMERICAL SIMULATION OF THE NANO PARTICLE DEPOSITION USING A THREE-DIMENSIONAL MODEL OF LUNG AIRWAYS

A. F. Tena[1], P. Casan[1], J. Fernandez[2], A. Marcos[2], and R Barrio[3]

[1] Instituto Nacional de Silicosis. C/ Dr Bellmunt. 33006 Oviedo. E-mail: anafertena@gmail.com, pcasan@ins.es
[2] Universidad de Extremadura. Avda de Elvas, 06006 Badajoz, Spain. E-mail: ffrancos@unex.es, acmarcos@unex.es
[3] Universidad de Oviedo. Campus de Viesques 33203 Gijón, Spain. E-mail: barrioraul@uniovi.es

ABSTRACT

One of the main health problems to the urban population is the exposure to air pollution. Suspended particles (made up of soot, smoke, dust and liquid droplets) can cause a wide range of respiratory diseases such as asthma and chronic obstructive pulmonary disease, as well as worsening heart diseases and other conditions. Knowing the particle deposition in realistic models of the human respiratory system is fundamental to prevent these diseases, and this is the objective of this work.

A 3D numerical model of the bronchial tree has been developed, from the trachea to the seventh level bronchioles. The geometry follows the model developed by Weibel and Kitaoka. It has been discretized with a mesh of about one million cells. The Navier-Stokes equations have been solved with a commercial CFD finite volume code.

Keywords: CFD, Lung, Particles.

NOMENCLATURE

CFD	[-]	Computational Fluid Dynamics
COPD	[-]	Chronic Obstructive Pulmonary Disease
DF	[-]	Deposition fraction
DPM	[-]	Discrete Phase Model
SIMPLE	[-]	Semi-Implicit Method for Pressure-Linked Equations
UDF	[-]	User Defined Function
d	[m]	Branch diameter
d_a	[m]	Aerodynamic diameter
d_p	[m]	Particle diameter
n	[-]	Order of the branch
Q	[ℓ/min]	Flow rate
$\vec{u}$	[m/s]	Velocity vector
$(\nabla \times \vec{u})\cdot\vec{u}$	[m/s^2]	Helicity
$y+$	[-]	Wall Yplus ($\rho y u_t / \mu$)
β	[º]	angle

1. INTRODUCTION

In the rush hour in the city, cars, with diesel engines, start up, move for a few meters, slow down and then start again, releasing particles into the atmosphere. Depending on their size, particles can be classified into:

- Particles of aerodynamic diameter between 15 and 100 μm: Particles over 15 μm are deposited by their weight and are rarely inhaled.
- Particles of aerodynamic diameter between 5 and 10 μm: The human nose and trachea filter particles from 10 to 15 μm, preventing its entrance into the lungs.
- Particles of aerodynamic diameter between 2.5 and 5 μm: The cilia of the respiratory epithelium of the trachea expel the captured particles of 3-5 μm through the nasopharynx.
- Particles of aerodynamic diameter less than 2.5 μm. These finer particles are the most important from the standpoint of health.

Aerodynamic diameter is the diameter of a sphere of density 1,000 kg/m^3 that has the same gravitational settling velocity as the particle in question.

$$d_a = d_p \left(\frac{\rho_p}{1{,}000} \right)^{\frac{1}{2}} \quad (1)$$

The effect of particles on health is directly dependent on its size, since the human body is designed to remove larger particles and prevent them from accumulating in the lungs, which are the filters that prevent the passage of particles to the blood stream.

The upper airways consist of the nose, inner nasal cavity, paranasal sinuses, pharynx and larynx. For this work we will focus on the anatomy of the lower airways, which begin at the trachea. The

trachea is divided into two main bronchus. Then each bronchi continue to divide in a dichotomous way, reaching a minimum of 23 generations. Generations 1, 2 and 3 are called bronchi. Generations 4 to 16 are the bronchioles. The latter is called the terminal bronchiole and it is the smallest portion of the airways devoid of alveoli.

The basic objective of the experimental and numerical studies of flow in the lungs is to deepen in the knowledge of the gas exchange (O_2 and CO_2) and in the particle deposition, and optimize the application of pharmaceutical aerosols for the treatment of lung diseases. The deposition of aerosols in the lungs is a non-stationary phenomenon due to the complexity of the lungs' geometry, the existence of interactions between air, water and solids, the cells' mechanics and heat transfer. This means that the velocity, density, pressure or temperature can change over time. Not all phenomena occurring in the lungs' airways can be simulated. Experimental and numerical simplifications are needed, such as considering the airflow as isothermal, rigid ducts (which would be the bronchi), and a spherical shape of the particles.

The earlier studies of particle deposition were based on one-dimensional models based on empirical formulas. One of the pioneering researchers in this field was Martonen [1-2], who proposed in 1982 a system of equations to determine the particle deposition. For its formulation took into account a number of assumptions such as the behaviour of particles in the lung (that are deposited by impaction, sedimentation and diffusion) and the velocity of air in the lungs in function of tidal volume and respiratory rate. In the larger particles the impaction behaviour predominates, while in the smaller ones diffusion is the main behaviour. The intermediate particles tend to deposit by sedimentation because of the effect of gravity.

For over a decade, several studies about the airflow behaviour were performed, starting in the mouth and ending in the alveolar region [3-6]. These studies have mainly focused on isolated sections of the lung, such as the trachea and the first generations of alveolar ducts or sacs.

Current studies are based predominantly in Computational Fluid Dynamics (CFD). Increased computer power has allowed the development of this technique, in which the Navier-Stokes equations are solved in the domain under study. Walters [7] uses a model with a finite number of flow paths, each of which is fully resolved, to provide a detailed description of the entire complex small-scale flowfield. This model was tested for three inspiratory flowrates and compared in terms of pressure drop, flow distribution characteristics, and flow structure with the fully resolved geometry. Robinson [8, 9] focuses her work in studying the three main modes of particle deposition (impact, sedimentation and diffusion) using simplified ducts. The techniques of imaging (e.g., SPECT) can detect with a high degree of resolution the deposition patterns of particles, but not clearly the airway composition. Martonen [10] shows a protocol to aid in the interpretation of these images, where the interior of lung was partitioned into a series of nested shells, each one containing its part of the airways, helping the interpretation of scintigraphy images. To our knowledge, the use of CFD in Spain has been only developed in the Universidad Autónoma de Madrid [11] and in the Universidad de Valladolid [12], although both cases were limited to the upper airways.

This work is part of a broader one, which tries to model the airflow in the lung with all their characteristics: unsteady flow, inhalation and exhalation of particles, common diseases (asthma, bronchitis, etc.). A first step was [13] the construction and simulation of a particular 7-level model, using a single way to study the unsteady flow that occurs during the execution of a spirometry test. The main innovation was the unsteady boundary conditions applied in conjunction with an adaptive time step. Such conditions required the use of two UDF. The fluid dynamic phenomenon of different obstructive diseases, and how it is perceived in the tests, was characterized varying the geometry and the unsteady boundary conditions.

A second step of the investigation is the main objective of this work, to study the lung deposition of inhaled particles through a numerical model. To achieve the overall objective we have established the following specific objectives:

- Preparation of a geometrical model of human airway.
- Preparation of numerical model to determine the airflow through the airway.
- Determining the transport and deposition of particles under different conditions of speed and particle sizes.

2. METHODOLOGY

A 3D numerical model of the bronchial tree has been developed, from the trachea to the seventh level bronchioles with the commercial code Ansys Gambit© [14]. The geometry follows the models developed by Weibel [15] and Kitoaka et al [16].

This model begins at the trachea, which has a length of 12 *cm* and a diameter of around 1.8 *cm*. The right main bronchus is shorter and wider. It leaves the trachea with an angle of 25 to 30 degrees, with a diameter of approximately 1.5 *cm* and a length of 2 *cm*. The left main bronchus leaves the trachea with an angle of approximately 45 degrees. It is substantially longer than the right main bronchus, with an average length of 5 *cm* and a diameter of 1.2 *cm*. Levels 2 and 3 are made with Kitoaka recommendations [16] and the rest following Weibel [15]. The bifurcation angle β was set to 35º

according to the guidelines given in [15]. The dimensions of the built model can be seen in table 1.

Table 1. Model dimensions

Gen n	Branches number	Diam (m)	Lengh (m)	Area (m^2)
0	1	0.01800	0.12000	2.54E-08
1	2	0.01221	0.04782	1.17E-08
2	4	0.00828	0.01906	5.39E-09
3	8	0.00562	0.00760	2.56E-09
4	16	0.00445	0.01267	1.56E-09
5	32	0.00351	0.01069	9.69E-10
6	64	0.00281	0.00901	6.19E-10
7	128	0.00227	0.00761	4.05E-10

The geometry of the bifurcations in the bronchioles at all the generations is created by a similar procedure. The diameter d and the length ℓ, deduced from the relations proposed by Weibel and Kitaoka, are:

$$\begin{cases} d = 0.018\exp(-0.388\,n) & \text{if } n \le 3 \\ d = 0.013\exp\left[-(0.2929 - 0.00624\,n)\,n\right] & \text{if } n > 3 \end{cases} \quad (2)$$

$$\begin{cases} l = 0.12\exp(-0.92\,n) & \text{if } n \le 3 \\ l = 0.025\exp(-0.17\,n) & \text{if } n > 3 \end{cases} \quad (3)$$

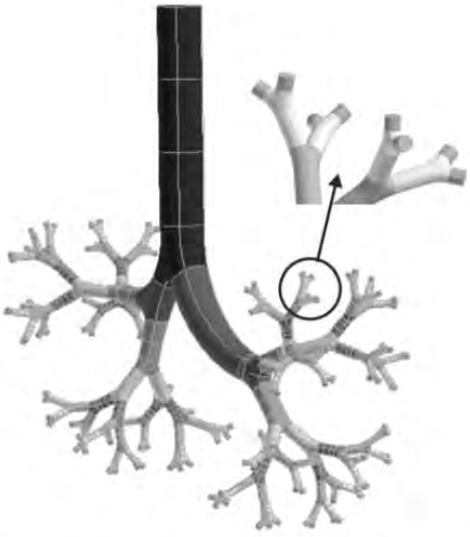

Figure 1. Numerical model geometry from the trachea to the 7th order bronchioles

Figure 1 shows a global image of the model. The complete morphology of the lung can be generated from this model by imposing symmetry at each of the branches. The entire lung is presented in Figure 2 for showing purposes only; of course, the numerical simulation of this complete morphology would be simply unavoidable.

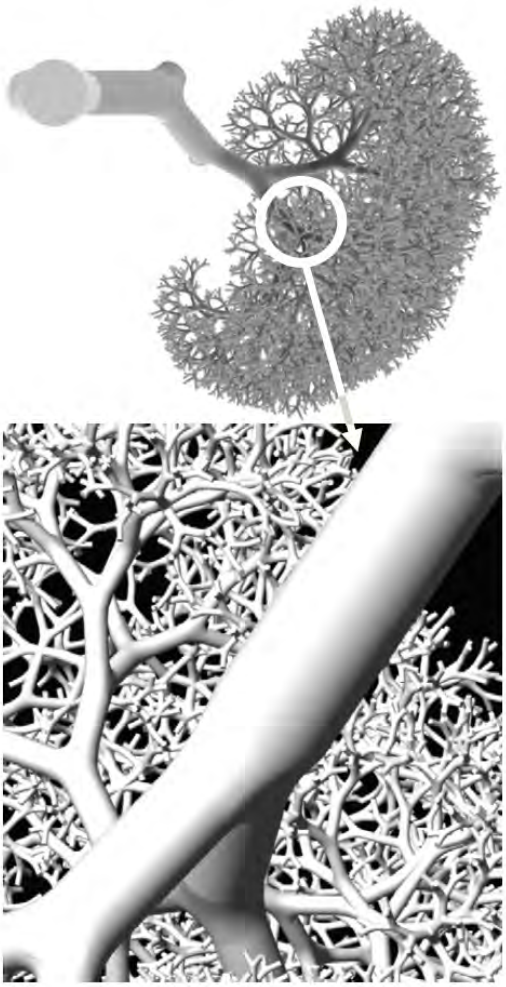

Figure 2. Complete morphology of the lung

Figure 3 shows a detail of the unstructured mesh generated. The model of the lung was meshed with tetrahedral cells due to their better adaptation to complex geometries. The size of the tetrahedrons diminishes while descending from the high-order to the low-order generations. A boundary layer mesh was built before meshing the volumes in order to obtain a better description of the boundary layer in the numerical calculations. The size of the tetrahedrons was consistent with the size of the boundary layer cells. The volume of the cells ranges between $2.96\text{x}10^{-12}$ and $2.01\text{x}10^{-10}$. The maximum equiangle skew was restricted to 0.6 for 97.60% of the cells in the mesh.

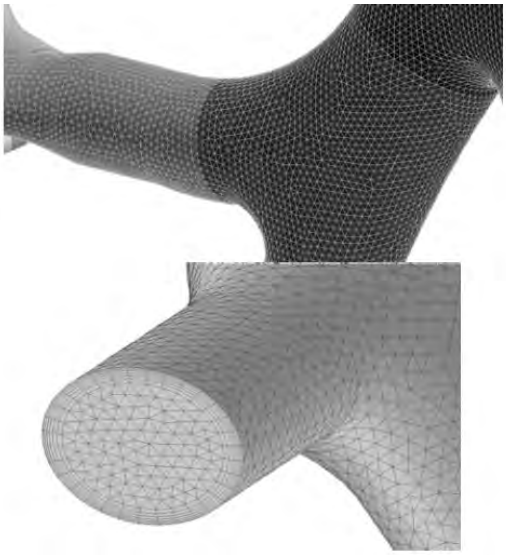

Figure 3. Detail of the mesh

The total number of cells used to begin the simulations was about 10^6, though other meshes of different size ($2x10^6$ and $4x10^6$) were generated in order to investigate the dependence of the numerical predictions. As can be seen in Figure 4, the variation observed in the outlet static pressure rate when considering different mesh sizes is not very significant. For the mesh size used for the calculations (about 1,000,000 cells) this variation is lower than 1.77%, and with 2,000,000 cells is lower than 1.04% compared with the model of 4,000,000 cells.

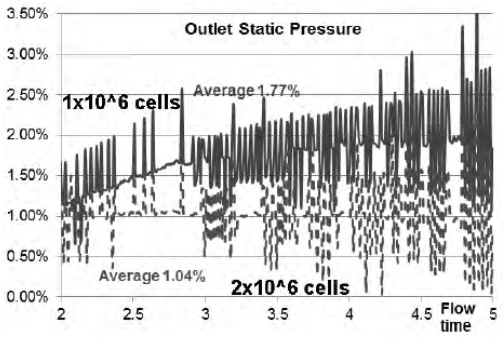

Figure 4. Results of the independence tests

The numerical simulations were performed with the code Ansys Fluent© [17]. This code was used to solve the full steady 3D Reynolds-averaged Navier-Stokes equations by the finite volume method. The fluid used in the calculations was air. The velocities will vary between 0.4 and 8 *m/s*, so the Reynolds number is between $4.93x10^2$ and $9.83x10^3$. The flow was considered as incompressible and turbulent. To effectively address both laminar and turbulent flow conditions, the model used for turbulent closure was the SST k-omega together with the transitional flows option to enable a low-Reynolds-number correction to the turbulent viscosity. This model provides a good approximation to transitional flows because the value of ω does not reach the zero value as the laminar flow limit is approached. Furthermore, the turbulence is simulated all the way to the viscous sublayer, avoiding the use of standard wall functions, which are inaccurate for transitional flows. The pressure-velocity coupling was established by means of the SIMPLE algorithm. Second-order upwind discretizations were used for the convection terms and central difference discretizations were established for the diffusion terms. The $y+$ values were maintained to be on the order of approximately 2 or less at all wall boundaries.

This model has already been tested in the first step of this broad work [13].

The particle trajectory equation can either be solved with the momentum and energy equation for the continuum flow (coupled) or after the momentum and energy equations have converged (uncoupled). The coupled option allows particles to interact with the flow fluid and affect the flow solution. In this case, the uncoupled option was chosen. The inlet boundary condition was mass flow rate, and the outlet boundary condition was pressure outlets. Each of the 128 terminal airway branches were held constant at atmospheric pressure, instead of constant outflow, since the flow rate in the branches is allowed to vary. Convergence was accepted with a criteria of 0.00001 residuals for continuity and each velocity component in the momentum equation. Convergence required about 1,600 iterations and approximately 10 min CPU time.

Once the static simulation has finished, the Discrete Phase Model (DPM) is switched on to predict the trajectory of discrete phase particles. To study particle deposition, the Lagrangian approach was used; particle trajectories were calculated within the steady flow fields of interest as a post processing step. Forces on the particles of interest include drag, pressure gradient, gravity, lift, and Brownian motion. To model the effects of turbulent fluctuations on particle motion, a random walk method has been employed. The tracking parameters used were 50,000 for the "maximum number steps" and 5 for the "step length factor".

Particles are introduced by means of an injection type called surface, specifying particle properties and velocity. The particles must be introduced from a surface close to the entrance (0.1 *mm*) and not near the walls (0.5 *mm*) to avoid the immediate deposition. Robinson [18] founded that 50,000 particles are necessary to minimize random variation in the deposition efficiency predictions due to the randomness of the particle position profile. Figure 5 shows the spatial distribution of particles

employed at the inlet in DPM. Only 188 of the 50,058 particles are shown.

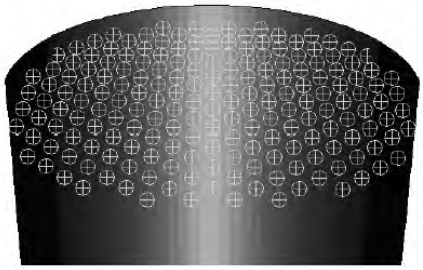

Figure 5. Particles distribution at the inlet.

Deposition is determined by summing up the "trapped" fate particles, which occurs when their centre of mass touches the wall. Fluent also reports the number of incomplete, aborted, or unable to be tracked particles. These numbers can be minimized by adjusting various input parameters.

3. RESULTS

The flow rates tested were 8, 31, 95 and 122 *ℓ/min*, which are equivalent to different respiratory rhythms. The seeding conditions of the particles were:

- Inert material density: 1,000 kg/m^3.
- Particle size: 5 *nm*, 10 *nm*, 50 *nm*, 0.1 *μm*, 0.2 *μm*, 0.5 *μm*, 1 *μm*, 2 *μm*, 5 *μm*, 10 *μm* and 20 *μm*.
- Velocity: the same that air.
- Density 0.5%.
- Number of injected particles: 50,058.

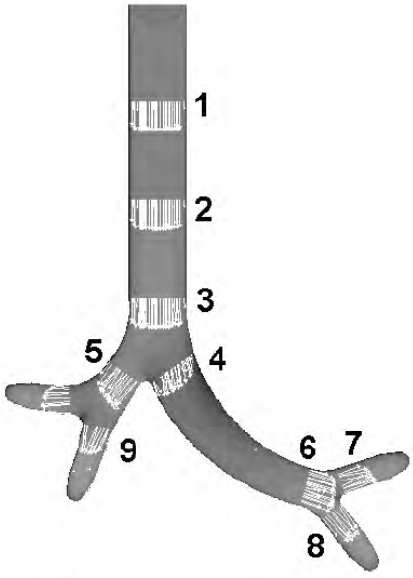

Figure 6. Velocity vectors and contours (range 0-6.5 *m/s*) in the first 3 levels, flowrate 31 *ℓ/min*

Figure 6 shows the velocity contours in the first 3 levels as well as the velocity profiles at several positions.

In figure 7, the helicity inside the lung at various positions is mapped. Helicity is defined by the dot product of the vorticity and the velocity vectors, that is $(\nabla \times \vec{u}) \cdot \vec{u}$. It provides information about the vorticity aligned with the fluid stream. It has been plotted here looking for the secondary flows. The surfaces are tangential planes and two counter-rotating vortices are captured. It can be observed that the vortex centres are kept more or less at the same distance from the lung centre. Only small differences are found at both sides of the centre plane (middle surface in the axis direction).

Because the input boundary condition, the fluid begins to have vorticity at the end of the trachea, which favours the deposition of particles carried by the air.

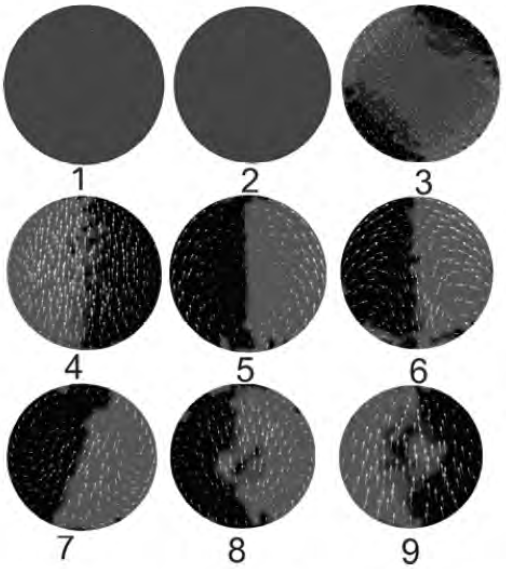

Figure 7. Helicity at various sections (figure 6) in m/s^2, flow rate 31 *ℓ/min*.

The regional deposition of particles can be quantified in terms of the deposition fraction (DF), defined as the mass ratio of deposited particles in a specific region to the particles entering the lung. Here (figure 8) is the ratio of the particles trapped in the first seven levels and entering the lung. These results agree with Dolovich [18], shown in figure 6, except in the range of particles between 0.1 and 2 *microns*, where numerical values are greater than those obtained experimentally. This difference may be due mainly to lung numerical model used, but can also be influenced by the parameters used.

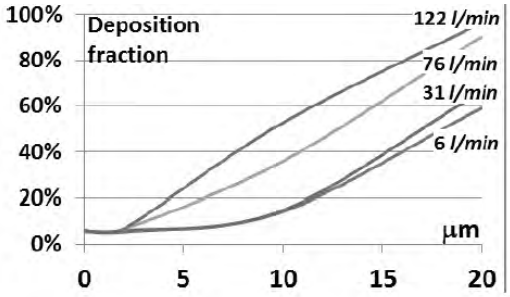

Figure 8. Relationship between particle size and lung deposition. Numerical results.

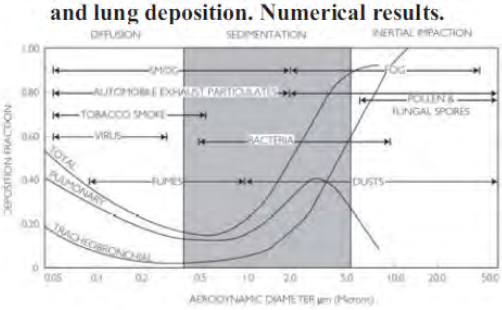

Figure 8. Relationship between particle size and lung deposition. Experimental results (Dolovich et al.).

Figures 9 to 14 show the concentration of the particles (kg/m^2) settled on the duct walls for a flow rate of 31 *ℓ/min* and for all size of particles. Black colour with white border means "high concentration" of settled particles on the wall, and gray colour means absence of settled particles. It can be observed that the number of escaped particles decreases when the particle size increases. This is due to the gravitational force, which also increases, forcing the particles to settle on the walls. In these figures it also can be observed that the black areas reach more distant regions as the particles are smaller.

4. CONCLUSIONS

The distribution of particles in the lung airways depends of its size. Small particles are distributed more uniformly than bigger particles, which follow the mean flow. The main objective of this work, to study the particle transport in the lung from the trachea to level 7 has been achieved. The next step is a combination of this work with the previous one. We will try to determine the particle deposition from the mouth to the level 17 during a respiratory cycle, using a mixture of particles of different sizes. Due to the high number of branches (131,072), it is necessary to work with a single pathway, so the boundary conditions applied in the truncated branches will be very important.

ACKNOWLEDGEMENTS

The authors gratefully acknowledge the financial support provided by Junta de Extremadura and FEDER under project GR10047 and also by Ministerio de Ciencia e Innovación under project DPI 2010-21103-C04-04.

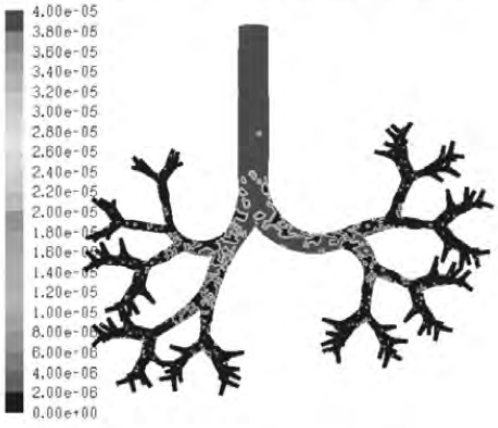

Fig. 9: Flowrate 31 *ℓ/min*, size 1 *pm*

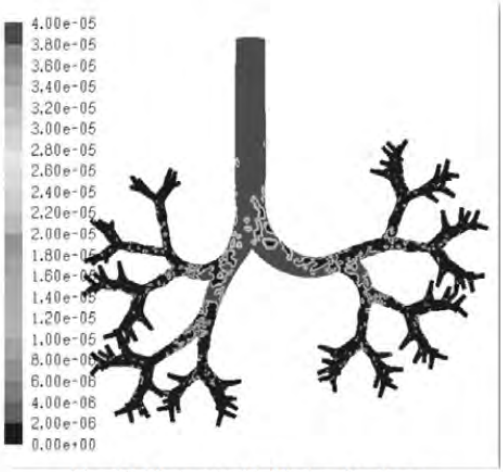

Fig. 10 Flowrate 31 *ℓ/min*, size 1 *nm*

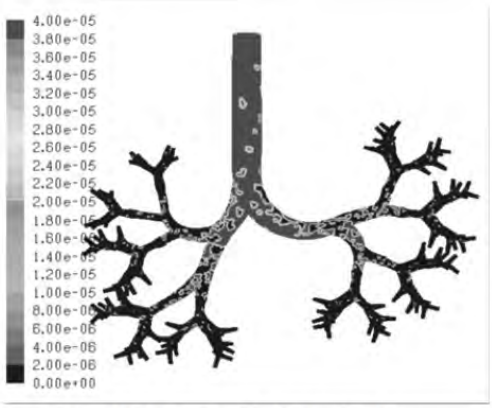

Fig. 11: Flowrate 31 *ℓ/min*, size 1 *μm*

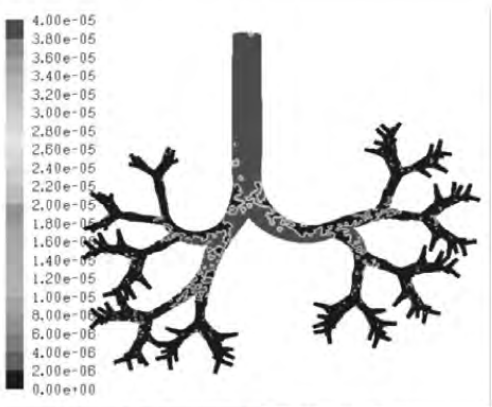

Fig. 12: Flowrate 31 *ℓ/min*, size 5 *μm*

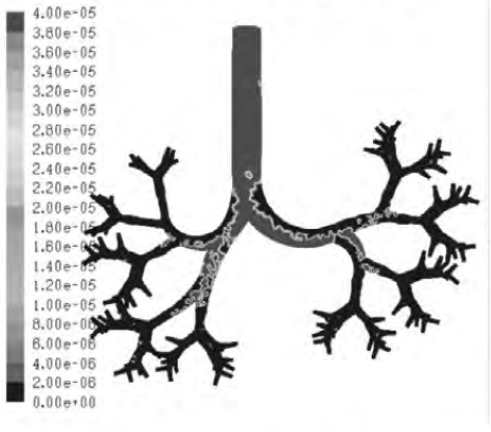

Fig. 13: Flowrate 31 *ℓ/min*, size 10 *μm*

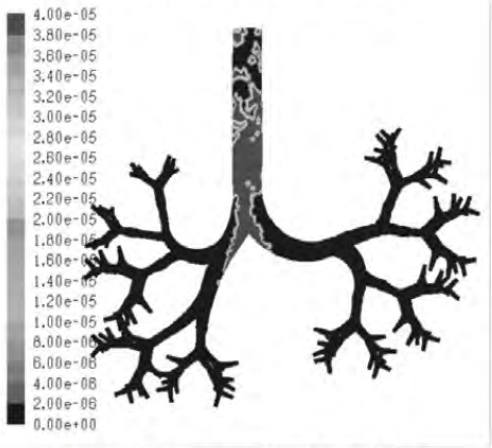

Fig. 14: Flowrate 31 *ℓ/min*, size 50 *μm*

REFERENCES

[1] Martonen TB. Analytical model of hygroscopic particle behavior in human airways. *Bull Math Biol. 1982; 44:425–442.*

[2] Martonen TB, Katz I. Inter-related effects of morphology and ventilation on drug deposition patterns. *STP Pharm Sci. 1994; 4:11–18.*

[3] Adler K, Brucker C. Dynamic flow in a realistic model of the upper human lung airways. *Exp. Fluids. 2007; 43:411–23.*

[4] Ball CG, Uddin M, Pollard A. High resolution turbulence modelling of airflow in an idealised human extrathoracic airway. *Comput. Fluids. 2008; 37:943–64.*

[5] Gemci T, Ponyavin V, Chen Y, Chen H, Collins R. Computational model of airflow in upper 17 generations of human respiratory tract. *J. Biomech. 2008; 41:2047–54.*

[6] Zhang Z, Kleinstreuer C, Kim CS. Airflow and nanoparticle deposition in a 16-generation tracheobronchial airway model. *Ann. Biomed. Eng. 2008; 36:2095–110.*

[7] D. Keith Walters and William H. Luke, A Method for Three-Dimensional Navier-Stokes Simulations of Large-Scale Regions of the Human Lung Airway. *J. Fluids Eng. 132, 051101, 2010, vol. 132, 051101-1-8.*

[8] Robinson, RJ., Snyder, P., Oldham MJ. Comparison of Particle Tracking Algorithms in Commercial CFD Packages: Sedimentation and Diffusion. *Inhalation Toxicology, 19:517–531, 2007.*

[9] Robinson, RJ., Snyder, P., Oldham MJ. Comparison of Analytical and Numerical Particle Deposition Using Commercial CFD Packages: Impaction and Sedimentation. *Inhalation Toxicology, 20:485 - 497, 2008.*

[10] Martonen T. B, Schroeter, J.D., Fleming J.S. 3D In Silico Modeling of the Human Respiratory System for Inhaled Drug Delivery and Imaging Analysis. *Journal of Pharmaceutical Sciences, Vol. 96, 603–617, 2007.*

[11] Castro Ruiz Pilar. *Análisis computarizado del flujo aéreo en cavidad nasal. Tesis Doctoral*. Universidad Autónoma de Madrid. 2003.

[12] Quispe Apaclla César, 2010. *Estudio del flujo de aire a través de las fosas nasales en la inspiración y espiración, considerando el intercambio de calor existente. Tesis Doctoral*. Universidad de Valladolid.

[13] Tena, Ana T, Casan, P, Marcos, A, Barrio, R, Blanco, E, 2011. Analysis of the fluid dynamic characteristics of the obstructive pulmonary diseases using a three-dimensional cfd model of the upper conductive zone of the lung airways. *Proceedings of the ECCOMAS. Conference on Simulation and Modeling of Biological Flows, VUB, Brussels, Belgium.*

[14] *Gambit version 2.4.6* (2006). ©ANSYS Inc.

[15] Weibel, E.R., *Morphometry of the human lung*, Springer-Verlag (1963).

[16] Kitaoka H, Takaki R, Suki B. A three-dimensional model of the human tree. *J. Applied Physiology. 1999; 87: 2207-2217.*

[17] *Fluent version 6.3.26* (2006). ©ANSYS Inc.

[18] Robinson, R. J., Oldham, M. J., Clinkenbeard, R. E., and Rai, P. 2006. Experimental and numerical analysis of a 7 generation human replica tracheobronchial model. Ann. Biomed. Eng. 34(3):373–383

[19] Dolovich MB, Newhouse MT. Aerosols. *Generation, methods of administration, and therapeutic applications in asthma. In Allergy. Principles and practice*, 4th edn, eds Middleton E Jr, Reed CE, Ellis EF, Adkinson NF Jr, Yunginger JW, Busse WW. St Louis: Mosby Year Book, Inc., 1993; 712–739.

Proceedings of the ECCOMAS Thematic International Conference on Simulation and Modeling of Biological Flows (SIMBIO 2011) September 21-23, 2011, VUB, Brussels, Belgium

Analysis of the fluid dynamic characteristics of the obstructive pulmonary diseases using a three-dimensional cfd model of the upper conductive zone of the lung airways.

Ana F. Tena[1], Pere Casan[1], Alfonso Marcos[2], Raúl Barrio[3], Eduardo Blanco[3]

1 Instituto N. de Silicosis. C/ Dr Bellmunt. 33006 Oviedo, Spain. E-mail: anafertena@gmail.com, pcasan@ins.es
3 Universidad de Oviedo. C. de Viesques 33203 Gijón, Spain. E-mail: barrioraul@uniovi.es; eblanco@uniovi.es

2 Universidad de Extremadura. Avda de Elvas, 06071 Badajoz, Spain. E-mail: acmarcos@unex.es

Abstract

The main objective of this work is the analysis of the fluid dynamic characteristics of the obstructive pulmonary diseases (Cronic Obstructive Pulmonary Disease, COPD, bronchitis and emphysema). Its obstructive pattern can be easily detected in the spirometry, but they usually need more complex tests to distinguish between them. However, their fluid dynamic features are quite different.

A 3D numerical model of the bronchial tree has been developed, from the trachea to the seventh level bronchioles, following the model developed by Weibel and Kitaoka . The main innovation in the numerical model is the unsteady boundary conditions applied and an adaptive time step, using two User Defined Function (UDF). The analysis of the results obtained varying the geometry and the unsteady boundary conditions, allows the characterization of the particular fluid dynamic phenomenon of each disease and how it is perceived in the tests.

Keywords: obstructive pulmonary disease, spirometry, CFD.

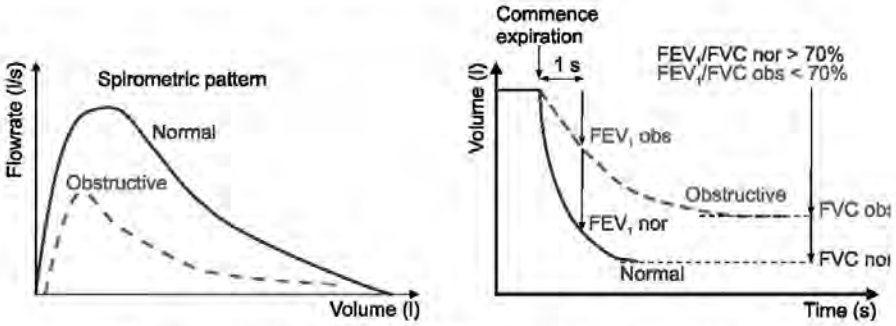

Fig.1 Normal and obstructive curves obtained in the forced spirometry test

Introduction

Lung diseases with an obstructive diagnosis are, basically, COPD (Cronic Obstructive Pulmonary Disease, both bronchitis and emphysema), and asthma although some other diseases and entities as tumors can also hinder the air flow. Its obstructive pattern can be easily detected in the spirometry (figure 1), but they usually need more complex tests to distinguish between them. However, their fluid dynamic features are quite different.

The distinctive attribute between COPD and asthma is the chronic quality of the first. A nearly normal pulmonary function can be observed in asthma patients after a bronchodilator treatment.

The main fluid dynamic effect in bronchitis is produced by the section reduction of the airways, mainly due to the chronic inflammation. The pressure loss increases and the flow rate diminish, mainly during the first second, when air velocity is the highest. As the global airways section increases going down the bronchial tree, is to be expected that the obstruction of the lower order branches is the most significant part of the phenomena. As the flow can be considered laminar, at

least in the less severe phase of the illness, the pressure loss should be more or less proportional to the flow rate. The presence of an obstruction originated by a tumor, on the other hand, can be considered as a singular pressure loss, and influenced by the square of the flow rate.

The respiratory obstruction generated by emphysema has a completely different source: the pressure driving the flow during the expiratory maneuver is due to the elastic lung recoil; in emphysema, the loss of elastic tissue elements reduces this pressure, hampering the lungs deflation [1].

A normal description of the human lung with 24 branches must have 16 million of segments (2^{24}). A full CFD resolution requires an estimated mesh size of thousands of millions of elements. CFD simulations have been limited to relatively small subsections of the lung geometry, being the flow in the lower airways either ignored or modeled using simple 1D or axisymmetric approximations. The earliest morphological description of the lung was the symmetric model of Weibel [2]. A complementary alternative was proposed by Kitaoka et al. [3]. Now, there are several models, most of them derived from these. Realistic morphologies for lung airways up to nine branches can be obtained using CT-scan and MRI techniques [4, 5].

Several works have demonstrated the complexity of the pulmonary flow. Zhang and Kleinstreuer [6] performed CFD simulations in a four-generation symmetric branching model and found that unsteady typical flow of normal breathing led to different flow features than in the steady state case, being greater during high frequency ventilation. Luo et al. [7] investigated the effect of COPD on particle deposition in the upper lung airways for a symmetric four-generation model. Yang et al. [8] worked with a three-generation airway model for both healthy and COPD cases, and found that the velocity profile entering the segments has great influence on flow patterns and pressure drop.

The main innovation in this numerical model is the unsteady boundary conditions applied [9, 10]. Volume and flow rate (vs. time) real data have been obtained from forced spirometry tests of patients without obstructive pulmonary diseases. This data has been used with the model to obtain the pressure vs. volume and pressure vs. time patterns at the end of the smaller bronchioles studied. Then, with these boundary conditions, were made simulations under obstructive pulmonary diseases (bronchitis and emphysema). The analysis of the results obtained varying the geometry and the unsteady boundary conditions, allows the characterization of the particular fluid dynamic phenomenon of each disease and how it is perceived in the tests.

Methodology and numerical model

Few forced spirometry tests of patients without obstructive pulmonary diseases were realized to simulate realistic conditions. From these data relations between volume, flow rate and time have been obtained (Fig. 2).

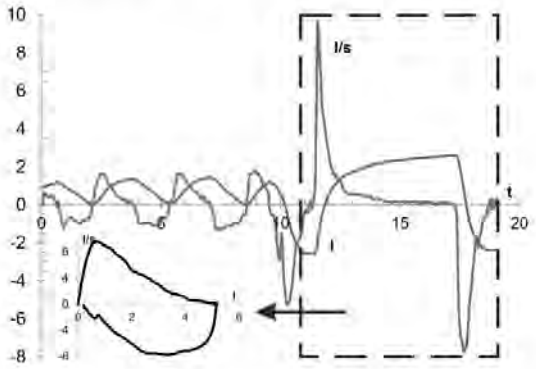

Fig.2 Forced spirometry tests.

A 3D numerical model of the bronchial tree has been developed, from the trachea to the seventh level bronchioles. The geometry follows the model developed by Weibel [2] and Kitoaka et al [3]. The dimensions of the built model can be seen in table 1.

Table 1: model dimensions

Gen	Branches	Diam (m)	Lengh (m)	Area (m^2)
0	1	0.018	0.12	0.000254469
1	2	0.012211422	0.047822285	0.000117118
2	4	0.00828438	0.019058091	5.39026E-05
3	8	0.005620225	0.007595012	2.48083E-05
4	16	0.00445127	0.012665425	1.55617E-05
5	32	0.003512926	0.010685373	9.69232E-06
6	64	0.002807205	0.009014874	6.18925E-06
7	128	0.002271429	0.007605532	4.05218E-06

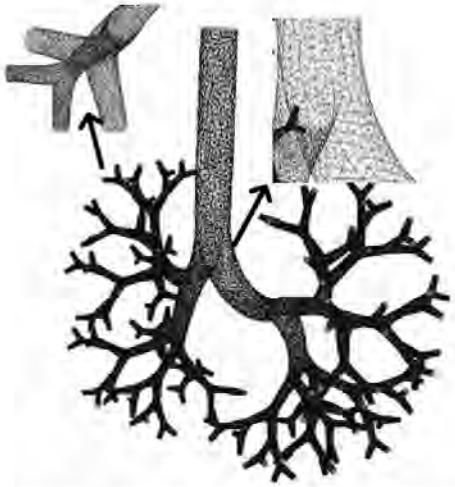

Fig.3 Numerical model and detail of the surface mesh.

Figure 3 shows a global image of the unstructured mesh generated. The total number of cells used to begin with the simulations was about 10^6, though other meshes of different size ($2\,10^6$ and $4\,10^6$) were generated in order to investigate the dependence of the numerical predictions. As can be seen in Fig 4, the variation observed in the outlet flow rate when considering different mesh sizes is not very significant. For the mesh size used for the calculations (about 1,000,000 cells) this variation is lower than 1.11%, and with 2,000,000 cells is lower than 0.67% compared with the model of 4,000,000 cells.

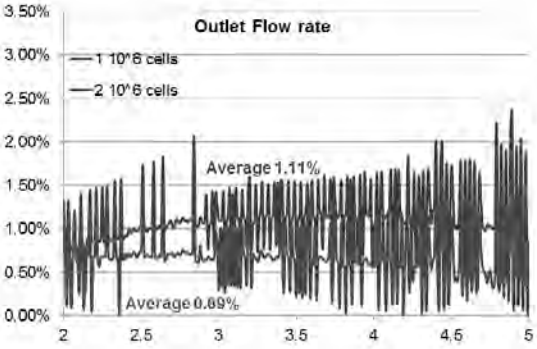

Fig.4 Results of the independence tests.

The maximum equiangle skew was restricted below 0.6 for 98% of the cells in the mesh.

The numerical simulations were performed with the code Ansys Fluent [11]. This code was used to solve the full unsteady 3D Navier-Stokes equations by the finite volume method. Air is the working fluid with a constant density of 1.225 kg/m^3 and dynamic viscosity of 1.7894 10^{-5} kg/(m s).

The boundary conditions imposed were firstly an unsteady velocity distribution (using a User Defined Function) at the inlet (G0, trachea) and gauge static pressure at the outlet (G7).

The number of time steps was 400. Due to non-uniformity of breathing cycle, it was applied an adaptive time step method by means of the before User Defined Function. The number of iterations in each time step was adjusted to reduce the magnitude of the residuals below an acceptable level. The residuals converged quickly and reached negligible magnitudes.

The time required for each simulation was 4 days working in parallel with 4 cores. Over 5 breathing cycles are necessary to achieve the periodic unsteady solution convergence.

Figure 5 shows the inlet boundary condition (unsteady flow rate) obtained from a forced spirometry test, and the unsteady pressure pick-up from the simulation.

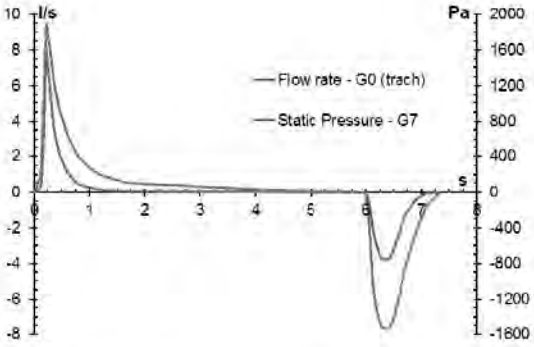

Fig.5 Unsteady flow rate imposed and static pressure obtained.

One way to check if the simulation is right is to repeat the test, but in this case the unsteady pressure obtained before as inlet boundary condition (G7) and see if it matches the obtained unsteady output velocity (G0, trachea) with the first valor (fig. 6). Results look like rights.

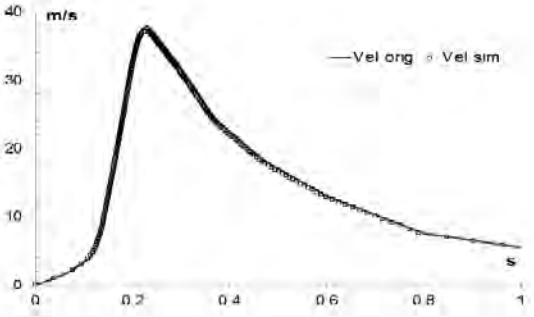

Fig.6. Real and simulated velocities in the trachea (G0)

To simulate the COPD conditions (bronchitis and emphysema) the unsteady total pressure obtained in the past step is imposed as the inlet (G7) boundary condition using an udf whereas a gauge pressure is established as the outlet boundary condition. In the case of bronchitis, the roughness of the walls was increased, whereas in the case of emphysema, a branch of order 3 was closed, which is equivalent to having 1/8 of inoperable lung.

Results

First of all, the results will be compared with those existing in the literature. Hofmann et al [12] say that the velocity is increasing in the first branches, from the branch 0 (trachea) to branch 3. Rest of the branches, from G4 to 24, the velocity is decreasing.

The total sections of the built model are in the table 2. Figure 7 shows the velocity magnitude obtained in the simulation in the different pulmonary branches for a healthy lung. From the G0 (trachea) to G3 the velocity is increasing, whereas in the rest is decreasing. Therefore, both results are in agreement.

Table 2: Variation of the total section in the airways

Gen	Total area (m^2)	Gen	Total area (m^2)
0	0.00025447	4	0.00024899
1	0.00023424	5	0.00031015
2	0.00021561	6	0.00039611
3	0.00019847	7	0.00051868

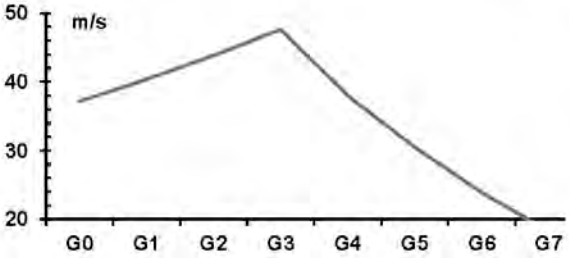

Fig.7. Velocity magnitude in the pulmonary branches

Figure 8 shows the pahtlines from G7 to the trachea (G0) colored by inlet surface, and the velocity vectors in first 3 branches at a given moment of the expiratory flow.

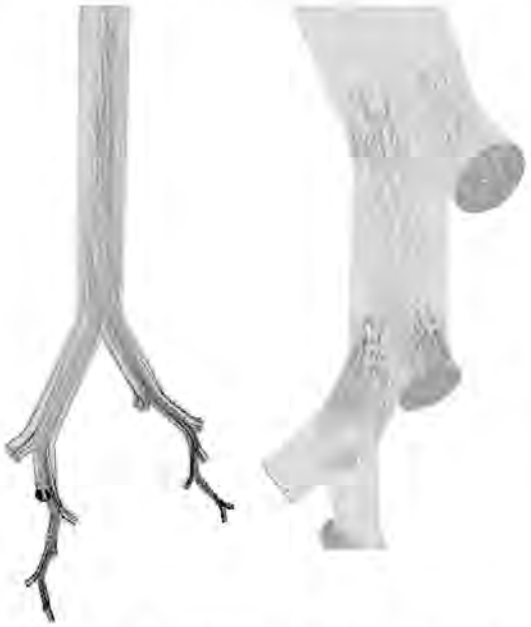

Fig.8. Pathlines from G7 to G0 in two branches and velocity vector in first 3 branches.

For the same flow conditions, Figure 9 shows the contours of velocity in cross sections of different branches, in the sense of clockwise. In general, the flow is axisymmetric, with predominant axial component of velocity.

Fig.9. Contours of velocity in cross sections of different branches.

Figure 10 shows the unsteady velocity in the trachea (G0) for the three study cases, with the same inlet boundary condition (static pressure), as has been said previously. The conditions imposed to simulate bronchitis and emphysema correspond, in this first study, a mild conditions. The simulation perfectly captures these situations, with results similar to those obtained by spirometry tests. The spirometry results are shown as graphics of flow rate versus volume and volume versus time. To obtain these values, previous results are integrated, being shown in Figures 11 (flow rate vs volume) and 12 (volume vs time).

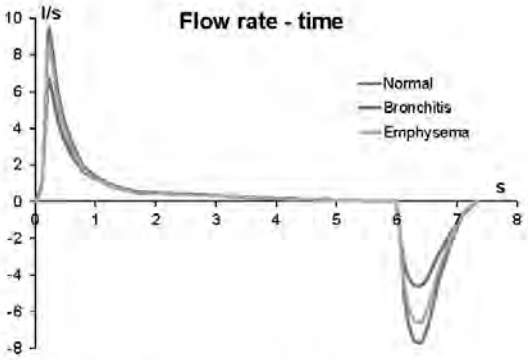

Fig.10. Velocity magnitude in the pulmonary branches

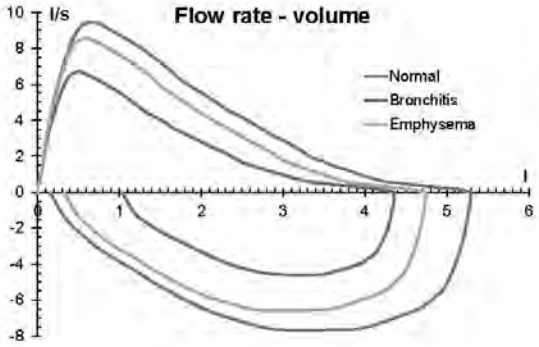

Fig.11. Flowrate versus volume.

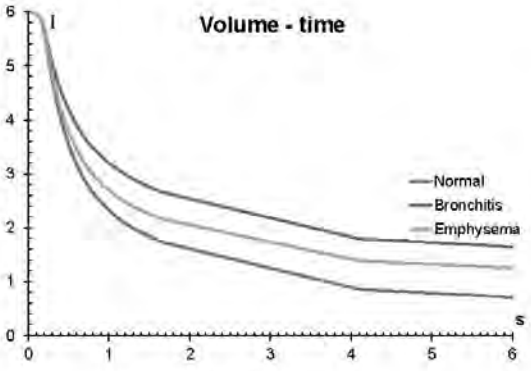

Fig.12. Volume versus time.

From these data it can be obtained the most used parameters in pneumological studies (FVC, Forced Vital Capacity; FVC_1, Forced Expiratory Volume in first second; FEF_{25-75}, Forced Expiratory Flow at 25% point to the 75% point of Forced Vital Capacity; PEF, Peak Expiratory Flow). Table 3 shows these parameters.

Table 3

	Normal	Bronchitis	Emphysema
	l	*l*	*l*
FVC	5.29	4.35	4.74
FVC_1	3.69	2.81	3.29
	l/s	*l/s*	*l/s*
PEF	9.46	6.70	8.54
	%	%	%
FVC_1/FVC	72.68%	64.56%	69.34%

Conclusions

A numerical study of lung diseases with an obstructive diagnosis (COPD) was made using unsteady boundary conditions. These boundary conditions were imposed by means of two User Defined Functions (UDF's), one to obtain the unsteady pressure in the branch G7 and the other to obtain the spirometry data in the three study cases.

Once verified the functioning of the model, further studies will be directed to simulate different cases of existing spirometry.

Acknowledgements

The authors gratefully acknowledge the financial support provided by Junta de Extremadura and FEDER under project GR10047 and also by Ministerio de Ciencia e Innovación under project DPI 2010-21103-C04-04.

References

[1] R.J. Altiere and D.C. Thompson, Physiology and Pharmacology of the Airways. In: Inhalation Aerosols, 2d Edition, Informa Healthcare (2007).

[2] E.R. Weibel, Morphometry of the human lung, Springer-Verlag (1963).

[3] Kitaoka, H., Takaki, R., and Suki, B., 1999, "A Three Dimensional Model of the Human Airway Tree" J. Appl. Physiol., 87(6), pp. 2207–2217.

[4] Sera, T., Fujioka, H., Yokota, H., Makinouchi, A., Himeno, R., Schroter, R. C., and Tanishita, K., 2003, "Three-Dimensional Visualization and Morphometry of Small Airways From Microfocal X-Ray Computed Tomography," J. Biomech., 36(11), pp. 1587–1594.

[5] Burton, R. T., Isaacs, K. K., Fleming, J. S., and Martonen, T. B., 2004, "Computer Reconstruction of a Human Lung Boundary Model From Magnetic Resonance Images," Respir. Care, 49(2), pp. 180–185.

[6] Zhang, Z., and Kleinstreuer, C., 2011, "Computational analysis of airflow and nano particle deposition in a combined nasal-oral-tracheobronchial airway model," Journal of Aerosol Science 42, pp. 174–194.

[7] Luo, H. Y., Liu, Y., and Yang, X. L., 2007, "Particle Deposition in Obstructed Airways," J. Biomech., 40(14), pp. 3096–3104.
[8] Yang, X. L., Liu, Y., So, R. M. C., and Yang, J. M., 2006, "The Effect of Inlet Velocity Profile on the Bifurcation COPD Airway Flow," Comput. Biol. Med., 36(2), pp. 181–194.
[9] R.K. Freitas and W. Schröder, 2008, Numerical investigation of the three-dimensional flow in a human lung model, Journal of Biomechanics 41, pp. 2446–2457.
[10] C-L. Lin, M.H. Tawhai, G. McLennan, E.A. Hoffman, 2009, Multiscale simulation of gas flow in subject-specific models of the human lung, IEEE Engineering in Medicine and Biology Magazine 28(3), pp. 25–33.
[11] Fluent Inc. User's Guide, 2006, 10 Cavendish Court, Lebanon, NH03766.
[12] Hofmann W, Martonen TB, Graham RC. Predicted deposition of nonhygroscopic aerosols in the human lung as a function of subject age. J Aerosol Med 1989; 2:49–68.
[13] Agustí, A. G. N. 1995, Función pulmonar aplicada: puntos clave. Mosby/Doyma Libros, Barcelona.

APPENDIX B
UDF: boundary conditions

```
#include "udf.h"
#if !PARALLEL
        #define node_serial myid
        #define node_host 999999
        #define node_zero 0
        #define node_one 1
        #define compute_node_count 1
        #define PRF_CRECV_INT(a,b,c,d)
        #define PRF_CSEND_INT(a,b,c,d)
        #define PRF_CRECV_REAL(a,b,c,d)
        #define PRF_CSEND_REAL(a,b,c,d)
#endif

#define NUM_C 104
#define ID_BC

293,292,291,290,289,288,287,286,285,284,283,282,281,187,186,185,184,183,182,181,180,179,
178,177,176,175,505,504,503,502,501,500,499,498,497,496,49

5,494,493,399,398,397,396,395,394,393,392,391,390,389,388,387,901,900,899,898,897,896,89
5,894,893,892,891,890,889,821,820,819,818,817,816,815,814,

813,812,811,810,809,715,714,713,712,711,710,709,708,707,706,705,704,703,610,609,608,607,
606,605,604,603,602,601,600,599,598

#define ID_IN

280,279,278,277,276,275,274,273,272,271,270,269,268,174,173,172,171,170,169,168,167,166,
165,164,163,162,492,491,490,489,488,487,486,485,484,483,48

2,481,480,386,385,384,383,382,381,380,379,378,377,376,375,374,888,887,886,885,884,883,88
2,881,880,879,878,877,876,808,807,806,805,804,803,802,801,

800,799,798,797,796,702,701,700,699,698,697,696,695,694,693,692,691,690,597,596,595,594,
593,592,591,590,589,588,587,586,585

#define DENS 1.225
#define MAX_F 400
#define MAX_NDS 8
#define RELAJ 1

int nc = NUM_C;
int bcID[NUM_C] = {ID_BC};
int inID[NUM_C] = {ID_IN};
int inS[NUM_C];
int rel[NUM_C][MAX_NDS][MAX_F];
real vu_mirror[NUM_C][ND_ND];
real in_mflow[NUM_C][MAX_F];
real in_vel[NUM_C][MAX_F][ND_ND];

DEFINE_EXECUTE_ON_LOADING(Load_copyVel, libname)
{
        face_t f;
        Thread *t;
        Domain *dom;

        real inCoor[MAX_F][ND_ND], inSup[MAX_F][ND_ND];
        real inCentro[ND_ND], bcCentro[ND_ND];
        real inVector[ND_ND], bcVector[ND_ND];
        int innf;
        real coor[MAX_NDS][MAX_F][ND_ND], sup[ND_ND];
        real centr[MAX_NDS][ND_ND], vect[MAX_NDS][ND_ND];
        int nod, nf[MAX_NDS];
        real tprod1, tprod2, tresta[ND_ND], dis;
        int i, j, n, c, ia;

        if (myid == node_host) return;

        Message0("\nEXECUTE_ON_LOADING\nRelaciones entre caras...\n");

        dom = Get_Domain(1);
        nod = (myid == node_serial ? 0 : myid);
```

```
        for (c=0;c<NUM_C;c++) for (n=0;n<MAX_NDS;n++) for (i=0;i<MAX_F;i++) rel[c][n][i]
= -1;
        for (c=0;c<nc;c++)
        {
                t = Lookup_Thread(dom, inID[c]);
                NV_S (centr[nod], =, 0);
                NV_S (vect[nod], =, 0);
                i = 0;
                begin_f_loop(f,t)
                {
                        if PRINCIPAL_FACE_P(f,t)
                        {
                                F_AREA(sup,f,t);
                                NV_V(vect[nod], +=, sup);
                                F_CENTROID(coor[nod][i],f,t);
                                NV_VS(centr[nod], +=, coor[nod][i], *, NV_MAG(sup));
                                i++;
                        }
                }
                end_f_loop(f,t)
                nf[nod] = i;
                if (myid == node_serial || myid == node_zero)
                {
                        NV_V (inVector, =, vect[nod]);

                        NV_V (inCentro, =, centr[nod]);
                        for (i=0;i<nf[nod];i++) NV_V (inCoor[i], =, coor[nod][i]);
                        innf = nf[nod];
                }
                else
                {
                        PRF_CSEND_INT(node_zero, &nf[nod], 1, myid);
                        PRF_CSEND_REAL(node_zero, vect[nod], ND_ND, myid);
                        PRF_CSEND_REAL(node_zero, centr[nod], ND_ND, myid);
                        PRF_CSEND_REAL(node_zero, coor[nod][0], MAX_F*ND_ND, myid);
                }
                if (myid == node_zero)
                {
                        for (n=node_one;n<compute_node_count;n++)
                        {
                                PRF_CRECV_INT(n, &nf[n], 1, n);
                                PRF_CRECV_REAL(n, vect[n], ND_ND, n);
                                PRF_CRECV_REAL(n, centr[n], ND_ND, n);
                                PRF_CRECV_REAL(n, coor[n][0], MAX_F*ND_ND, n);
                                NV_V (inVector, +=, vect[n]);
                                NV_V (inCentro, +=, centr[n]);
                                for (i=0;i<nf[n];i++) NV_V (inCoor[i+innf], =, coor[n][i]);
                                innf += nf[n];
                        }
                }

                t = Lookup_Thread(dom, bcID[c]);
                NV_S (centr[nod], =, 0);
                NV_S (vect[nod], =, 0);
                i = 0;
                begin_f_loop(f,t)
                {
                        if PRINCIPAL_FACE_P(f,t)
                        {
                                F_AREA(sup,f,t);
                                NV_V(vect[nod], +=, sup);
                                F_CENTROID(coor[nod][i],f,t);
                                NV_VS(centr[nod], +=, coor[nod][i], *, NV_MAG(sup));
                                i++;
                        }
                }
                end_f_loop(f,t)
                nf[nod] = i;
                if (myid == node_serial || myid == node_zero)
                {
                        NV_V (bcVector, =, vect[nod]);
                        NV_V (bcCentro, =, centr[nod]);
                }
```

```
        else
        {
                PRF_CSEND_INT(node_zero, &nf[nod], 1, myid);
                PRF_CSEND_REAL(node_zero, vect[nod], ND_ND, myid);
                PRF_CSEND_REAL(node_zero, centr[nod], ND_ND, myid);
                PRF_CSEND_REAL(node_zero, coor[nod][0], MAX_F*ND_ND, myid);
        }

        if (myid == node_zero)
        {

                for (n=node_one;n<compute_node_count;n++)
                {
                        PRF_CRECV_INT(n, &nf[n], 1, n);
                        PRF_CRECV_REAL(n, vect[n], ND_ND, n);
                        PRF_CRECV_REAL(n, centr[n], ND_ND, n);
                        PRF_CRECV_REAL(n, coor[n][0], MAX_F*ND_ND, n);
                        NV_V (bcVector, +=, vect[n]);
                        NV_V (bcCentro, +=, centr[n]);
                }
        }

        if (myid == node_serial || myid == node_zero)
        {
                dis = NV_MAG(inVector);
                NV_S(inCentro, /=, dis);
                NV_S(inVector, /=, dis);
                dis = NV_MAG(bcVector);
                NV_S(bcCentro, /=, dis);
                NV_S(bcVector, /=, dis);
                NV_VV(tresta, =, bcCentro, -, inCentro);
                tprod1 = NV_DOT(tresta,bcVector);
                tprod2 = NV_DOT(tresta,inVector);
                inS[c] = ((tprod1 * tprod2) < 0 ? 1 : -1);
                NV_VS_VS(vu_mirror[c], =, inVector, *, inS[c], -, bcVector, *, 1);
                dis = NV_MAG(vu_mirror[c]);
                NV_S(vu_mirror[c], /=, dis);
                for (i=0; i<innf; i++)
                {
                        NV_V(inCoor[i], -=, inCentro);
                        dis = 2*NV_DOT(vu_mirror[c], inCoor[i]);
                        NV_V_VS(inCoor[i], +=, bcCentro, -, vu_mirror[c], *, dis);
                }
                for(n=0; n<compute_node_count;n++)
                {
                        for (i=0;i<nf[n];i++)
                        {
                                ia = 0;
                                NV_VV(tresta, =, coor[n][i], -, inCoor[0]);
                                dis = NV_MAG2(tresta);
                                for (j=1; j<innf; j++)
                                {
                                        NV_VV(tresta, =, coor[n][i], -, inCoor[j]);
                                        if (NV_MAG2(tresta) < dis)
                                        {
                                                ia = j;
                                                dis = NV_MAG2(tresta);
                                        }
                                }
                                rel[c][n][i] = ia;
                        }
                }
        }
}
if (myid == node_zero)
        for (n=node_one;n<compute_node_count;n++)
        {
                PRF_CSEND_INT(n, rel[0][0], NUM_C*MAX_NDS*MAX_F, myid);
                PRF_CSEND_INT(n, inS, NUM_C, myid);
                PRF_CSEND_REAL(n, vu_mirror[0], NUM_C*ND_ND, myid);
        }
else if (myid != node_serial)
{
```

```
                PRF_CRECV_INT(node_zero, rel[0][0], NUM_C*MAX_NDS*MAX_F, node_zero);
                PRF_CRECV_INT(node_zero, inS, NUM_C, node_zero);
                PRF_CRECV_REAL(node_zero, vu_mirror[0], NUM_C*ND_ND, node_zero);
        }
        for (c=0;c<NUM_C;c++)
                for (i=0;i<MAX_F;i++)
                {
                        in_mflow[c][i] = 0;
                        for (n=0;n<MAX_NDS;n++)
                                in_vel[c][i][n] = 0;
                }

        Message0("Hecho\n\n");
}

DEFINE_INIT(Init_copyVel,d)
{
        int c, i, n;

        Message0("\nINIT\nInicializacion de las matrices de flujo y velocidad en las
faces de las intasoc...\n");

        for (c=0;c<NUM_C;c++)
                for (i=0;i<MAX_F;i++)
                {
                        in_mflow[c][i] = 0;
                        for (n=0;n<MAX_NDS;n++)
                                in_vel[c][i][n] = 0;
                }

        Message0("Hecho\n\n");
}

DEFINE_EXECUTE_AT_END(Iter_copyVel)
{
        face_t f;
        Thread *t;
        Domain *dom;
        cell_t  c0,  c1 = -1;
        Thread *t0, *t1 = NULL;
        real tvel0, tvel1;
        real mflow[MAX_NDS][MAX_F], vel[MAX_NDS][MAX_F][ND_ND];
        int nod, innf, nf[MAX_NDS];
        int i, j, n, c;

        if (myid == node_host) return;

        dom = Get_Domain(1);
        nod = (myid == node_serial ? 0 : myid);

        for (c=0;c<nc;c++)
        {
                t = Lookup_Thread(dom, inID[c]);
                innf = 0;

                i = 0;
                begin_f_loop(f,t)
                {
                        if PRINCIPAL_FACE_P(f,t)
                        {
                                mflow[nod][i] = F_FLUX(f,t);
                                c0 = F_C0(f,t);
                                t0 = F_C0_THREAD(f,t);
                                c1 = F_C1(f,t);
                                t1 = F_C1_THREAD(f,t);
                                tvel0 = C_U(c0,t0);
                                tvel1 = C_U(c1,t1);
                                vel[nod][i][0] = (tvel0 + tvel1) / 2;
                                tvel0 = C_V(c0,t0);
                                tvel1 = C_V(c1,t1);
                                vel[nod][i][1] = (tvel0 + tvel1) / 2;
                                if (ND_ND == 3)
                                {
```

```
                                        tvel0 = C_W(c0,t0);
                                        tvel1 = C_W(c1,t1);
                                        vel[nod][i][2] = (tvel0 + tvel1) / 2;
                                }
                                i++;
                        }
                }
                end_f_loop(f,t)
                nf[nod] = i;
                if (myid == node_serial || myid == node_zero)
                        for (i=0;i<nf[nod];i++)
                        {
                                in_mflow[c][i] = mflow[nod][i];
                                for (j=0;j<ND_ND;j++) in_vel[c][i][j] = vel[nod][i][j];
                        }
                        innf = nf[nod];
                }
                else
                {
                        PRF_CSEND_INT(node_zero, &nf[nod], 1, myid);
                        PRF_CSEND_REAL(node_zero, mflow[nod], MAX_F, myid);
                        PRF_CSEND_REAL(node_zero, vel[nod][0], MAX_F*ND_ND, myid);
                }
                if (myid == node_zero)
                {
                        for (n=node_one;n<compute_node_count;n++)
                        {
                                PRF_CRECV_INT(n, &nf[n], 1, n);
                                PRF_CRECV_REAL(n, mflow[n], MAX_F, n);
                                PRF_CRECV_REAL(n, vel[n][0], MAX_F*ND_ND, n);
                                for (i=0;i<nf[n];i++)
                                {
                                        in_mflow[c][i+innf] = mflow[n][i];
                                        for (j=0;j<ND_ND;j++) in_vel[c][i+innf][j] =
vel[n][i][j];
                                }
                                innf += nf[n];
                        }
                }
        }

        if (myid == node_zero)
                for (n=node_one;n<compute_node_count;n++)
                {
                        PRF_CSEND_REAL(n, in_mflow[0], NUM_C*MAX_F, myid);
                        PRF_CSEND_REAL(n, in_vel[0][0], NUM_C*MAX_F*ND_ND, myid);
                }
        else if (myid != node_serial)
        {
                PRF_CRECV_REAL(node_zero, in_mflow[0], NUM_C*MAX_F, node_zero);
                PRF_CRECV_REAL(node_zero, in_vel[0][0], NUM_C*MAX_F*ND_ND, node_zero);
        }


}

DEFINE_PROFILE(copyVel_Mag_NtB,tbc,ind)
{
        face_t fbc;
        real sup[ND_ND];
        real bcmflow, inmflow, newmflow;
        int thID, ibc, nod;
        int i, n;

        if (! Data_Valid_P()) return;

        thID = THREAD_ID(tbc);
        ibc = 0;
        while ((bcID[ibc] != thID) && (ibc < nc)) ibc++;
        if (ibc == nc)
        {
                Message0("\n\n********* error ***********");
                Message0("\nID de condicion de contorno incorrecto");
```

```
                Message0("\nProfile asignado a ID: %d, que no esta en la lista", thID);
                return;
        }

        nod = (myid == node_serial ? 0 : myid);
        i = 0;
        begin_f_loop(fbc,tbc)
        {
                if PRINCIPAL_FACE_P(fbc,tbc)
                {
                        F_AREA(sup,fbc,tbc);
                        bcmflow = F_FLUX(fbc,tbc);
                        inmflow = inS[ibc] * in_mflow[ibc][rel[ibc][nod][i]];
                        newmflow =  bcmflow + 0.5 * RELAJ * (inmflow - bcmflow);
                        F_PROFILE(fbc,tbc,ind) = - newmflow / NV_MAG(sup) / DENS;
                        i++;
                }
        }
        end_f_loop(fbc,tbc)
}

DEFINE_PROFILE(copyVel_X,tbc,ind)
{
        face_t fbc;
        real bcvelx, tinvelx;
        real invel[ND_ND], vumirror[ND_ND];
        real proy;
        int thID, ibc, nod;
        int i, j;

        if (! Data_Valid_P()) return;

        thID = THREAD_ID(tbc);
        ibc = 0;
        while ((bcID[ibc] != thID) && (ibc < nc)) ibc++;
        if (ibc == nc)
        {
                Message0("\n\n********* error ***********");
                Message0("\nID de condicion de contorno incorrecto");
                Message0("\nProfile asignado a ID: %d, que no esta en la lista", thID);
                return;
        }

        nod = (myid == node_serial ? 0 : myid);
        i = 0;
        begin_f_loop(fbc,tbc)
        {
                if PRINCIPAL_FACE_P(fbc,tbc)
                {
                        bcvelx = F_U(fbc,tbc);
                        for (j=0;j<ND_ND;j++)
                        {
                                invel[j] = in_vel[ibc][rel[ibc][nod][i]][j];
                                vumirror[j] = vu_mirror[ibc][j];
                        }
                        proy = NV_DOT(vumirror, invel);
                        tinvelx = invel[0] - 2 * proy * vumirror[0];
                        F_PROFILE(fbc,tbc,ind) =  bcvelx + 0.5 * RELAJ * (tinvelx -
bcvelx);
                        i++;
                }
        }
        end_f_loop(fbc,tbc)
}

DEFINE_PROFILE(copyVel_Y,tbc,ind)
{
        face_t fbc;
        real bcvely, tinvely;
        real invel[ND_ND], vumirror[ND_ND];
        real proy;
        int thID, ibc, nod;
        int i, j;
```

```
        if (! Data_Valid_P()) return;

        thID = THREAD_ID(tbc);
        ibc = 0;
        while ((bcID[ibc] != thID) && (ibc < nc)) ibc++;
        if (ibc == nc)
        {
                Message0("\n\n********* error ***********");
                Message0("\nID de condicion de contorno incorrecto");
                Message0("\nProfile asignado a ID: %d, que no esta en la lista", thID);
                return;
        }

        nod = (myid == node_serial ? 0 : myid);
        i = 0;
        begin_f_loop(fbc,tbc)
        {
                if PRINCIPAL_FACE_P(fbc,tbc)
                {
                        bcvely = F_V(fbc,tbc);
                        for (j=0;j<ND_ND;j++)
                        {
                                invel[j] = in_vel[ibc][rel[ibc][nod][i]][j];
                                vumirror[j] = vu_mirror[ibc][j];
                        }
                        proy = NV_DOT(vumirror, invel);
                        tinvely = invel[1] - 2 * proy * vumirror[1];
                        F_PROFILE(fbc,tbc,ind) =  bcvely + 0.5 * RELAJ * (tinvely -
bcvely);
                        i++;
                }
        }
        end_f_loop(fbc,tbc)
}

DEFINE_PROFILE(copyVel_Z,tbc,ind)
{
        face_t fbc;
        real bcvelz, tinvelz;
        real invel[ND_ND], vumirror[ND_ND];
        real proy;
        int thID, ibc, nod;
        int i, j;

        if (! Data_Valid_P()) return;

        thID = THREAD_ID(tbc);
        ibc = 0;
        while ((bcID[ibc] != thID) && (ibc < nc)) ibc++;
        if (ibc == nc)
        {
                Message0("\n\n********* error ***********");
                Message0("\nID de condicion de contorno incorrecto");
                Message0("\nProfile asignado a ID: %d, que no esta en la lista", thID);
                return;
        }

        nod = (myid == node_serial ? 0 : myid);
        i = 0;
        begin_f_loop(fbc,tbc)
        {
                if PRINCIPAL_FACE_P(fbc,tbc)
                {
                        bcvelz = F_W(fbc,tbc);
                        for (j=0;j<ND_ND;j++)
                        {
                                invel[j] = in_vel[ibc][rel[ibc][nod][i]][j];
                                vumirror[j] = vu_mirror[ibc][j];
                        }
                        proy = NV_DOT(vumirror, invel);
                        tinvelz = invel[2] - 2 * proy * vumirror[2];
```

```
                        F_PROFILE(fbc,tbc,ind) =  bcvelz + 0.5 * RELAJ * (tinvelz -
bcvelz);
                        i++;
                }
        }
        end_f_loop(fbc,tbc)
}
```

APPENDIX C
UDF: unsteady conditions

```
#include "udf.h"
#if !PARALLEL
        #define node_serial myid
        #define node_host 999999
        #define node_zero 0
        #define node_one 1
        #define compute_node_count 1
        #define PRF_CRECV_INT(a,b,c,d)
        #define PRF_CSEND_INT(a,b,c,d)
        #define PRF_CRECV_REAL(a,b,c,d)
        #define PRF_CSEND_REAL(a,b,c,d)
        #define PRF_CRECV_DOUBLE(a,b,c,d)
        #define PRF_CSEND_DOUBLE(a,b,c,d)
#endif

#define LEEDEFICH 1
#define FICHDATOS "Datos_espiro.txt"
#define MAX_NT 2000
#define ADAPTIMESTEP 1
#define NUM_PASOS 200

void leerDatosInternos(void);
void leerDatosFich(void);
void errorDatos(int m);
void distribuyeDatos(void);
void inicTiempos(void);
double InterpolaXY(double x[MAX_NT], double y[MAX_NT], int nd, double xi);
double yamismo(double tmax);

double dt[MAX_NT];
double dd[MAX_NT];
double ddc[MAX_NT];
int nt;

DEFINE_INIT(Cargar_datos,d)
{
        int i,j;

        if (myid == node_serial || myid == node_host)
        {
                if (!LEEDEFICH) leerDatosInternos();
                else leerDatosFich();

                Message("\nNumero de datos: %d\n", nt);
                Message("Tiempo   Dato\n");
                for (i=0; i<nt; i++) Message("%8.2f    %-10.4f\n", dt[i], dd[i]);
                Message("\n");

                inicTiempos();
        }
        if (myid != node_serial) distribuyeDatos();
}


DEFINE_PROFILE(Dato_instantaneo,t,ind)
{
        face_t f;
        double idd;
        double instante;
        int i;

        instante = yamismo(dt[nt-1]);
        if(instante >= 0) idd = InterpolaXY(dt, dd, nt, instante);
        else idd = 0;
        begin_f_loop(f,t)
        {
                F_PROFILE(f,t,ind) = idd;
        }
        end_f_loop(f,t)
}


DEFINE_DELTAT(delta_t_variable,d)
```

```
{
        double paso_temp = 0;
        double instante;
        double datcor;
        int i;

        if (ADAPTIMESTEP)
        {
                instante = yamismo(dt[nt-1]);

                if (instante < 0) return 0;

                datcor = InterpolaXY(dt, ddc, nt, instante);
                datcor += (ddc[nt-1] - ddc[0]) / NUM_PASOS;

                if (datcor < ddc[nt-1]) paso_temp = InterpolaXY(ddc, dt, nt, datcor) -
instante;
                else paso_temp = dt[nt-1] - instante;

                if((paso_temp + instante) > dt[nt-1])  paso_temp = dt[nt-1] - instante;
                if(paso_temp <= 0.000001)  paso_temp = (dt[nt-1] - dt[0]) / NUM_PASOS;
                if(paso_temp > 10)  paso_temp = (dt[nt-1] - dt[0]) / NUM_PASOS;
        }
        else paso_temp = (dt[nt-1] - dt[0]) / NUM_PASOS;

        return paso_temp;
}

void inicTiempos(void)
{
        int i;

        ddc[0] = dd[0];
        for(i=1; i<nt; i++) ddc[i] = ddc[i-1] + fabs(dd[i]-dd[i-1]);

        Message("\nComprobacion de datos...");

        if (dt[0] != 0) errorDatos(3);
        i = 1;
        while((dt[i-1] <= dt[i]) && (i < nt)) i++;
        if(i < nt) errorDatos(4);

        if ((dd[0] != 0) || (dd[nt-1] != 0)) errorDatos(5);
        i = 1;
        while((ddc[i-1] <= ddc[i]) && (i < nt)) i++;
        if(i < nt) errorDatos(6);

        Message(" Comprobados\n");
}

double yamismo(double tmax)
{
        double ya;

        if (!Data_Valid_P()) return -1;

        ya = CURRENT_TIME;

        ya = fmod(ya, tmax);
        if (fabs(ya - tmax) < 0.0001) ya = 0;
        return ya;
}

double InterpolaXY(double x[MAX_NT], double y[MAX_NT], int nd, double xi)
{
        double yi, denom;
        int it;

        it = 0;
        while (x[it] < xi && it < nd) it++;
        if (it == 0) it++;
        if (it == nd) it--;
        denom = x[it] - x[it-1] ;
```

```
        if (fabs(denom) > 0.00001) yi = y[it-1] + (y[it] - y[it-1]) * (xi - x[it-1]) /
denom;
        else yi = y[it];

        return yi;
}

void distribuyeDatos(void)
{
        int i;

        if (myid == node_host) Message("\nDistribucion de datos...");

        if (myid != node_serial)
        {
                if (myid == node_host)
                {
                        PRF_CSEND_INT(node_zero, &nt, 1, myid);
                        PRF_CSEND_DOUBLE(node_zero, &dt[0], MAX_NT, myid);
                        PRF_CSEND_DOUBLE(node_zero, &dd[0], MAX_NT, myid);
                        PRF_CSEND_DOUBLE(node_zero, &ddc[0], MAX_NT, myid);
                }
                else if (myid == node_zero)
                {
                        PRF_CRECV_INT(node_host, &nt, 1, node_host);
                        PRF_CRECV_DOUBLE(node_host, &dt[0], MAX_NT, node_host);
                        PRF_CRECV_DOUBLE(node_host, &dd[0], MAX_NT, node_host);
                        PRF_CRECV_DOUBLE(node_host, &ddc[0], MAX_NT, node_host);
                        for(i=node_one;i<compute_node_count;i++)
                        {
                                PRF_CSEND_INT(i, &nt, 1, myid);
                                PRF_CSEND_DOUBLE(i, &dt[0], MAX_NT, myid);
                                PRF_CSEND_DOUBLE(i, &dd[0], MAX_NT, myid);
                                PRF_CSEND_DOUBLE(i, &ddc[0], MAX_NT, myid);
                        }
                }
                else
                {
                        PRF_CRECV_INT(node_zero, &nt, 1, node_zero);
                        PRF_CRECV_DOUBLE(node_zero, &dt[0], MAX_NT, node_zero);
                        PRF_CRECV_DOUBLE(node_zero, &dd[0], MAX_NT, node_zero);
                        PRF_CRECV_DOUBLE(node_zero, &ddc[0], MAX_NT, node_zero);
                }
        }

        if (myid == node_host) Message(" Distribuidos\n");
}

void leerDatosInternos(void)
{
        int i;
        double dtp[38] = {0, 0.03, 0.07, 0.11, 0.12, \
                0.13, 0.14, 0.16, 0.18, 0.2, \
                0.21, 0.22, 0.23, 0.24, 0.3, \
                0.37, 0.47, 0.6, 0.8, 1, \
                1.28, 1.7, 2.85, 6, 6.03, \
                6.05, 6.08, 6.13, 6.18, 6.28, \
                6.33, 6.37, 6.43, 6.53, 6.7, \
                6.9, 7.1, 7.33};
        double ddp[38] = {0, -0.785950336, -1.964875841, -3.929751681, -4.912189602, \
                -6.680577858, -9.431404035, -16.89793223, -24.75743559, -32.99026536, \
                -36.07512043, -37.61951284, -38.01641776, -37.41909551, -31.88600514, \
                -24.49807198, -18.27334532, -13.0782136, -7.631577765, -5.501652354, \
                -3.536776513, -1.996313854, -0.943140404, 0, 1.599408934, \
                3.285272406, 10.87755265, 21.19315082, 25.75166277, 30.25908795, \
                30.8485507, 30.76995566, 30.25908795, 26.72231143, 17.2909074, \
                9.077726384, 2.432516291, 0};

        nt = 38;
        for (i=0; i<nt; i++)
        {
                dt[i] = dtp[i];
                dd[i] = ddp[i];
```

```
	}
}

void leerDatosFich(void)
{
	FILE *fp;
	int i,j;
	char linea[1000], comas[20];
	int cc;

	if ((fp = fopen(FICHDATOS, "r")) == NULL)
	{
		errorDatos(1);
		return;
	}
	else
	{
		nt = 0;
		Message("\n\n");
		while (fgets(linea, 1000, fp) != NULL)
		{
			if (linea[0] == '/' && linea[1] == '/') Message("%s", linea);
			else
			{
				cc = sscanf(linea, "%lf %lf", &dt[nt], &dd[nt]);
				if (cc == 2) nt++;
				else if (cc == EOF) Message("%s", linea);
				else
				{
					errorDatos(2);
					fclose(fp);
					return;
				}
			}
		}
		if (nt < 2) errorDatos(2);

		fclose(fp);
	}
}

void errorDatos(int m)
{
	if (m == 1) Message("\n\n¡¡¡¡Error de apertura del fichero!!!!\n\n");
	else if (m == 2) Message("\n\n¡¡¡¡Error en los datos del fichero!!!!\n\n");
	else if (m == 3) Message("\n\n¡¡¡¡Error en el tiempo inicial: no es 0!!!!\n\n");
	else if (m == 4) Message("\n\n¡¡¡¡Error en el orden de los tiempos!!!!\n\n");
	else if (m == 5) Message("\n\n¡¡¡¡Error en los datos inicial y final: no son
0!!!!\n\n");
	else if (m == 6) Message("\n\n¡¡¡¡Error en el cálculo de los incrementos de los
datos!!!!\n\n");
	else Message("\n\n¡¡¡¡Error (desconocido) en los datos!!!!\n\n");

	nt = 3;
	dt[0] = 0;
	dd[0] = 0;
	dt[1] = 1;
	dd[1] = 1;
	dt[2] = 2;
	dd[2] = 0;
}
```